REPORT NO.
UCB/EERC-97/14
DECEMBER 1997

EARTHQUAKE ENGINEERING RESEARCH CENTER

PB99-106106

VIBRATION PROPERTIES OF BUILDINGS DETERMINED FROM RECORDED EARTHQUAKE MOTIONS

by

RAKESH K. GOEL
ANIL K. CHOPRA

A Report on Research Conducted Under
Grant No. CMS-9416265
from the National Science Foundation

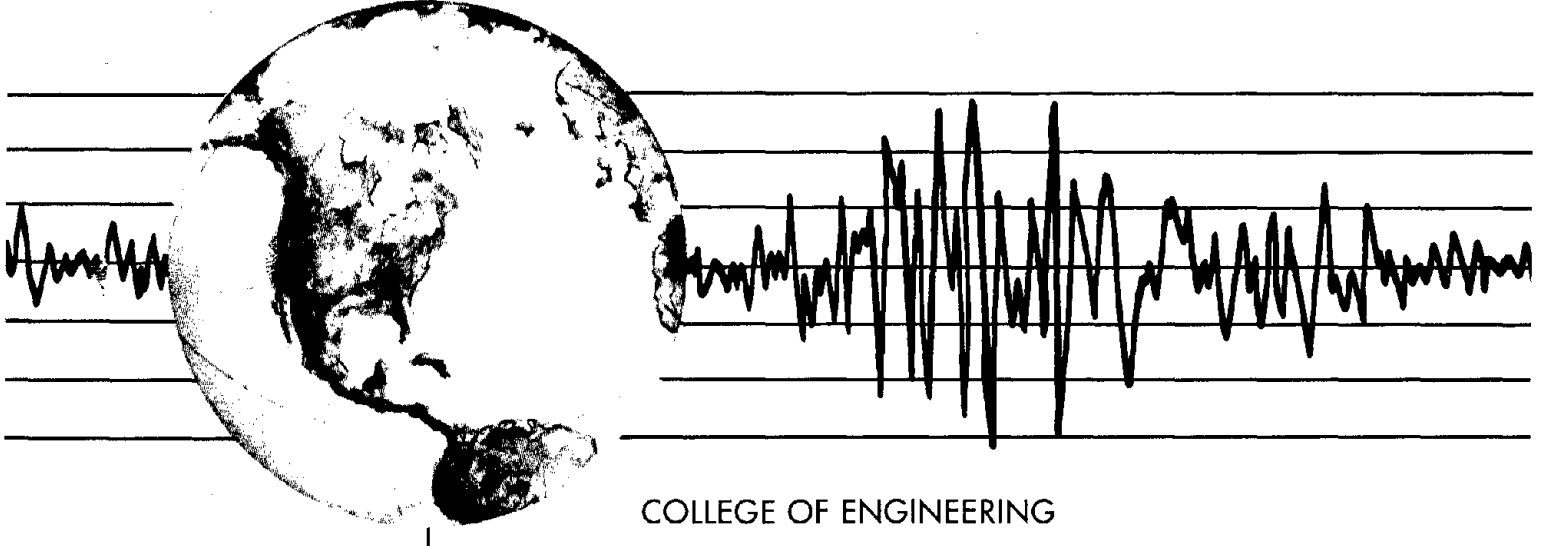

COLLEGE OF ENGINEERING

UNIVERSITY OF CALIFORNIA AT BERKELEY

For sale by the National Technical Information Service, U.S. Department of Commerce, Springfield, Virginia 22161

See back of report for up to date listing of EERC reports.

DISCLAIMER

Any opinions, findings, and conclusions or recommendations expressed in this publication are those of the authors and do not necessarily reflect the views of the National Science Foundation or the Earthquake Engineering Research Center, University of California at Berkeley.

50272-101

REPORT DOCUMENTATION PAGE	1. REPORT NO. UCB/EERC-97/14	2.	PB99-106106

4. Title and Subtitle

Vibration Properties of Buildings Determined from Recorded Earthquake Motions

5. Report Date

December 1997

6.

7. Author(s)

Rakesh K. Goel and Anil K. Chopra

8. Performing Organization Rept. No.

UCB/EERC-97/14

9. Performing Organization Name and Address

Earthquake Engineering Research Center
University of California, Berkeley
1301 S. 46th Street
Richmond, CA 94804

10. Project/Task/Work Unit No.

11. Contract(C) or Grant(G) No.

(C)

(G)

12. Sponsoring Organization Name and Address

National Science Foundation
1800 G Street N.W.
Washington, D.C. 20550

13. Type of Report & Period Covered

14.

15. Supplementary Notes

16. Abstract (Limit: 200 words)

Most seismic codes specifiy empirical formulas to estimate the fundamental vibration period of buildings. Developed first is a database on vibration properties - period and damping ratio of the first two longitudinal, transverse, and torsional vibration modes - of buildings "measured" from their motions recorded during eight California earthquakes, starting from the 1971 San Fernando earthquake and ending with the 1994 Northridge earthquake. To this end, the natural vibration periods of 21 buildings have been measured by system identification methods applied to the motions of buildings recorded during the 1994 Northridge earthquake. These data have been combined with similar data from the motions of buildings recorded during the 1971 San Fernando, 1984 Morgan Hill, 1986 Mt. Lewis and Palm Springs, 1987 Whittier, 1989 Loma Prieta, 1990 Upland, and 1991 Sierra Madre earthquakes reported by several investigators. The "measured" fundamental periods of moment-resisting frame and shear wall buildings, extracted from the database, are then used to evaluate the empirical formulas specified in present US codes. It is shown that although current code formulas provide periods of moment-resisting frame buildings that are generally shorter than measured periods, these formulas can be improved to provide better correlation with the measured period data. The code formulas for concrete shear wall buildings are, however, inadequate. Subsequently, improved formulas are developed by calibrating the theoretical formulas against the measured period data through regression analysis.

17. Document Analysis a. Descriptors

b. Identifiers/Open-Ended Terms

c. COSATI Field/Group

18. Availability Statement	19. Security Class (This Report) unclassified	21. No. of Pages 281
	20. Security Class (This Page) unclassified	22. Price

(See ANSI-Z39.18) *See Instructions on Reverse*

OPTIONAL FORM 272 (4-77)
(Formerly NTIS-35)
Department of Commerce

VIBRATION PROPERTIES OF BUILDINGS DETERMINED FROM RECORDED EARTHQUAKE MOTIONS

by

Rakesh K. Goel
Department of Civil and Environmental Engineering
Cal Poly State University
San Luis Obispo, CA 93407

and

Anil K. Chopra
Department of Civil and Environmental Engineering
University of California
Berkeley, CA 93720

A Report on Research Conducted Under
Grant no. CMS-9416265 from the National Science Foundation

Report No. UCB/EERC-97/14
Earthquake Engineering Research Center
University of California at Berkeley

December, 1997

ABSTRACT

Most seismic codes specify empirical formulas to estimate the fundamental vibration period of buildings. Developed first in this investigation is a database on vibration properties – period and damping ratio of the first two longitudinal, transverse, and torsional vibration modes – of buildings "measured" from their motions recorded during eight California earthquakes, starting from the 1971 San Fernando earthquake and ending with the 1994 Northridge earthquake. To this end, the natural vibration periods of 21 buildings have been measured by system identification methods applied to the motions of buildings recorded during the 1994 Northridge earthquake. These data have been combined with similar data from the motions of buildings recorded during the 1971 San Fernando, 1984 Morgan Hill, 1986 Mt. Lewis and Palm Springs, 1987 Whittier, 1989 Loma Prieta, 1990 Upland, and 1991 Sierra Madre earthquakes reported by several investigators. The "measured" fundamental periods of moment-resisting frame and shear wall buildings, extracted from the database, are then used to evaluate the empirical formulas specified in present US codes. It is shown that although current code formulas provide periods of moment-resisting frame buildings that are generally shorter than measured periods, these formulas can be improved to provide better correlation with the measured period data. The code formulas for concrete shear wall buildings are, however, inadequate. Subsequently, improved formulas are developed by calibrating the theoretical formulas against the measured period data through regression analysis. The theoretical formula for moment-resisting frame buildings is developed using Rayleigh's method whereas that for shear wall buildings is developed using Dunkerley's method. Finally factors to limit the period calculated by a "rational" analysis, such as Rayleigh's method or computer-based eigen-analysis, of both types of buildings are recommended for code applications.

ACKNOWLEDGMENTS

This research investigation is supported by the National Science Foundation under Grant CMS-9416265. The authors are grateful for this support. The authors also acknowledge the assistance provided by Anthony Shakal, Moh Huang, Bob Darragh, Gustavo Maldonado, and Praveen Malhotra of California Strong Motion Instrumentation Program in obtaining recorded motions and structural plans; and by Professors S. T. Mau and J. L. Beck, and Dr. M. Celebi in implementing the system identification procedures.

TABLE OF CONTENTS

PREFACE

This work on vibration properties of buildings determined from recorded earthquake motions is divided into three parts. Part I is concerned with the code formulas for the fundamental periods of reinforced concrete (RC) and steel moment-resisting frame buildings, whereas Part II is focused on the code formulas for the fundamental period of concrete shear wall (SW) buildings. Appendices containing details that could not be included in the Part I and II are presented in Part III.

Each of the Part I and II first presents a brief introduction followed by the measured period database for the type of buildings under consideration. The fundamental period formulas in current US codes are reviewed and evaluated next. Subsequently, theoretical formulas are developed and calibrated against the measured period data using regression analysis techniques. Each part ends with recommendations for improved formula to estimate the fundamental period of a building and a factor to limit the period calculated by a "rational" analysis, such as Rayleigh's method.

Part III contains several appendices where detailed information on several aspects of the project is presented. Appendix A presents the complete database on vibration properties of buildings determined from recorded earthquake motions. The database was compiled using Microsoft Access 2.0; the database is available electronically from the Earthquake Engineering Research Center at the University of California at Berkeley via their web page at www.eerc.berkeley.edu. Described is the format of the database followed by the techniques that can be used to add and extract data from the database. Although only the fundamental period data is used in Parts I and II of this report, the database includes the vibration period and damping ratio of the first two longitudinal, transverse, and torsional vibration modes.

Appendix B presents the theoretical background, along with examples, for various system identification techniques used in this investigation. Appendix C summarizes results of system identification for twenty-two buildings, conducted as part of this investigation. Appendix D develops theoretical formula and associated assumptions, which form the basis for empirical formulas in current US codes to estimate the fundamental period. Appendix E presents development of the fundamental period formula for moment-resisting frame buildings using Rayleigh's method. Appendix F describes the regression analysis method. Appendix G presents detailed development of theoretical formulas for fundamental period of concrete shear wall buildings using Rayleigh's and Dunkerley's methods. These formulas are used in Part II of this report for developing improved period formula for shear wall buildings. Appendix H presents sketches of structural plans and information on shear wall dimensions for nine buildings (this information was not available for the remaining seven shear wall buildings) followed by the computations for the fundamental period using the code empirical formula and the proposed formula involving shear wall dimensions. Finally, Appendix I includes an exhaustive list of references on system identification techniques, data on period and damping ratio values for buildings, their recorded motions, and other relevant publications.

PART I:
MOMENT-RESISTING FRAME BUILDINGS

INTRODUCTION

The fundamental vibration period of a building appears in the equation specified in building codes to calculate the design base shear and lateral forces. Because this building property can not be computed for a structure that is yet to be designed, building codes provide empirical formulas that depend on the building material (steel, R/C, etc.), building type (frame, shear wall etc.), and overall dimensions.

The period formulas in the 1997 UBC (*Uniform Building Code*, 1997) and the 1996 SEAOC recommendations (*Recommended Lateral Force Requirements*, 1996) are derived from those developed in 1975 as part of the ATC3-06 project (*Tentative Provisions*, 1978), based largely on periods of buildings "measured" from their motions recorded during the 1971 San Fernando earthquake. However, motions of many more buildings recorded during recent earthquakes, including the 1989 Loma Prieta and 1994 Northridge earthquakes, are now available. These recorded motions provide an opportunity to expand greatly the existing database on the fundamental vibration periods of buildings. To this end, the natural vibration periods of 21 buildings have been measured by system identification methods applied to the motions of buildings recorded during the 1994 Northridge earthquake (Goel and Chopra, 1997). These data have been combined with similar data from the motions of buildings recorded during the 1971 San Fernando, 1984 Morgan Hill, 1986 Mt. Lewis and Palm Springs, 1987 Whittier, 1989 Loma Prieta, 1990 Upland, and 1991 Sierra Madre earthquakes reported by several investigators (an exhaustive list of references is available in Appendix I).

The objective of this investigation is to develop improved empirical formulas to estimate the fundamental vibration period of reinforced-concrete (R/C) and steel moment-resisting frame (MRF) buildings for use in equivalent lateral force analysis specified in building codes. Presented

first is the expanded database for measured values of fundamental periods of MRF buildings, against which the empirical formulas in present US codes are evaluated. Subsequently, regression analysis of the measured data is used to develop improved formulas for estimating the fundamental periods of R/C MRF buildings and of steel MRF buildings. Finally, factors to limit the period calculated by a rational analysis, such as Rayleigh's method, are recommended.

PERIOD DATABASE

The data that are most useful but hard to come by are from structures shaken strongly but not deformed into the inelastic range. Such data are slow to accumulate because relatively few structures are installed with permanent accelerographs, and earthquakes causing strong motions of these instrumented buildings are infrequent. Thus, it is very important to investigate comprehensively the recorded motions when they do become available, as during the 1994 Northridge earthquake. Unfortunately, this obviously important goal is not always accomplished, as indicated by the fact that the vibration properties of only a few of the buildings whose motions were recorded during post-1971 earthquakes have been determined.

Available data on the fundamental vibration period of buildings measured from their motions recorded during several California earthquakes have been collected (Appendix A). This database contains data for a total of 106 buildings, including twenty-one buildings that experienced peak ground acceleration, $\ddot{u}_{go} \geq 0.15g$ during the 1994 Northridge earthquake. The remaining data comes from motions of buildings recorded during the 1971 San Fernando earthquake and subsequent earthquakes (*Tentative Provisions*, 1978; Bertero et al., 1988; Cole et al., 1992; Hart and Vasudevan, 1975; Goel and Chopra, 1997).

Shown in Tables 1 and 2 is the subset of this database pertaining to MRF buildings including 37 data points for 27 R/C MRF buildings, and 53 data points for 42 steel MRF buildings; buildings subjected to $\ddot{u}_{go} \geq 0.15g$ are identified with an asterisk (*). "C", "U", and "N" denote buildings instrumented by the California Strong Motion Instrumentation Program (CSMIP), United States Geological Survey (USGS), and National Oceanic and Atmospheric Administration (NOAA); "ATC" denotes buildings included in the ATC3-06 report (*Tentative Provisions*, 1978). The number of data points exceeds the number of buildings because the

period of some buildings was determined from their motions recorded during more than one earthquake, or was reported by more than one investigator for the same earthquake.

Table 1. Period data for R/C MRF buildings.

No.	Location	ID Number	No. of Stories	Height (ft)	Earthquake	Period T (sec)	
						Longitudinal	Transverse
1	Emeryville	NA	30	300.0	Loma Prieta	2.80	2.80
2	Los Angeles	NA	9	120.0	San Fernando	1.40	1.30
3	Los Angeles	NA	14	160.0	San Fernando	1.80	1.60
4	Los Angeles	NA	13	166.0	San Fernando	1.90	2.40
5	Los Angeles	ATC_12	10	137.5	San Fernando	1.40	1.60
6	Los Angeles	ATC_14	7	61.0	San Fernando	0.90	1.20
7	Los Angeles	ATC_2	7	68.0	San Fernando	1.00	1.00
8	Los Angeles	ATC_3	12	159.0	San Fernando	SW	1.33
9	Los Angeles	ATC_5	19	196.8	San Fernando	2.15	2.22
10	Los Angeles	ATC_6	11	124.0	San Fernando	1.43	1.60
11	Los Angeles	ATC_7	22	204.3	San Fernando	1.90	2.20
12	Los Angeles	ATC_9	16	152.0	San Fernando	1.10	1.80
13*	Los Angeles	C24236	14	148.8	Northridge	NA	2.28
14*	Los Angeles	C24463	5	119.0	Northridge	1.46	1.61
15*	Los Angeles	C24463	5	119.0	Whittier	1.40	1.30
16*	Los Angeles	C24569	15	274.0	Northridge	3.11	3.19
17*	Los Angeles	C24579	9	141.0	Northridge	1.39	1.28
18*	Los Angeles	N220-2	20	196.8	San Fernando	2.27	2.09
19*	Los Angeles	N220-2	20	196.8	San Fernando	2.27	2.13
20*	Los Angeles	N220-2	20	196.8	San Fernando	2.24	1.98
21*	Los Angeles	N446-8	22	204.3	San Fernando	1.94	2.14
22*	Los Angeles	N446-8	22	204.3	San Fernando	1.84	2.17
23*	North Hollywood	C24464	20	169.0	Northridge	2.60	2.62
24	North Hollywood	C24464	20	169.0	Whittier	2.15	2.21
25	Pomona	C23511	2	30.0	Upland	0.28	0.30
26	Pomona	C23511	2	30.0	Whittier	0.27	0.29
27	San Bruno	C58490	6	78.0	Loma Prieta	0.85	1.10
28	San Bruno	C58490	6	78.0	Loma Prieta	0.85	1.02
29	San Jose	NA	5	65.0	Morgan Hill	0.83	0.83
30	San Jose	C57355	10	124.0	Loma Prieta	1.01	SW
31	San Jose	C57355	10	124.0	Morgan Hill	0.91	SW
32	San Jose	C57355	10	124.0	Mount Lewis	0.91	SW
33*	Sherman Oaks	ATC_4	13	124.0	San Fernando	1.20	1.40
34*	Sherman Oaks	C24322	13	184.5	Whittier	1.90	2.30
35*	Sherman Oaks	C24322	13	184.5	Whittier	NA	2.44
36	Van Nuys	ATC_1	7	65.7	San Fernando	0.79	0.88
37*	Van Nuys	C24386	7	65.7	Whittier	1.40	1.20

* Denotes buildings with $\ddot{u}_{go} \geq 0.15$g.

NA Indicates data not available.

SW Implies shear walls form the lateral load resisting system.

Number followed by "C" or "N" indicates the station number, and by "ATC" indicates the building number in ATC3-06 report.

Table 2. Period data for steel MRF buildings (continues ...).

No.	Location	ID Number	No. of Stories	Height (ft)	Earthquake Name	Period T (sec)	
						Longitudinal	Transverse
1*	Alhambra	U482	13	198.0	Northridge	2.15	2.20
2*	Burbank	C24370	6	82.5	Northridge	1.36	1.38
3*	Burbank	C24370	6	82.5	Whittier	1.32	1.30
4	Long Beach	C14323	7	91.0	Whittier	1.19	1.50
5	Los Angeles	ATC_1	19	208.5	San Fernando	3.00	3.21
6	Los Angeles	ATC_10	39	494.0	San Fernando	5.00	4.76
7	Los Angeles	ATC_11	15	202.0	San Fernando	2.91	2.79
8	Los Angeles	ATC_12	31	336.5	San Fernando	3.26	3.00
9	Los Angeles	ATC_13	NA	102.0	San Fernando	1.71	1.62
10	Los Angeles	ATC_14	NA	158.5	San Fernando	2.76	2.38
11	Los Angeles	ATC_15	41	599.0	San Fernando	6.00	5.50
12	Los Angeles	ATC_17	NA	81.5	San Fernando	1.85	1.71
13	Los Angeles	ATC_3	NA	120.0	San Fernando	2.41	2.23
14	Los Angeles	ATC_4	27	368.5	San Fernando	4.38	4.18
15	Los Angeles	ATC_5	19	267.0	San Fernando	3.97	3.50
16	Los Angeles	ATC_6	17	207.0	San Fernando	3.00	2.28
17	Los Angeles	ATC_7	NA	250.0	San Fernando	4.03	3.88
18	Los Angeles	ATC_8	32	428.5	San Fernando	5.00	5.40
19	Los Angeles	ATC_9	NA	208.5	San Fernando	3.20	3.20
20*	Los Angeles	C24643	19	270.0	Northridge	3.89	BF
21	Los Angeles	N151-3	15	202.0	San Fernando	2.84	2.77
22	Los Angeles	N157-9	39	459.0	San Fernando	4.65	NA
23	Los Angeles	N163-5	41	599.0	San Fernando	6.06	5.40
24*	Los Angeles	N172-4	31	336.5	San Fernando	3.38	2.90
25*	Los Angeles	N172-4	31	336.5	San Fernando	3.42	2.94
26	Los Angeles	N184-6	27	398.0	San Fernando	4.27	4.26
27	Los Angeles	N184-6	27	398.0	San Fernando	4.37	4.24
28*	Los Angeles	N187-9	19	270.0	San Fernando	3.43	3.41
29	Los Angeles	N428-30	32	443.5	San Fernando	4.86	5.50
30	Los Angeles	N440-2	17	207.0	San Fernando	2.85	3.43
31*	Los Angeles	N461-3	19	231.7	San Fernando	3.27	3.34
32*	Los Angeles	N461-3	19	231.7	San Fernando	3.02	3.30
33*	Los Angeles	N461-3	19	231.7	San Fernando	3.28	3.34
34*	Los Angeles	U5208	6	104.0	Northridge	0.94	0.96
35*	Los Angeles	U5233	32	430.0	Northridge	3.43	4.36
36*	Norwalk	U5239	7	96.0	Whittier	1.54	1.54
37*	Norwalk	U5239	7	98.0	Whittier	1.30	1.22

* Denotes buildings with $\ddot{u}_{go} \geq 0.15$g.

NA Indicates data not available.

BF Implies braced frame and EBF means eccentric braced frame form the lateral load resisting system.

Number followed by "C", "N", or "U" indicates the station number, and by "ATC" indicates the building number in ATC3-06 report.

Table 2. Period data for steel MRF buildings (... continued).

No.	Location	ID Number	No. of Stories	Height (ft)	Earthquake Name	Period T (sec)	
						Longitudinal	Transverse
38*	Palm Springs	C12299	4	51.5	Palm Springs	0.71	0.63
39	Pasadena	ATC_2	9	128.5	San Fernando	1.29	1.44
40*	Pasadena	C24541	6	92.3	Northridge	2.19	1.79
41	Pasadena	N267-8	9	130.0	Lytle Creek	1.02	1.13
42	Pasadena	N267-8	9	130.0	San Fernando	1.26	1.42
43	Richmond	C58506	3	45.0	Loma Prieta	0.63	0.74
44	Richmond	C58506	3	45.0	Loma Prieta	0.60	0.76
45	San Bernardino	C23516	3	41.3	Whittier	0.50	0.46
46*	San Francisco	C58532	47	564.0	Loma Prieta	6.25	EBF
47*	San Francisco	C58532	47	564.0	Loma Prieta	6.50	EBF
48	San Francisco	NA	60	843.2	Loma Prieta	3.57	3.57
49*	San Jose	C57357	13	186.6	Loma Prieta	2.22	2.22
50*	San Jose	C57357	13	186.6	Loma Prieta	2.23	2.23
51	San Jose	C57357	13	186.6	Morgan Hill	2.05	2.16
52	San Jose	C57562	3	49.5	Loma Prieta	0.67	0.69
53	San Jose	C57562	3	49.5	Loma Prieta	0.69	0.69

* Denotes buildings with $\ddot{u}_{go} \geq 0.15$g.

NA Indicates data not available.

BF Implies braced frame and EBF means eccentric braced frame form the lateral load resisting system.

Number followed by "C", "N", or "U" indicates the station number, and by "ATC" indicates the building number in ATC3-06 report.

CODE FORMULAS

The empirical formulas for the fundamental vibration period of MRF buildings specified in US building codes -- UBC-97 (*Uniform Building Code*, 1997), ATC3-06 (*Tentative Provisions*, 1978), SEAOC-96 (*Recommended Lateral Force Requirements*, 1996), and NEHRP-94 (*NEHRP*, 1994) -- are of the form:

$$T = C_t H^{3/4} \tag{1}$$

where H is the height of the building in feet above the base and the numerical coefficient C_t = 0.030 and 0.035 for R/C and steel MRF buildings, respectively, with one exception: in ATC3-06 recommendations C_t = 0.025 for R/C MRF buildings.

Equation (1), which first appeared in the ATC3-06 report, was derived using Rayleigh's method (Chopra, 1995) with the following assumptions: (1) equivalent static lateral forces are distributed linearly over the height of the building; (2) seismic base shear is proportional to $1/T^{2/3}$; and (3) deflections of the building are controlled by drift limitations (Appendix D). While the first two assumptions are evident, the third assumption implies that the height-wise distribution of stiffness is such that the inter-story drift under linearly distributed forces is uniform over the height of the building. Numerical values of C_t = 0.035 and 0.025 for steel and R/C MRF buildings were established in the ATC3-06 report based on measured periods of buildings from their motions recorded during the 1971 San Fernando earthquake. The commentary to SEAOC-88 (*Recommended Lateral Force Requirements*, 1988) states that "... data upon which the ATC3-06 values were based were re-examined for concrete frames and the 0.030 value judged to be more appropriate." This judgmental change was adopted by other codes.

The NEHRP-94 provisions also recommend an alternative formula for R/C and steel MRF buildings:

$$T = 0.1N \tag{2}$$

in which N is the number of stories. The simple formula is restricted to buildings not exceeding 12 stories in height and having a minimum story height of 10 ft. This formula was also specified in earlier versions of other seismic codes before it was replaced by Eq. (1).

UBC-97 (*Uniform Building Code*, 1997) and SEAOC-96 codes specify that the design base shear should be calculated from:

$$V = CW \tag{3}$$

in which W is the total seismic dead load and C is the seismic coefficient defined as

$$C = \frac{C_v}{R}\frac{I}{T}; \quad 0.11 C_a I \le C \le \frac{2.5 C_a}{R} I \tag{4}$$

and for seismic zone 4

$$C \ge \frac{0.8 Z N_v I}{R} \tag{5}$$

in which coefficients C_v and C_a depend on the near-source factors, N_v and N_a, respectively, along with the soil profile and the seismic zone factor Z; I is the important factor; and the R is the numerical coefficient representative of the inherent overstrength and global ductility capacity of the lateral-load resisting system. The upper limit of $2.5 C_a I \div R$ on C applies to very-short period buildings, whereas the lower limit of $0.11 C_a I$ (or $0.8 Z N_v I \div R$ for seismic zone 4) applies to very-long period buildings. These limits imply that C becomes independent of the period for very-short or very-tall buildings. The upper limit existed, although in slightly different form, in

previous versions of UBC and SEAOC blue book; the lower limit, however, appeared only recently in UBC-97 and SEAOC-96.

The fundamental period T, calculated using the empirical Eq. (1), should be smaller than the "true" period to obtain a conservative estimate for the base shear. Therefore, code formulas are intentionally calibrated to underestimate the period by about 10 to 20 percent at first yield of the building (*Tentative Provisions*, 1978; *Recommended Lateral Force Requirements*, 1988).

The codes permit calculation of the period by a rational analysis, such as Rayleigh's method, but specify that the resulting value should not be longer than that estimated from the empirical formula (Eq. 1) by a certain factor. The factors specified in various US codes are: 1.2 in ATC3-06; 1.3 for high seismic region (Zone 4) and 1.4 for other regions (Zones 3, 2, and 1) in UBC-97; and a range of values with 1.2 for regions of high seismicity to 1.7 for regions of very low seismicity in NEHRP-94. The restriction in SEAOC-88 that the base shear calculated using the rational period shall not be less than 80 percent of the value obtained by using the empirical period corresponds to a factor of 1.4 (Cole et al., 1992). These restrictions are imposed in order to safeguard against unreasonable assumptions in the rational analysis, which may lead to unreasonably long periods and hence unconservative values of base shear.

EVALUATION OF CODE FORMULAS

For buildings listed in Tables 1 and 2, the fundamental period identified from their motions recorded during earthquakes (subsequently denoted as measured period) is compared with the value given by the empirical code formula (Figures 1 to 4, part a); the measured periods in two orthogonal lateral directions are shown by solid circles connected by a vertical line, whereas code periods are shown by a single solid curve because the code formula gives the same period in the two directions if the lateral resisting systems are of the same type. Also included are curves for $1.2T$ and $1.4T$ representing the limits imposed by codes on the rational value of the period for use in high seismic regions like California. Also compared are the two values of the seismic coefficient for each building calculated according to Eqs. (4) and (5) with $I = 1$ for standard occupancy structures; $R = 3.5$ for ordinary concrete moment-resisting frames or $R = 4.5$ for ordinary steel moment-resisting frames; and $C_v = 0.64$ and $C_a = 0.44$ for seismic zone 4 with $Z = 0.4$, soil profile type S_D, i.e., stiff soil profile with average shear wave velocity between 180 and 360 m/s, and $N_v = N_a = 1$. The seismic coefficients corresponding to the measured periods in the two orthogonal directions are shown by solid circles connected by a vertical line, whereas the value based on the code period is shown by a solid curve.

R/C MRF Buildings

The data shown in Figure 1 for all R/C MRF buildings (Table 1) permit the following observations. The code formula is close to the lower bound of measured periods for buildings up to 160 ft high, but leads to periods significantly shorter than the measured periods for buildings in the height range of 160 ft to 225 ft. For such buildings, the lower bound tends to be about 1.2 times the code period. Although data for R/C MRF buildings taller than 225 ft is limited, it appears that the measured period of such buildings is much longer than the code value. The

measured periods of most R/C MRF buildings fall between the curves for $1.2T$ and $1.4T$, indicating that the code limits on the period calculated from rational analysis may be reasonable for high seismic regions like California; improved limits are proposed later. Data on measured periods of buildings in regions of low seismicity are needed to evaluate the much higher values of $1.7T$ permitted in NEHRP-94 to reflect the expectation that these buildings are likely to be more flexible (Commentary for NEHRP-94). The seismic coefficient calculated from the code period is conservative for most buildings because the code period is shorter than the measured period. For very-short (H less than about 50 ft) or very-tall (H more than about 250 ft) buildings, measured and code periods lead to the same seismic coefficient as C becomes independent of the period.

Since for design applications, it is most useful to examine the periods of buildings that have been shaken strongly but did not reach their yield limit, the data for buildings subjected to $\ddot{u}_{go} \geq 0.15$g (denoted with an * in Table 1) are separated in Figure 2. These data permit the following observations. For buildings of similar height, the fundamental period of strongly shaken buildings is longer compared to less strongly shaken buildings because of increased cracking of R/C that results in reduced stiffness. As a result the measured periods are in all cases longer than their code values, in most cases much longer. The lower bound of measured periods of strongly shaken buildings is close to 1.2 times the code period. Thus the coefficient $C_t = 0.030$ in current codes seems to be too small, and a value like 0.035, as will be seen later from the results of regression analysis, may be more appropriate. Just as observed from the data for all buildings, the seismic coefficient value calculated using the code period is conservative for most strongly shaken buildings and the conservatism is larger; exception occurs for very-short or very-tall buildings for which the seismic coefficient is independent of the period.

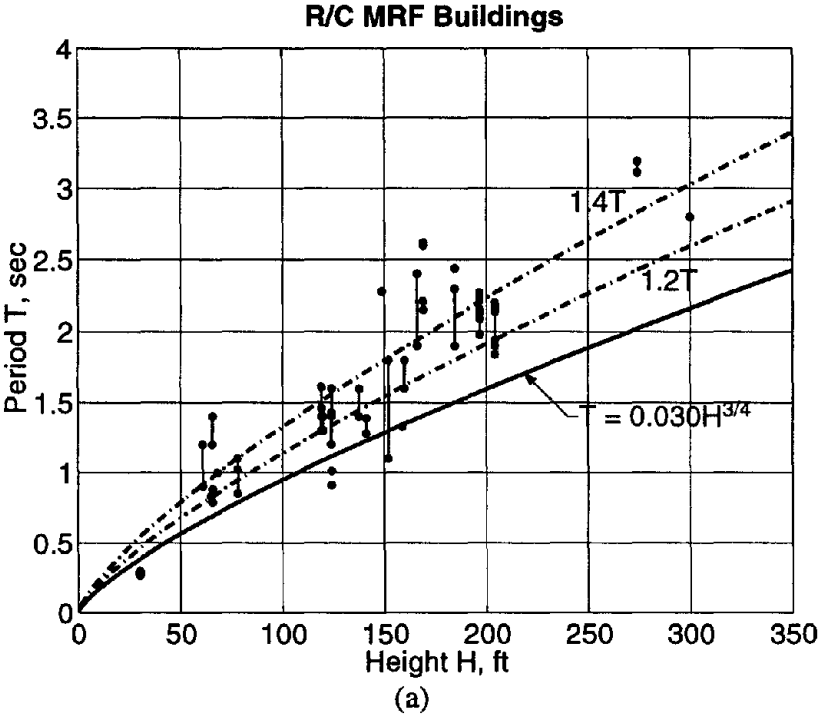

(a)

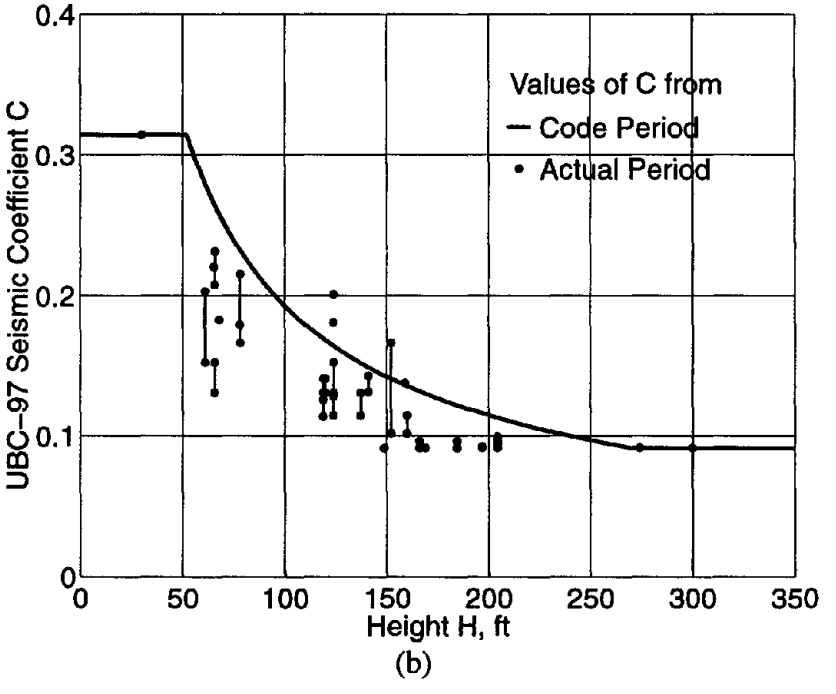

(b)

Figure 1. Comparison of (a) measured and code periods, and (b) UBC-97 seismic coefficients from measured and code periods, for R/C MRF buildings.

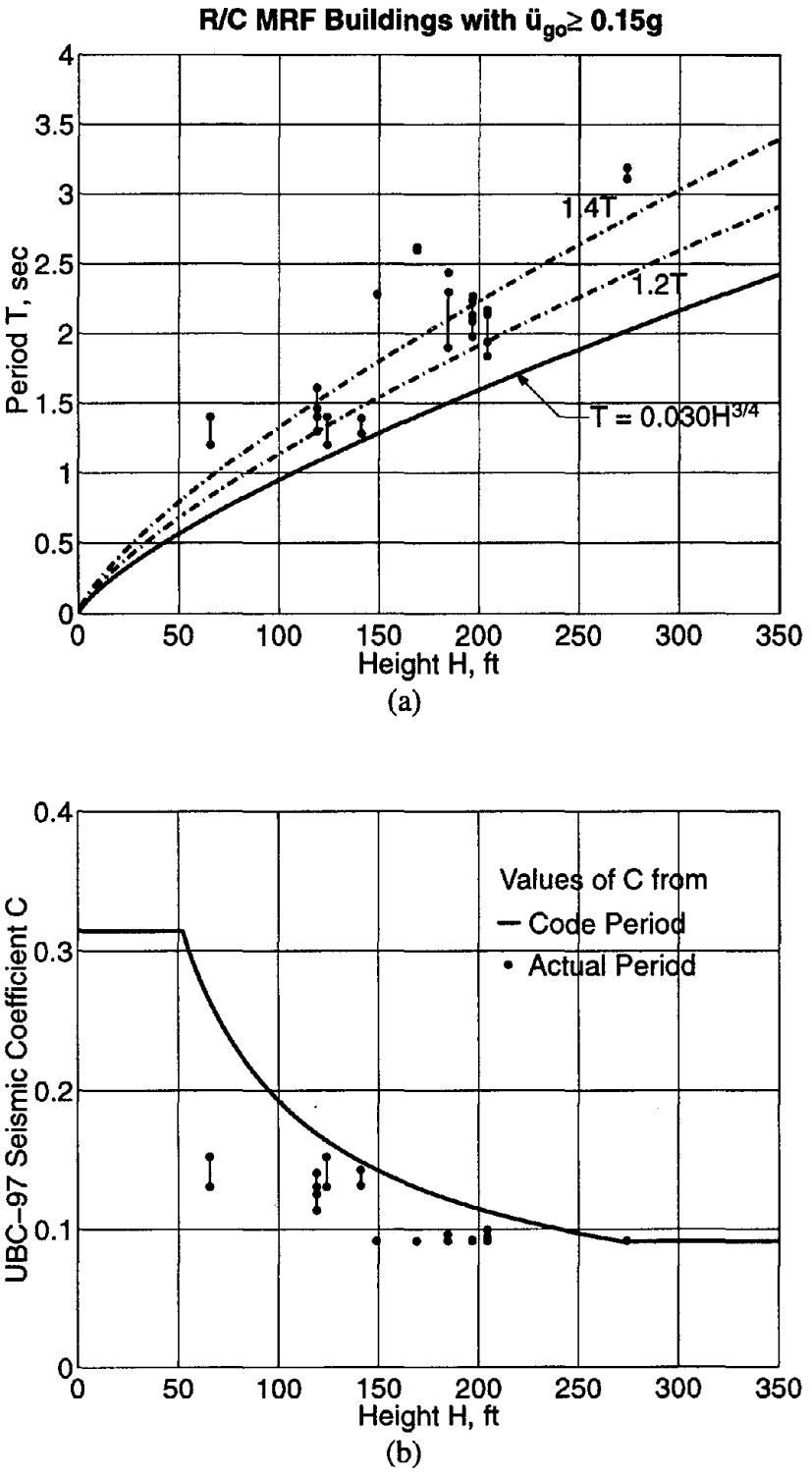

Figure 2. Comparison of (a) measured and code periods, and (b) UBC-97 seismic coefficients from measured and code periods, for R/C MRF buildings with $\ddot{u}_{go} \geq 0.15$g.

Steel MRF Buildings

The data presented in Figure 3 for all steel MRF buildings (Table 2) permit the following observations. The code formula leads to periods that are generally shorter than measured periods, with the margin between the two being much larger than for R/C MRF buildings (Figure 1a). The code formula gives periods close to the lower bound of measured periods for buildings up to about 120 ft high, but 20-30% shorter for buildings taller than 120 ft; this conclusion is based on a larger data set compared to the meager data for R/C MRF buildings. For many buildings the measured periods exceed $1.4T$, indicating that the code limits on the period calculated from rational analysis are too restrictive. The seismic coefficient value calculated from the code period is conservative for most buildings and the degree of conservatism is larger compared to R/C buildings; as noted previously for R/C buildings, exception occurs for very-short or very-tall buildings for which the seismic coefficient is independent of the period.

The data for steel MRF buildings subjected to ground acceleration of $0.15g$ or more (denoted with an * in Table 2) are separated in Figure 4. Comparing these data with Figure 3, it can be observed that the intensity of ground shaking has little influence on the measured period. The period elongates slightly due to stronger shaking but less than for R/C buildings which exhibit significantly longer periods due to increased cracking. Thus period data from all levels of shaking of buildings remaining essential elastic may be used to develop improved formulas for fundamental periods of steel MRF buildings.

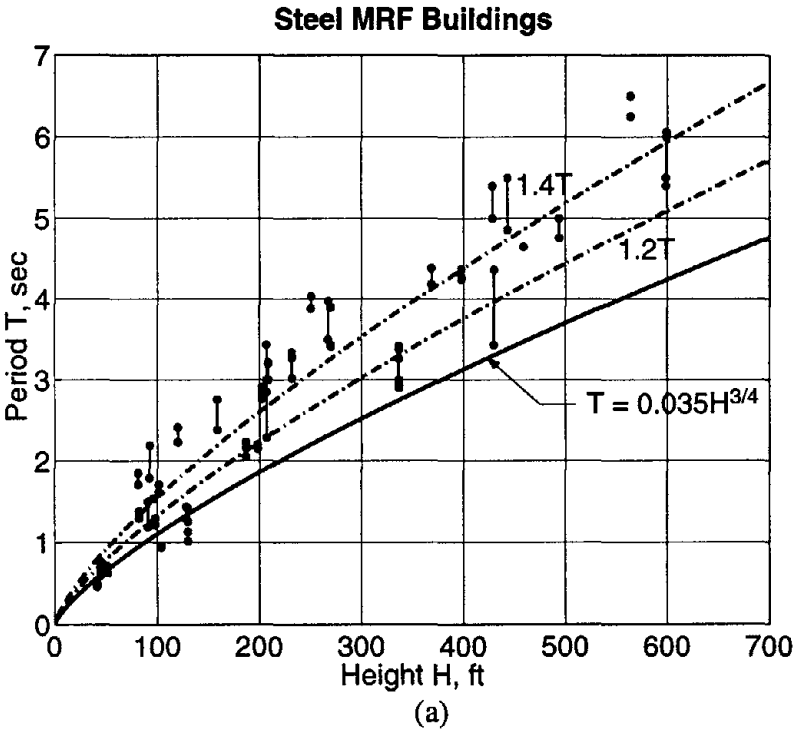

(a)

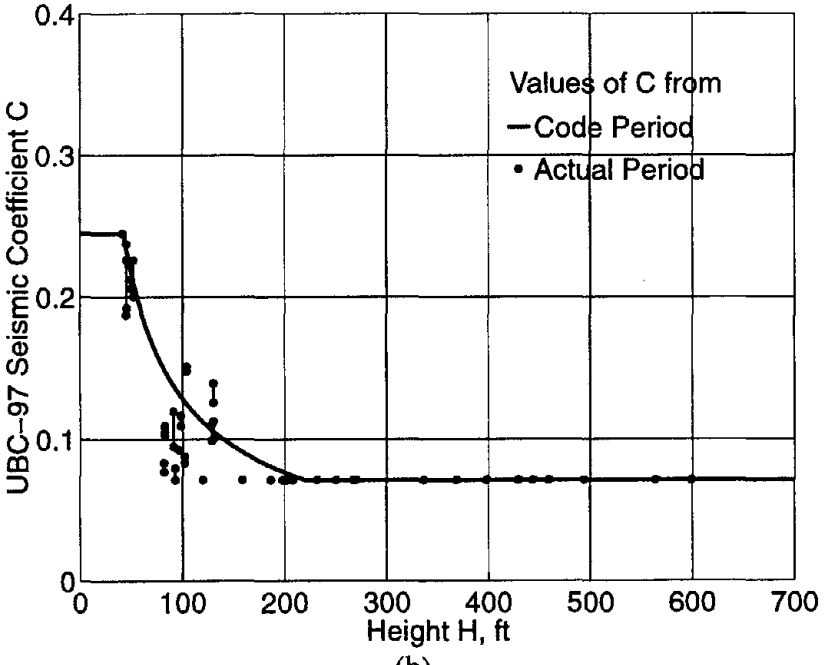

(b)

Figure 3. Comparison of (a) measured and code periods, and (b) UBC-97 seismic coefficients from measured and code periods, for steel MRF buildings.

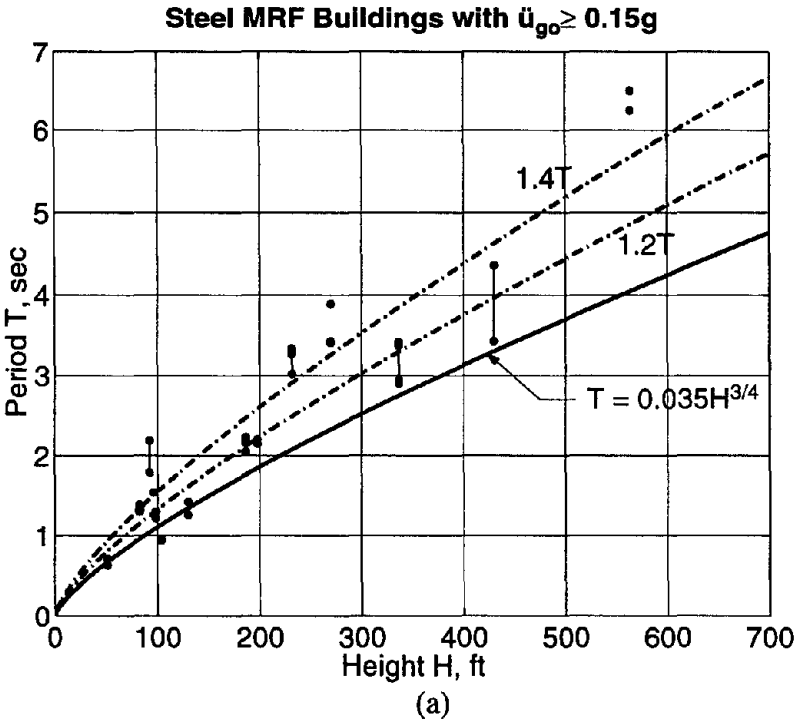

(a)

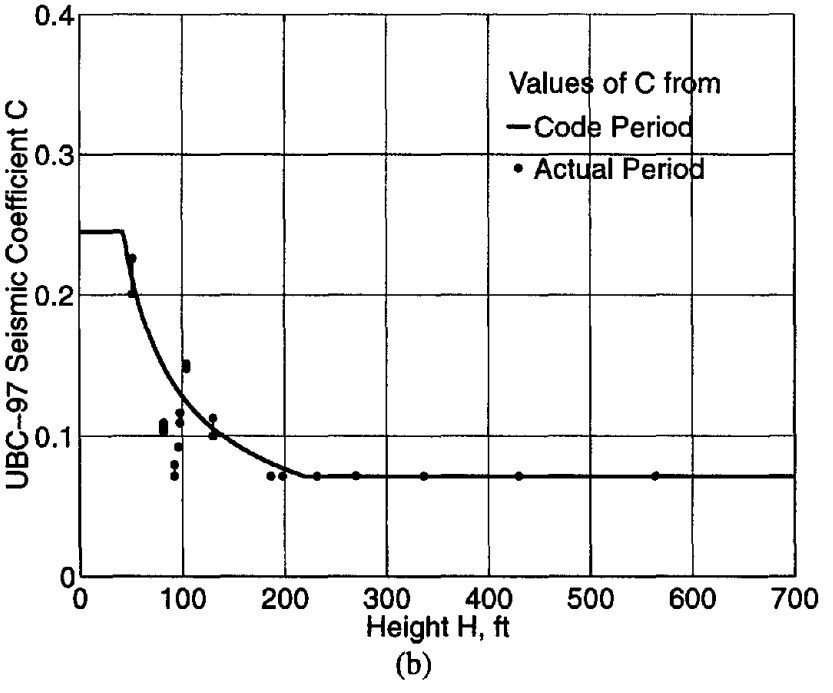

(b)

Figure 4. Comparison of (a) measured and code periods, and (b) UBC-97 seismic coefficients from measured and code periods, for steel MRF buildings with $\ddot{u}_{go} \geq 0.15$g.

THEORETICAL FORMULAS

Although the results presented in the preceding section indicate that the code formulas provide periods that are, in general, shorter than the measured periods, leading to conservative estimates of design forces, these formulas may be improved to provide better correlation with the measured periods. The relation between the period and building height in the improved formulas should be consistent with theoretical formulas presented next.

Using Rayleigh's method, the following relationships for fundamental period of multistory building frames with equal floor masses and story heights have been determined (Housner and Brady, 1963; Appendix E):

$$T = C_1\sqrt{H} \text{ or } C_2 H \tag{6}$$

The exponent of H and the numerical values of C_1 and C_2 depends on the stiffness properties, including their height-wise variation.

Another formula for the fundamental period has been derived by Rayleigh's method under the following assumptions: (1) lateral forces are distributed linearly (triangular variation of forces) over the building height; (2) base shear is proportional to $1/T^{\gamma}$; (3) weight of the building is distributed uniformly over its height; and (4) deflected shape of the building, under application of the lateral forces, is linear over its height, which implies that the inter-story drift is the same for all stories. The result of this derivation (Appendix D) is:

$$T = C_3 H^{\frac{1}{2-\gamma}} \tag{7}$$

If the base shear is proportional to $1/T^{2/3}$, as in US codes (Eq. 4), $\gamma = 2/3$ and Eq. (7) gives:

$$T = C_4 H^{3/4} \tag{8}$$

which is in the ATC3-06 report and appears in current US codes.

The formulas presented in Eqs. (6) to (8) are of the form:

$$T = \alpha H^{\beta} \tag{9}$$

in which constants α and β depend on building properties, with β bounded between one-half and one. This form is adopted in the present investigation and constants α and β are determined by regression analysis of the measured period data.

REGRESSION ANALYSIS METHOD

For the purpose of regression analysis, it is useful to recast Eq. (9) as:

$$y = a + \beta x \tag{10}$$

in which $y = log(T)$, $a = log(\alpha)$, and $x = log(H)$. The intercept a at $x = 0$ and slope β of the straight line of Eq. (10) were determined by minimizing the squared error between the measured and computed periods, and then α was back calculated from the relationship $a = log(\alpha)$. The standard error of estimate is:

$$s_e = \sqrt{\frac{\sum_{i=1}^{n}\left[y_i - (a+\beta x_i)\right]^2}{(n-2)}} \tag{11}$$

in which $y_i = \log(T_i)$ is the observed value (with T_i = measured period) and $(a + \beta x_i) = \left[\log(\alpha) + \beta \log(H_i)\right]$ is the computed value of the *i*th data, and *n* is the total number of data points. The s_e represents scatter in the data and approaches, for large *n*, the standard deviation of the measured periods from the best-fit equation.

This procedure leads to values of α_R and β for Eq. (9) to represent the best-fit, in the least squared sense, to the measured period data. However, for code applications, the formula should provide lower values of the period, and this was obtained by lowering the best-fit line (Eq. 10) by s_e without changing its slope. Thus α_L, the lower value of α, is computed from:

$$\log(\alpha_L) = \log(\alpha_R) - s_e \tag{12}$$

Since s_e approaches the standard deviation for a large number of samples and *y* is log-normal, α_L is the mean-minus-one-standard-deviation or 15.9 percentile value, implying that 15.9 percent of the measured periods would fall below the curve corresponding to α_L (subsequently

referred to as the best-fit - 1σ curve). If desired, α_L corresponding to other non-exceedance probabilities may be selected. Additional details of the regression analysis method and the procedure to estimate α_L are available elsewhere (Appendix F).

As mentioned previously, codes also specify an upper limit on the period calculated by rational analysis. This limit is established in this investigation by raising the best-fit line (Eq. 10) by s_e without changing its slope. Thus α_U, the value of α corresponding to the upper limit, is computed from:

$$\log(\alpha_U) = \log(\alpha_R) + s_e \tag{13}$$

Eq. (9) with α_U and β represents the best-fit + 1σ curve which will be exceeded by 15.9 percent of the measured periods.

RESULTS OF REGRESSION ANALYSIS

For each of the two categories of MRF buildings -- R/C and steel -- results are presented for the following regression analyses:

1. Unconstrained regression analysis to determine α and β.
2. Constrained regression analysis to determine α with the value of β from unconstrained regression analysis rounded-off to the nearest 0.05, e.g., $\beta = 0.92$ is rounded-off to 0.90, and $\beta = 0.63$ to 0.65.
3. Constrained regression analysis to determine α with β fixed at 0.75, the value in some current building codes (Eq. 1).
4. Constrained regression analysis to determine α with β fixed at 1.0, the value which corresponds to the alternative formula specified in NEHRP-94 (Eq. 2).

These regression analyses, implemented using the data from all buildings (Tables 1 and 2), lead to the formulas in Table 3 for R/C MRF buildings and in Table 4 for steel MRF buildings. In order to permit visual inspection, the formulas obtained from the second, third, and fourth regression analyses are presented in Figures 5 and 6 together with the measured period data. In order to preserve clarity in the plots, the formulas from the first regression, which are close to those from the second regression, are not included in these figures. The best-fit curves are labeled as T_R and the best-fit - 1σ curves as T_L.

R/C MRF Buildings

Figure 5 gives an impression of the scatter in the data of the measured periods relative to curves from regression analyses. As expected, the data fall above and below the curve, more or less evenly, and most of the data are above the best-fit - 1σ curve. Observe that, as expected,

constrained regression generally implies a larger standard error of estimate, s_e (Table 3), indicating greater scatter of the data about the best-fit curve; s_e increases as the value of β deviates increasingly from its unconstrained regression value. However, s_e is insensitive to β in the immediate vicinity of its unconstrained regression value, as evident from nearly identical values (up to three digits after the decimal point) of s_e from the first two regression analyses (Table 3). The value of s_e is significantly larger if $\beta = 0.75$ or 1.0, demonstrating that the period formula with either of these β values, as in present US codes, is less accurate. Thus the best choice is $\beta = 0.90$ with the associated $\alpha = 0.015$.

The values of α and β, determined from all available data, should be modified to recognize that the period of a R/C building lengthens at levels of motion large enough to cause cracking of concrete. The data from buildings experiencing $\ddot{u}_{go} \geq 0.15g$ are too few (Figure 2) to permit a reliable value of β from unconstrained regression analysis. Therefore, constrained regression analysis of these data with $\beta = 0.90$, determined from the full set of data, was conducted to obtain $\alpha_L = 0.016$ and $\alpha_U = 0.023$ leading to:

$$T_L = 0.016 H^{0.90} \tag{14}$$

and

$$T_U = 0.023 H^{0.90} \tag{15}$$

Eqs. (14) and (15) are plotted in Figure 7 together with the measured period data. As expected, very few data fall above the curve for T_U or below the curve for T_L. This indicates that Eq. (14) is suitable for estimating, conservatively, the fundamental period and Eq. (15) for limiting the

period computed from rational analysis. This period should not be longer than $1.4T_L$; the factor 1.4 is determined as the ratio 0.023/0.016, rounded-off to one digit after the decimal point.

Steel MRF Buildings

Figure 6 gives an impression of the scatter in the measured period data relative to the best-fit curve. As expected, the data fall above and below the curve, more or less evenly, and most of the data are above the best-fit - 1σ curve. Observe that values of s_e are almost identical for unconstrained regression and constrained regression with rounded-off value of β because this value is close to the regressed value (Table 4); however, s_e increases as the value of β deviates increasingly from its unconstrained regression value. It is larger if β = 0.75 or 1.0, demonstrating that the period formula with either of these β values, as in present US codes, is less accurate. Thus the best choice is β = 0.80 with the associated $\alpha_L = 0.028$ and $\alpha_U = 0.045$ leading to:

$$T_L = 0.028\,H^{0.80} \tag{16}$$

and

$$T_U = 0.045\,H^{0.80} \tag{17}$$

Eqs. (16) and (17) are plotted in Figure 8 together with the measured period data. As observed earlier for R/C buildings, Eq. (16) is suitable for estimating, conservatively, the fundamental period and Eq. (17) for limiting the period from rational analysis. The period from rational analysis should not be longer than $1.6T_L$; the factor 1.6 is determined as the ratio 0.045/0.028, rounded-off to one digit after the decimal point. The period formula (Eq. 16) and the factor 1.6, determined from all available data, also apply to strongly shaken buildings because, as observed earlier, the intensity of shaking has little influence on the period of steel MRF buildings, so long as there is no significant yielding of the structure.

Table 3. Results from regression analysis: R/C MRF buildings.

Regression Analysis Type	Period Formula		
	Best Fit	**Best-Fit - 1σ**	s_e
Unconstrained	$T_R = 0.017\,H^{0.92}$	$T_L = 0.014\,H^{0.92}$	0.209
Constrained with β = 0.90	$T_R = 0.018\,H^{0.90}$	$T_L = 0.015\,H^{0.90}$	0.209
Constrained with β = 0.75	$T_R = 0.038\,H^{0.75}$	$T_L = 0.030\,H^{0.75}$	0.229
Constrained with β = 1	$T_R = 0.011H$	$T_L = 0.009H$	0.214

Table 4. Results from regression analysis: steel MRF buildings.

Regression Analysis Type	Period Formula		
	Best-Fit	**Best-Fit - 1σ**	s_e
Unconstrained	$T_R = 0.035\,H^{0.805}$	$T_L = 0.027\,H^{0.805}$	0.233
Constrained with β = 0.80	$T_R = 0.035\,H^{0.80}$	$T_L = 0.028\,H^{0.80}$	0.233
Constrained with β = 0.75	$T_R = 0.046\,H^{0.75}$	$T_L = 0.036\,H^{0.75}$	0.237
Constrained with β = 1.0	$T_R = 0.013H$	$T_L = 0.009H$	0.277

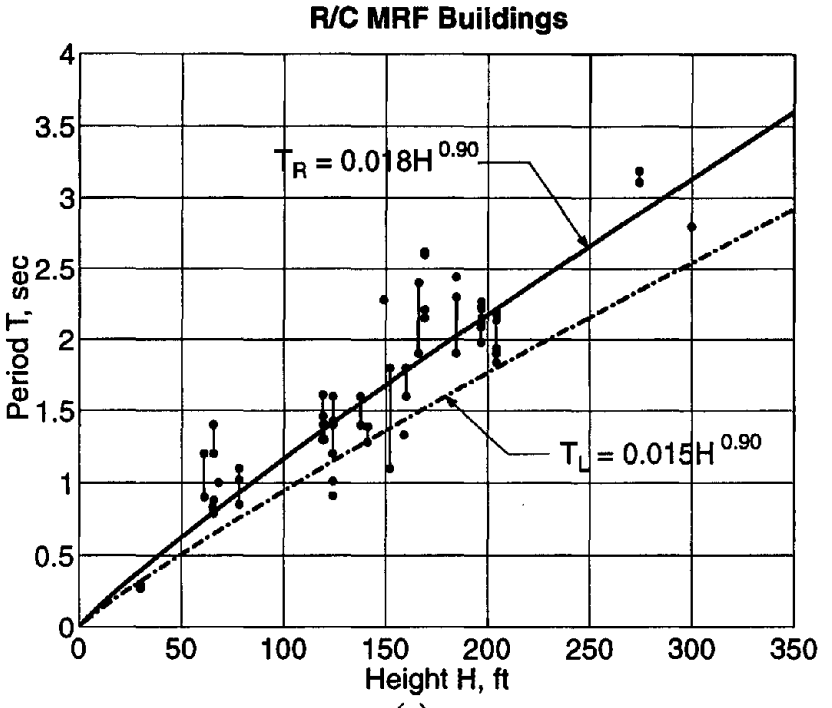

(a)

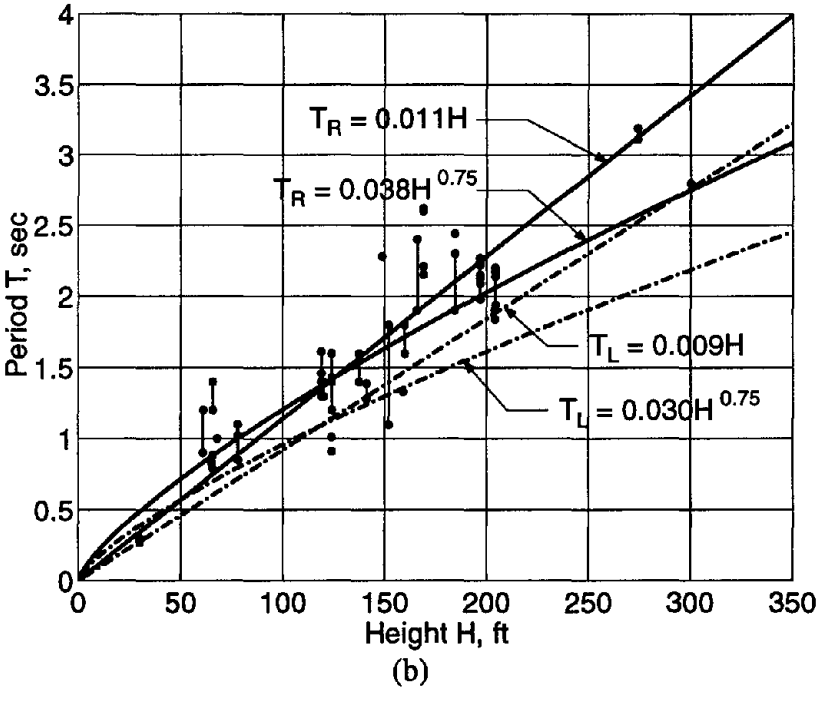

(b)

Figure 5. Regression analysis for R/C MRF buildings: (a) $\beta = 0.90$, and (b) $\beta = 0.75$ and 1.0.

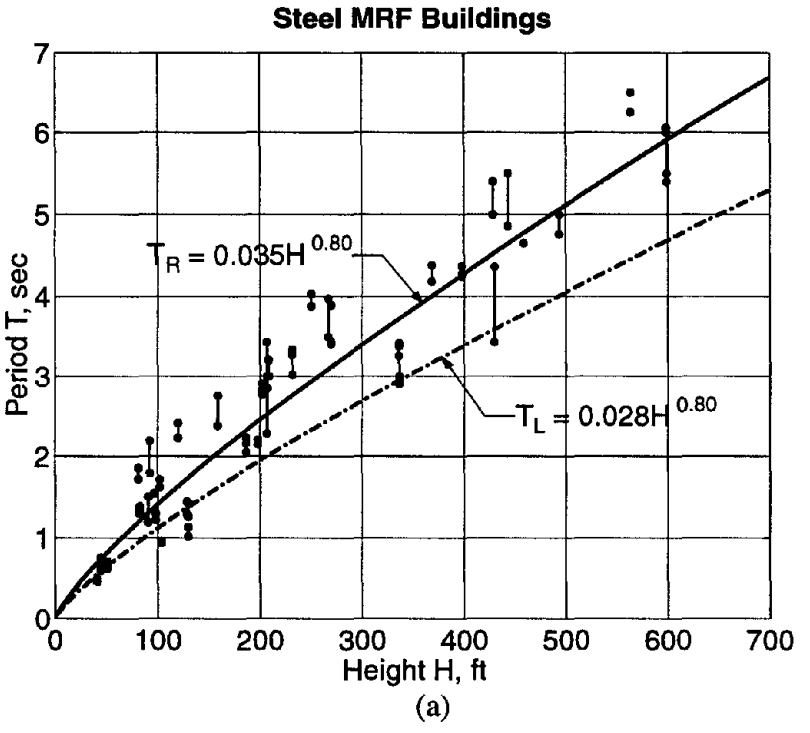

Figure 6. Regression analysis for steel MRF buildings: (a) $\beta = 0.80$, and (b) $\beta = 0.75$ and 1.0.

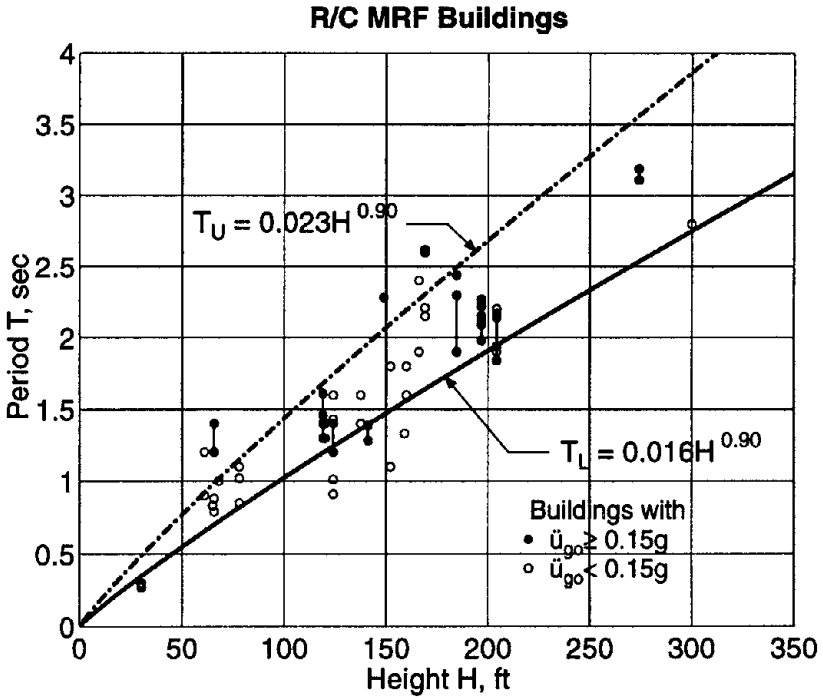

Figure 7. Recommended period formula and upper limit for the fundamental period of R/C MRF buildings.

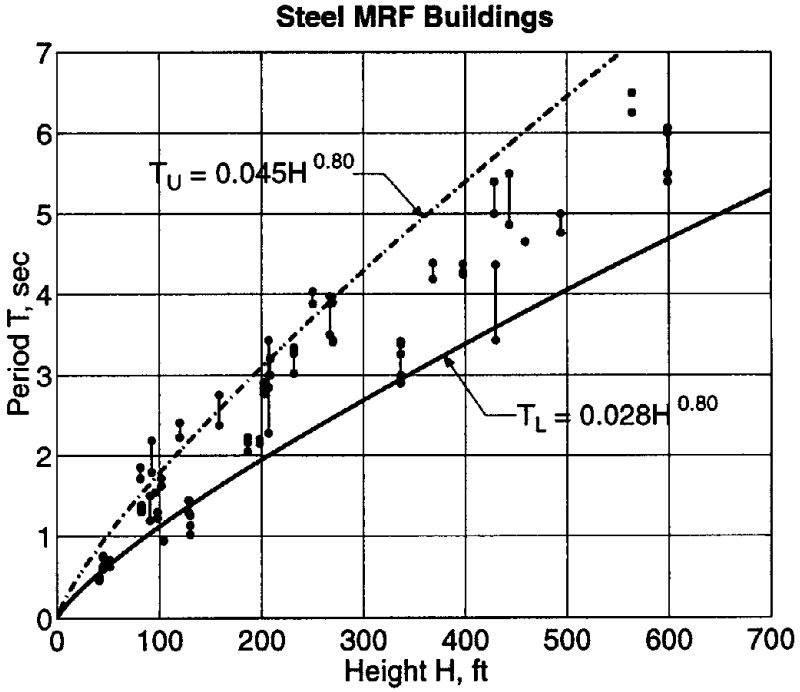

Figure 8. Recommended period formula and upper limit for the fundamental period of steel MRF buildings.

CONCLUSIONS AND RECOMMENDATIONS

Based on analysis of the available data for the fundamental vibration period of 27 R/C MRF buildings and 42 steel MRF buildings, measured from their motions recorded during earthquakes, Eqs. (14) and (16) are recommended for estimating, conservatively, the period of R/C and steel buildings, respectively. These formulas provide the "best" fit of Eq. (9) to the available data; the fit is better than possible with $\beta = 0.75$ or 1.0 in current US codes. Furthermore, the period from rational analysis should not be allowed to exceed the value from the recommended equations by a factor larger than 1.4 for R/C MRF buildings or 1.6 for steel MRF buildings. Since these recommendations are developed based on data from buildings in California, they should be applied with discretion to buildings in less seismic regions of the US or other parts of the world where building design practice is significantly different than in California.

Regression analyses that led to the recommended formulas should be repeated periodically on larger data sets. The database can be expanded by including buildings, other than those in Tables 1 and 2, whose motions recorded during past earthquakes have, so far, not been analyzed. Period data should also be developed for additional buildings when records of their motions during future earthquakes become available.

REFERENCES

Bertero, V. V., Bendimerad, F. M., and Shah, H. C. (1988). *Fundamental Period of Reinforced R/C Moment-Resisting Frame Structures*, Report No. 87, John A. Blume Earthquake Engineering Center, Stanford University, CA, October.

Chopra, A. K. (1995). *Dynamics of Structures: Theory and Applications to Earthquake Engineering*, Prentice Hall, Upper Saddle River, New Jersey.

Cole, E. E., Tokas, C. V. and Meehan, J. F. (1992). "Analysis of Recorded Building Data to Verify or Improve 1991 Uniform Building Code (UBC) Period of Vibration Formulas," *Proceedings of SMIP92*, Strong Motion Instrumentation Program, Division of Mines and Geology, California Department of Conservation, Sacramento, 6-1 - 6-12, May.

Hart, G. C. and Vasudevan, R. (1975). "Earthquake Design of Buildings: Damping," *Journal of the Structural Division*, ASCE, Vol. 101, No. ST1, 11-30, January.

Housner, G. W. and Brady, A. G. (1963). "Natural Periods of Vibration of Buildings," *Journal of Engineering Mechanics Division*, ASCE, Vol. 89, No. EM4, 31-65, August.

NEHRP Recommended Provisions for the Development of seismic Regulations for New Buildings. (1994). Building Seismic Safety Council, Washington, D. C.

Recommended Lateral Force Requirements and Tentative Commentary. (1988). Seismological Committee, Structural Engineers Association of California, San Francisco, CA.

Recommended Lateral Force Requirements and Commentary. (1996). Seismological Committee, Structural Engineers Association of California, San Francisco, CA.

Tentative Provisions for the Development of Seismic Regulations for Buildings. (1978). ATC3-06, Applied Technological Council, Palo Alto, CA.

Uniform Building Code. (1997). International Conference of Building Officials, Whittier, CA.

PART II:
SHEAR WALL BUILDINGS

INTRODUCTION

The fundamental vibration period of a building appears in the equation specified in building codes to calculate the design base shear and lateral forces. Because this building property can not be computed for a structure that is yet to be designed, building codes provide empirical formulas that depend on the building material (steel, R/C, etc.), building type (frame, shear wall etc.), and overall dimensions.

The empirical period formulas for concrete shear wall (SW) buildings in the 1997 UBC (*Uniform Building Code*, 1997) and the 1996 SEAOC bluebook (*Recommended Lateral Force Requirements*, 1996) were derived, by modifying the ATC3-06 formulas (*Tentative Provisions*, 1978), during development of the 1988 SEAOC bluebook to more accurately reflect the configuration and material properties of these systems (*Recommended Lateral Force Requirements*, 1988: Appendix 1E2b(1)-T). The period formulas in ATC3-06 (*Tentative Provisions*, 1978) are based largely on motions of buildings recorded during the 1971 San Fernando earthquake. However, motions of many more buildings recorded during recent earthquakes, including the 1989 Loma Prieta and 1994 Northridge earthquakes, are now available. These recorded motions provide an opportunity to expand greatly the existing database on the fundamental vibration periods of buildings. To this end, the natural vibration periods of twenty-one buildings have been measured by system identification methods applied to the motions of buildings recorded during the 1994 Northridge earthquake (Appendix A). These data have been combined with similar data from the motions of buildings recorded during the 1971 San Fernando, 1984 Morgan Hill, 1986 Mt. Lewis and Palm Springs, 1987 Whittier, 1989 Loma Prieta, 1990 Upland, and 1991 Sierra Madre earthquakes.

The objective of this investigation is to develop improved empirical formulas to estimate the fundamental vibration period of concrete SW buildings for use in equivalent lateral force analysis specified in building codes. Presented first is the expanded database for "measured" values of fundamental periods of SW buildings, against which the code formulas in present US codes are evaluated; similar work on limited data sets has appeared previously (e.g., Arias and Husid, 1962; Cole et al., 1992; Housner and Brady, 1963; Lee and Mau, 1997). It is shown that current code formulas for estimating the fundamental period of concrete SW buildings are grossly inadequate. Subsequently, an improved formula is developed by calibrating a theoretical formula, derived using Dunkerley's method, against the measured period data through regression analysis. Finally, a factor to limit the period calculated by a "rational" analysis, such as Rayleigh's method, is recommended.

PERIOD DATABASE

The data that are most useful but hard to come by are from structures shaken strongly but not deformed into the inelastic range. Such data are slow to accumulate because relatively few structures are installed with permanent accelerographs and earthquakes causing strong motions of these instrumented buildings are infrequent. Thus, it is very important to investigate comprehensively the recorded motions when they do become available, as during the 1994 Northridge earthquake. Unfortunately, this obviously important goal is not always accomplished, as indicated by the fact that the vibration properties of only a few of the buildings whose motions were recorded during post-1971 earthquakes have been determined.

Available data on the fundamental vibration period of buildings measured from their motions recorded during several California earthquakes have been collected (Appendix A). This database contains data for a total of 106 buildings, including twenty-one buildings that experienced peak ground acceleration, $\ddot{u}_{go} \geq 0.15g$ during the 1994 Northridge earthquake. The remaining data comes from motions of buildings recorded during the 1971 San Fernando earthquake and subsequent earthquakes (Cole et al., 1992; Gates et al., 1994; Hart et al., 1975; Hart and Vasudevan, 1975; Marshall et al., 1994; MacVerry, 1979; Werner et al., 1992).

Shown in Table 1 is the subset of this database pertaining to 16 concrete SW buildings (27 data points); buildings subjected to peak ground acceleration, $\ddot{u}_{go} \geq 0.15g$ are identified with an asterisk (*). "C" and "N" denote buildings instrumented by the California Strong Motion Instrumentation Program (CSMIP) and National Oceanic and Atmospheric Administration (NOAA); "ATC" denotes one of the buildings included in the ATC3-06 report (*Tentative Provisions*, 1978) for which the height and base dimensions were available from other sources, but these dimensions for other buildings could not be discerned from the plot presented in the

ATC3-06 report. The number of data points exceeds the number of buildings because the period of some buildings was determined from their motions recorded during more than one earthquake, or was reported by more than one investigator for the same earthquake.

Table 1. Period data for concrete SW buildings.

No.	Location	ID Number	No. of Stories	Height (ft)	Earthquake	Period T (sec)		Width (ft)	Length (ft)
						Longi-tudinal	Trans-verse		
1	Belmont	C58262	2	28.0	Loma Prieta	0.13	0.20	NA	NA
2*	Burbank	C24385	10	88.0	Northridge	0.60	0.56	75.0	215.0
3*	Burbank	C24385	10	88.0	Whittier	0.57	0.51	75.0	215.0
4	Hayward	C58488	4	50.0	Loma Prieta	0.15	0.22	NA	NA
5	Long Beach	C14311	5	71.0	Whittier	0.17	0.34	81.0	205.0
6	Los Angeles	ATC_3	12	159.0	San Fernando	1.15	MRF	60.0	161.0
7*	Los Angeles	C24468	8	127.0	Northridge	1.54	1.62	63.0	154.0
8*	Los Angeles	C24601	17	149.7	Northridge	1.18	1.05	80.0	227.0
9	Los Angeles	C24601	17	149.7	Sierra Madre	1.00	1.00	80.0	227.0
10*	Los Angeles	N253-5	12	161.5	San Fernando	1.19	1.14	76.0	156.0
11*	Los Angeles	N253-5	12	161.5	San Fernando	1.07	1.13	76.0	156.0
12	Palm Desert	C12284	4	50.2	Palm Springs	0.50	0.60	60.0	180.0
13	Pasadena	N264-5	10	142.0	Lytle Creek	0.71	0.52	69.0	75.0
14*	Pasadena	N264-5	10	142.0	San Fernando	0.98	0.62	69.0	75.0
15*	Pasadena	N264-5	10	142.0	San Fernando	0.97	0.62	69.0	75.0
16	Piedmont	C58334	3	36.0	Loma Prieta	0.18	0.18	NA	NA
17	Pleasant Hill	C58348	3	40.6	Loma Prieta	0.38	0.46	77.0	131.0
18	San Bruno	C58394	9	104.0	Loma Prieta	1.20	1.30	84.0	192.0
19	San Bruno	C58394	9	104.0	Loma Prieta	1.00	1.45	84.0	192.0
20	San Jose	C57355	10	124.0	Loma Prieta	MRF	0.75	82.0	190.0
21	San Jose	C57355	10	124.0	Morgan Hill	MRF	0.61	82.0	190.0
22	San Jose	C57355	10	124.0	Mount Lewis	MRF	0.61	82.0	190.0
23	San Jose	C57356	10	96.0	Loma Prieta	0.73	0.43	64.0	210.0
24	San Jose	C57356	10	96.0	Loma Prieta	0.70	0.42	64.0	210.0
25	San Jose	C57356	10	96.0	Morgan Hill	0.65	0.43	64.0	210.0
26	San Jose	C57356	10	96.0	Mount Lewis	0.63	0.41	64.0	210.0
27*	Watsonville	C47459	4	66.3	Loma Prieta	0.24	0.35	71.0	75.0

* Denotes buildings with $\ddot{u}_{go} \geq 0.15$g.

NA Indicates data not available.

MRF Implies moment-resisting frames form the lateral load resisting system.

Number followed by "C" or "N" indicates the station number, and by "ATC" indicates the building number in ATC3-06 report.

CODE FORMULAS

The empirical formula for fundamental vibration period of concrete SW buildings specified in current US building codes -- UBC-97 (*Uniform Building Code*, 1997), SEAOC-96 (*Recommended Lateral Force Requirements*, 1996), and NEHRP-94 (*NEHRP*, 1994) -- is of the form:

$$T = C_t H^{3/4} \tag{1}$$

where H is the height of the building in feet above the base and the numerical coefficient $C_t = 0.02$. UBC-97 and SEAOC-96 permit an alternative value for C_t to be calculated from:

$$C_t = 0.1/\sqrt{A_c} \tag{2}$$

where A_c, the combined effective area (in square feet) of the shear walls, is defined as:

$$A_c = \sum_{i=1}^{NW} A_i \left[0.2 + \left(D_i/H\right)^2\right]; \qquad D_i/H \le 0.9 \tag{3}$$

in which A_i is the horizontal cross-sectional area (in square feet) and D_i is dimension in the direction under consideration (in feet) of the *i*th shear wall in the first story of the structure; and NW is the total number of shear walls. The value of D_i/H in Eq. (3) should not exceed 0.9.

ATC3-06 (*Tentative Provisions*, 1978) and earlier versions of other US codes specify a different formula:

$$T = \frac{0.05H}{\sqrt{D}} \tag{4}$$

where D is the dimension, in feet, of the building at its base in the direction under consideration.

UBC-97 and SEAOC-96 codes specify that the design base shear should be calculated from:

$$V = CW \tag{5}$$

in which W is the total seismic dead load and C is the seismic coefficient defined as

$$C = \frac{C_v}{R}\frac{I}{T}; \quad 0.11 C_a I \le C \le \frac{2.5 C_a}{R} I \text{ and for seismic zone 4 } C \ge \frac{0.8 Z N_v I}{R} \tag{6}$$

in which coefficients C_v and C_a depend on the near-source factors, N_v and N_a, respectively, along with the soil profile and the seismic zone factor Z; I is the importance factor; and the R is the numerical coefficient representative of the inherent overstrength and global ductility capacity of the lateral-load resisting system. The upper limit of $2.5 C_a I \div R$ on C applies to very-short period buildings, whereas the lower limit of $0.11 C_a I$ (or $0.8 Z N_v I \div R$ for seismic zone 4) applies to very-long period buildings. These limits imply that C becomes independent of the period for very-short or very-tall buildings. The upper limit existed, although in slightly different form, in previous versions of UBC and SEAOC bluebook; the lower limit, however, appeared only recently in UBC-97 and SEAOC-96.

The fundamental period T, calculated using the empirical Eqs. (1) or (4), should be smaller than the "true" period to obtain a conservative estimate for the base shear. Therefore, code formulas are intentionally calibrated to underestimate the period by about 10 to 20 percent at first yield of the building (*Tentative Provisions*, 1978; *Recommended Lateral Force Requirements*, 1988).

The codes permit calculation of the period by established methods of mechanics (referred to as "rational" analyses in this investigation), such as Rayleigh's method or computer-based eigen-value analysis, but specify that the resulting value should not be longer than that estimated from the empirical formula (Eqs. 1 or 4) by a certain factor. The factors specified in various US codes are: 1.2 in ATC3-06; 1.3 for high seismic region (Zone 4) and 1.4 for other regions (Zones 3, 2, and 1) in UBC-97 and SEAOC-96; and a range of values with 1.2 for regions of high

seismicity to 1.7 for regions of very low seismicity in NEHRP-94. The restriction in SEAOC-88 that the base shear calculated using the "rational" period shall not be less than 80 percent of the value obtained by using the empirical period corresponds to a factor of 1.4 (Cole et al., 1992). These restrictions are imposed in order to safeguard against unreasonable assumptions in the "rational" analysis, which may lead to unreasonably long periods and hence unconservative values of base shear.

EVALUATION OF CODE FORMULAS

For buildings listed in Table 1, the fundamental period identified from their motions recorded during earthquakes (subsequently denoted as "measured" period) is compared with the values given by the code empirical formulas (Figures 1 to 3, part a). Also compared are the two values of the seismic coefficient for each building calculated according to Eq. (6) with $I = 1$ for standard occupancy structures; $R = 5.5$ for concrete shear walls; and $C_v = 0.64$ and $C_a = 0.44$ for seismic zone 4 with $Z = 0.4$, soil profile type S_D, i.e., stiff soil profile with average shear wave velocity between 180 and 360 m/s, and $N_v = N_a = 1$ (Figures 1 to 3, part b).

Code Formula: Eq. (1) With $C_t = 0.02$

For all buildings in Table 1, the periods and seismic coefficients are plotted against the building height in Figure 1. The measured periods in two orthogonal directions are shown by circles (solid for $\ddot{u}_{go} \geq 0.15g$, open for $\ddot{u}_{go} < 0.15g$) connected by a vertical line, whereas the code period is shown by a solid curve because the code formula gives the same period in the two directions if the lateral-force resisting systems are of the same type. Also included are the curves for $1.2T$ and $1.4T$ representing the limits imposed by codes on a "rational" value of the period for use in high seismic regions like California. The seismic coefficients (Eq. 6) corresponding to the measured periods in the two orthogonal directions are also shown by circles connected by a vertical line, whereas the value based on the code period is shown by a solid curve.

Figure 1 leads to the following observations. For a majority of buildings, the code formula gives a period longer than the measured value. In contrast, for concrete and steel moment-resisting frame buildings, the code formula almost always gives a period shorter than the measured value (Part I). The longer period from the code formula leads to seismic coefficient smaller than the value based on the measured period if the period falls outside the flat portion of

the seismic coefficient spectrum; otherwise the two periods lead to the same seismic coefficient. For most of the remaining buildings, the code formula gives a period much shorter than the measured value and seismic coefficient much larger than the value based on the measured period. Since the code period for many buildings is longer than the measured period, the limits of $1.2T$ or $1.4T$ for the period calculated from a "rational" analysis are obviously inappropriate.

The building height alone is not sufficient to estimate accurately the fundamental period of SW buildings because measured periods of buildings with similar heights can be very different, whereas they can be similar for buildings with very different heights. For example, in Table 1 the measured longitudinal periods of buildings 4 and 12 of nearly equal heights differ by a factor of more than three; the heights of these buildings are 50 ft and 50.2 ft whereas the periods are 0.15 sec and 0.50 sec, respectively. On the other hand, measured longitudinal periods of buildings 13 and 23 are close even though building 13 is 50% taller than building 23; periods of these buildings are 0.71 sec and 0.73 sec, whereas the heights are 142 ft and 96 ft, respectively. The poor correlation between the building height and the measured period is also apparent from the significant scatter of the measured period data (Figure 1a).

Alternate Code Formula: Eq. (1) With C_t From Eqs. (2) and (3)

Table 2 lists a subset of nine buildings (17 data points) with their A_c values calculated from Eq. (3) using shear wall dimensions obtained from structural drawings; for details see Appendix H. These dimensions were not available for the remaining seven buildings in Table 1.

In Figure 2 the alternate code formula for estimating the fundamental period is compared with the measured periods of the nine buildings. The code period is determined from Eqs. (1) to (3) using the calculated value of A_c and plotted against $H^{3/4} \div \sqrt{A_c}$. This comparison shows that

the alternate code formula almost always gives a value for the period that is much shorter than the measured periods, and a value for the seismic coefficient that is much higher than from the measured periods. The measured periods of most buildings are longer than the code imposed limits of $1.2T$ and $1.4T$ on the period computed from a "rational" analysis. Although the code period formula gives a conservative value for the seismic coefficient, the degree of conservatism seems excessive for most buildings considered in this investigation.

Table 2. Measured periods and areas of selected concrete SW buildings.

No.	ID No.	Height (ft)	Measured Period		A_c (Sq. ft)		$\overline{A}_e$ (%)	
			Longi-tudinal	Trans-verse	Longi-tudinal	Trans-verse	Longi-tudinal	Trans-verse
1*	C24385	88.0	0.60	0.56	83.5	92.1	0.1642	0.1677
2*	C24385	88.0	0.57	0.51	83.5	92.1	0.1642	0.1677
3*	C24468	127.0	1.54	1.62	13.8	34.2	0.0265	0.0345
4*	C24601	149.7	1.18	1.05	63.3	106.9	0.0635	0.0939
5	C24601	149.7	1.00	1.00	63.3	106.9	0.0635	0.0939
6	C12284	50.2	0.50	0.60	21.5	17.7	0.0537	0.0550
7	C58334	36.0	0.18	0.18	26.2	26.2	0.1311	0.1311
8	C58348	40.6	0.38	0.46	26.6	12.2	0.1118	0.0501
9	C58394	104.0	1.20	1.30	21.5	22.2	0.0330	0.0189
10	C58394	104.0	1.00	1.45	21.5	22.2	0.0330	0.0189
11	C57355	124.0	MRF	0.75	MRF	104.5	MRF	0.2751
12	C57355	124.0	MRF	0.61	MRF	104.5	MRF	0.2751
13	C57355	124.0	MRF	0.61	MRF	104.5	MRF	0.2751
14	C57356	96.0	0.73	0.43	60.7	84.5	0.1280	0.1547
15	C57356	96.0	0.70	0.42	60.7	84.5	0.1280	0.1547
16	C57356	96.0	0.65	0.43	60.7	84.5	0.1280	0.1547
17	C57356	96.0	0.63	0.41	60.7	84.5	0.1280	0.1547

* Denotes buildings with $\ddot{u}_{go} \geq 0.15$g.

MRF Implies moment-resisting frames form the lateral load resisting system.
Number followed by "C" indicates the station number.

ATC3-06 Formula

In Figure 3, the ATC3-06 formula for estimating the fundamental period is compared with the measured periods of all buildings listed in Table 1. The code period is determined from Eq. (4) using the H and D dimensions of the building (Table 1) and plotted against $H \div \sqrt{D}$. This comparison demonstrates that Eq. (4) significantly underestimates the period and

considerably overestimates the seismic coefficient for many buildings and the ATC3-06 imposed limit of $1.2T$ is too restrictive.

The ratio $H \div \sqrt{D}$ is not sufficient to estimate accurately the fundamental period of concrete SW buildings because measured periods of buildings with similar values of this ratio can be very different, whereas they can be similar for buildings with very different values of $H \div \sqrt{D}$. For example, in Table 1 the measured transverse period of building 18 and measured longitudinal period of building 27 -- two buildings with similar values of $H \div \sqrt{D}$ -- differ by nearly a factor of five; $H \div \sqrt{D}$ = 7.51 and 7.87, and measured periods = 1.30 sec and 0.24 sec, respectively. On the other hand, the measured longitudinal and transverse periods of building 9 are the same, equal to 1 sec, even though the values of $H \div \sqrt{D}$ in the two directions are 16.7 and 9.93. The poor correlation between the ratio $H \div \sqrt{D}$ and the measured periods is also apparent from a large scatter of the measured period data (Figure 3a).

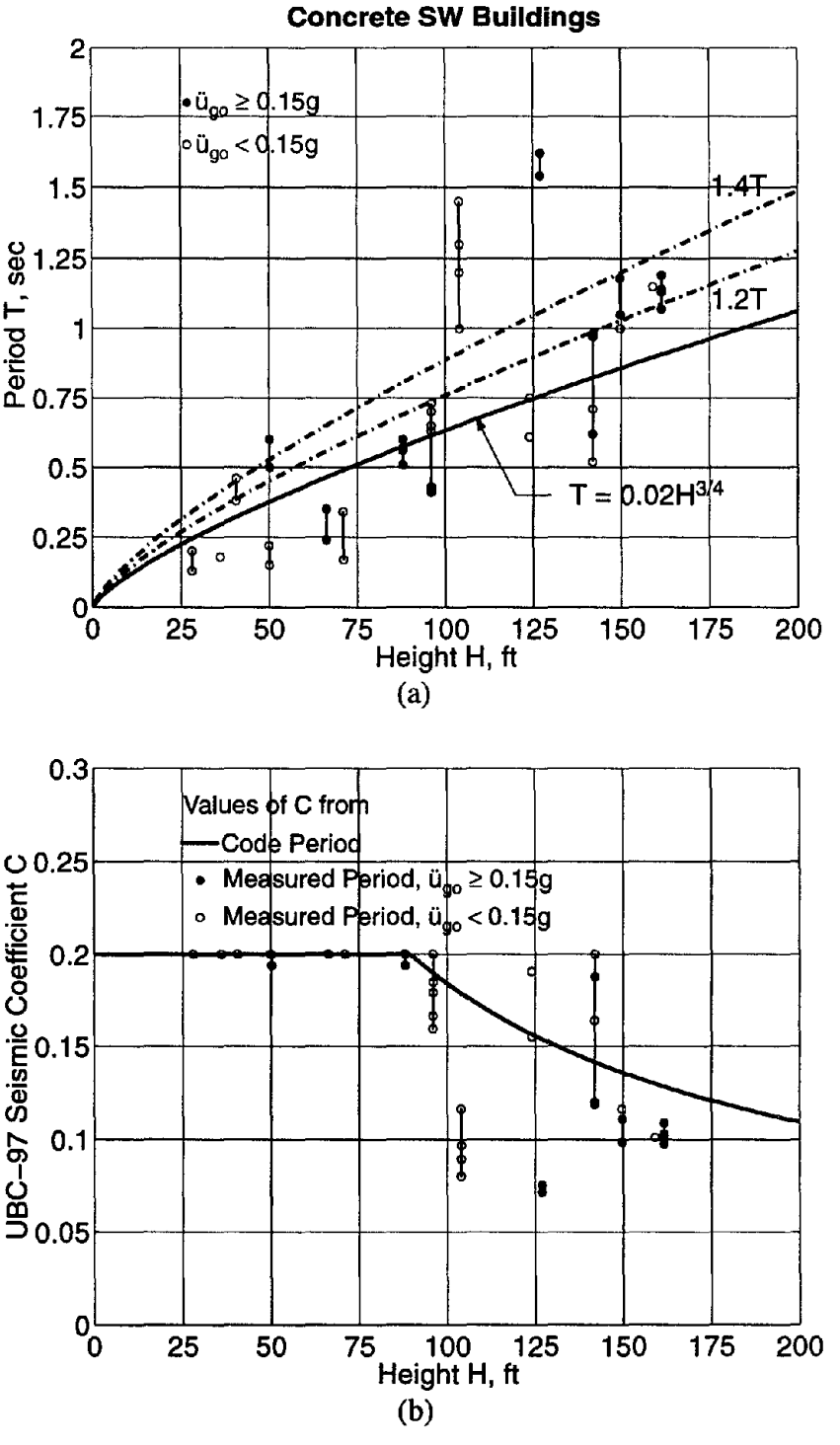

Figure 1. Comparison of (a) measured and code periods, and (b) UBC-97 seismic coefficients from measured and code periods.

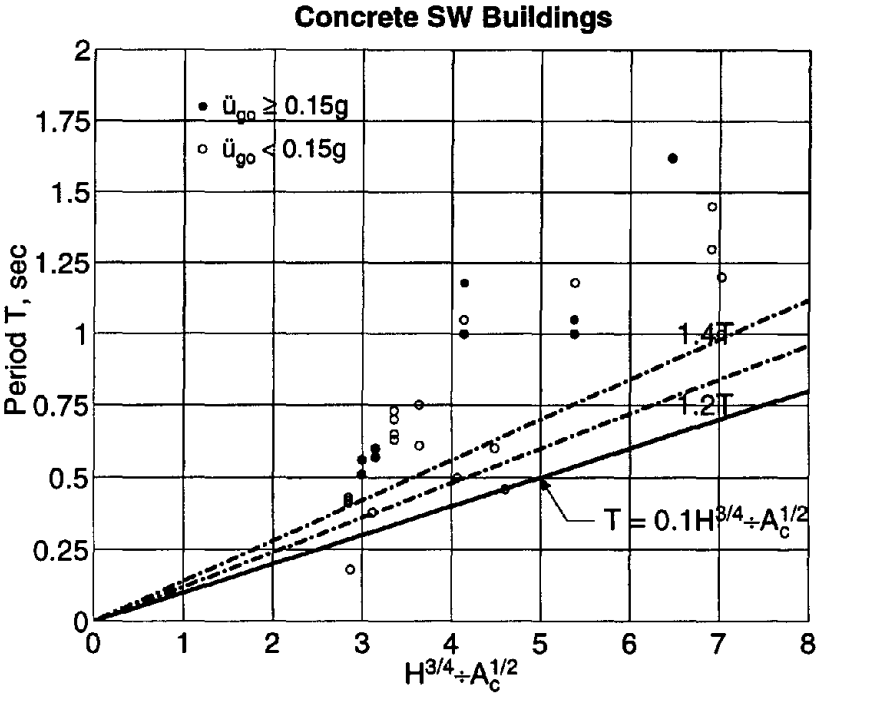

(a)

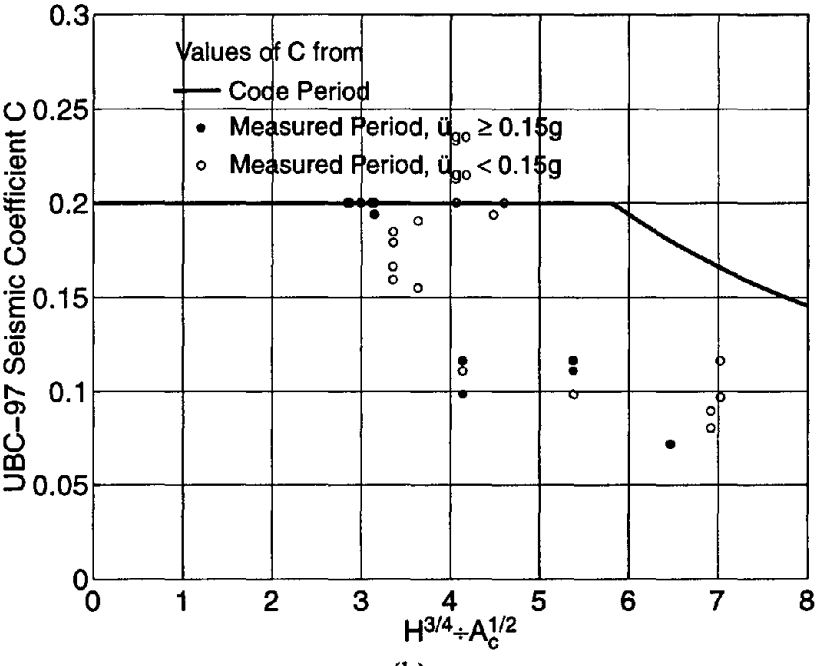

(b)

Figure 2. Comparison of (a) measured and code periods, and (b) UBC-97 seismic coefficients from measured and code periods; code periods are calculated from the alternate formula.

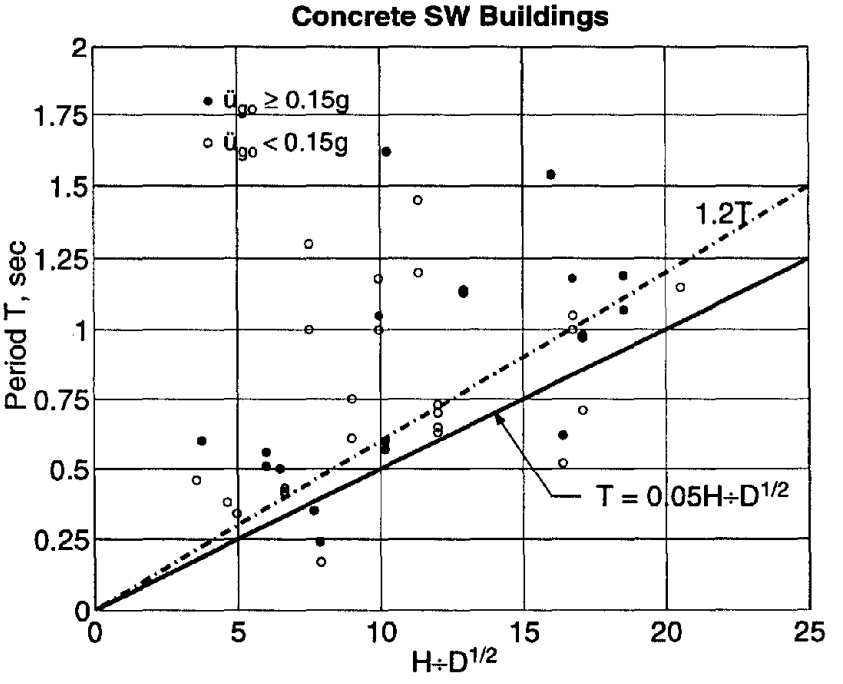

(a)

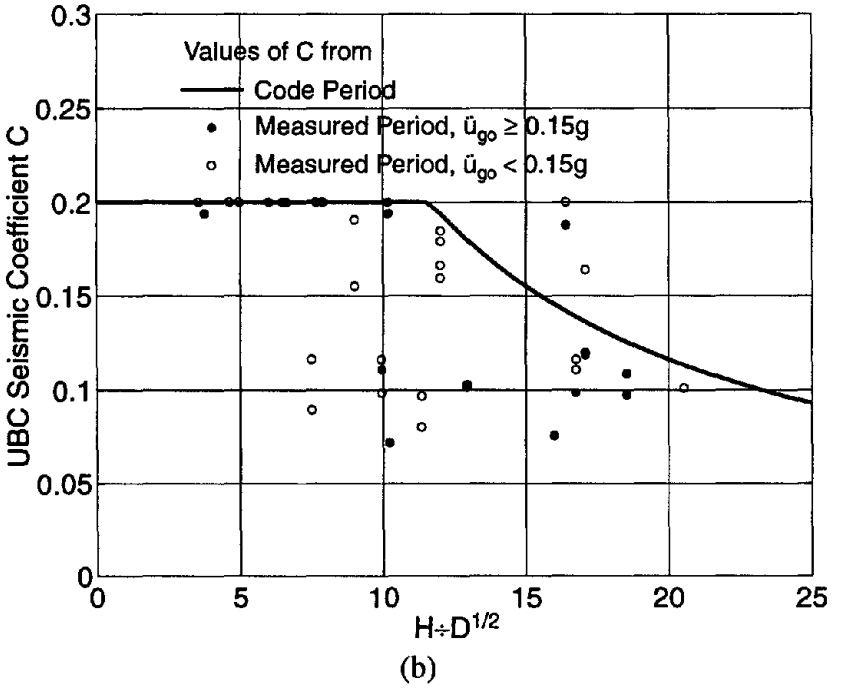

(b)

Figure 3. Comparison of (a) measured and code periods, and (b) UBC-97 seismic coefficients from measured and code periods; code periods are calculated from the ATC3-06 formula.

THEORETICAL FORMULAS

The observations in the preceding section clearly indicate that the current code formulas for estimating the fundamental period of concrete SW buildings are grossly inadequate. For this purpose, equations for the fundamental period are derived using established analytical procedures. Based on Dunkerley's method (Jacobsen and Ayre, 1958: pages 119-120 and 502-505; Inman, 1996: pages 442-449; Veletsos and Yang, 1977), the fundamental period of a cantilever, considering flexural and shear deformations, is:

$$T = \sqrt{T_F^2 + T_S^2} \tag{7}$$

in which T_F and T_S are the fundamental periods of pure-flexural and pure-shear cantilevers, respectively. For uniform cantilevers T_F and T_S are given by (Chopra, 1995: page 592; Timoshenko et al., 1974: pages 424-431; Jacobsen and Ayre, 1958: pages 471-496):

$$T_F = \frac{2\pi}{3.516}\sqrt{\frac{m}{EI}}H^2 \tag{8}$$

$$T_S = 4\sqrt{\frac{m}{\kappa G}}\frac{1}{\sqrt{A}}H \tag{9}$$

In Eqs. (8) and (9), m is the mass per unit height, E is the modulus of elasticity, G is the shear modulus, I is the section moment of inertia, A is the section area, and κ is the shape factor to account for nonuniform distribution of shear stresses (= 5/6 for rectangular sections). Combining Eqs. (7) to (9) and recognizing that $G = E \div 2(1+\mu)$, where the Poison's ratio $\mu = 0.2$ for concrete, leads to:

$$T = 4\sqrt{\frac{m}{\kappa G}}\frac{1}{\sqrt{A_e}}H \tag{10}$$

with

$$A_e = \frac{A}{\left[1 + 0.83\left(\frac{H}{D}\right)^2\right]} \tag{11}$$

where D is the plan dimension of the cantilever in the direction under consideration. Comparing Eqs. (10) and (11) with Eq. (9) reveals that the fundamental period of a cantilever considering flexural and shear deformations may be computed by replacing the area A in Eq. (9) with the equivalent shear area A_e given by Eq. (11).

The period T from Eq. (10) normalized by T_F is plotted in Figure 4 against the ratio $H \div D$ on a logarithmic scale. Also shown is the period of a pure-shear cantilever and of a pure-flexural cantilever. Eq. (10) approaches the period of a pure-shear cantilever (Eq. 9) as $H \div D$ becomes small and the period of a pure-flexural cantilever (Eq. 8) for large values of $H \div D$. For all practical purposes, the contribution of flexure can be neglected for shear walls with $H \div D < 0.2$ whereas the contribution of shear can be neglected for shear walls with $H \div D > 5$; the resulting error is less than 2%. However, both shear and flexural deformations should be included for shear walls with $0.2 \leq H \div D \leq 5$.

Equation (10), based on Dunkerley's method, provides a highly accurate value for the true fundamental period of a shear-flexural cantilever. This can be demonstrated by recognizing that the exact period is bounded by the periods obtained from Dunkerley's and Rayleigh's methods; Dunkerley's method gives a period longer than the exact value (Jacobsen and Ayre, 1958: pages 113-120; Inman, 1996: pages 442-449), whereas Rayleigh's method provides a shorter period

(Chopra, 1995: page 554). Also shown in Figure 4 is the period determined by Rayleigh's method using the deflected shape due to lateral forces varying linearly with height, considering both shear and flexural deformations; details are available in Appendix G. The resulting period is very close to that obtained from Eq. (10), derived using Dunkerley's method; the difference between the two periods is no more than 3%. Since the exact period lies between the two approximate values, Eq. (10) errs by less than 3%.

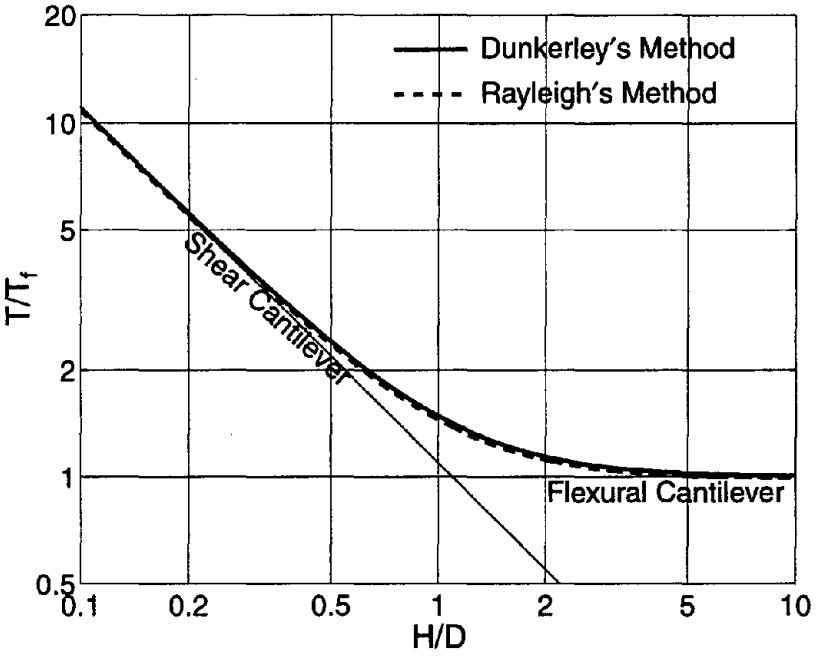

Figure 4. Fundamental period of cantilever beams.

Now consider a class of symmetric-plan buildings -- symmetric in the lateral direction considered -- with lateral-force resisting system comprised of a number of uncoupled (i.e., without coupling beams) shear walls connected through rigid floor diaphragms. Assuming that the stiffness properties of each wall are uniform over its height, the equivalent shear area, A_e, is given by a generalized version of Eq. (11) (details are available in Appendix G):

$$A_e = \sum_{i=1}^{NW}\left(\frac{H}{H_i}\right)^2 \frac{A_i}{\left[1+0.83\left(\frac{H_i}{D_i}\right)^2\right]} \tag{12}$$

where A_i, H_i, and D_i are the area, height, and dimension in the direction under consideration of the *i*th shear wall, and NW is the number of shear walls. With A_e so defined, Eq. (10) is valid for a system of shear walls of different height.

Equation (10) is now expressed in a form convenient for buildings:

$$T = 40\sqrt{\frac{\rho}{\kappa G}}\frac{1}{\sqrt{\bar{A}_e}}H \tag{13}$$

where ρ is the average mass density, defined as the total building mass (= mH) divided by the total building volume (= $A_B H$ -- A_B is the building plan area), i.e., $\rho = m/A_B$; and $\bar{A}_e$ is the equivalent shear area expressed as a percentage of A_B, i.e.,

$$\bar{A}_e = 100\frac{A_e}{A_B} \tag{14}$$

Equation (13) applies only to those buildings in which lateral load resistance is provided by uncoupled shear walls. Theoretical formulas for the fundamental period of buildings with coupled shear walls are available in Rutenberg (1975), and for buildings with a combination of shear walls and moment-resisting frames in Heiderbrecht and Stafford-Smith (1973) and Stafford-Smith and Crowe (1986). It seems that these formulas can not be simplified to the form of Eq. (13).

Sozen (1989) and Wallace and Moehle (1992) also presented a formula for the fundamental vibration period of SW buildings. Their formula was developed based on pure-flexural cantilever idealization of SW buildings and ignored the influence of shear deformations. Furthermore, the numerical constant in their formula was determined based on assumed material

properties and effective member stiffness equal to half its initial value. In contrast, the formula developed in this investigation (Eq. 13) includes both flexural and shear deformations and the numerical constant is determined directly from regression analysis of measured period data as described in the following sections.

REGRESSION ANALYSIS METHOD

Although $\overline{C} = 40\sqrt{\rho/\kappa G}$ in Eq. (13) can be calculated from building properties, it is determined from regression analysis to account for variations in properties among various buildings and for differences between building behavior and its idealization. For this purpose, it is useful to write Eq. (13) as:

$$T = \overline{C}\frac{1}{\sqrt{\overline{A}_e}}H \tag{15}$$

and recast it as:

$$y = a + x \tag{16}$$

in which $y = log(T)$, $a = \log(\overline{C})$, and $x = \log(H \div \sqrt{\overline{A}_e})$. The intercept a at $x = 0$ of the straight line in Eq. (16) was determined by minimizing the squared error between the measured and computed periods, and then $\overline{C}$ was back-calculated from the relationship $a = \log(\overline{C})$. The standard error of estimate is:

$$s_e = \sqrt{\frac{\sum_{i=1}^{n}\left[y_i - (a + x_i)\right]^2}{(n-2)}} \tag{17}$$

in which $y_i = \log(T_i)$ is the observed value (with T_i = measured period) and $(a + x_i) = \log(\overline{C}) + \log\left(\left(H \div \sqrt{\overline{A}_e}\right)\right)$ is the computed value of the ith data, and n is the total number of data points. The s_e represents scatter in the data and approaches, for large n, the standard deviation of the measured period data from the best-fit equation.

This procedure leads to the value of $\overline{C}_R$ for Eq. (15) to represent the best-fit, in the least squared sense, to the measured period data. However, for code applications the formula should

provide a lower value of the period and this was obtained by lowering the best-fit line (Eq. 16) by s_e without changing its slope. Thus $\overline{C}_L$, the lower value of $\overline{C}$, is computed from:

$$\log(\overline{C}_L) = \log(\overline{C}_R) - s_e \tag{18}$$

Since s_e approaches the standard deviation for large number of samples and y is log-normal, $\overline{C}_L$ is the mean-minus-one-standard-deviation or 15.9 percentile value, implying that 15.9 percent of the measured periods would fall below the curve corresponding to $\overline{C}_L$ (subsequently referred to as the best-fit – 1σ curve). If desired, $\overline{C}_L$ corresponding to other non-exceedance probabilities may be selected. Additional details of the regression analysis method and the procedure to estimate $\overline{C}_L$ are available in Appendix F.

As mentioned previously, codes also specify an upper limit on the period calculated by a "rational" analysis. This limit is established in this investigation by raising the best-fit line (Eq. 16) by s_e without changing its slope. Thus $\overline{C}_U$, the upper value of $\overline{C}$ corresponding to the upper limit, is computed from:

$$\log(\overline{C}_U) = \log(\overline{C}_R) + s_e \tag{19}$$

Eq. (15) with $\overline{C}_U$ represents the best-fit + 1σ curve which will be exceeded by 15.9 percent of the measured periods.

Regression analysis in the log-log space (Eq. 16) is preferred over the direct regression on Eq. (15) because it permits convenient development of the best-fit – 1σ and best-fit + 1σ curves; both regression analyses give essentially identical values of $\overline{C}_R$.

RESULTS OF REGRESSION ANALYSIS

The formula for estimating the fundamental period of concrete SW buildings was obtained by calibrating the theoretical formula of Eq. (15) by regression analysis of the measured period data for nine concrete SW buildings (17 data points) listed in Table 2. For each building, the equivalent area $\overline{A}_e$ was calculated from Eqs. (12) and (14) using dimensions from structural plans (Appendix H); for shear walls with dimensions varying over height, A_i and D_i were taken as the values at the base. Regression analysis gives $\overline{C}_R = 0.0023$ and $\overline{C}_L = 0.0018$. Using these values for $\overline{C}$ in Eq. (15) give T_R and T_L, the best-fit and best-fit – 1σ values of the period, respectively.

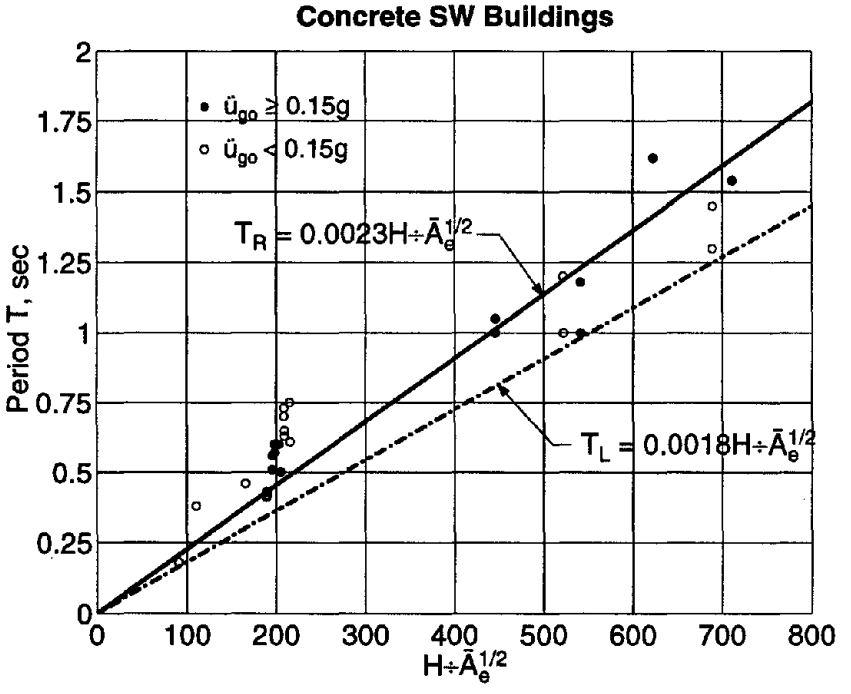

Figure 5. Results of regression analysis: all buildings.

These period values are plotted against $H \div \sqrt{\overline{A}_e}$ in Figure 5, together with the measured periods shown in circles; the measured periods of a building in the two orthogonal directions are

not joined by a vertical line because the ratio $H \div \sqrt{\overline{A}_e}$ is different if the shear wall areas are not the same in the two directions. Figure 5 permits the following observations. As expected the measured period data falls above and below (more or less evenly) the best-fit curve. The best-fit equation correlates with measured periods much better (error of estimate $s_e = 0.143$) than formulas (Eqs. 1 to 3) in UBC-97 ($s_e = 0.546$). It is apparent that the form of Eq. (15) includes many of the important parameters that influence the fundamental period of concrete SW buildings.

In passing, observe that the value of $\overline{C}_R = 0.0023$ for concrete buildings with E = 3.1×10^6 psi (21.4×10^3 MPa) and $\mu = 0.2$ corresponds to $\rho \approx 0.47$ lb-sec^2/ft^4 = 240 Kg/m^3 or unit weight = 15 pcf, implying approximately 10% solids and 90% voids in the building, which seem reasonable for many buildings.

The values of $\overline{C}$ determined from all available data, should be modified to recognize that the period of a concrete building lengthens at moderate to high levels of ground shaking. Regression analysis of the data from buildings experiencing peak ground acceleration $\ddot{u}_{go} \geq 0.15g$ (denoted with * in Table 2) gives:

$$T_L = 0.0019 \frac{1}{\sqrt{\overline{A}_e}} H \tag{20}$$

$$T_U = 0.0026 \frac{1}{\sqrt{\overline{A}_e}} H \tag{21}$$

Eqs. (20) and (21) are plotted in Figure 6 with the measured period data. As expected, very few data fall above the curve for T_U or below the curve for T_L, indicating that Eq. (20) is suitable for estimating, conservatively, the fundamental periods and Eq. (21) for limiting the period computed from "rational" analysis. Thus the period from "rational" analysis should not be

longer than $1.4T_L$; the factor is determined as the ratio 0.0026÷0.0019, rounded-off to one digit after the decimal point.

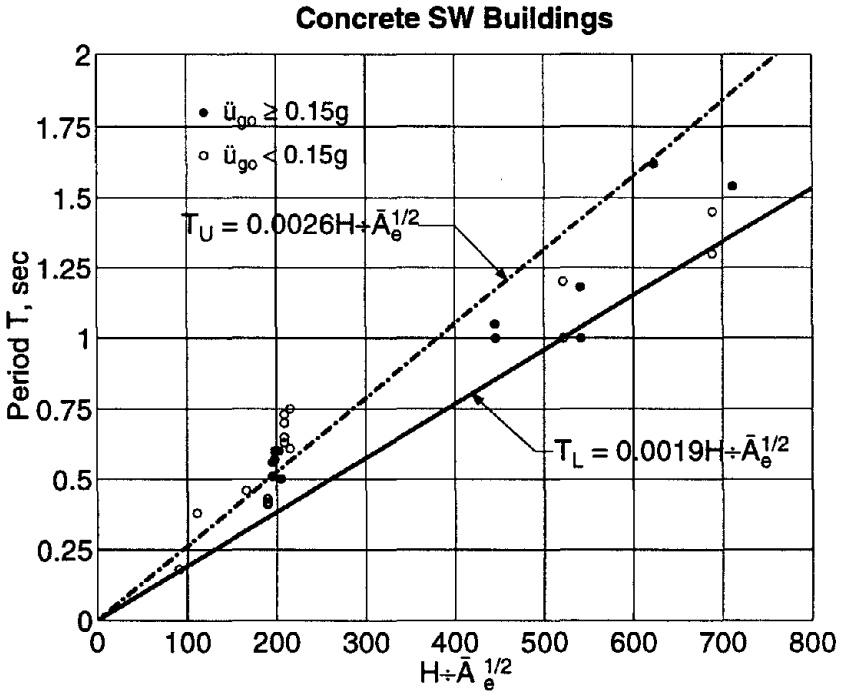

Figure 6. Results of regression analysis: buildings with $\ddot{u}_{go} \geq 0.15$g.

In using Eq. (12) to calculate A_e for nonuniform shear walls, A_i and D_i should be defined as the area and the dimension in the direction under consideration, respectively, at the base of the wall. To provide support for this recommendation, consider the building identified as C57356 in Table 2. The thickness of the shear walls in this ten-story building is 11 inch (30 cm) in the first story, 9 inch (23 cm) in second to fourth stories, 8 inch (20 cm) in fifth to eighth stories, and 7 inch (18 cm) in ninth and tenth stories. Calculating $\overline{A}_e$ by using D_i = 11 inch (at the base), 8 inch (at mid height) and 7 inch (at the roof), and substituting in Eq. (20) gives period values 0.36 sec, 0.42 sec, and 0.45 sec, respectively. Although the mid-height-value of D_i gives the period value close to the "measured" period (0.41 to 0.43 sec, by different investigators), the base value of D_i provides a shorter period, leading to a conservative value of base shear. This

recommendation is consistent with the current codes (*Uniform Building Code*, 1997; *Recommended Lateral Force Requirements*, 1996).

CONCLUSIONS AND RECOMMENDATIONS

Based on the analysis of the available data for the fundamental vibration period of nine concrete SW buildings (17 data points), measured from their motions recorded during earthquakes, Eq. (20) with $\overline{A}_e$ calculated from Eqs. (12) and (14) using wall dimensions at the base is recommended for conservatively estimating the fundamental period of concrete SW buildings. This formula provides the "best" fit of Eq. (15) to the available data; the fit is better than possible from formulas (Eqs. 1 to 3) in current US codes. Furthermore, the period from "rational" analysis should not be allowed to exceed the value from the recommended equation by a factor larger than 1.4. Since these recommendations are developed based on data from buildings in California, they should be applied with discretion to buildings in less seismic regions of the US or other parts of the world where building design practice is significantly different than in California.

Regression analyses that led to the recommended formulas should be repeated periodically on larger data sets. The database can be expanded by including buildings, other than those in Tables 1 and 2, whose motions recorded during past earthquakes have, so far, not been analyzed. Period data should also be developed for additional buildings when records of their motions during future earthquakes become available.

REFERENCES

Arias, A. and Husid, R. (1962). "Empirical Formula for the Computation of Natural Periods of Reinforced Concrete Buildings with Shear Walls," Reinsta del IDIEM, 39(3).

Chopra, A. K. (1995). *Dynamics of Structures: Theory and Applications to Earthquake Engineering*, Prentice Hall, Englewood Cliffs, N.J.

Cole, E. E., Tokas, C. V. and Meehan, J. F. (1992). "Analysis of Recorded Building Data to Verify or Improve 1991 Uniform Building Code (UBC) Period of Vibration Formulas," *Proceedings of SMIP92*, Strong Motion Instrumentation Program, Division of Mines and Geology, California Department of Conservation, Sacramento, 6-1 - 6-12.

Gates, W. E., Hart, G. C., Gupta, S. and Srinivasan, M. (1994). "Evaluation of Overturning Forces of Shear Wall Buildings," *Proceedings of SMIP94*, Strong Motion Instrumentation Program, Division of Mines and Geology, California Department of Conservation, Sacramento, 105-120.

Hart, G. C. and Vasudevan, R. (1975). "Earthquake Design of Buildings: Damping," *Journal of the Structural Division*, ASCE, 101(ST1), 11-30.

Hart, G. C., DiJulio, R. M. and Lew, M. (1975). "Torsional Response of High-Rise Buildings," *Journal of the Structural Division*, ASCE, 101(ST2), 397-416.

Heidebrecht, A. C. and Stafford-Smith, B. (1973). "Approximate Analysis of Tall Wall-Frame Structures," *Journal of Structural Division*, ASCE, 99(ST2), 199-221.

Housner, G. W. and Brady, A. G. (1963). "Natural Periods of Vibration of Buildings," *Journal of Engineering Mechanics Division*, ASCE, 89(EM4), 31-65.

Inman, D. J. (1996). *Engineering Vibrations*, Prentice Hall, Englewood Cliffs, New Jersey.

Jacobsen, L. S. and Ayre, R. S. (1958). *Engineering Vibrations*, McGraw-Hill, New York.

Li, Y. and Mau, S. T. (1997). "Learning from Recorded Earthquake Motion of Buildings," *Journal of Structural Engineering*, ASCE, 123(1), 62-69.

Marshall, R. D., Phan, L. T. and Celebi, M. (1994). "Full-Scale Measurement of Building Response to Ambient Vibration and the Loma Prieta Earthquake," *Proceedings of Fifth U. S. National Conference of Earthquake Engineering*, Vol. II, 661-670.

McVerry, G. H. (1979). *Frequency Domain Identification of Structural Models from Earthquake Records*, Report No. EERL 79-02, Earthquake Engineering research Laboratory, California Institute of Technology, Pasadena, CA, October.

NEHRP Recommended Provisions for the Development of seismic Regulations for New Buildings. (1994). Building Seismic Safety Council, Washington, D. C.

Recommended Lateral Force Requirements and Commentary. (1988). Seismological Committee, Structural Engineers Association of California, San Francisco, CA.

Recommended Lateral Force Requirements and Commentary. (1996). Seismological Committee, Structural Engineers Association of California, San Francisco, CA.

Rutenberg, A. (1975). "Approximate Natural Frequencies for Coupled Shear Walls," *Journal of Earthquake Engineering and Structural Dynamics*, 4(1), 95-100.

Sozen, M. A. (1989). "Earthquake Response of Buildings with Robust Walls," *Proceedings of the Fifth Chilean Conference on Seismology and Earthquake Engineering*, Association Chilean de Sismologia e Ingenieria Antisismica, Santiago, Chile.

Stafford-Smith, B. and Crowe, E. (1986). "Estimating Periods of Vibration of Tall Buildings," *Journal of Structural Engineering*, ASCE, 112(5), 1005-1019.

Tentative Provisions for the Development of Seismic Regulations for Buildings. (1978). ATC3-06, Applied Technological Council, Palo Alto, CA.

Timoshenko, S., Young, D. H., and Weaver, W. Jr. (1974). *Vibration Problems in Engineering*, Wiley, New York.

Uniform Building Code. (1997). International Conference of Building Officials, Whittier, CA.

Veletsos, A. S. and Yang, J. Y. (1977). "Earthquake Response of Liquid Storage Tanks," *Advances in Civil Engineering Through Engineering Mechanics*, Proceedings of the Engineering Mechanics Division Specialty Conference, Rayleigh, North Carolina, 1-24.

Wallace, J. W. and Moehle, J. P. (1992). "Ductility and Detailing Requirements of Bearing Wall Buildings," *Journal of Structural Engineering*, ASCE, 118(6), 1625-1643.

Werner, S. D., Nisar, A. and Beck, J. L. (1992). *Assessment of UBC Seismic Design Provisions Using Recorded Building Motion from the Morgan Hill, Mount Lewis, and Loma Prieta Earthquakes*, Dames and Moor, Oakland, CA, April.

PART III:
APPENDICES

APPENDIX A: DATABASE

The vibration periods and modal damping ratios of about twenty-five buildings have been identified from their recorded motions during the Northridge earthquake using system identification techniques. These results are combined with similar data available from the 1971 San Fernando earthquake and other recent earthquakes to form a comprehensive set of data. This data set includes the period and damping values along with information on other factors that could influence these vibration properties. These data are compiled on an electronic database that can be easily updated after every major earthquake. This appendix describes the information included in the database followed by the procedures to update the database and to extract the relevant information for further evaluation.

Database Format

A master database containing information on the vibration properties and other relevant information is compiled using Microsoft Access 2.0, a commercially-available database management software package. Contents of this database are arranged into the following five broad categories:

1. General information
2. Structure characteristics
3. Excitation characteristics
4. Recorded motion characteristics
5. Response characteristics

For each of these general categories, a series of individual parameters are defined. These parameters are defined in more details in subsequent sections. This information is extracted for each of the building considered in this study and entered into the master database. A separate set

of data, or "record" is established for each different building. In addition, a separate record is created for data obtained for the same building but for different earthquakes or by different investigators for the same earthquake. If the information on a particular parameter in a record is not available, that parameter is left blank.

General Information

The following general information is included for building identification purposes and for future reference.

Location: This parameter indicates the city where the structure is located.

Identification Number: Each building is assigned a unique identification number. This parameter includes a single character followed by a number. The character indicates the agency that instrumented the building. For example, "C" indicates that this building was instrumented by the California Strong Motion Instrumentation Program (CSMIP). Similarly, "U" and "N" indicate that the building was instrumented by the United States Geological Survey (USGS) or the National Oceanographic and Atmospheric Agency (NOAA), respectively. The number followed by the first character indicates the station number or the instrument identification numbers assigned by the instrumenting agency. For buildings instrumented by the CSMIP or the USGS, this number represents the station number assigned by the respective agency. For example, a number "58262" following the character "C" indicates the station number assigned to the building by the CSMIP. Similarly, a number "482" following the character "U" implies the station number assigned to the building by the USGS. However, for buildings instrumented by the NOAA, the number represents the identification numbers of the instruments used to measure motions of the buildings. For example, a number "151-3" followed by the character "N" indicates that the motions of the building were recorded by the instruments numbered 151 to 153.

Occupancy: This parameter indicates the building usage, for example, office, residential, hospital, or hotel.

Name: This parameter lists the name, if available, of the building. For example, building with identification number "N151-3" is known as the "Kajima International Building".

Address: Several buildings, especially those instrumented by the NOAA, are identified by their address. Thus, this information is also included in the database.

Reference: This parameter identifies the source of the vibration data if these data were not identified in this study. If the properties are identified in this study, "Goel and Chopra" is entered in the database.

Structure Characteristics

The following quantitative and qualitative parameters associated with characteristics of the building are included in the database:

Height: This parameter lists the height in feet from base level of the building. This height is used for estimating the fundamental vibration period of the building from code formulas.

Width: Width is the base dimension in feet along the longitudinal direction of the building.

Length: Length is the base dimension in feet along the transverse direction of the building.

Number of Stories: This parameter represents the number of stories above the ground level.

Number of Basements: This parameter represents the number of stories below the ground level (or the number of basements).

Base to Roof Height: Base to roof height lists the height in feet between the locations of instruments recording the input ground accelerations and the output ground accelerations. This parameter is used to estimate the average drift of the building during an earthquake. Since the instrument measuring the input ground acceleration may not always be located at the base of the

building or the instrument measuring the output acceleration may not be located at the top-most floor level, this height can be different than the height of the building described previously.

Material: The construction materials encountered in the building data included: Reinforced concrete (R/C); Steel; Masonry (MS); Unreinforced Masonry (URM); mixed materials such as Steel and R/C, Steel and URM, and R/C and URM.

Longitudinal Resisting System: This parameter categorizes the lateral system used in the longitudinal direction of the building for resisting the earthquake loads. Following is a list of lateral load resisting systems encountered in the building data:

- Moment-Resisting Frame (MRF): This category identifies a structure constructed of an assemblage of beams and columns that resist earthquake loads by frame action. The frames may be constructed of steel or reinforced concrete.
- Shear Wall (SW): This category identifies reinforced concrete or masonry systems that resist lateral loads by walls loaded in their own plane.
- Braced Frame (BF): This category identifies a structure whose frames are braced by diagonal members such that lateral loads are resisted by axial forces in the members.
- Eccentric Braced Frame (EBF): This system transfers the load through axial forces in members as well as dissipates earthquake energy through inelastic deformations in the shear links formed by the eccentric bracing.
- Moment Frames and Shear Walls (MRF/SW): This category is assigned to buildings having dual shear wall and moment frame systems or shear wall buildings with moment frames that contribute significantly to the earthquake resistance.

Transverse Resisting System: Similar to the longitudinal resisting system, this parameter indicates the lateral load resisting system of the building in the transverse direction.

Excitation Characteristics

This category includes the following two parameters to indicate the information on the earthquake for which the building vibration properties are identified:

Earthquake Name: This parameter indicates the name of the earthquake, usually indicating the location of the earthquake epicenter.

Earthquake Date: This is the date on which the earthquake occurred.

Recorded Motion Characteristics

This category includes the information on the building motions that is either recorded or derived directly from the recorded motions. This information is useful for estimating the intensity of the earthquake shaking at the building site or deformations of the building itself.

Longitudinal Base Acceleration: This parameter indicates the base peak acceleration recorded in the longitudinal direction of the building.

Longitudinal Roof Acceleration: This parameter indicates the roof peak acceleration recorded in the longitudinal direction of the building.

Transverse Base Acceleration: This parameter indicates the base peak acceleration recorded in the transverse direction of the building.

Transverse Roof Acceleration: This parameter indicates the roof peak acceleration recorded in the transverse direction of the building.

Longitudinal Roof Deformation: The longitudinal roof deformation, specified in feet, is calculated as the difference between the displacements at the roof level and the base level. The displacements used are obtained by double integrating the corrected accelerations.

Transverse Roof Deformation: Similar to longitudinal roof deformation, this parameter indicates the roof deformation in the transverse direction of the building.

Longitudinal Drift: Measured in percentage (%), this value indicates the average drift over the height of the building in the longitudinal direction. This drift is obtained by dividing the longitudinal roof deformation by the base to roof height of the building.

Transverse Drift: Similar to the longitudinal drift, this value is the average drift of the building in the transverse direction.

Vibration Properties

This category lists the vibration properties of the building identified from its motions recorded during the earthquake. The information includes the vibration period (T) and modal damping ratio (ξ) for the first two modes of the building in each of the following directions: longitudinal, transverse, and torsional.

Database Manipulation

The database for vibration properties should be amenable to easy update after each earthquake to include data for vibration properties of additional buildings. Furthermore, it should also be possible to easily extract the relevant data required for further studies. This section describes how the data can be added to or extracted from the database.

Adding Data

The data for each building can be entered in the database using two alternative approaches. These approaches are described next.

Tables: In Microsoft Access 2.0, the entire database can be viewed in the form of a table. Each row of this table contains data for a record. The various data properties (or fields), mentioned previously, are arranged in columns of this table. Thus, to enter data for each additional building, one can enter the appropriate row and column of the table and type in value of that field. For data records containing a large number of fields, this may become cumbersome because it may not be

possible to view the entire record on the computer screen. In such situations, forms, described next, offer a more attractive alternative.

Forms: Forms present the data for all fields of one record in an organized and attractive manner. In order to enter information on various fields of a record, one can navigate the form by using tab key of the keyboard and typing in the appropriate data. Furthermore, data in forms can also be organized differently compared to the tables, with category titles and more descriptive field names. The form designed for entering the vibration property database and used in this study is shown in Figure A.1.

Extracting Data

One of the primary advantages of organizing the data in databases is that it is easy to extract portions of the data, arrange various fields in a manner different compared to the original database, and sort them in ascending or descending order. The process of selectively extracting a subset of data from the larger database is facilitated by the queries.

Queries: Queries are used to extract data selectively from a larger data set stored in the database. To extract this data, the following options may be used:

- The data fields in the records that are to be extracted. Using this information, only selected data fields may be extracted and they may be arranged in a manner different than the main database.
- The order in which the records are to be sorted. The database stores the records in their order of entry. Using this information, the data may be sorted either in ascending or descending order of one or more fields.
- Whether the field is to be displayed. Using this option, a field may be hidden from the final printout but all other options and criteria may be applied to this field.

- The criteria to be used to extract the data. This criteria in usually in the form of Boolean operators and may be specified on more than one field simultaneously.

Example: The following example illustrates the use of queries in selectively extracting data from the main database. The fields to be extracted are: (1) Location, (2) Identification Number, (3) Height, (4) First Longitudinal Period, and (5) First Transverse Period. The data is to be extracted only for the Northridge earthquake and the steel buildings; the earthquake name or the material should not be printed. Furthermore, the records extracted are arranged in ascending order by the location and the height. The query designed to extract this data is shown in Figure A.2 and the extracted data in Figure A.3.

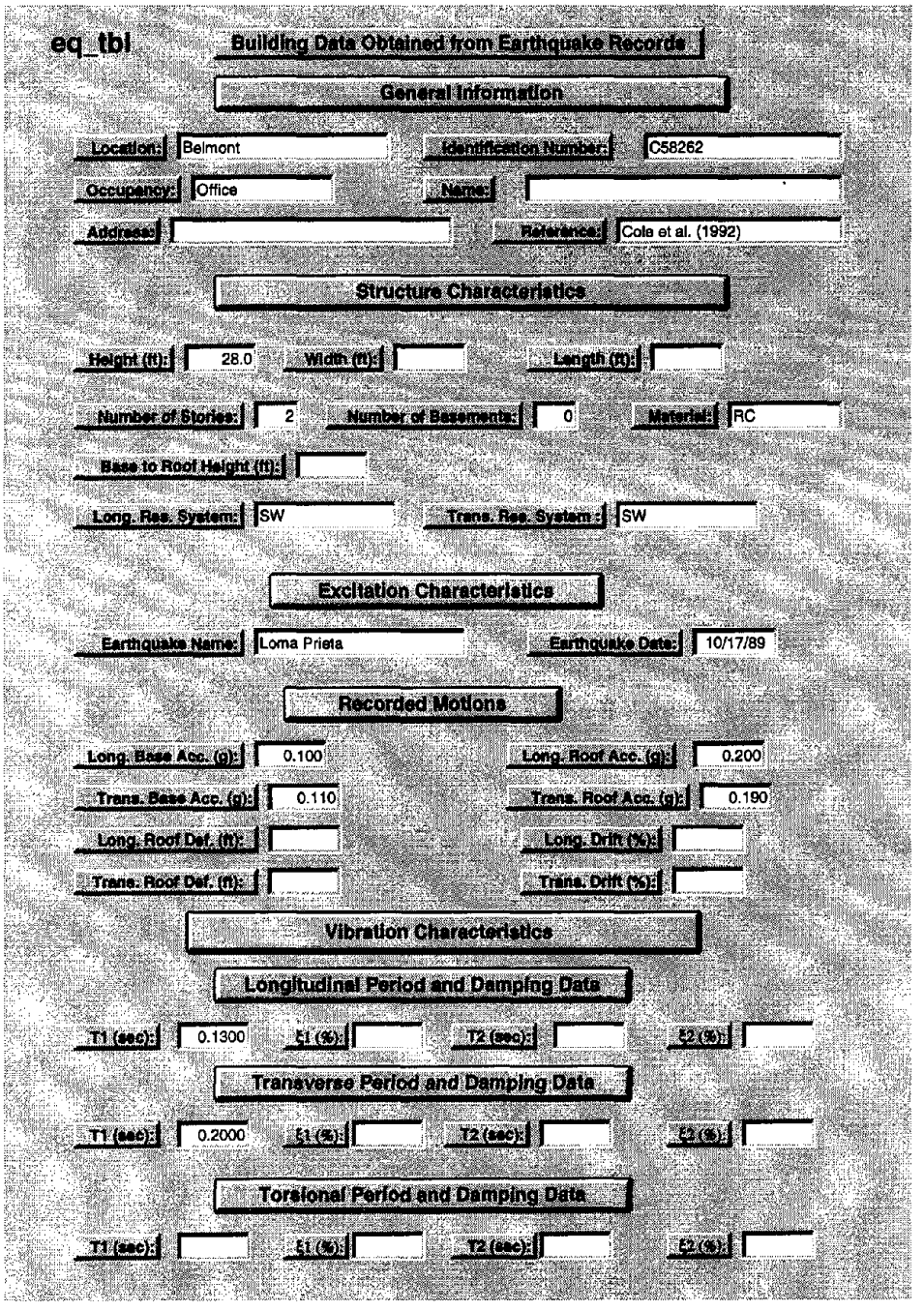

Figure A.1. Form designed for the vibration properties database.

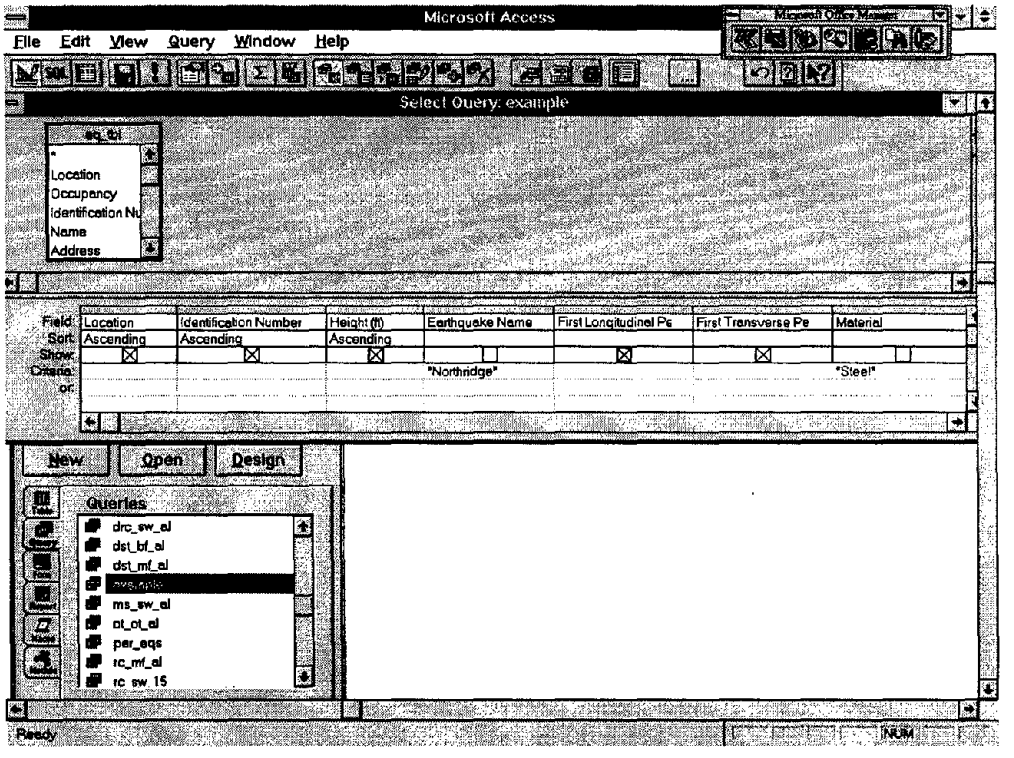

Figure A.2. Example query design in Microsoft Access 2.0.

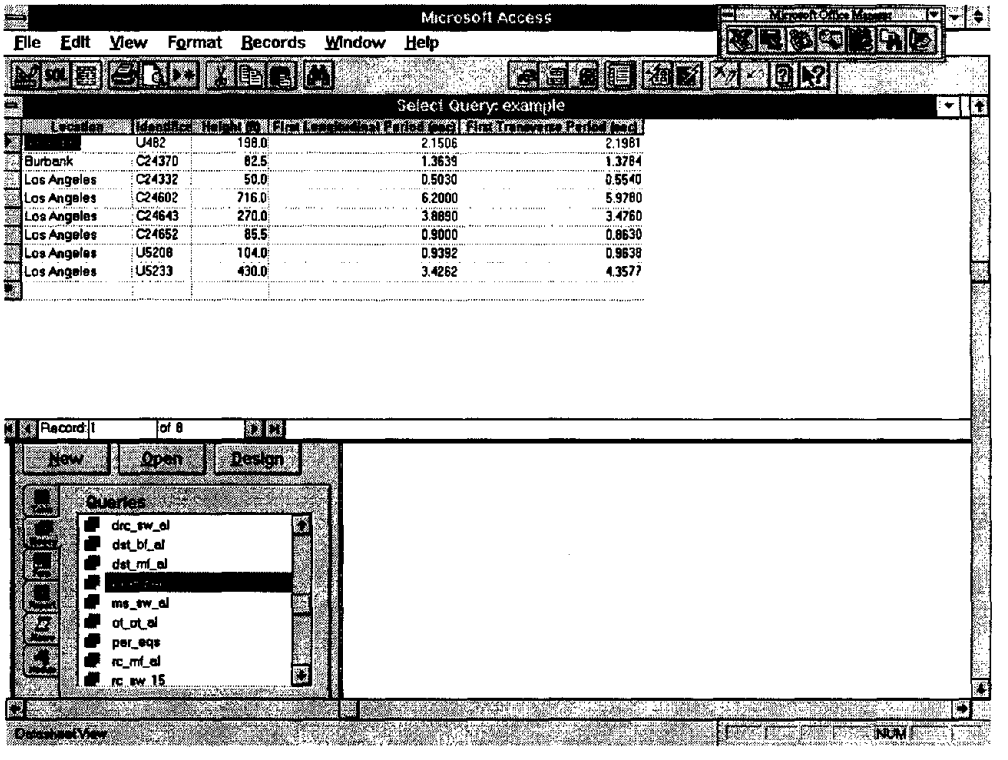

Figure A.3. Results of example query.

APPENDIX B: SYSTEM IDENTIFICATION METHODS

System identification techniques are used to identify the vibration periods and modal damping ratios of buildings from their motions recorded during earthquakes. Although, a number of parametric and nonparametric system identification techniques are available (Appendix I), this appendix describes the following three more commonly used techniques for system identification of the vibration properties from recorded motion: (a) the transfer function method, (b) the modal minimization method, and (c) the autoregressive modeling method. Described first is the theory for each of these techniques followed by an example.

Transfer Function Method

The transfer function method is a nonparametric system identification approach designed to work for linear and time-invariant systems. This approach involves determining the transfer function, $H(i\omega)$, from the Fourier transforms of input and output accelerations. The modal frequencies are estimated from the locations of the resonant peaks in the absolute value, $|H(i\omega)|$, of the transfer function; and the modal damping ratios are determined from their half-power bandwidths.

The transfer function method usually works well for steady-state harmonic test data or ambient vibration data where the level of noise in the data is small. When applied to earthquake data, difficulties arise because the transfer function is characterized by extreme variability. Furthermore, the transfer function exhibits numerous peaks that are not related to the resonant peaks but are a function of the noise in the data and the model error. Smoothing of the transfer function can reduce the variability and thus make the resonant peaks more apparent, but leads to a loss of information that can result in the damping ratios being overestimated. Generally, past work suggests that the only vibration properties that can be reliably estimated from the transfer

function are the frequencies of the first few modes and possibly the damping ratio in the fundamental vibration mode. Since the goal of this study is to estimate the vibration frequencies as well as the modal damping ratios for at least first two modes, the transfer function method is used only to obtain initial estimates that are to be supplied to the parametric system identification techniques described in the next two sections.

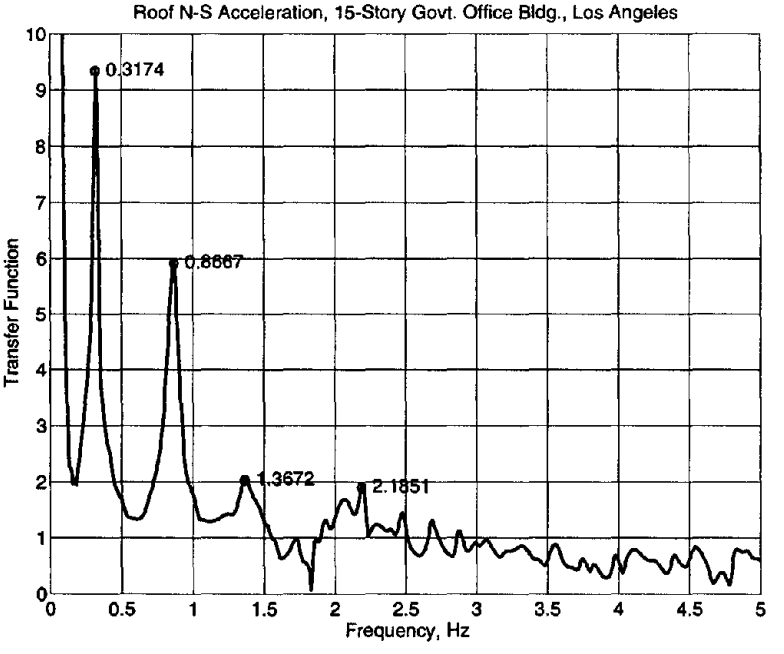

Figure B.1. Smoothed transfer function and initial frequency estimates.

Figure B.1 shows the smoothed transfer function determined from the base and roof accelerations of one of buildings considered in this study. The frequencies of the first and second modes of vibration estimated from this transfer function are 0.3175 Hz and 0.8667 Hz, respectively. Although two other peaks at 1.3672 Hz and 2.1851 Hz are also identified, these can not be reliably associated with higher modes of the building. Since the resonant peaks are very sharp, it is not possible to estimate the damping ratio even for the first mode of vibration; the

initial guess for modal damping ratios for these modes would be 2% and 3% of the critical damping value.

Modal Minimization Method

The modal minimization method is a parametric system identification approach for estimating the vibration properties of a linear system. This approach involves minimizing the error between the output acceleration and the input acceleration, in the least square sense, for the various vibration parameters of the building (Beck, 1978; Li and Mau, 1971). This section describes the theoretical background for the modal minimization method followed by an example. The approach presented is valid for multiple input and multiple output. The single input and single output approach adopted in the present study is a simplified version of this more general approach.

Theoretical Background

Using modal superposition for linear systems, the output acceleration, a_i, of the building can be expressed in terms of its modal acceleration responses, $\ddot{u}_j$, through the following equation:

$$a_i = \sum_j \phi_{ij} \ddot{u}_j \tag{B-1}$$

in which ϕ_{ij} is the mode shape component of the *j*th mode at location *I*. The modal accelerations are defined by the second order differential equation:

$$\ddot{u}_j + 2\xi_j \omega_j \dot{u}_j + \omega_j^2 u_j = \sum_k p_{jk} a_{gk} \tag{B-2}$$

where ξ_j and ω_j are the modal damping ratio and the natural frequency, respectively, of the *j*th mode, and p_{jk} is the participation factor of the *j*th mode with respect to the *k*th input motion. Since the input accelerations, a_{gk}, are linear within each time step Δt, the acceleration response,

$\ddot{u}_j$ for each mode can be computed using the exact solution to the piecewise linear excitation (Chopra, 1995); this computation requires the initial modal velocity, $\dot{u}_j(0)$, and modal displacement, $u_j(0)$ for each mode. Thus, the unknown modal parameters are: ω_j, ξ_j, p_{jk}, $\dot{u}_j(0)$, $u_j(0)$, and ϕ_{ij}.

The modal minimization method seeks to iteratively minimize the squared error:

$$J = \sum_i \sum_s [a_{oi}(s\Delta t) - a_i(s\Delta t)]^2 \tag{B-3}$$

between the recorded output acceleration, a_{oi}, and the output acceleration, a_i, of the linear model with respect the unknown modal parameters. A relative error corresponding to J of Eq. (B-3) is defined as:

$$E = \sqrt{\frac{\sum_i \sum_s [a_{oi}(s\Delta t) - a_i(s\Delta t)]^2}{\sum_i \sum_s [a_{oi}(s\Delta t)]^2}} \tag{B-4}$$

This modal minimization technique implemented on computer by Beck (1978) and Li and Mau (1991) generally follows the above-described methodology with minor differences in the minimization procedures; this study used the program developed by the latter authors. The iterative minimization procedure requires initial estimates of the unknown modal parameters. The initial estimates for the modal frequencies and damping ratios may be obtained from the transfer function approach described previously. Obtaining estimates of the other parameters requires some judgment.

The system identification process using the modal minimization method involves increasing the number of modes until the difference in the relative error E (Eq. B-4) is less than a certain value; a value of 3% is selected in this study. Although the last included mode often

contributes little to the output by itself, it improves the error estimate somewhat. This procedure is illustrated with an example next.

Example

The problem solved in the present study is that of single input at the building base and single output at the building roof. For such a problem, the unknown modal parameters are: ω_j, ξ_j, p_j, $\dot{u}_j(0)$, $u_j(0)$, and ϕ_j. Since one component of the mode shape can always be set arbitrarily equal to one, only the first five of these six parameters for each mode need to be identified. The various steps involved in the system identification process are:

1. Obtain initial estimates of the modal frequencies and damping ratios from the transfer function. Figure B.2 shows the transfer function between roof and base accelerations in the N-S direction of the 15-story Government Office Building in Los Angeles. Initial estimates of the modal frequencies are shown on this figure. Since it was not possible to obtain estimates of the modal damping ratio, the initial values for the first two modes is selected as 2% and remaining modes as 5% based on judgment.
2. Obtain initial estimates of the remaining modal parameters by judgment. The relative magnitude of the participation factor can be judged from the relative peak heights at the modal frequencies. Furthermore, initial modal velocities and displacements can be selected as zero. This selection is reasonable because the recorded motion used in the identification process starts at time zero when the initial motions of the building are for all practical purposes zero.
3. Identify the modal parameters using the modal minimization procedure. Start with first two modes and increase the number of modes until the difference between two successive values of the relative error is within 3%. For the example building, four modes are needed to satisfy

the convergence criteria. The results of the system identification are summarized in Table B.1.

4. Validate the identified model by comparing (a) the transfer functions, and (b) the time histories of the recorded motion and the motion of the identified model. Such comparisons are presented in Figures B.3 and B.4 for the example building. These comparisons also assist in reliably estimating the true modal frequencies and damping ratios of the building. For example, while the match in the time history is very good, only the first two peaks of the transfer function are matched well by the system identification procedure. Therefore, modal parameters for these two modes are considered to be reliable estimates of the true vibration properties of the building.

Table B.1. Results of system identification in N-S direction.

Mode No.	Frequency (Hz)	Damping	Part. Factor	Initial Disp.	Initial Velo.	Modal Cont.	Comments
1	0.3220	0.0241	-6.99E-00	-3.78E-04	2.24E-03	1.06E+00	1st Mode
2	0.8667	0.0390	1.05E-00	4.76E-05	7.97E-04	3.28E-01	2nd Mode
3	1.4200	0.0887	-3.89E-01	2.11E-05	-3.86E-05	1.28E-01	
4	2.1877	0.0358	1.06E-01	4.05E-06	-4.07E-05	4.89E-02	

Relative Error = 0.326 and Absolute Error = 0.683

Auto-Regressive Modeling Method

The auto-regressive modeling method is also a parametric system identification approach for estimating the vibration properties of a linear system. Similar to the modal minimization procedure, this approach involves minimizing the error between the output acceleration and the input acceleration, in the least squares sense, for the various parameters of the autoregressive model (Ljung, 1987). This section describes briefly the theoretical background for the autoregressive modeling method followed by an example; details of this method can be found elsewhere (Safak, 1988, 1989a, 1989b, 1991).

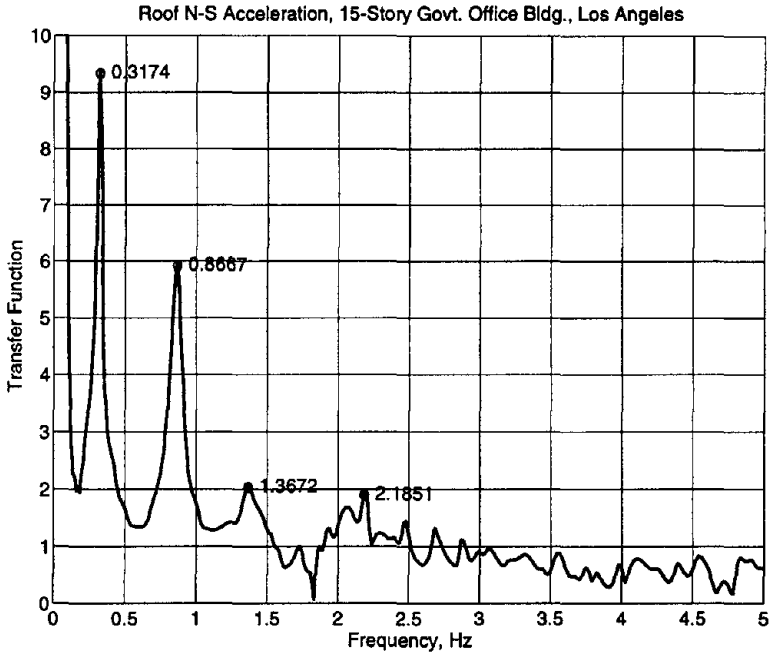

Figure B.2.. Initial frequency estimates from transfer function in N-S direction.

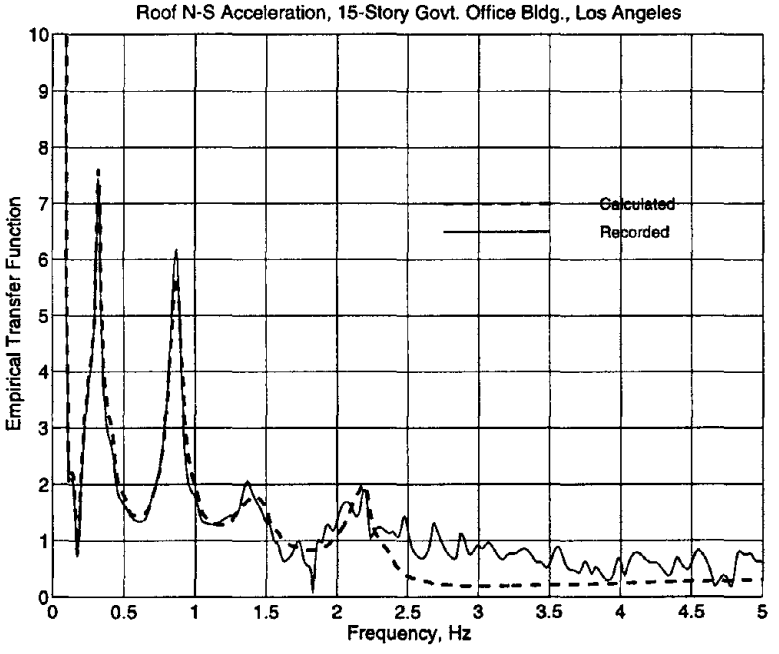

Figure B.3. Comparison of empirical transfer functions: recorded motions and calculated motions.

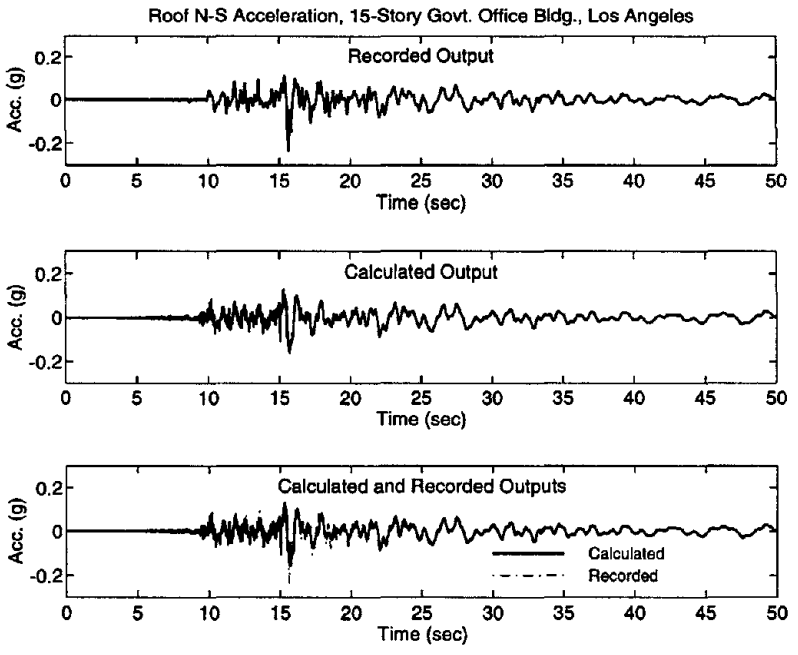

Figure B.4. Comparison of time-histories: recorded motions and calculated motions.

Theoretical Background

The set of second order differential equations governing the earthquake response of a linear system may be written as:

$$y(t) + \sum_{j=1}^{n_a} a_j y(t - j\Delta) = \sum_{k=1}^{n_b} b_k x(t - k\Delta - n_c\Delta) \tag{B-5}$$

in which $y(t)$ is the system output, $x(t)$ is the input, Δ is the sampling interval, a_j and b_k are the parameters of the autoregressive model numbering n_a and n_b, respectively, and n_c is the time delay, in terms of the number of discrete time steps, between the input and the output. The n_a and n_b are called the order of the auto-regressive model. The same equation can also be written in the frequency domain as:

$$Y(\omega) = H(i\omega)X(\omega) \tag{B-6}$$

where $Y(\omega)$ and $X(\omega)$ are the Fourier transforms of the output, $y(t)$, and the input $x(t)$, respectively, and $H(i\omega)$ is the transfer function defined as:

$$H(i\omega) = \frac{\sum_{k=1}^{n_b} b_k e^{-i\omega(k+n_c)\Delta}}{1 + \sum_{j=1}^{n_a} a_j e^{-i\omega j\Delta}} \tag{B-7}$$

in which $i = \sqrt{-1}$. The denominator of equation seven contains information about the dynamic properties of the building. The frequencies and the damping ratios are computed from the poles, p_j, of the transfer function which are determined as the roots of the following denominator polynomial:

$$p^{n_a} + a_1 p^{a_a - 1} + \cdots + a_{n_a - 1} p + a_{n_a} = 0 \tag{B-8}$$

For stable structures, i.e., structures with non negative damping, the poles are in complex-conjugate pairs. The modal frequencies, $\omega_j = 2\pi f_j$, and the damping ratios, ξ_j, are computed from these poles as:

$$\xi_j = \frac{\ln\left(\frac{1}{|p_j|}\right)}{\left[v_j + \ln\left(\frac{1}{|p_j|}\right)\right]^{1/2}} \tag{B-9}$$

$$f_j = \frac{\ln\left(\frac{1}{|p_j|}\right)}{2\pi \xi_j \Delta} \tag{B-10}$$

where v_j is argument of p_j. The frequencies and damping ratios corresponding to the complex-conjugate pairs are identical. Therefore, n_a poles result in $n_a/2$ distinct frequencies and damping ratios.

To compute the contribution of each mode to the response, the transfer functions are expanded into partial fractions and the pairs of terms corresponding to pairs of complex-conjugate poles are combined:

$$H(i\omega) = \sum_{j=1}^{n_a/2} \left(\frac{r_j z^{-(n_c+1)}}{1 - p_j z^{-1}} + \frac{r_j^* z^{-(n_c+1)}}{1 - p_j^* z^{-1}} \right) \text{ with } z = e^{i\omega\Delta} \tag{B-11}$$

where r_j denotes the residue for the jth transfer function corresponding to the jth pole. The contribution of the jth mode to the response is obtained by multiplying the input by the corresponding modal transfer function.

The autoregressive modeling method seeks to minimize the error between the output and the input in the least squared sense with respect to the parameters a_j and b_k. The next section describes the various step of the system identification using this method and illustrates these steps with an example.

Example

Various steps of this procedure are illustrated next with an example. For this purpose, the vibration properties of a 6-story commercial building located in Burbank are determined in the N-S direction from its roof and base accelerations recorded during the Northridge earthquake. Various steps of this procedure are implemented conveniently in the System Identification Toolbox of the commercially available software MATLAB. The steps are as follows:

1. Estimate the time delay, n_c, between the input and output. Time delay compensates the synchronization and discretization errors as well as errors introduced by considering only a limited number of modes. To determine the time delay, a single-mode system is assumed, i.e., n_a=2 and n_b=1, and variation of the squared error between the recorded output and the model output is investigated. The time delay that minimizes the error is selected as the time

delay for further system identification. Figure B.5a shows the variation for the example building where the error is minimized in the neighborhood of n_c=10. The time delay selected for the system identification is 9.

2. Determine the model order n_a. Similar to the time delay, the model order is also selected by investigating the error with increasing model orders. Generally the error decreases with increasing n_a with sharp decrease at the beginning and gradual flattening with further increase. The beginning of the flat region indicates the optimal model order. Figure B.5b shows variation of the error for n_a= 2 to 30 assuming n_b= n_a and n_c=10. This figure suggests that n_a= 4, i.e., two modes, would be sufficient as the model order. However, the model verification tests described next, showed that a much higher value of n_a= 32 is required for satisfactory identification.

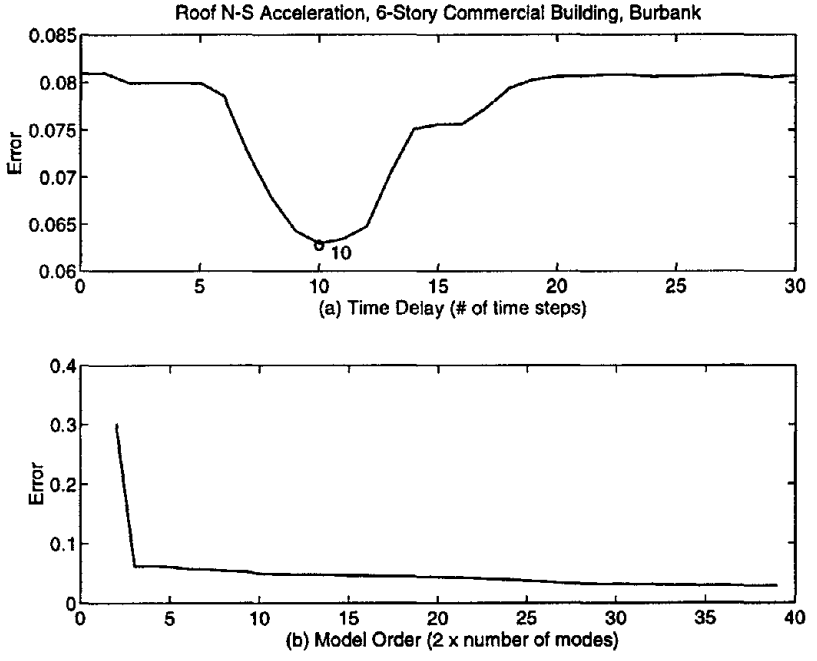

Figure B.5. Time delay and model order for the example building.

3. Select the parameter n_b. The error is not sensitive to the parameter n_b. This selection is based on zero-pole cancellation criteria rather than the minimum error criteria. Normally, the

accuracy of the identification increases with increasing n_b. However, if n_b becomes too high, one or more zeros may become equal to the poles of the transfer function. This results in a zero-pole cancellation eliminating some of the modes of the building. By trying several values, n_b = 16 is found to be appropriate for the example building. As shown in Figure B.6, it does not result in any zero-pole cancellation.

4. Identify the building. Using n_a=32, n_b = 16, and n_c= 9, the modal frequencies and damping ratios identified for the example building are presented in Table B.2. For this building the first mode is identified with a frequency of 4.607 Hz and damping ratio of 4.0%; the second mode values are 13.475 Hz and 5.3%, respectively. Figure B.7 and B.8 show the contribution of various modes to the output response.

5. Verify the identified model. The final step in the system identification using auto-regressive modeling is verification of the identified model. This is accomplished by ensuring the transfer function (Figure B.9) and time history (Figure B.10) of the auto-regressive model match closely with those of the recorded output motion. In addition, the autocorrelation and the cross correlation of the residuals are checked with the input (Figure B.11). For a valid identification, the residuals should be close to white noise and independent (uncorrelated) with the input. For this purpose, the dotted lines are also plotted in Figure B.11 for 95% confidence limits for whiteness in the autocorrelation and for independence in the cross correlation. The autocorrelation plot show that the residuals of the identified model satisfy the whiteness criteria. Although the cross correlation exceeds the confidence limit as a few places, the amplitude is generally small. Thus even the autocorrelation criteria is acceptable for the identified model.

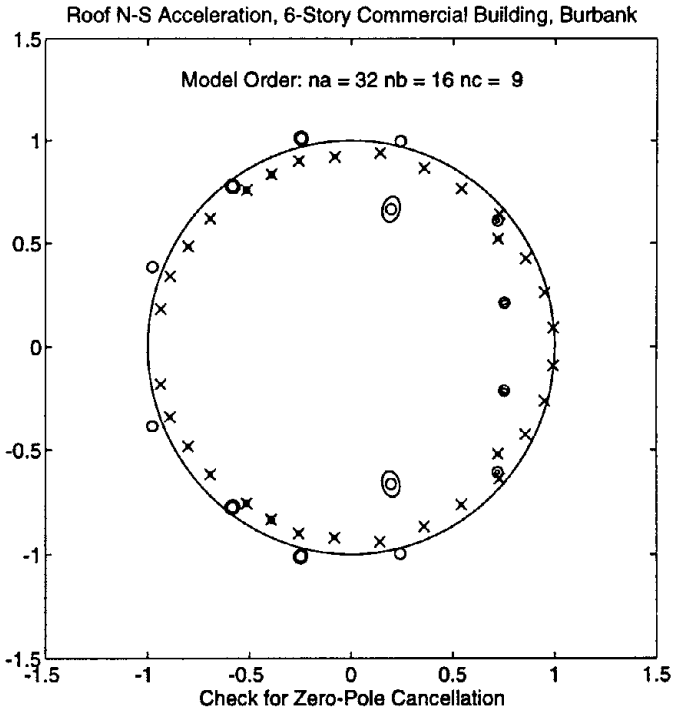

Figure B.6. Zero-pole cancellation for the example building.

Table B.2. Results of system identification for the example building.

j	Frequency (Hz)	Period (sec)	Damping	Pole Magnitude	Comments
1	4.607	1.364	0.040	0.996	1st Mode
2	4.607	1.364	0.040	0.996	
3	13.475	0.466	0.053	0.986	2nd Mode
4	13.475	0.466	0.053	0.986	
5	36.071	0.174	0.043	0.969	
6	36.071	0.174	0.043	0.969	
7	23.180	0.271	0.094	0.957	
8	23.180	0.271	0.094	0.957	
9	18.357	0.342	0.127	0.954	
10	18.357	0.342	0.127	0.954	
11	9.871	0.637	0.239	0.954	
12	9.871	0.637	0.239	0.954	
13	71.118	0.088	0.036	0.950	
14	71.118	0.088	0.036	0.950	
15	59.051	0.106	0.054	0.938	
16	59.051	0.106	0.054	0.938	
17	64.668	0.097	0.051	0.937	
18	64.668	0.097	0.051	0.937	
19	47.817	0.131	0.069	0.937	
20	47.817	0.131	0.069	0.937	
21	27.343	0.230	0.121	0.936	
22	27.343	0.230	0.121	0.936	
23	36.592	0.172	0.101	0.929	
24	36.592	0.172	0.101	0.929	
25	74.201	0.085	0.053	0.924	
26	74.201	0.085	0.053	0.924	
27	56.639	0.111	0.071	0.922	
28	56.639	0.111	0.071	0.922	
29	48.909	0.129	0.090	0.916	
30	48.909	0.129	0.090	0.916	
31	31.807	0.198	0.184	0.890	
32	31.807	0.198	0.184	0.890	

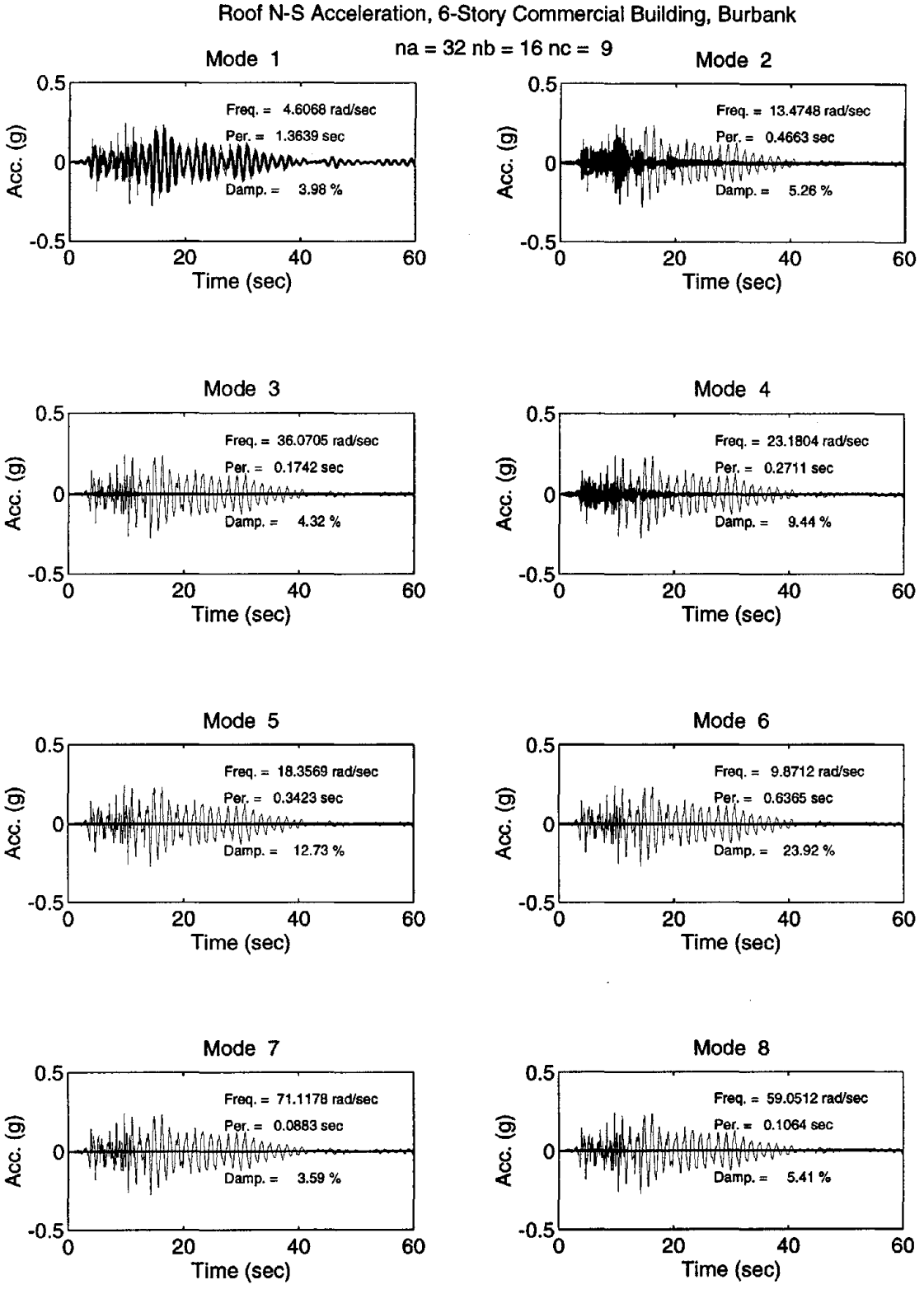

Figure B.7. Modal contributions of autoregressive model; modes 1 to 8.

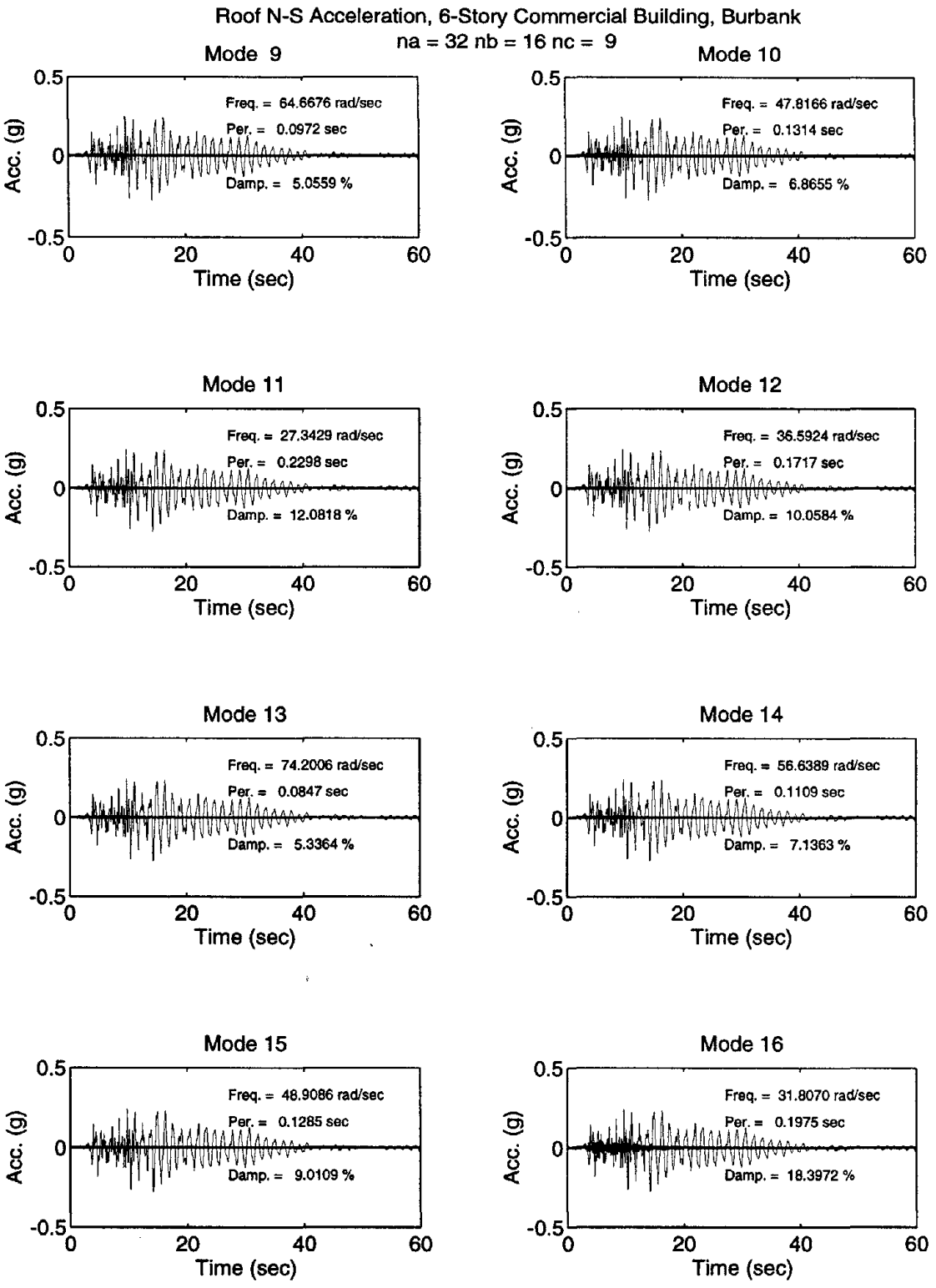

Figure B.8. Modal contributions of autoregressive model; modes 9 to 16.

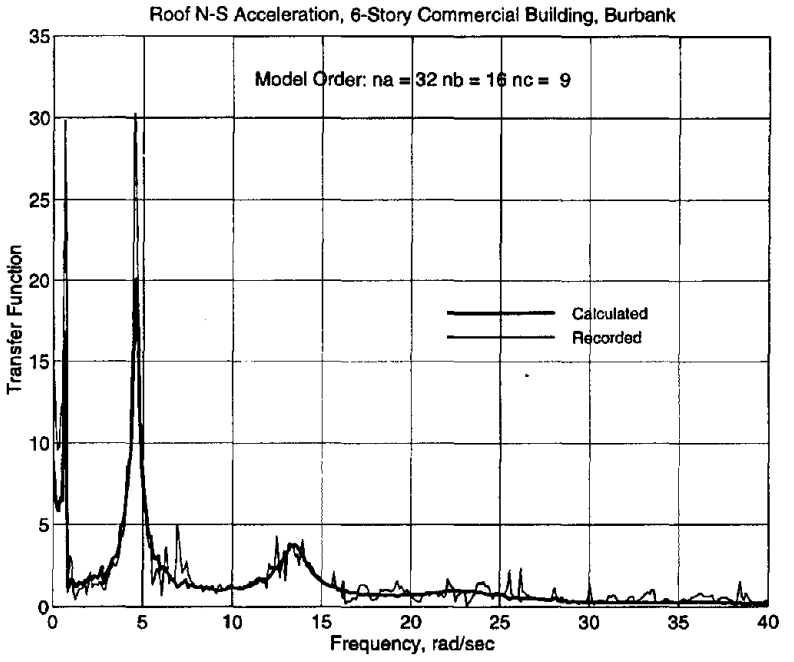

Figure B.9. Comparison of empirical transfer functions: recorded motions and calculated motions of autoregressive model.

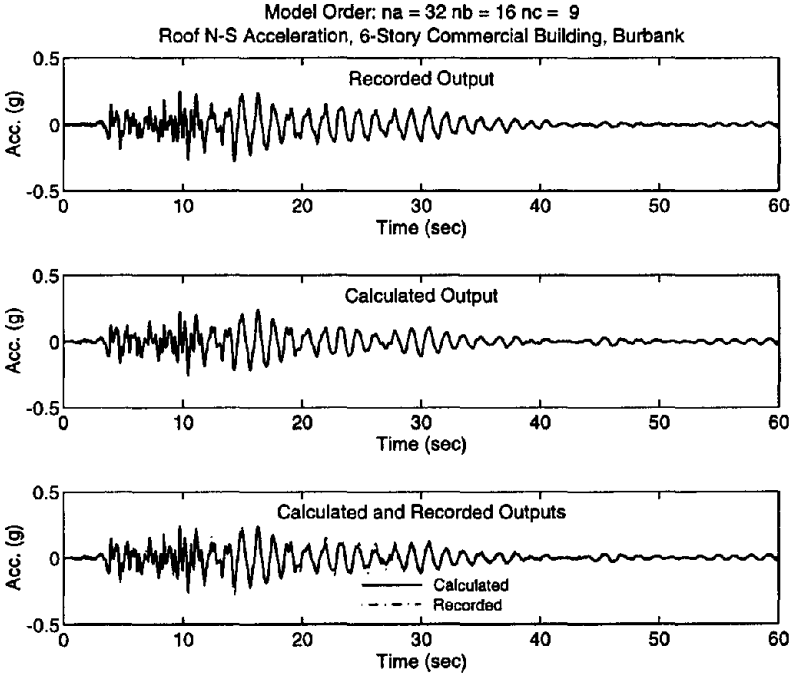

Figure B.10. Comparison of time-histories: recorded motions and calculated motions of autoregressive model.

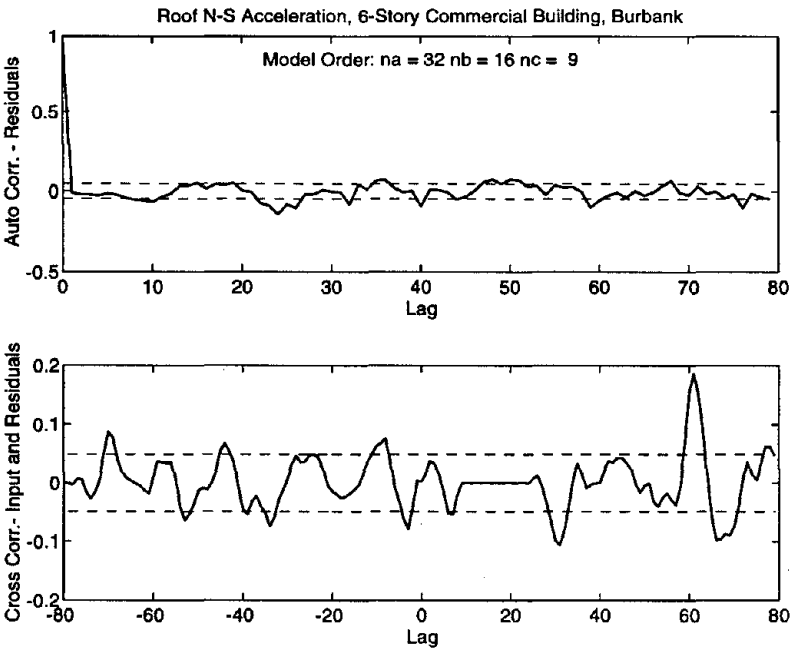

Figure B.11. Residuals for autoregressive model.

APPENDIX C: RESULTS OF SYSTEM IDENTIFICATION

Table C.1. List of identified buildings.

No.	Location	Station Name	ID Number	No. of Story	Material
1	Los Angeles	UCLA Math-Science Bldg.	C24231	7	Steel/RC
2	Burbank	Residential Bldg.	C24385	10	RC
3	Sylmar	County Hospital	C24514	6	Steel/RC
4	Burbank	Commercial Bldg.	C24370	6	Steel
5	Los Angeles	Office Bldg.	C24643	19	Steel
6	Los Angeles	Hollywood Storage Bldg.	C24236	14	RC
7	North Hollywood	Hotel	C24464	20	RC
8	Pasadena	Milikan Library	N264-5	10	RC
9	Los Angeles	Warehouse	C24463	5	RC
10	Los Angeles	Commercial Bldg.	C24332	3	Steel/RC
11	Los Angeles	Residential Bldg.	C24601	17	RC
12	Los Angeles	Govt. Office Bldg.	C24569	15	Steel
13	Los Angeles	Office Bldg.	C24602	52	Steel
14	Los Angeles	Office Bldg.	C24579	9	RC/URM
15	Los Angeles	CSULA Adm. Bldg.	C24468	8	RC
16	Pasadena	Office Bldg.	C24541	6	Steel/URM
17	Whittier	Hotel	C14606	8	MAS
18	Los Angeles	Office Bldg.	C24652	6	RC
19	Alhambra	900 South Fremont Street	U482	13	Steel
20	Los Angeles	1100 Wilshire Blvd.	U5233	32	Steel
21	Los Angeles	Wadsworth VA Hospital	U5082	6	Steel
22	Los Angeles	Office Bldg.	C24567	13	Steel/RC

1. Los Angeles - 7-Story UCLA Math-Science Building, CSMIP Station No. 24231

Los Angeles - 7-story UCLA Math-Science Bldg.
(CSMIP Station No. 24231)

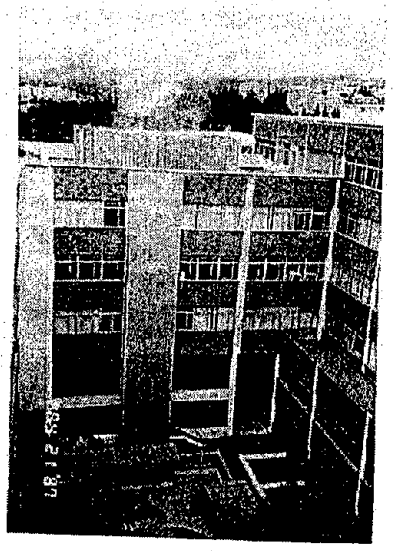

No. of Stories above/below ground: 7/0
Plan Shape: Rectangular
Base Dimensions: 60' x 48'
Typical Floor Dimensions: 60' x 48'
Design Date: 1969

Vertical Load Carrying System:
2.5" concrete slab over metal deck supported by steel framers at 5th, 6th, 7th floors and roof; thick concrete slab supported by concrete walls at 3rd floor.
Lateral Load Carrying System:
Thick concrete shear walls between Levels 1 and 3; moment resisting steel frames above.

Figure C.1.1a. Details of UCLA Math Science Building, CSMIP Station No. 24231

Los Angeles - 7-story UCLA Math-Science Bldg.
(CSMIP Station No. 24231)

SENSOR LOCATIONS

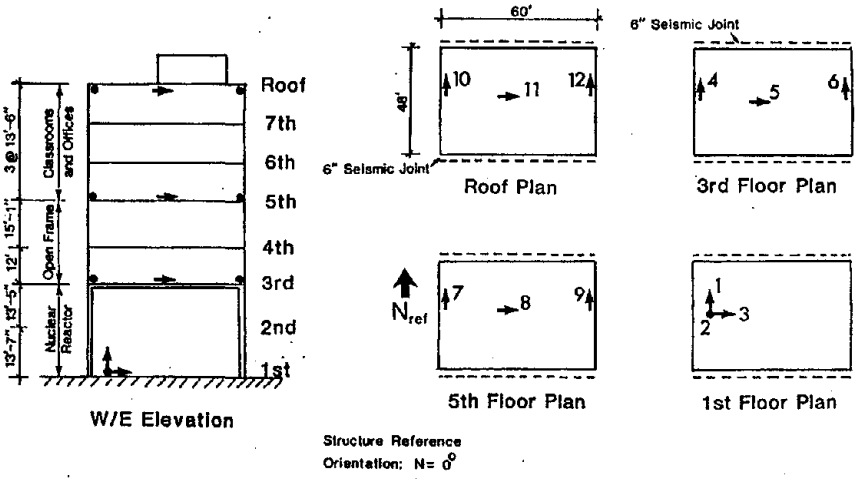

Figure C.1.1b. Sensor locations in UCLA Math Science Building, CSMIP Station No. 24231

Table C.1.1. Results of system identification in E-W (longitudinal) direction by autoregressive modeling.

j	Frequency (Hz)	Period (sec)	Damping	Pole Magnitude	Comments
1	0.902	1.108	0.071	0.992	1st Mode
2	0.902	1.108	0.071	0.992	
3	11.648	0.086	0.015	0.978	
4	11.648	0.086	0.015	0.978	
5	9.430	0.106	0.025	0.971	
6	9.430	0.106	0.025	0.971	
7	3.136	0.319	0.088	0.966	
8	3.136	0.319	0.088	0.966	
9	6.557	0.153	0.043	0.965	
10	6.557	0.153	0.043	0.965	
11	7.741	0.129	0.043	0.960	
12	7.741	0.129	0.043	0.960	
13	1.393	0.718	0.241	0.959	
14	1.393	0.718	0.241	0.959	
15	4.028	0.248	0.107	0.947	
16	4.028	0.248	0.107	0.947	
17	10.591	0.094	0.042	0.946	
18	10.591	0.094	0.042	0.946	
19	12.046	0.083	0.040	0.942	
20	12.046	0.083	0.040	0.942	
21	10.528	0.095	0.046	0.941	
22	10.528	0.095	0.046	0.941	
23	1.654	0.605	0.304	0.939	
24	1.654	0.605	0.304	0.939	
25	2.531	0.395	0.202	0.938	
26	2.531	0.395	0.202	0.938	
27	4.180	0.239	0.129	0.935	
28	4.180	0.239	0.129	0.935	
29	8.260	0.121	0.066	0.934	
30	8.260	0.121	0.066	0.934	
31	5.764	0.174	0.116	0.920	
32	5.764	0.174	0.116	0.920	
33	6.161	0.162	0.131	0.904	
34	6.161	0.162	0.131	0.904	
35	5.896	0.170	0.137	0.903	
36	5.896	0.170	0.137	0.903	
37	9.345	0.107	0.103	0.886	
38	9.345	0.107	0.103	0.886	

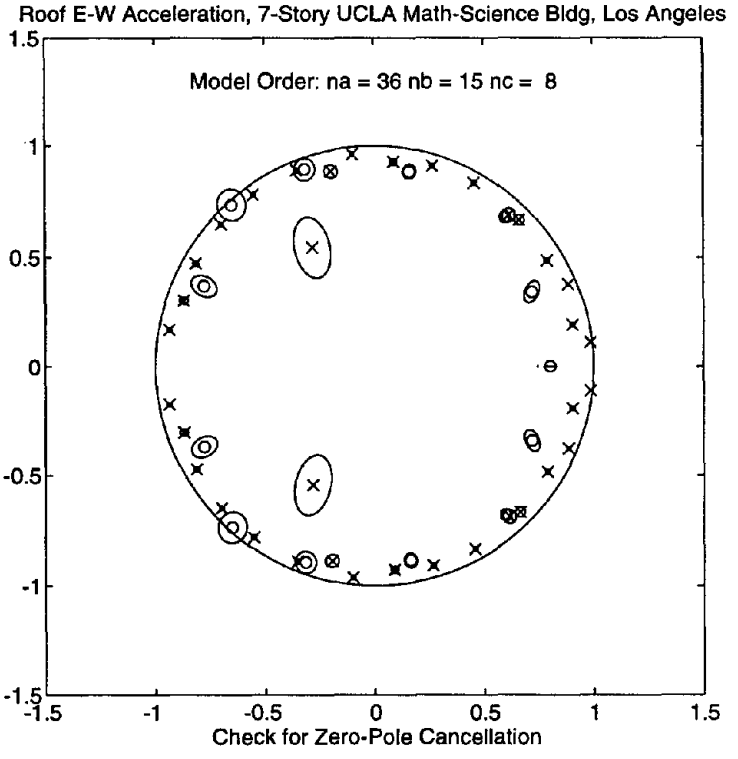

Figure C.1.2. Zero-pole cancellation for autoregressive model in E-W direction.

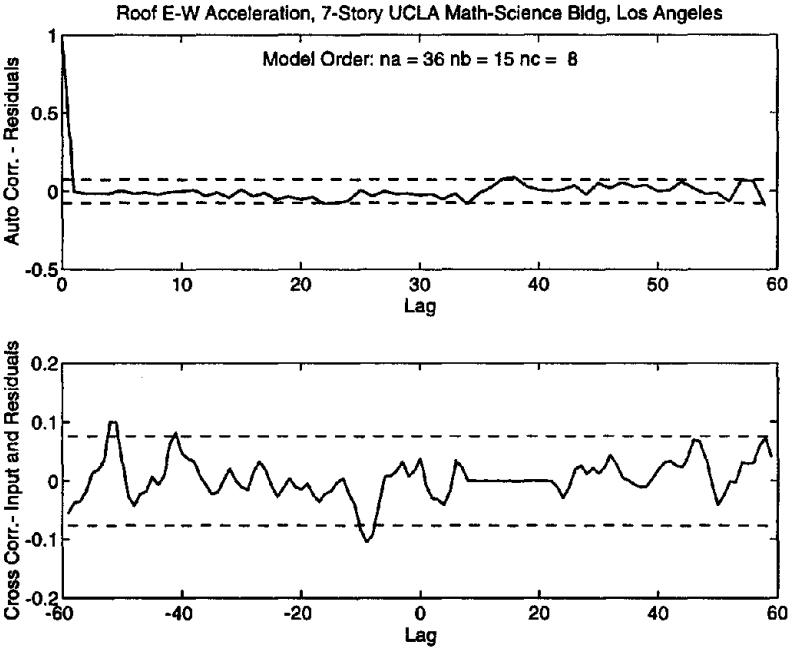

Figure C.1.3. Residuals for autoregressive model in E-W direction.

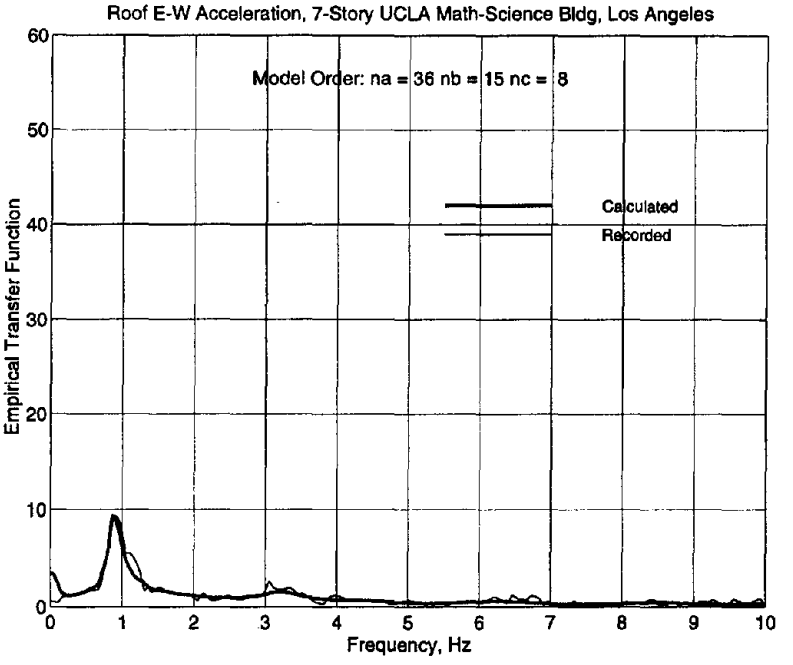

Figure C.1.4. Comparison of empirical transfer functions: recorded motion and calculated motion of autoregressive model in E-W direction.

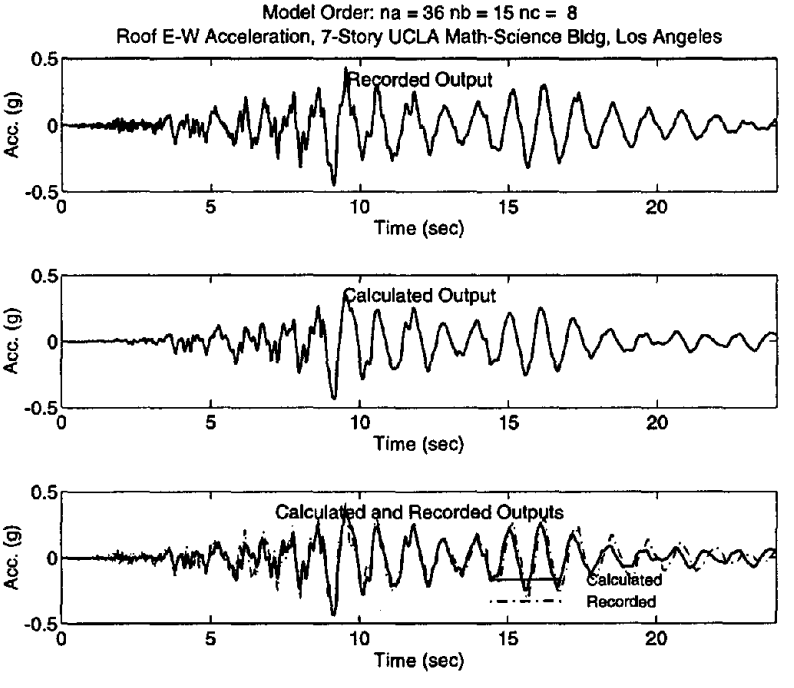

Figure C.1.5. Comparison of time-histories: recorded motion and calculated motion of autoregressive model in E-W direction.

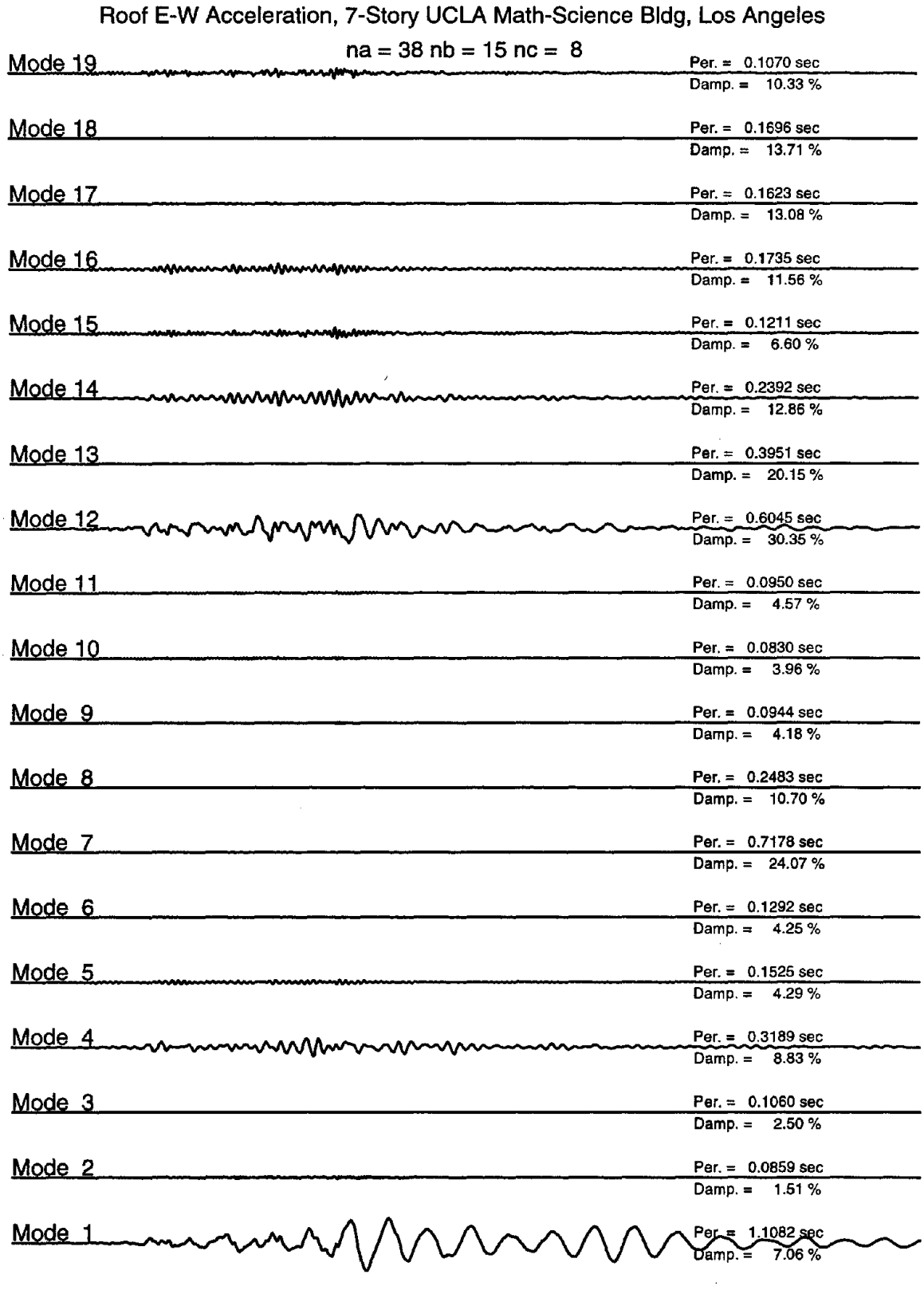

Figure C.1.6. Modal contributions of autoregressive model in E-W direction.

Table C.1.2. Results of system identification in N-S (transverse) direction by autoregressive modeling.

j	Frequency (Hz)	Period (sec)	Damping	Pole Magnitude	Comments
1	1.184	0.845	0.172	0.975	1st Mode
2	1.184	0.845	0.172	0.975	
3	2.696	0.371	0.123	0.959	
4	2.696	0.371	0.123	0.959	
5	3.583	0.279	0.100	0.956	
6	3.583	0.279	0.100	0.956	
7	4.235	0.236	0.093	0.952	
8	4.235	0.236	0.093	0.952	
9	5.703	0.175	0.070	0.951	
10	5.703	0.175	0.070	0.951	
11	1.756	0.569	0.236	0.949	
12	1.756	0.569	0.236	0.949	
13	6.105	0.164	0.071	0.947	
14	6.105	0.164	0.071	0.947	
15	7.669	0.130	0.058	0.946	
16	7.669	0.130	0.058	0.946	
17	1.337	0.748	0.331	0.946	
18	1.337	0.748	0.331	0.946	
19	11.485	0.087	0.041	0.943	
20	11.485	0.087	0.041	0.943	
21	4.235	0.236	0.121	0.938	
22	4.235	0.236	0.121	0.938	
23	9.839	0.102	0.053	0.937	
24	9.839	0.102	0.053	0.937	
25	8.938	0.112	0.059	0.936	
26	8.938	0.112	0.059	0.936	
27	7.396	0.135	0.072	0.935	
28	7.396	0.135	0.072	0.935	
29	10.671	0.094	0.063	0.919	
30	10.671	0.094	0.063	0.919	
31	11.961	0.084	0.066	0.906	
32	11.961	0.084	0.066	0.906	
33	8.521	0.117	0.095	0.904	
34	8.521	0.117	0.095	0.904	
35	10.442	0.096	0.462	0.545	
36	10.442	0.096	0.462	0.545	

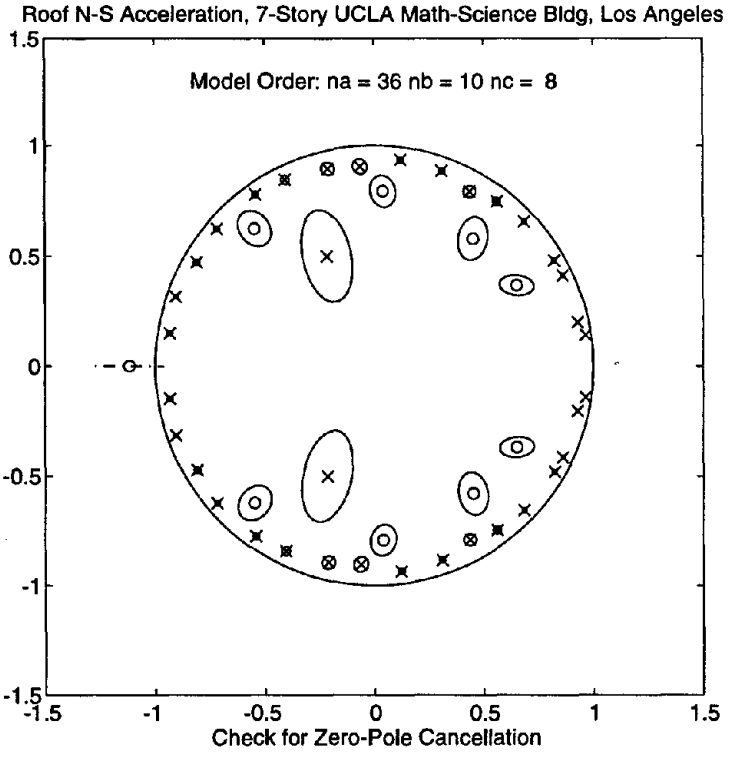

Figure C.1.7. Zero-pole cancellation for autoregressive model in N-S direction.

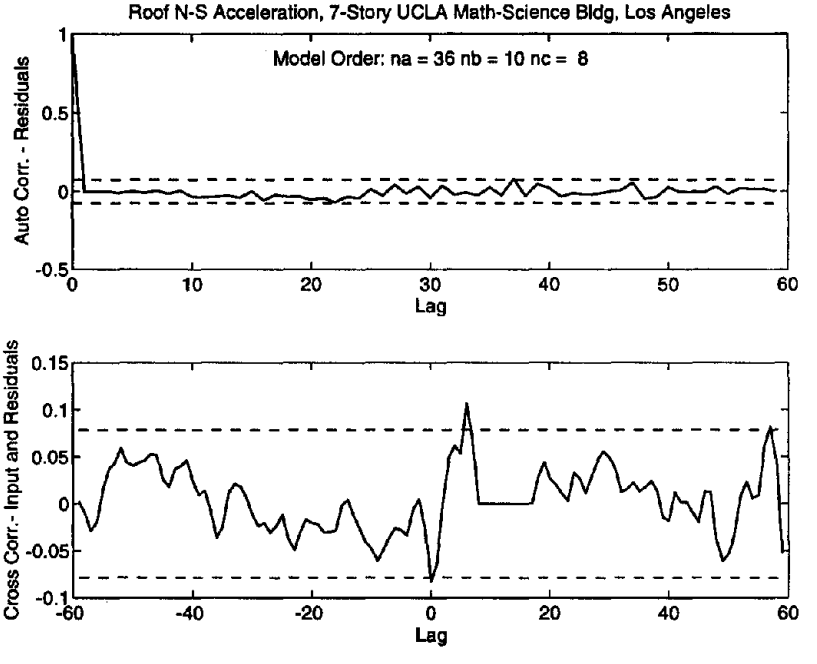

Figure C.1.8. Residuals for autoregressive model in N-S direction.

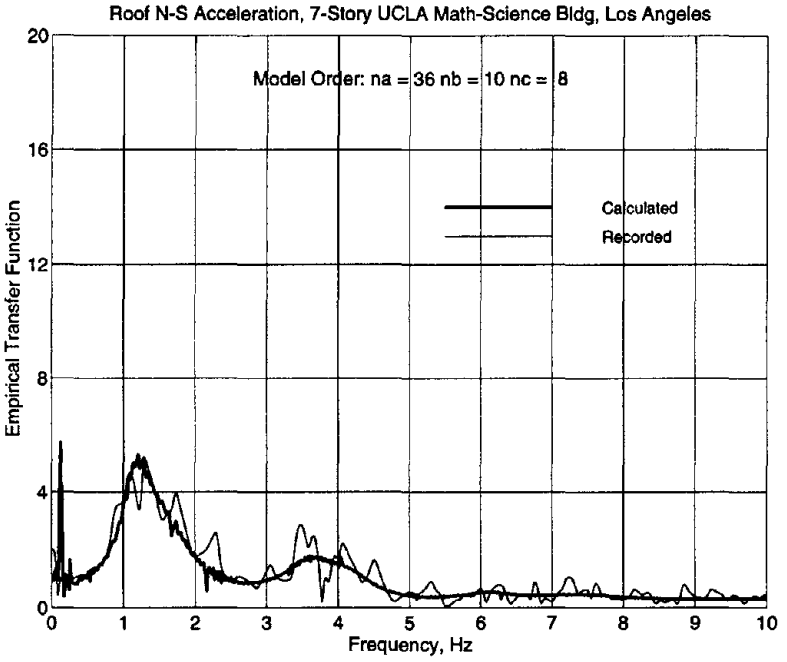

Figure C.1.9. Comparison of empirical transfer functions: recorded motion and calculated motion of autoregressive model in N-S direction.

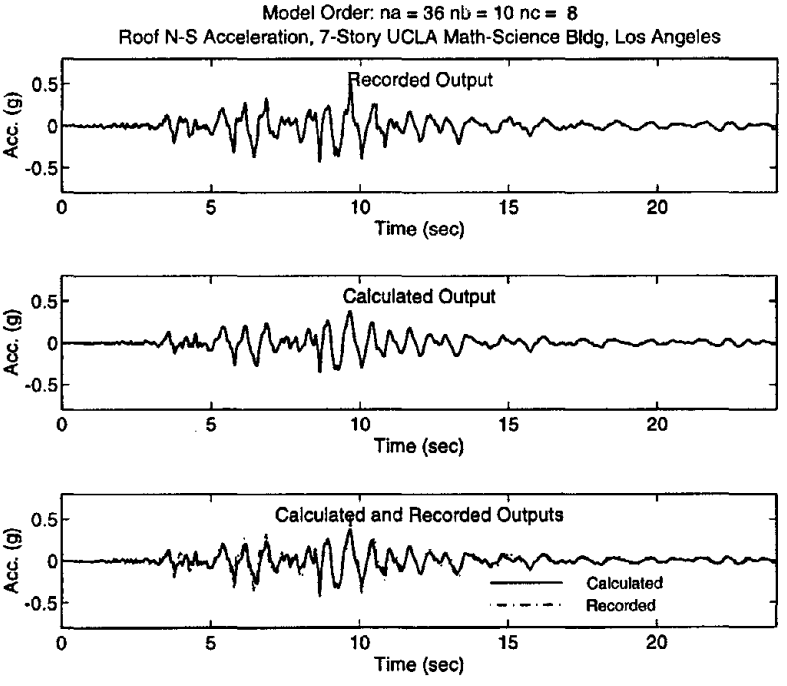

Figure C.1.10. Comparison of time-histories: recorded motion and calculated motion of autoregressive model in N-S direction.

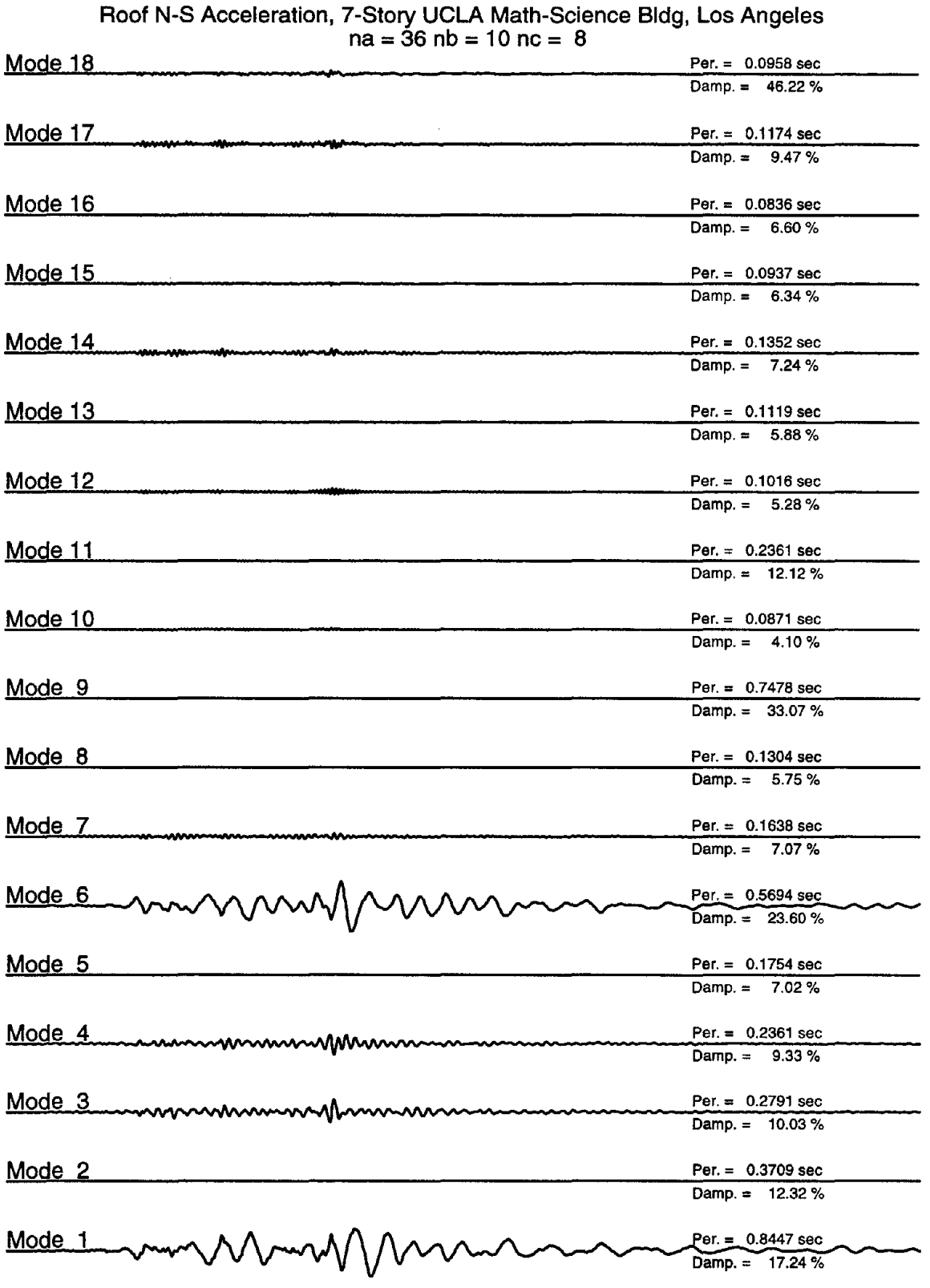

Figure C.1.11. Modal contributions of autoregressive model in N-S direction.

2. Burbank - 10-Story Residential Building, CSMIP Station No. 24385

No. of Stories above/below ground: 10/0
Plan Shape: Rectangular
Base Dimensions: 215' x 75'
Typical Floor Dimensions: 215' x 75'
Design Date: 1974
Construction Date: 1974

Vertical Load Carrying System:
Precast and poured-in-place concrete floor slabs supported by precast concrete bearing walls.
Lateral Force Resisting System:
Precast concrete shear walls in both directions.
Foundation Type:
Concrete caissons (25' to 35' deep).

Figure C.2.1a. Details of 10-story residential building, CSMIP Station No. 24385

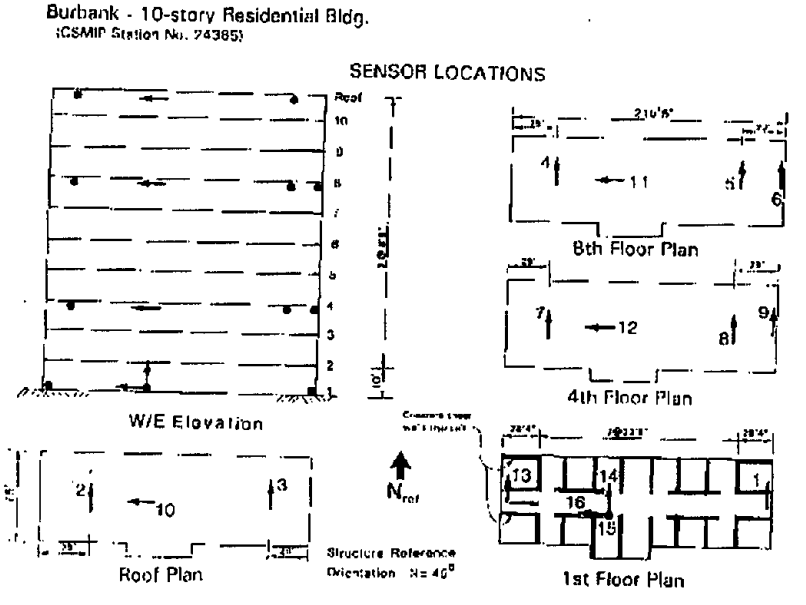

Figure C.2.1b. Sensor locations in 10-story residential building, CSMIP Station No. 24385

Table C.2.1 Results of system identification in E-W (longitudinal) direction by autoregressive modeling.

j	Frequency (Hz)	Period (sec)	Damping	Pole Magnitude	Comments
1	1.673	0.598	0.056	0.988	1st Mode
2	1.673	0.598	0.056	0.988	
3	7.199	0.139	0.073	0.936	2nd Mode
4	7.199	0.139	0.073	0.936	
5	3.147	0.318	0.290	0.892	
6	3.147	0.318	0.290	0.892	
7	9.995	0.100	0.094	0.888	
8	9.995	0.100	0.094	0.888	
9	6.263	0.160	0.162	0.880	
10	6.263	0.160	0.162	0.880	
11	12.029	0.083	0.128	0.824	
12	12.029	0.083	0.128	0.824	
13	9.212	0.109	0.174	0.818	
14	9.212	0.109	0.174	0.818	
15	5.127	0.195	0.502	0.724	
16	5.127	0.195	0.502	0.724	
17	9.538	0.105	0.514	0.540	
18	9.538	0.105	0.514	0.540	

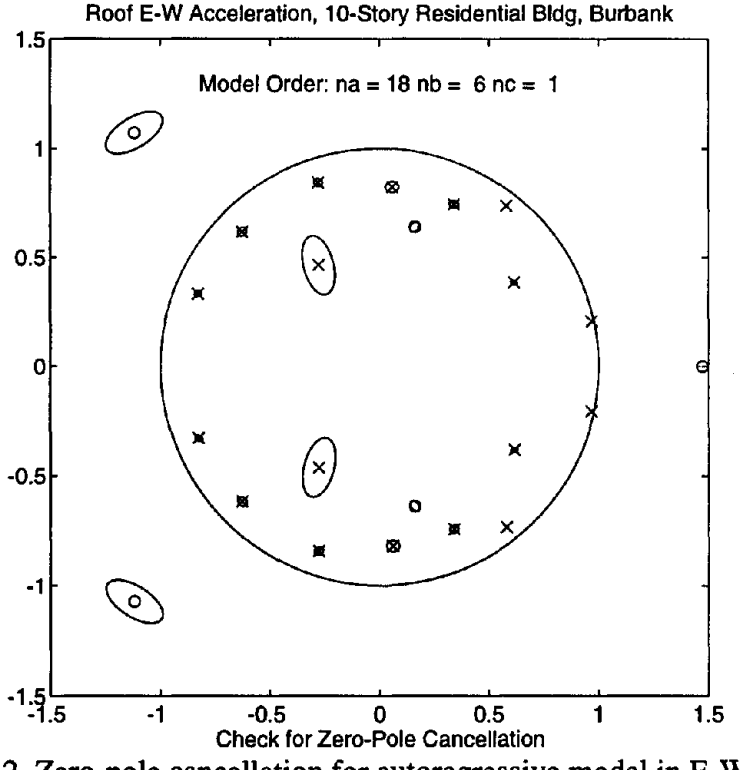

Figure C.2.2. Zero-pole cancellation for autoregressive model in E-W direction.

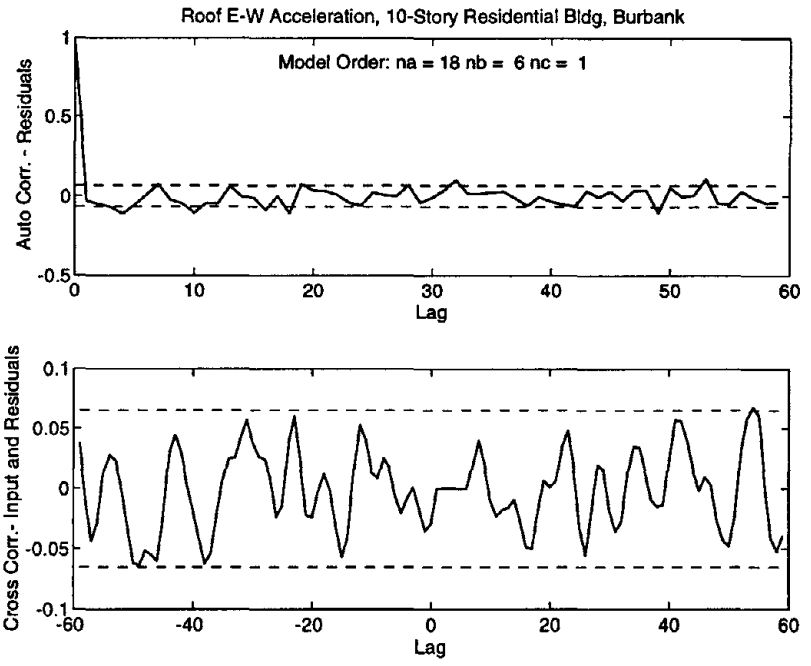

Figure C.2.3. Residuals for autoregressive model in E-W direction.

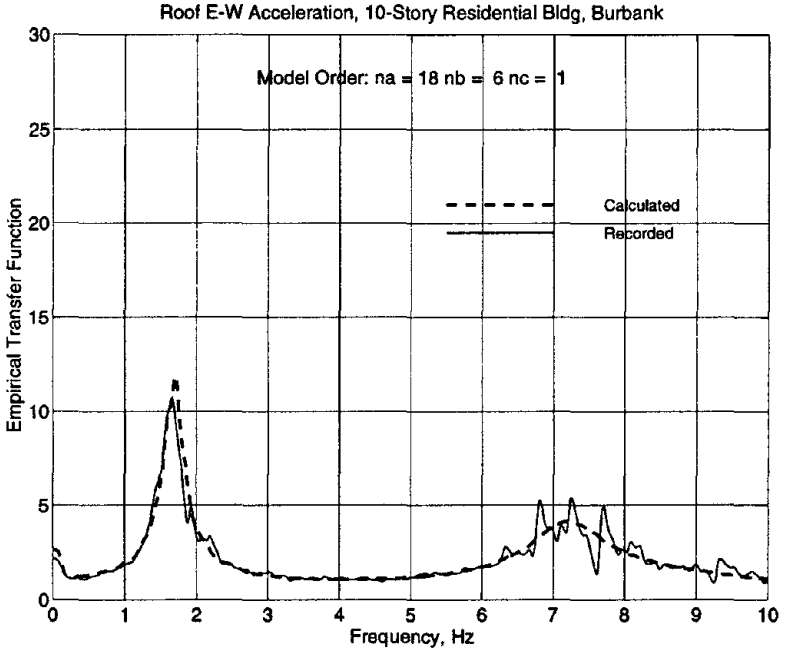

Figure C.2.4. Comparison of empirical transfer functions: recorded motions and calculated motions of autoregressive model in E-W direction.

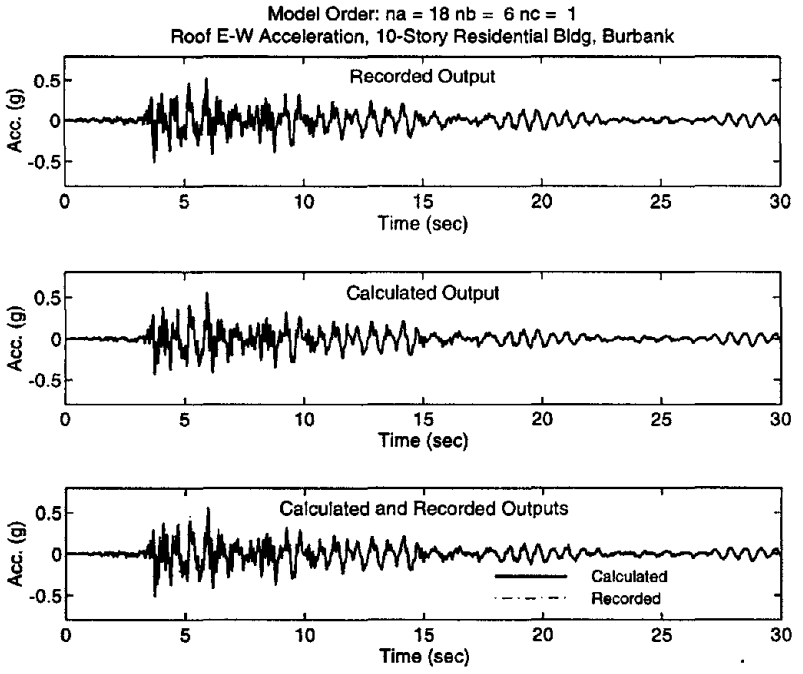

Figure C.2.5. Comparison of time-histories: recorded motions and calculated motions of autoregressive model in E-W direction.

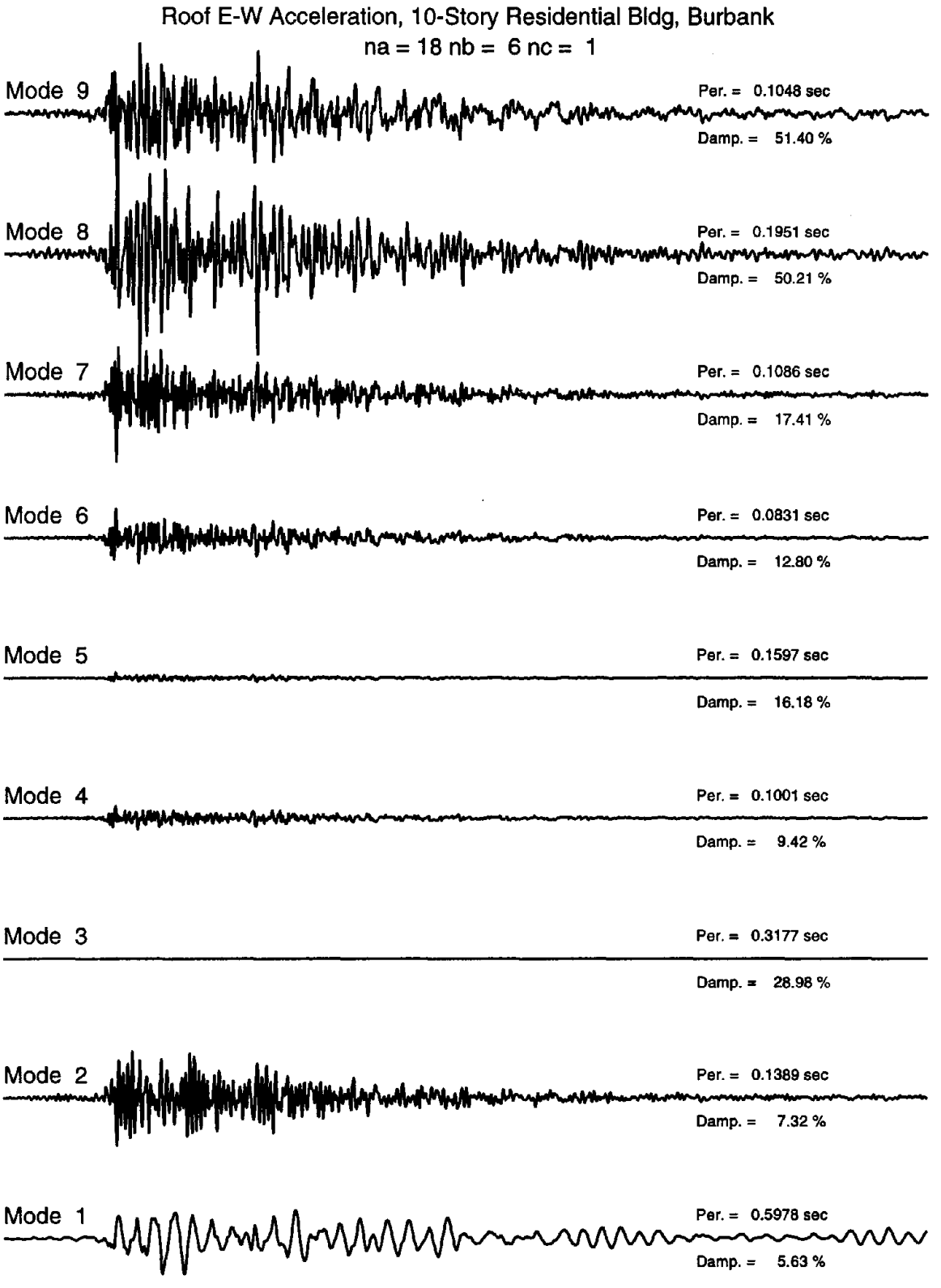

Figure C.2.6. Modal contributions of autoregressive model in E-W direction.

Table C.2.2 Results of system identification in N-S (transverse) direction by autoregressive modeling.

j	Frequency (Hz)	Period (sec)	Damping	Pole Magnitude	Comments
1	1.789	0.559	0.075	0.983	1st Mode*
2	1.789	0.559	0.075	0.983	
3	7.619	0.131	0.082	0.924	2nd Mode
4	7.619	0.131	0.082	0.924	
5	10.474	0.096	0.062	0.922	
6	10.474	0.096	0.062	0.922	
7	2.977	0.336	0.338	0.881	
8	2.977	0.336	0.338	0.881	
9	5.492	0.182	0.205	0.868	
10	5.492	0.182	0.205	0.868	
11	11.376	0.088	0.105	0.861	
12	11.376	0.088	0.105	0.861	
13	8.494	0.118	0.155	0.848	
14	8.494	0.118	0.155	0.848	
15	3.664	0.273	0.486	0.800	
16	3.664	0.273	0.486	0.800	
17	7.554	0.132	0.297	0.755	
18	7.554	0.132	0.297	0.755	

* Mode not used due to poor match in empirical transfer function

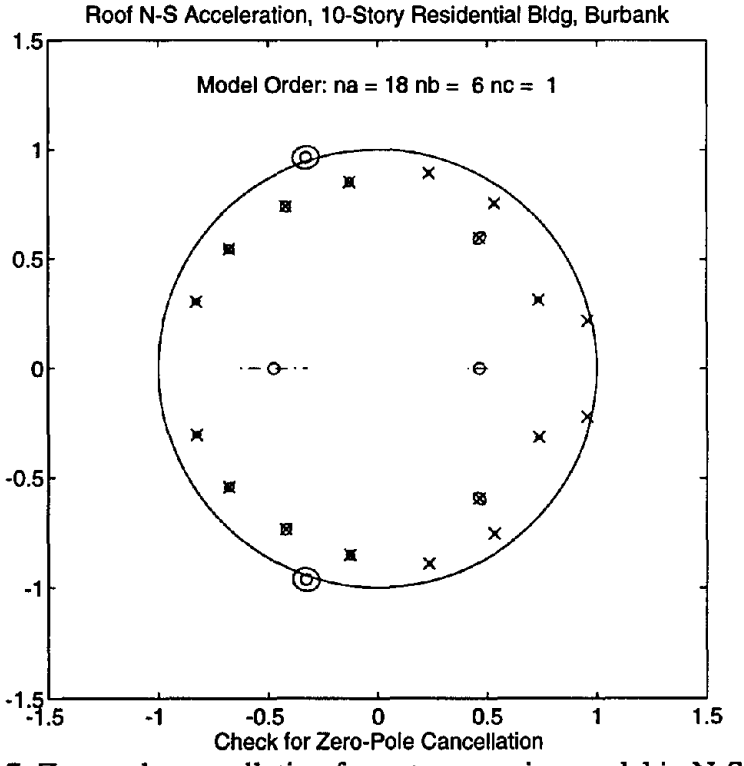

Figure C.2.7. Zero-pole cancellation for autoregressive model in N-S direction.

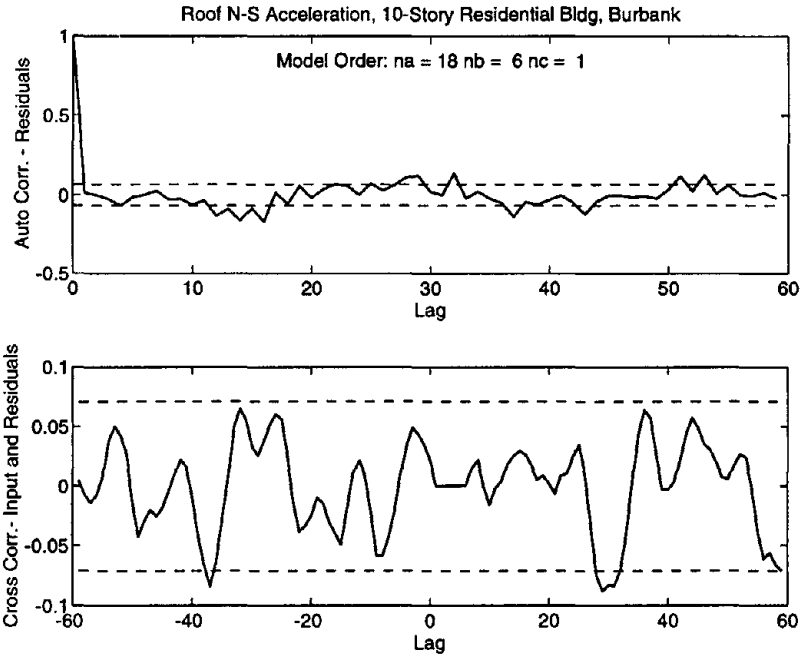

Figure C.2.8. Residuals for autoregressive model in N-S direction.

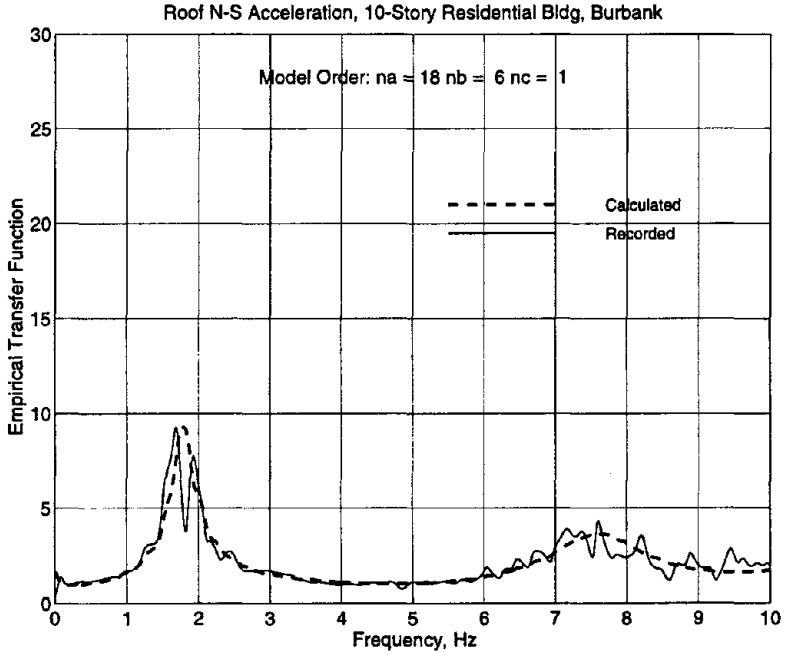

Figure C.2.9. Comparison of empirical transfer functions: recorded motions and calculated motions of autoregressive model in N-S direction.

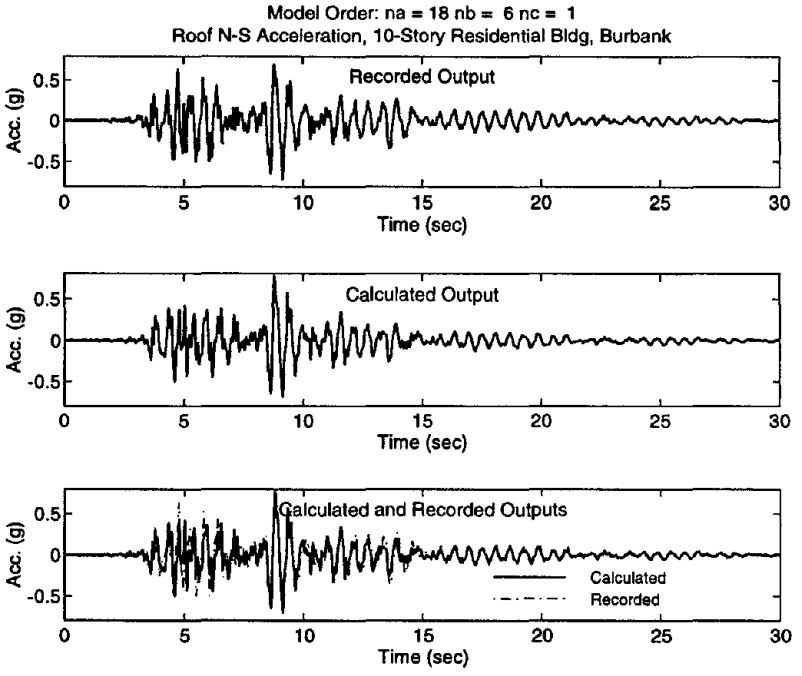

Figure C.2.10. Comparison of time-histories: recorded motions and calculated motions of autoregressive model in N-S direction.

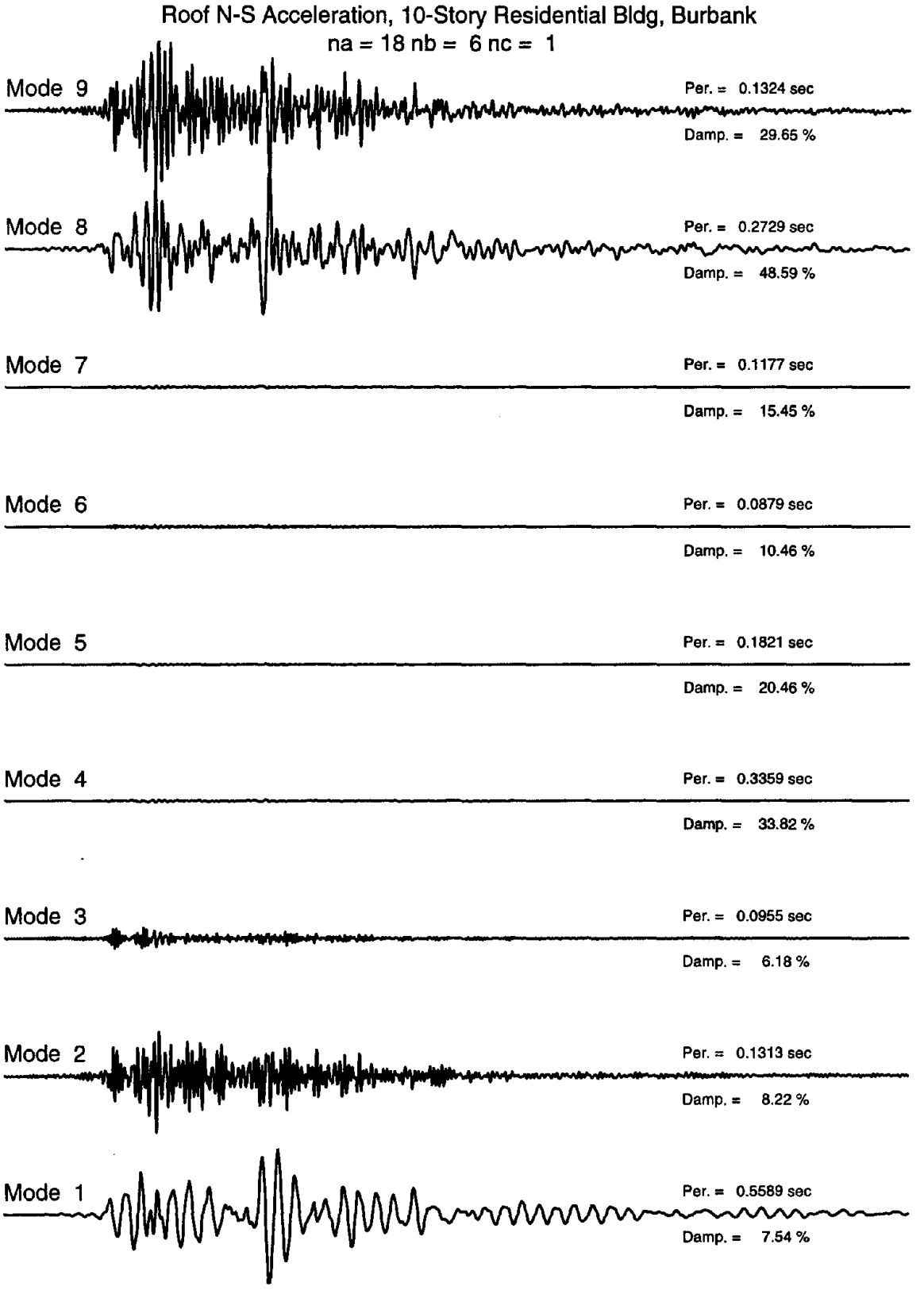

Figure C.2.11. Modal contributions of autoregressive model in N-S direction.

Table C.2.3. Results of system identification in N-S (transverse) direction by WPCMIMO.

Mode No.	Frequency (Hz)	Damping	Part. Factor	Initial Disp.	Initial Velo.	Modal Cont.	Comments
1	1.4379	0.016	7.06E-02	-6.74E-03	5.66E-02	1.28E-02	
2	1.7393	0.026	-2.58E-01	-3.14E-02	7.24E-02	1.55E-01	
3	1.8023	0.133	-1.73E-00	5.33E-02	-4.04E-01	7.24E-01	1st Tran. Mode*
4	1.8497	0.011	-3.55E-03	2.49E-03	2.48E-01	1.75E-01	1st Tor. Mode
5	7.5531	0.015	2.40E-02	-6.03E-06	-4.05E-05	5.23E-03	
6	8.1820	0.183	2.49E-01	1.75E-04	2.64E-02	4.85E-02	
7	10.0890	0.576	-1.05E-00	3.53E-03	-1.74E-01	1.16E-01	
8	12.3968	0.894	2.59E-00	-3.03E-03	9.94E-02	8.42E-02	
9	22.6437	0.098	4.14E-02	1.66E-05	2.10E-04	9.10E-05	

* Damping is not reliable

Relative Error = 0.223 and Absolute Error = 2.406

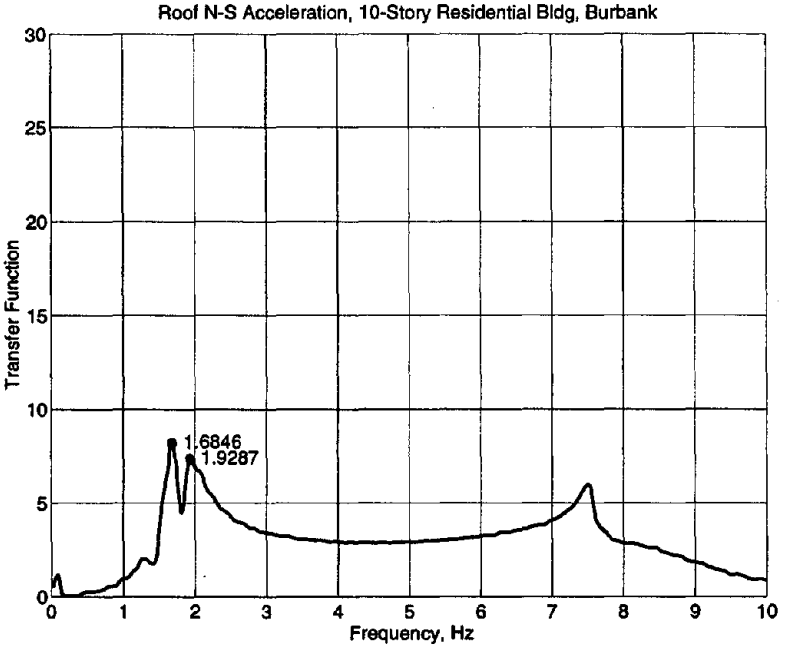

Figure C.2.12. Initial frequency estimates from transfer function in N-S direction.

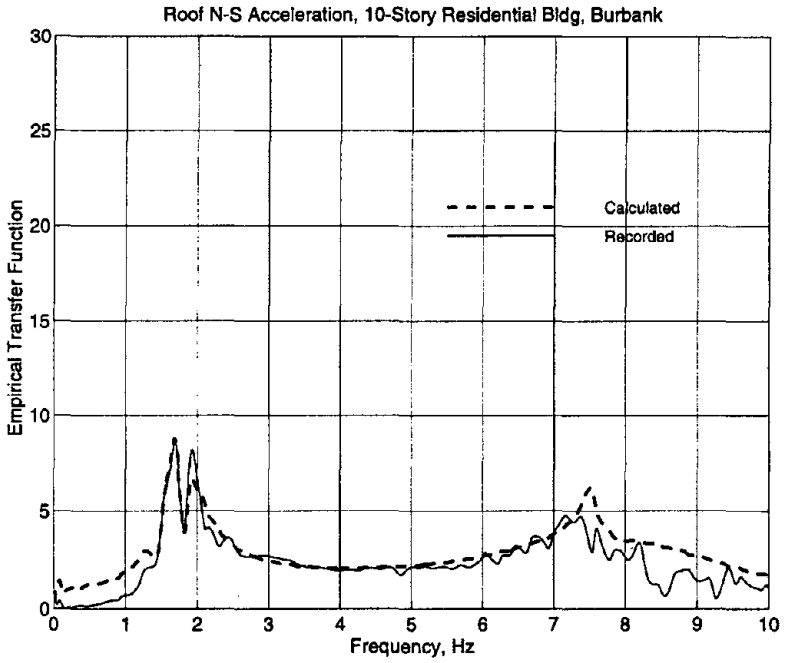

Figure C.2.13. Comparison of empirical transfer functions: recorded motions and calculated motions from WPCMIMO in N-S direction.

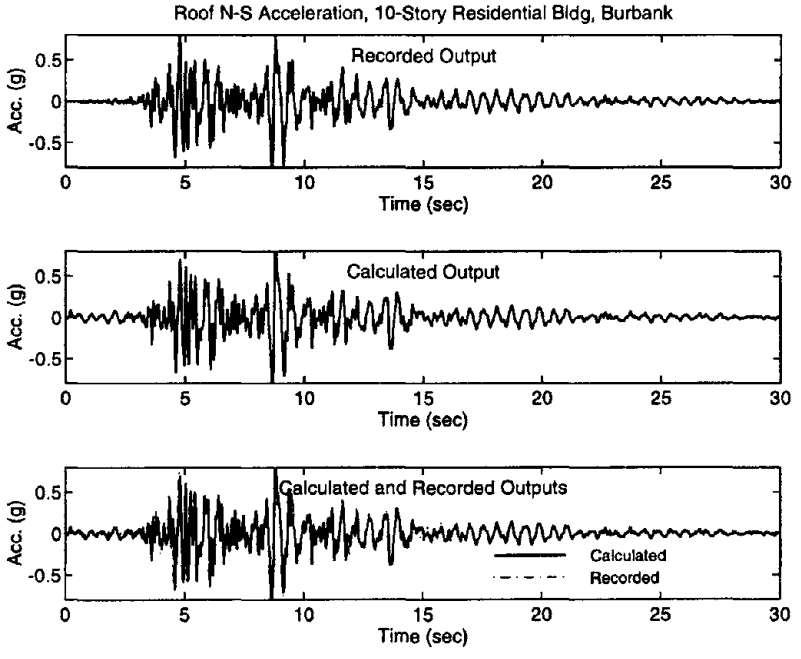

Figure C.2.14. Comparison of time-histories: recorded motions and calculated motions from WPCMIMO in N-S direction.

3. Sylmar - 6-Story County Hospital, CSMIP Station No. 24514

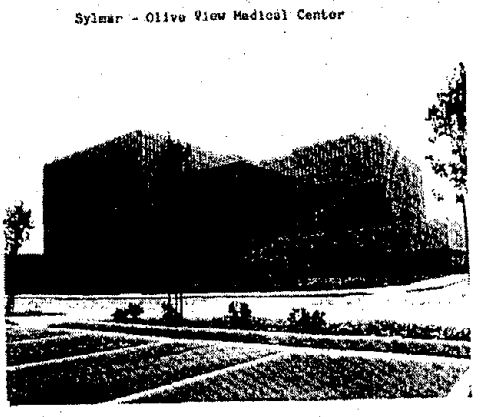

Address: 14445 Olive View Drive
Sylmar, CA
No. of Stories above/below ground: 6/0
Plan Shape:
Rectangular(lower 2 stories)
Cross-shaped(upper 4 stories)
Base Dimensions: 452' x 302'
Typical Floor Dimensions: 101' x 302'
Design Date: 1976
Construction Date: 1977-86

Vertical Load Carrying System:
Concrete slabs over metal deck supported by steel frame.
Lateral Force Resisting System:
Concrete shear walls on lower 2 stories, steel shear walls on the perimeter of upper 4 stories.
Foundation Type:
Spread footings.

Figure C.3.1a. Details of 6-story county hospital, CSMIP Station No. 24514

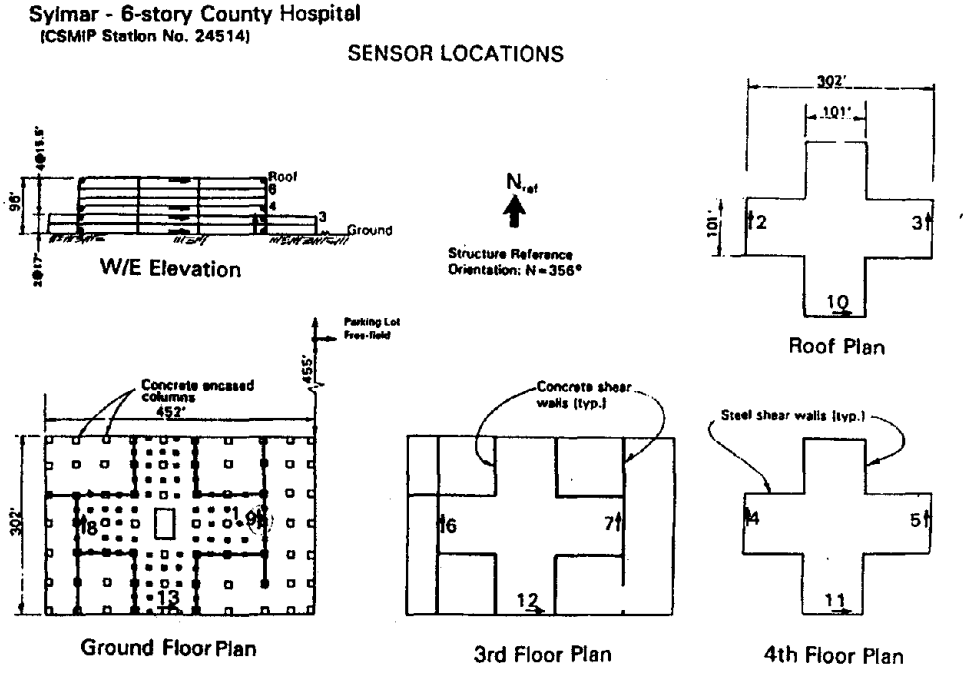

Figure C.3.1b. Sensor locations in 6-story county hospital, CSMIP Station No. 24514

Table C.3.1. Results of system identification in E-W (longitudinal) direction by WPCMIMO.

Mode No.	Frequency (Hz)	Damping	Part. Factor	Initial Disp.	Initial Velo.	Modal Cont.	Comments
1	2.8439	0.057	-1.67E-01	4.39E-04	-4.17E-02	1.96E-01	1st Mode
2	3.3200	0.088	-1.44E-01	-3.85E-03	3.11E-02	1.08E-01	
3	5.1094	0.020	-3.88E-02	5.65E-05	8.66E-03	7.01E-02	
4	6.0289	0.111	-7.94E-02	1.84E-04	2.27E-02	2.79E-02	
5	3.9917	0.011	2.60E-02	2.63E-04	6.78E-03	3.64E-02	
6	4.5870	0.009	-1.76E-02	-5.24E-05	6.25E-03	2.90E-02	
7	7.5857	0.003	1.37E-02	6.81E-05	2.22E-03	1.37E-02	
8	7.9046	0.005	4.43E-03	2.03E-05	-7.73E-03	4.17E-03	
9	6.9689	0.002	1.97E-03	1.98E-04	4.66E-04	1.20E-02	

Relative Error = 0.657 and Absolute Error = 7.180

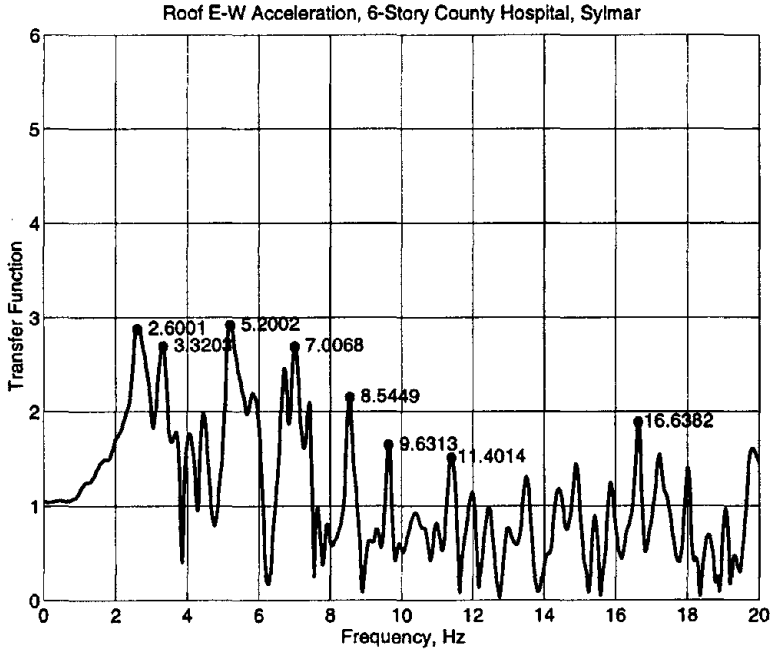

Figure C.3.2. Initial frequency estimates from transfer function in E-W direction.

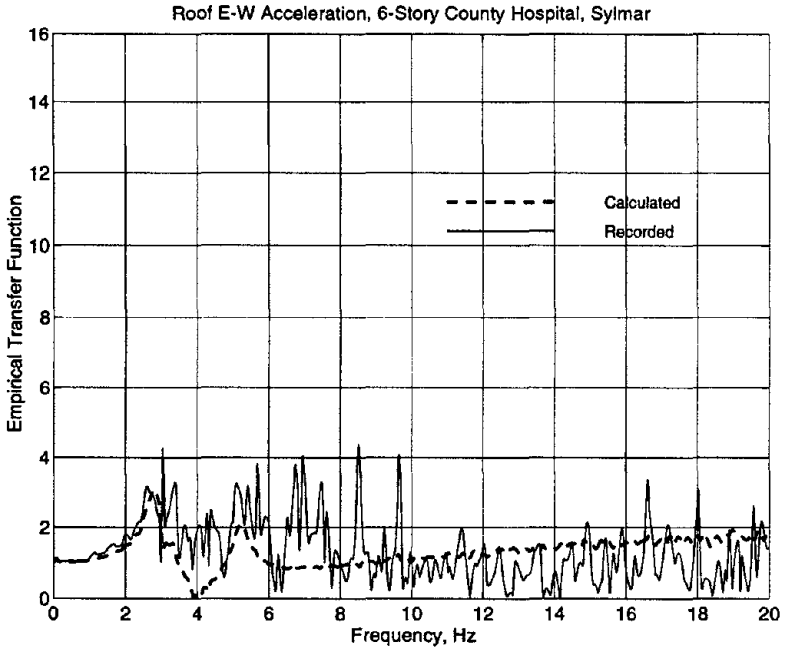

Figure C.3.3. Comparison of empirical transfer functions: recorded motions and calculated motions from WPCMIMO in E-W direction.

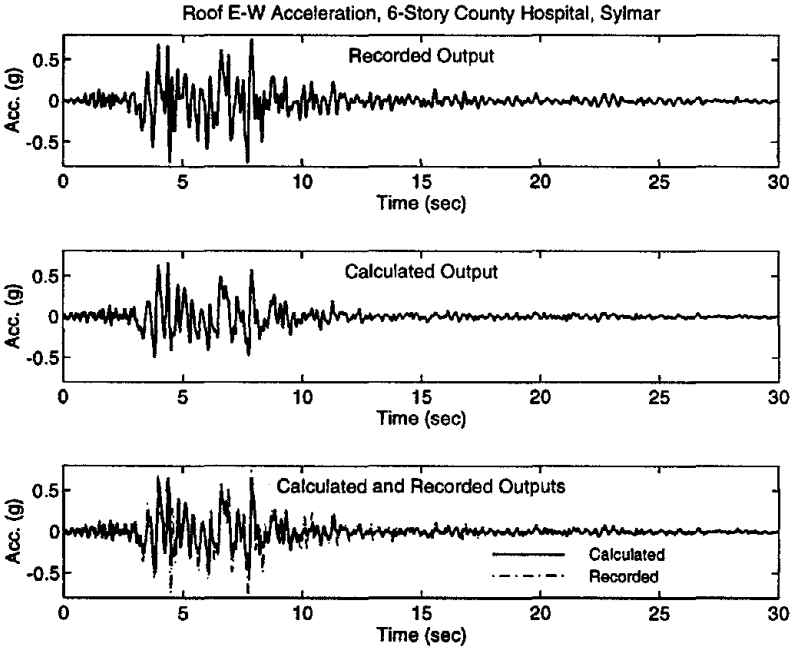

Figure C.3.4. Comparison of time-histories: recorded motions and calculated motions from WPCMIMO in E-W direction.

Table C.3.2. Results of system identification in N-S (longitudinal) direction by WPCMIMO.

Mode No.	Frequency (Hz)	Damping	Part. Factor	Initial Disp.	Initial Velo.	Modal Cont.	Comments
1	2.5134	0.045	-2.07E-01	3.36E-03	-2.51E-02	3.29E-01	1st Mode
2	2.8562	0.124	-3.24E-01	-5.45E-03	-2.61E-02	2.87E-01	
3	7.2613	0.039	4.66E-02	1.61E-04	-2.11E-02	1.26E-02	
4	7.7771	0.010	1.33E-02	-2.96E-04	4.79E-04	4.71E-03	
5	0.7825	0.900	1.56E-00	-7.50E-03	2.46E-02	2.11E-02	
6	7.0997	0.266	-2.74E-01	-5.52E-04	-1.89E-02	4.51E-02	
7	8.1373	0.230	1.13E-01	-4.98E-04	6.23E-02	1.02E-02	
8	13.1001	0.696	1.10E-01	-2.07E-04	3.68E-02	2.59E-03	

Relative Error = 0.343 and Absolute Error = 4.751

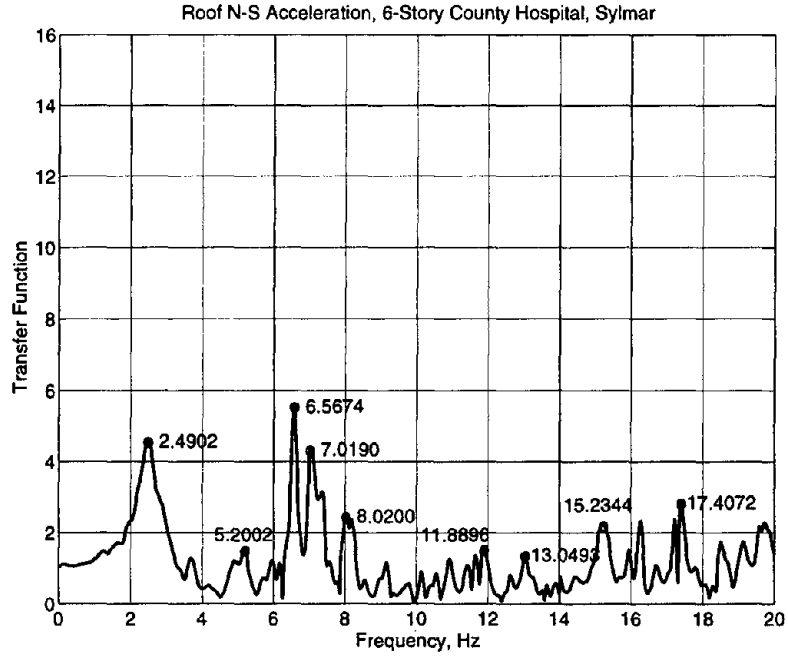

Figure C.3.5. Initial frequency estimates from transfer function in N-S direction.

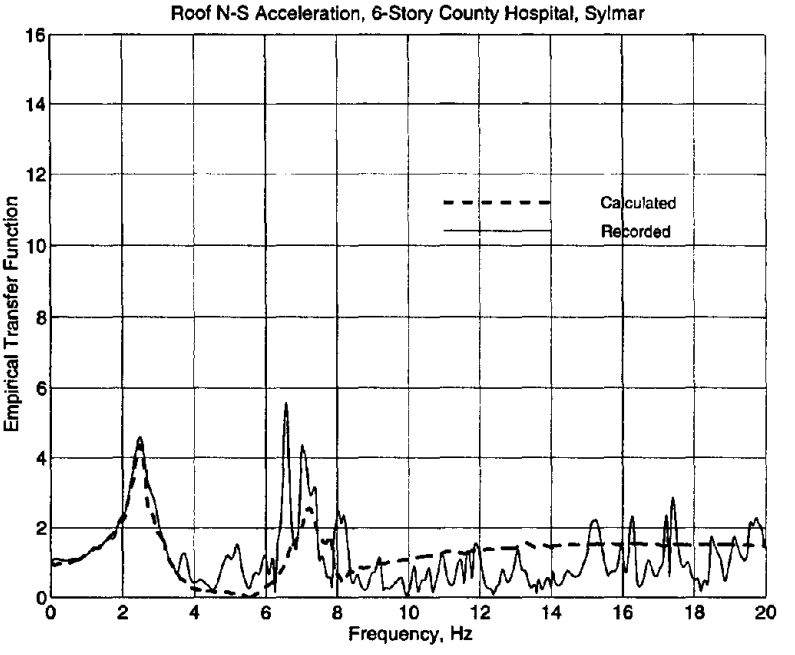

Figure C.3.6. Comparison of empirical transfer functions: recorded motions and calculated motions from WPCMIMO in N-S direction.

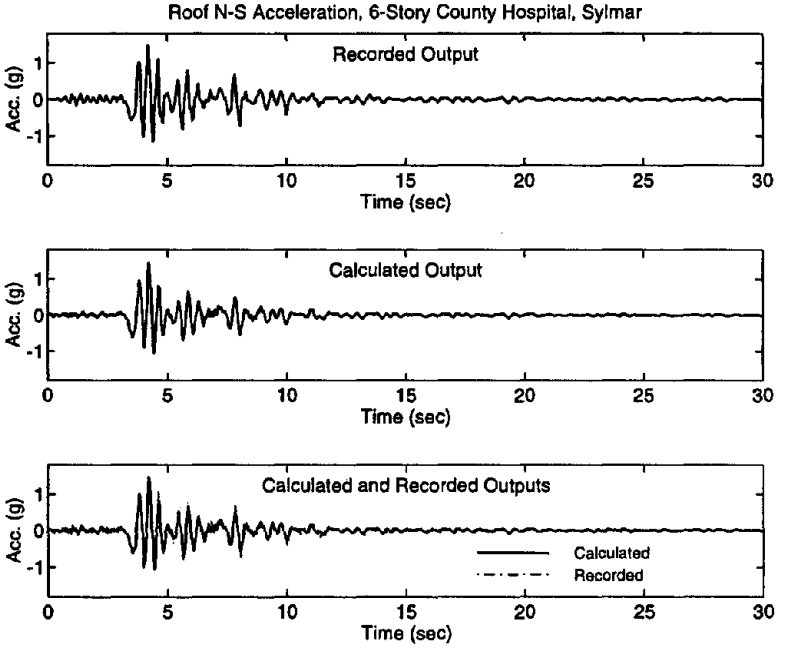

Figure C.3.7. Comparison of time-histories: recorded motions and calculated motions from WPCMIMO in N-S direction.

4. Burbank - 6-Story Commercial Building, CSMIP Station No. 24370

No. of Stories above/below ground: 6/0
Plan Shape: Rectangular
Base Dimensions: 120' x 120'
Typical Floor Dimensions: 120' x 120'
Design Date: 1976
Construction Date: 1977

Vertical Load Carrying System:
3" concrete slab over metal deck supported by steel frames.
Lateral Force Resisting System:
Perimeter moment resisting steel frames.
Foundation Type:
Concrete caissons (approx. 32' deep).

Figure C.4.1a. Details of 6-story commercial building, CSMIP Station No. 24370

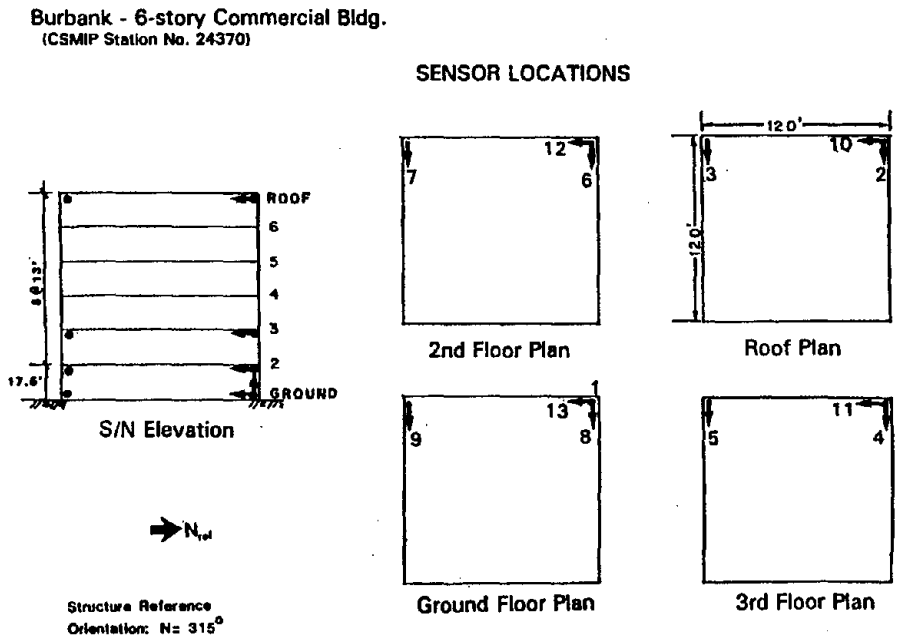

Figure C.4.1b. Sensor locations in 6-story commercial building, CSMIP Station No. 24370

Table C.4.1. Results of system identification in E-W (longitudinal) direction by autoregressive modeling.

j	Frequency (Hz)	Period (sec)	Damping	Pole Magnitude	Comments
1	4.558	1.378	0.041	0.996	1st Mode
2	4.558	1.378	0.041	0.996	
3	13.525	0.465	0.065	0.983	2nd Mode
4	13.525	0.465	0.065	0.983	
5	10.668	0.589	0.166	0.965	
6	10.668	0.589	0.166	0.965	
7	24.553	0.256	0.073	0.965	
8	24.553	0.256	0.073	0.965	
9	34.228	0.184	0.061	0.959	
10	34.228	0.184	0.061	0.959	
11	38.662	0.163	0.064	0.952	
12	38.662	0.163	0.064	0.952	
13	64.509	0.097	0.041	0.948	
14	64.509	0.097	0.041	0.948	
15	18.997	0.331	0.148	0.946	
16	18.997	0.331	0.148	0.946	
17	29.556	0.213	0.112	0.936	
18	29.556	0.213	0.112	0.936	
19	52.053	0.121	0.065	0.935	
20	52.053	0.121	0.065	0.935	
21	52.023	0.121	0.066	0.933	
22	52.023	0.121	0.066	0.933	
23	60.611	0.104	0.066	0.923	
24	60.611	0.104	0.066	0.923	
25	43.751	0.144	0.092	0.922	
26	43.751	0.144	0.092	0.922	
27	74.606	0.084	0.059	0.916	
28	74.606	0.084	0.059	0.916	
29	72.439	0.087	0.080	0.890	
30	72.439	0.087	0.080	0.890	

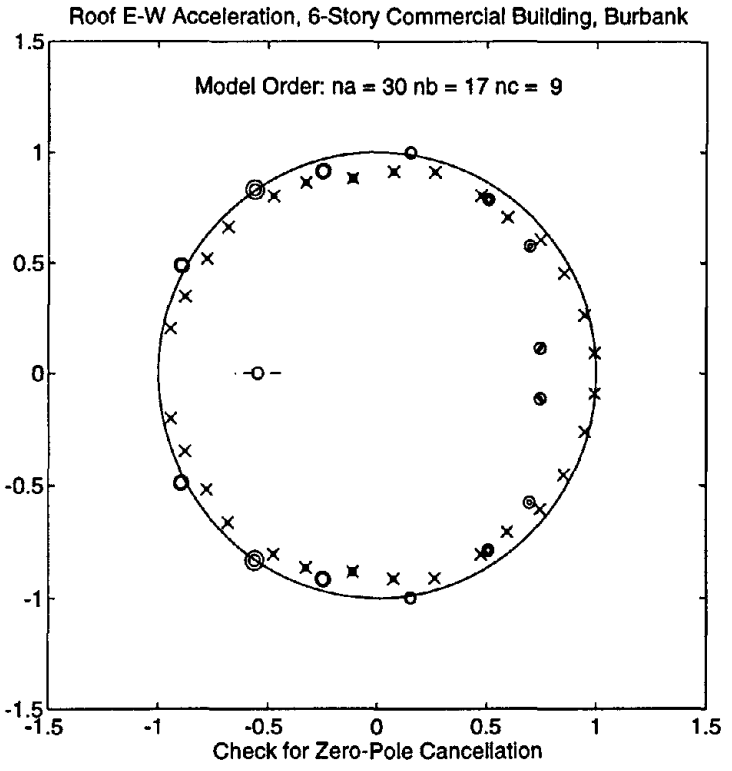

Figure C.4.2. Zero-pole cancellation for autoregressive model in E-W direction.

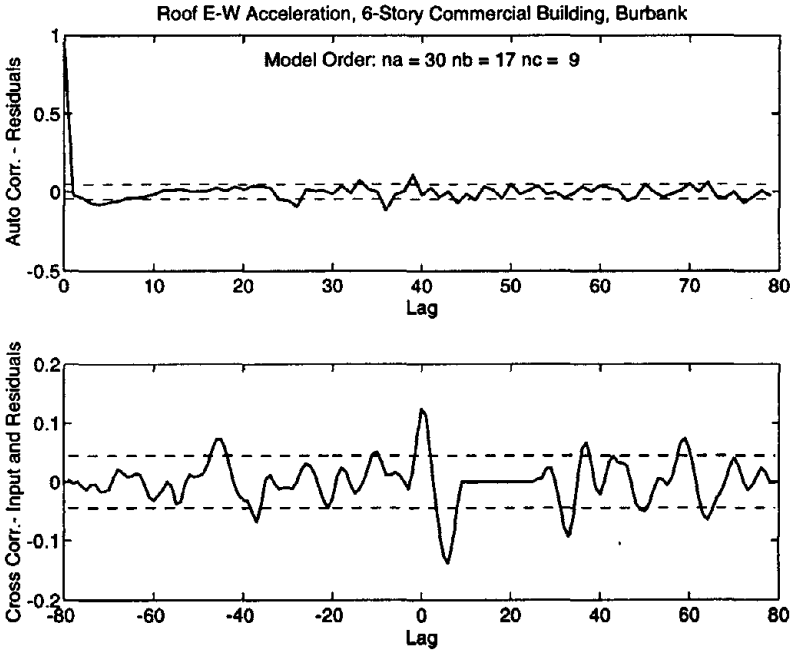

Figure C.4.3. Residuals for autoregressive model in E-W direction.

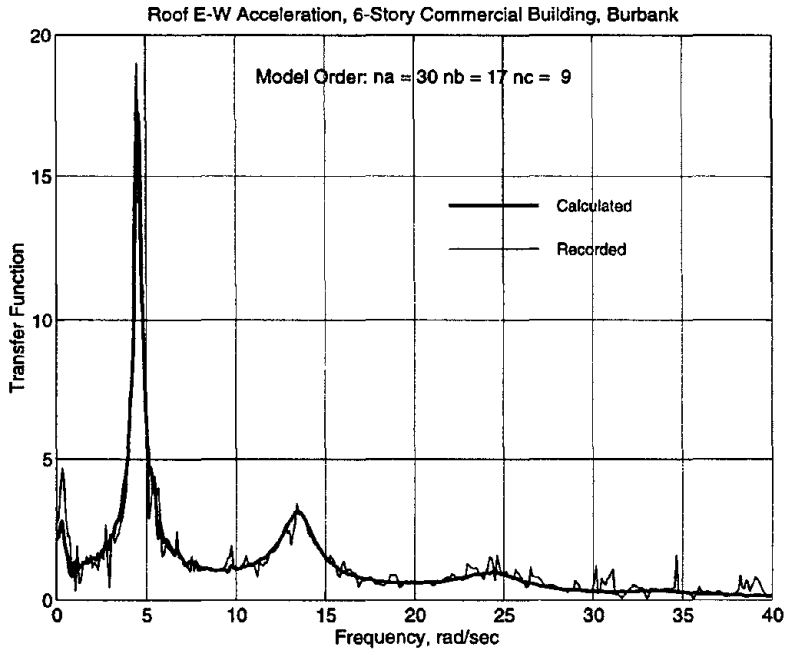

Figure C.4.4. Comparison of empirical transfer functions: recorded motions and calculated motions of autoregressive model in E-W direction.

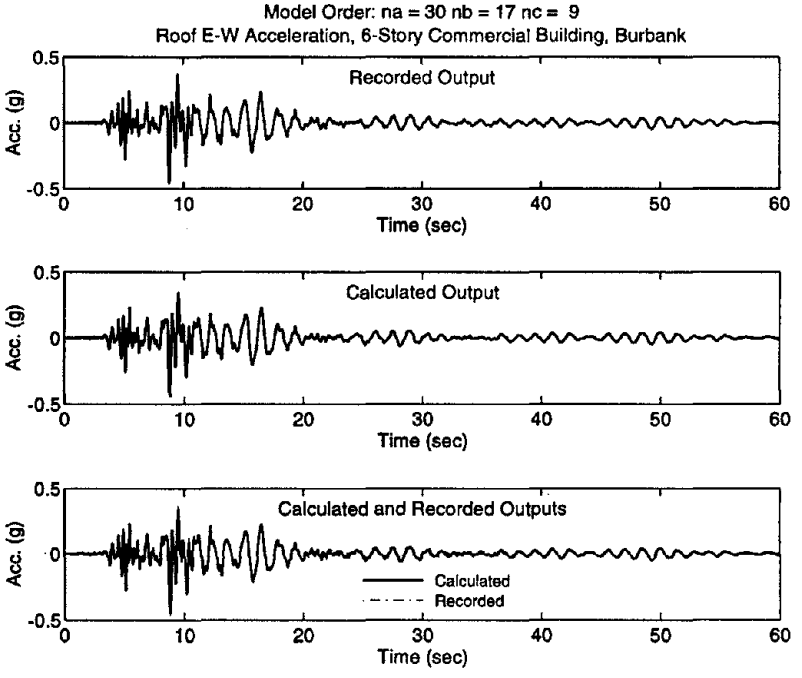

Figure C.4.5. Comparison of time-histories: recorded motions and calculated motions of autoregressive model in E-W direction.

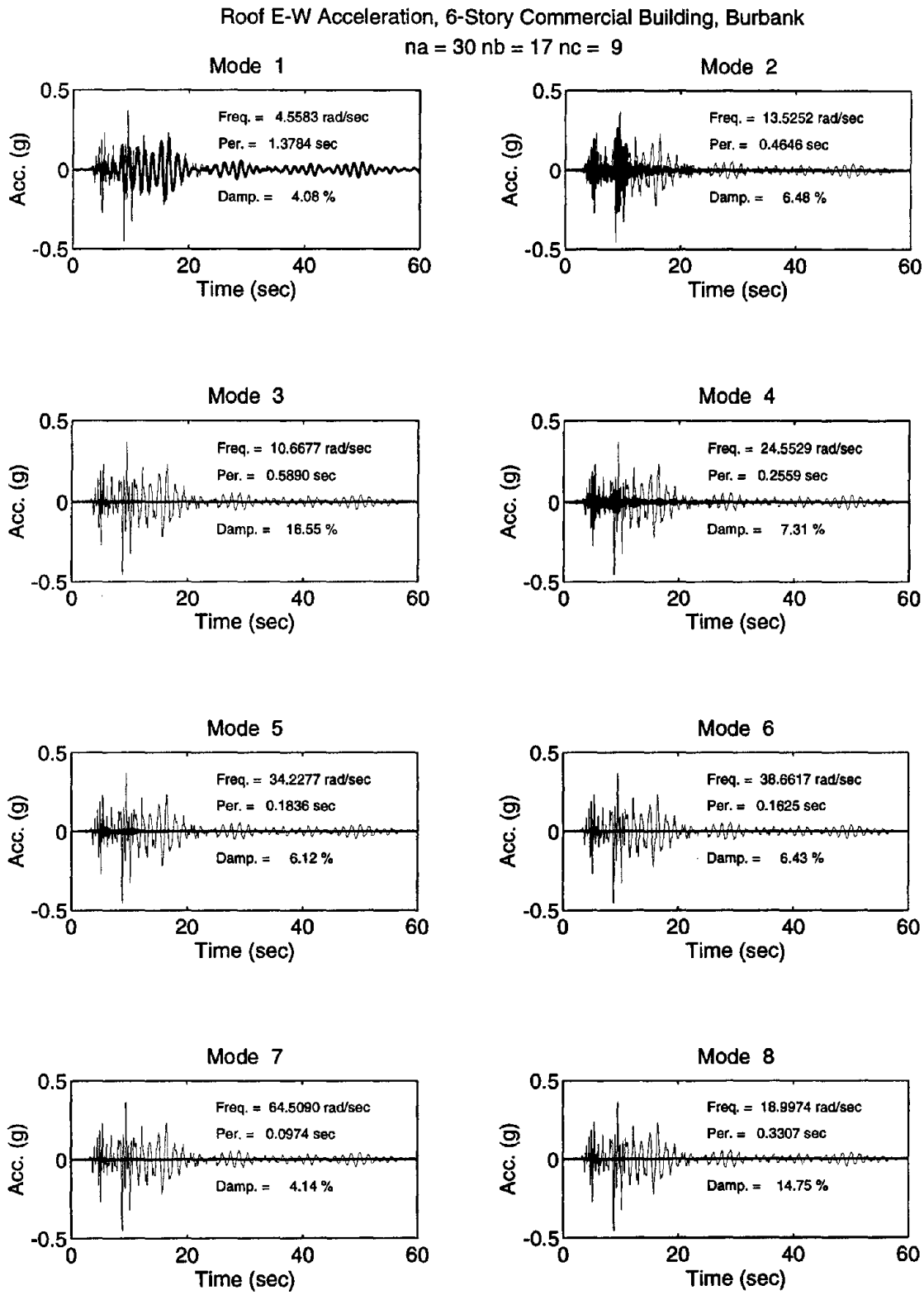

Figure C.4.6. Modal contributions of autoregressive model in E-W direction; modes 1 to 8.

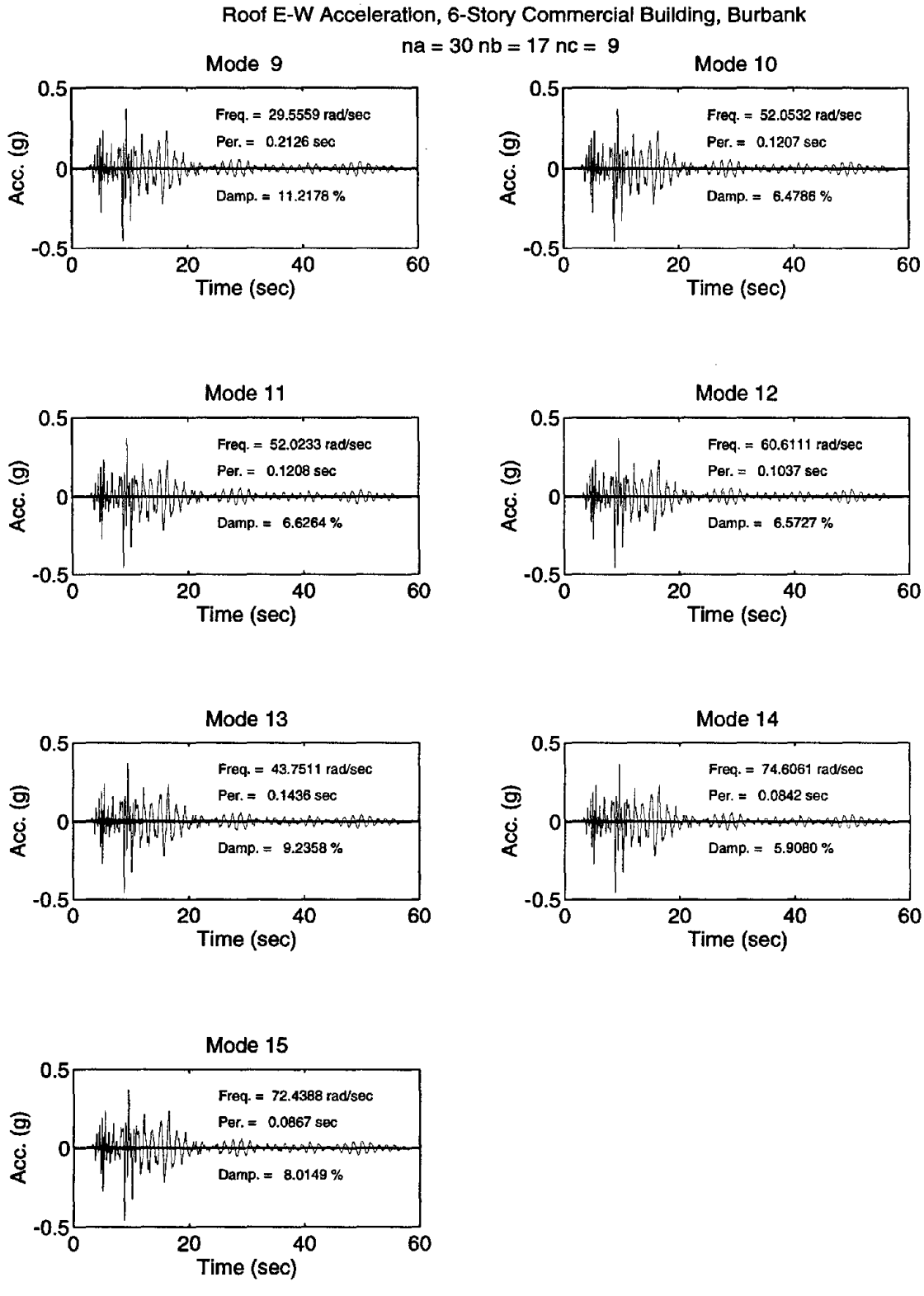

Figure C.4.7. Modal contributions of autoregressive model in E-W direction; modes 9 to 16.

Table C.4.2. Results of system identification in N-S (longitudinal) direction by autoregressive modeling.

j	Frequency (Hz)	Period (sec)	Damping	Pole Magnitude	Comments
1	4.607	1.364	0.040	0.996	1st Mode
2	4.607	1.364	0.040	0.996	
3	13.475	0.466	0.053	0.986	2nd Mode
4	13.475	0.466	0.053	0.986	
5	36.071	0.174	0.043	0.969	
6	36.071	0.174	0.043	0.969	
7	23.180	0.271	0.094	0.957	
8	23.180	0.271	0.094	0.957	
9	18.357	0.342	0.127	0.954	
10	18.357	0.342	0.127	0.954	
11	9.871	0.637	0.239	0.954	
12	9.871	0.637	0.239	0.954	
13	71.118	0.088	0.036	0.950	
14	71.118	0.088	0.036	0.950	
15	59.051	0.106	0.054	0.938	
16	59.051	0.106	0.054	0.938	
17	64.668	0.097	0.051	0.937	
18	64.668	0.097	0.051	0.937	
19	47.817	0.131	0.069	0.937	
20	47.817	0.131	0.069	0.937	
21	27.343	0.230	0.121	0.936	
22	27.343	0.230	0.121	0.936	
23	36.592	0.172	0.101	0.929	
24	36.592	0.172	0.101	0.929	
25	74.201	0.085	0.053	0.924	
26	74.201	0.085	0.053	0.924	
27	56.639	0.111	0.071	0.922	
28	56.639	0.111	0.071	0.922	
29	48.909	0.129	0.090	0.916	
30	48.909	0.129	0.090	0.916	
31	31.807	0.198	0.184	0.890	
32	31.807	0.198	0.184	0.890	

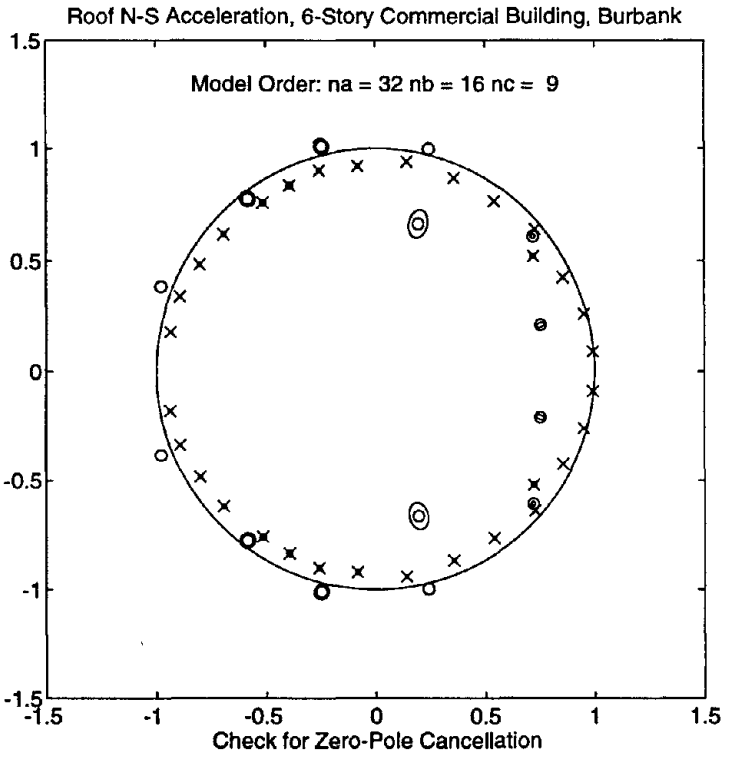

Figure C.4.8. Zero-pole cancellation for autoregressive model in N-S direction.

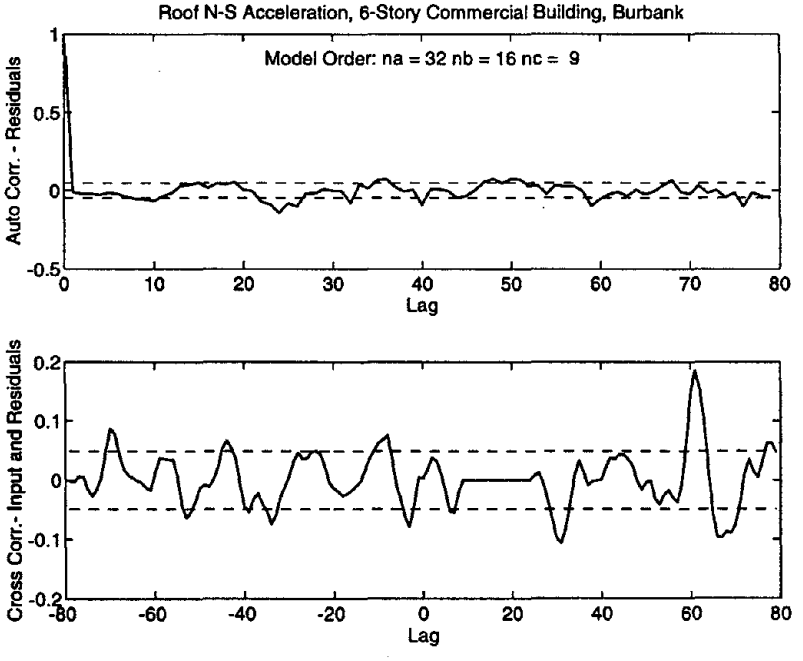

Figure C.4.9. Residuals for autoregressive model in N-S direction.

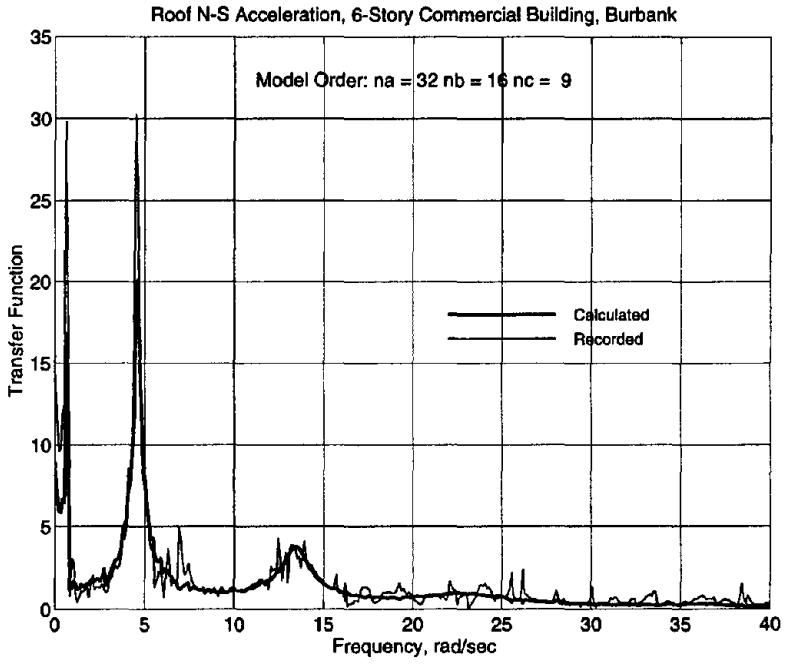

Figure C.4.10. Comparison of empirical transfer functions: recorded motions and calculated motions of autoregressive model in N-S direction.

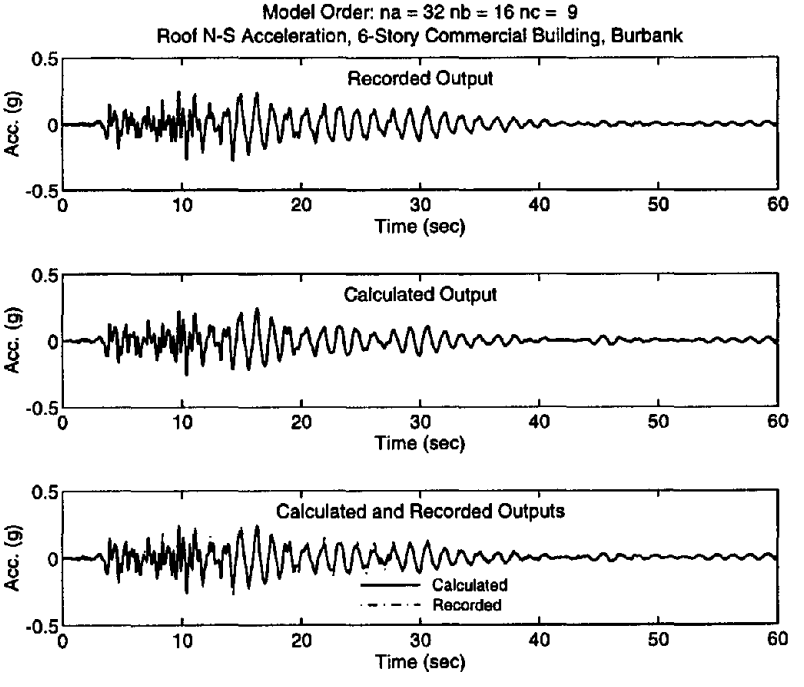

Figure C.4.11. Comparison of time-histories: recorded motions and calculated motions of autoregressive model in N-S direction.

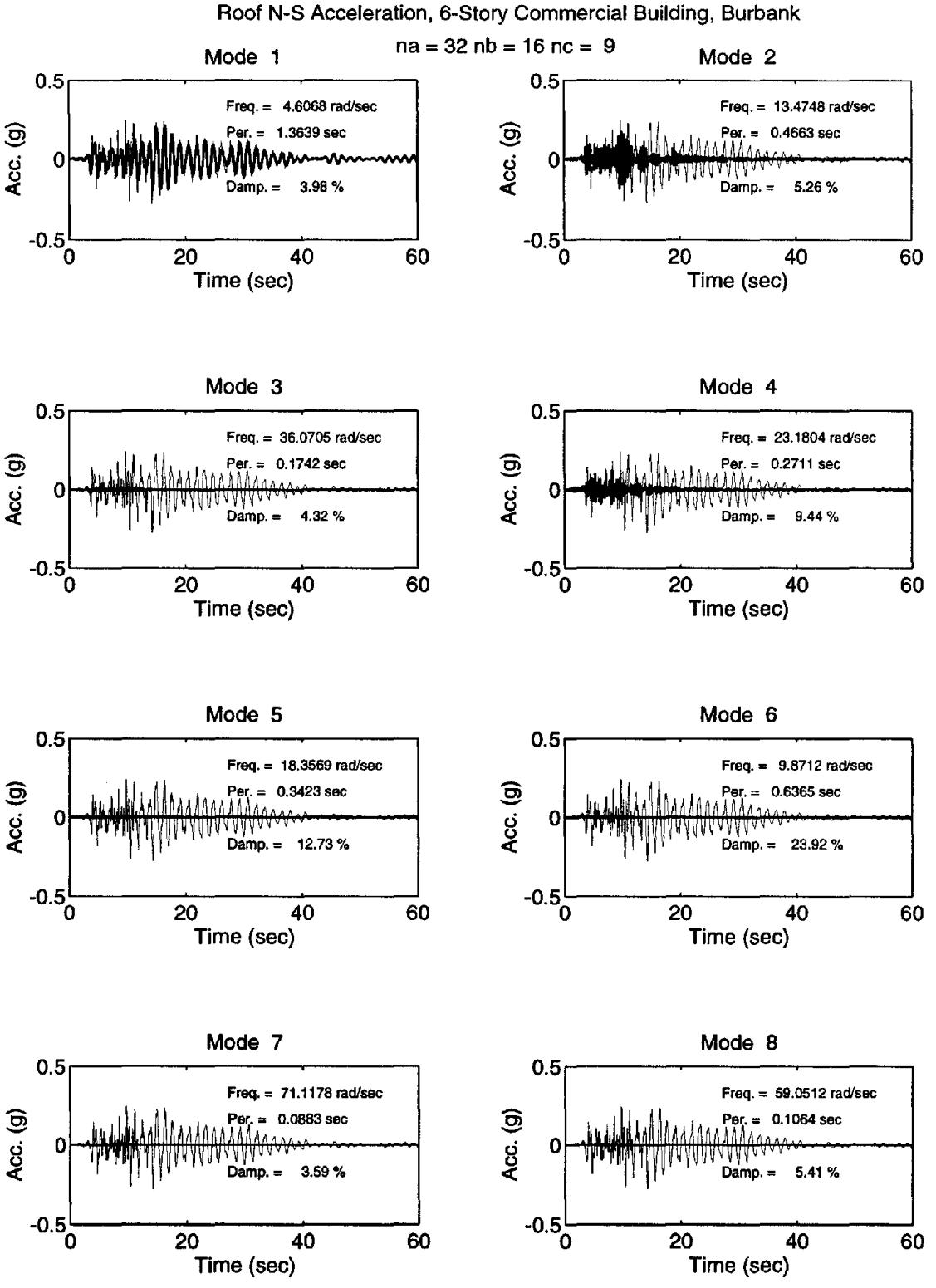

Figure C.4.12. Modal contributions of autoregressive model in N-S direction; modes 1 to 8.

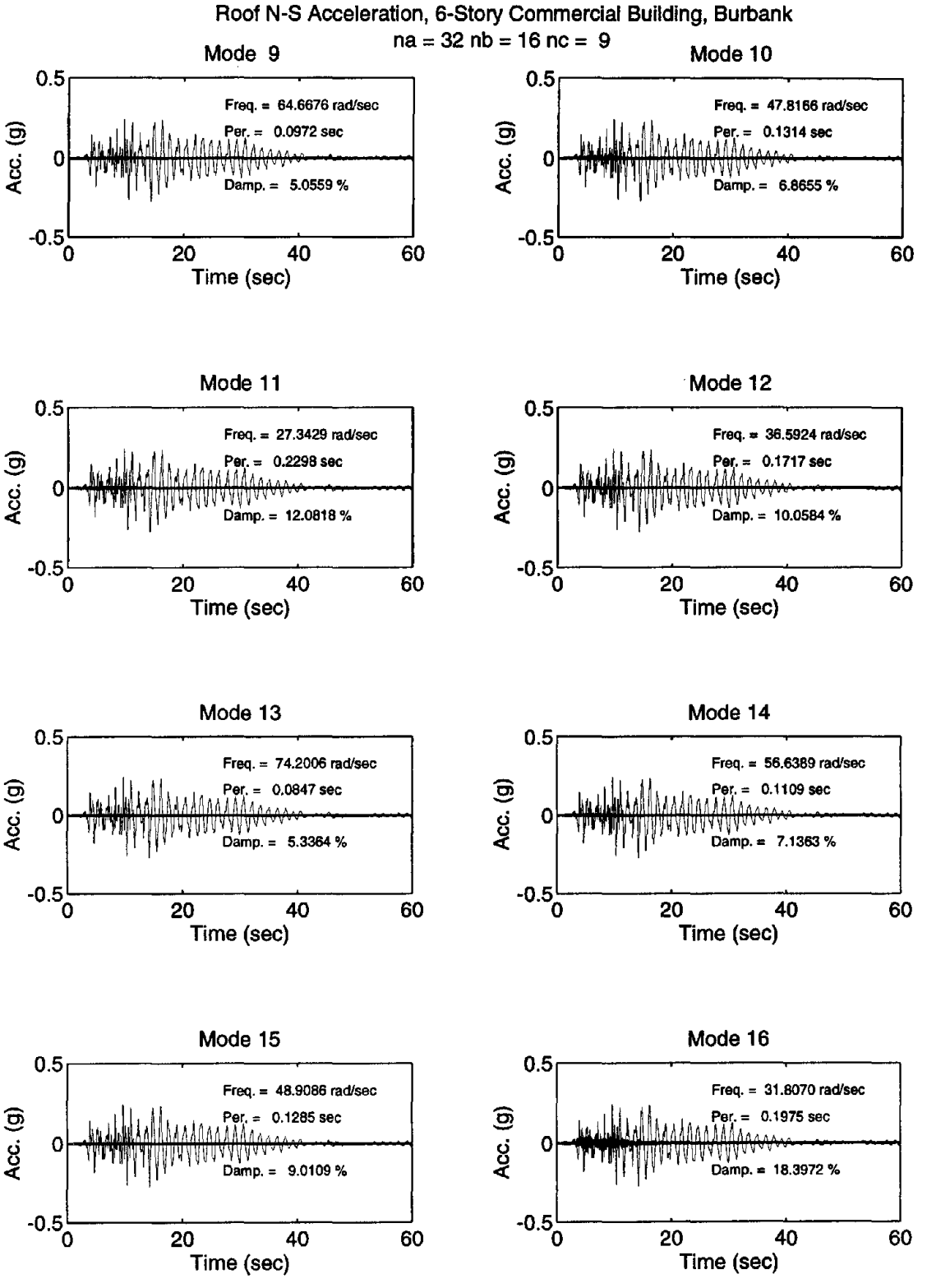

Figure C.4.13. Modal contributions of autoregressive model in E-W direction; modes 9 to 16.

5. Los Angeles - 19-Story Office Building, CSMIP Station No. 24643

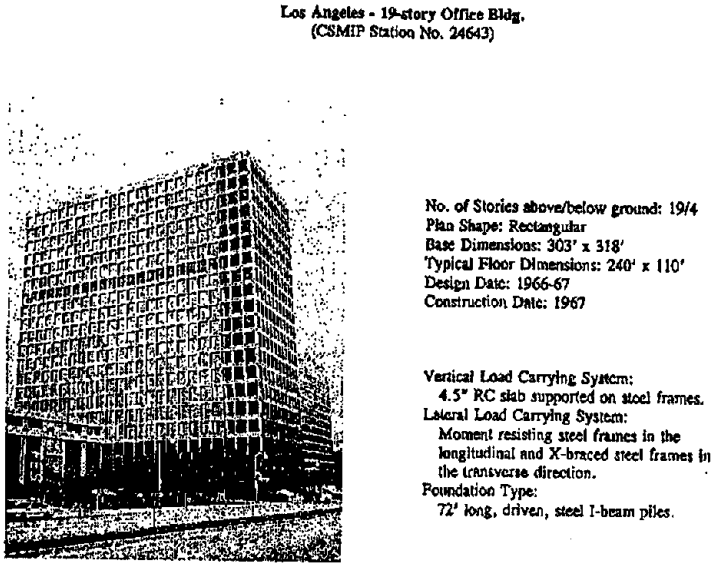

Figure C.5.1a. Details of 19-story office building, CSMIP Station No. 24643

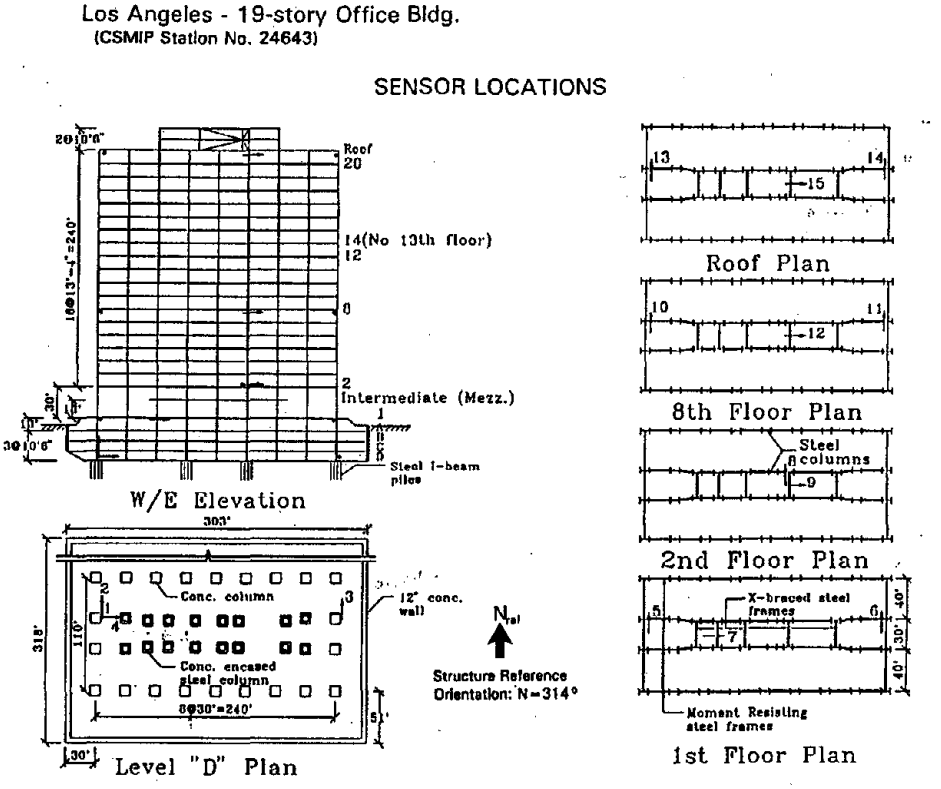

Figure C.5.1b. Sensor locations in 19-story office building, CSMIP Station No. 24643

Table C.5.1. Results of system identification in E-W (longitudinal) direction by WPCMIMO.

Mode No.	Frequency (Hz)	Damping	Part. Factor	Initial Disp.	Initial Velo.	Modal Cont.	Comments
1	0.2571	0.022	-8.63E-00	-1.57E-02	-4.13E-03	6.84E-01	1st Mode
2	0.7141	0.043	1.42E-00	-2.93E-04	1.87E-03	3.25E-01	2nd Mode
3	1.2481	0.051	-5.52E-01	-1.14E-04	1.60E-03	1.03E-01	
4	1.8057	0.078	2.82E-01	-2.59E-05	1.50E-03	7.41E-02	
5	2.3037	0.047	-1.55E-01	1.94E-05	7.05E-04	5.42E-02	
6	2.7331	0.036	2.14E-02	2.24E-05	1.80E-04	1.60E-03	

Relative Error = 0.203 and Absolute Error = 1.232

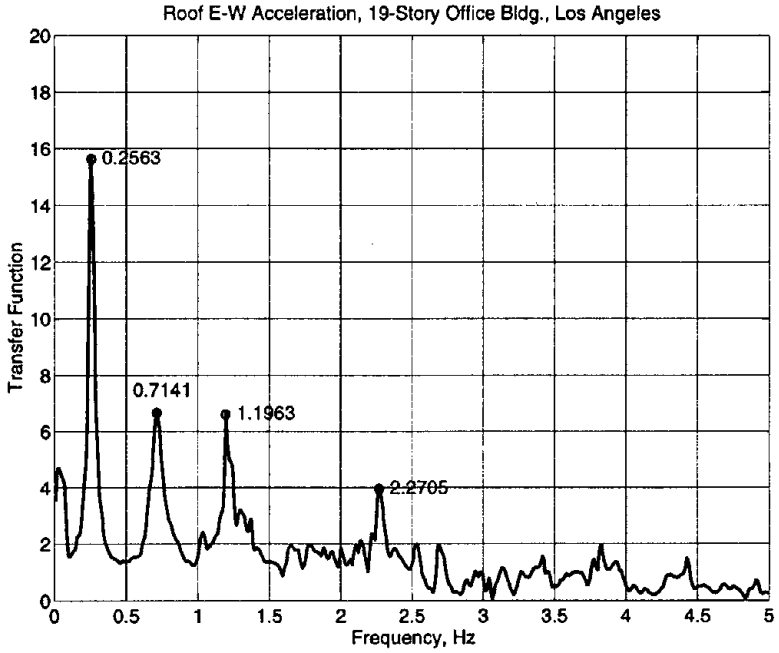

Figure C.5.2. Initial frequency estimate from transfer function in E-W direction.

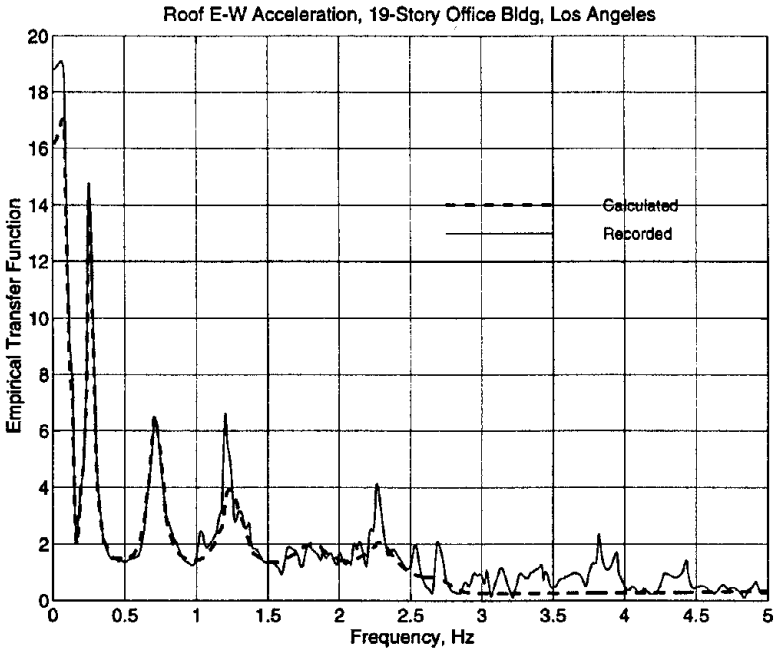

Figure C.5.3. Comparison of empirical transfer functions: recorded motions and calculated motions from WPCMIMO in E-W direction.

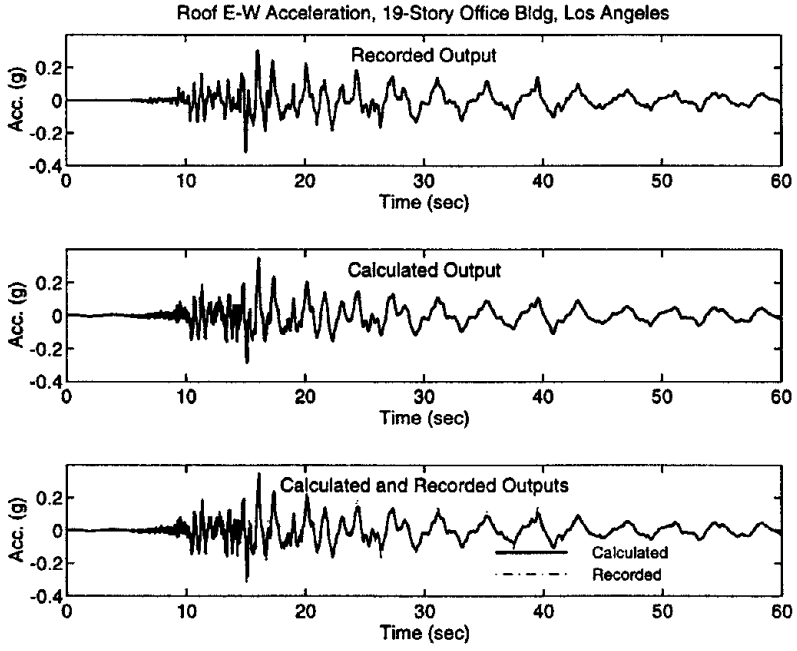

Figure C.5.4. Comparison of time-histories: recorded motions and calculated motions from WPCMIMO in E-W direction.

Table C.5.2. Results of system identification in N-S (transverse) direction by WPCMIMO.

Mode No.	Frequency (Hz)	Damping	Part. Factor	Initial Disp.	Initial Velo.	Modal Cont.	Comments
1	0.2877	0.029	-8.57E-00	-6.61E-03	1.39E-03	3.20E-01	1st Mode
2	1.2139	0.040	1.14E-00	9.30E-05	-1.06E-03	4.47E-01	2nd Mode
3	2.5687	0.107	-7.64E-01	-4.30E-05	-1.00E-03	4.14E-01	
4	2.9114	0.244	5.86E-01	-7.32E-05	2.47E-03	1.27E-01	
5	3.6779	0.030	9.09E-02	-1.37E-05	1.03E-04	1.64E-02	
6	3.8857	0.036	8.51E-02	1.56E-05	2.83E-04	1.62E-02	
7	4.5257	0.053	-1.48E-01	1.04E-05	-4.62E-05	8.37E-02	

Relative Error = 0.295 and Absolute Error = 3.953

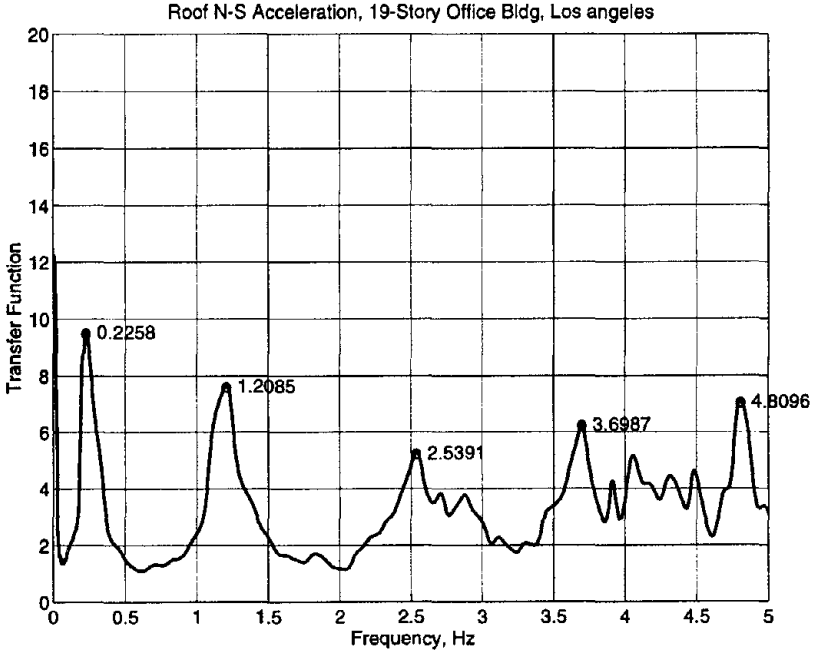

Figure C.5.5. Initial frequency estimate from transfer function in N-S direction.

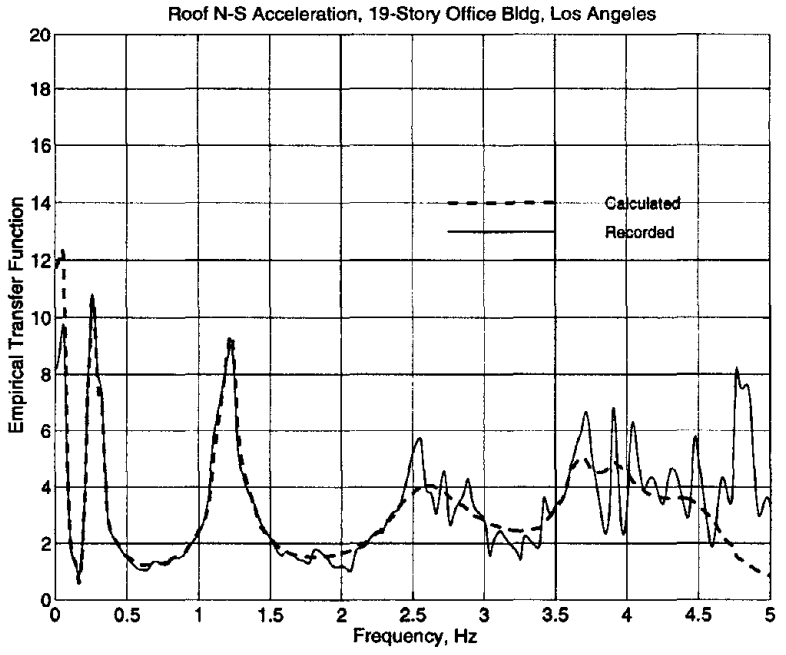

Figure C.5.6. Comparison of empirical transfer functions: recorded motions and calculated motions from WPCMIMO in N-S direction.

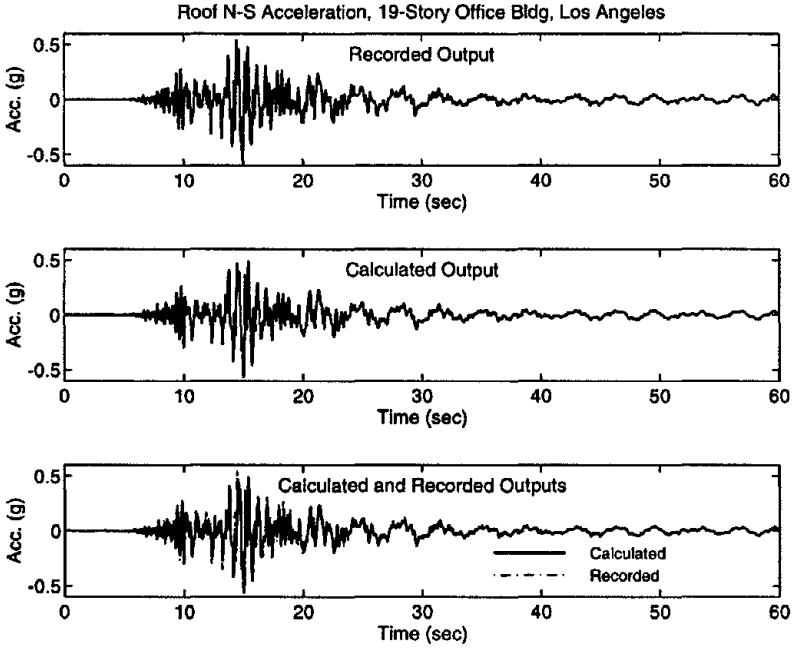

Figure C.5.7. Comparison of time-histories: recorded motions and calculated motions from WPCMIMO in N-S direction.

6. Los Angeles - Hollywood Storage Building, CSMIP Station No. 24236

No. of Stories above/below ground: 14/1
Plan Shape: Rectangular
Base Dimensions: 213' x 51'
Typical Floor Dimensions: 217' x 51'
Design Date: 1925

Vertical Load Carrying System:
8" concrete slabs supported by concrete frame.
Lateral Force Resisting System:
Reinforced concrete frames in both directions.
Foundation Type: Concrete piles.

Figure C.6.1a. Details of Hollywood Storage Building, CSMIP Station No. 24236

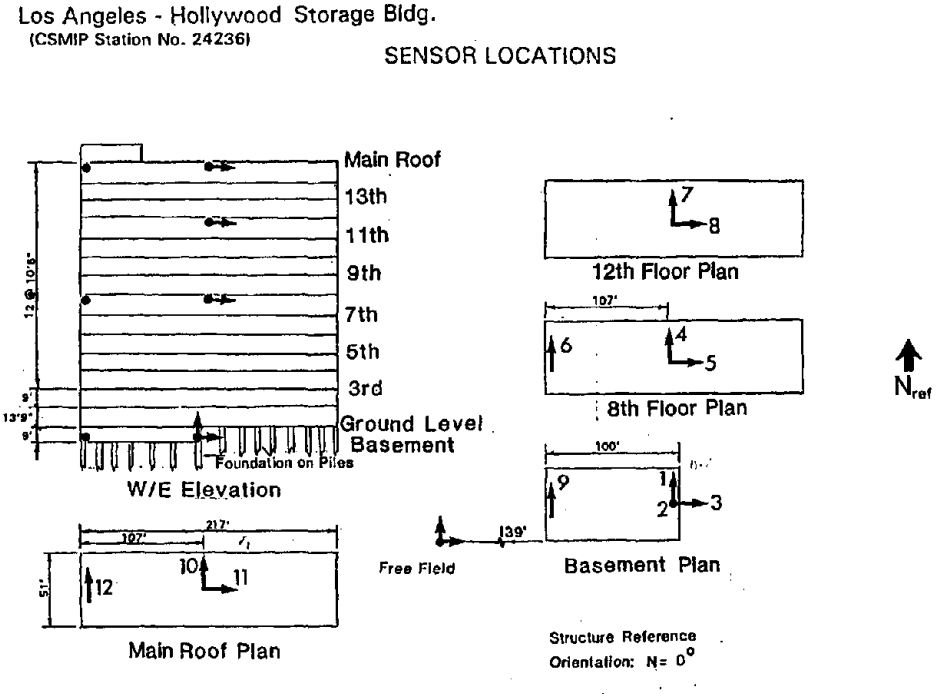

Figure C.6.1b. Sensor locations in Hollywood Storage Building, CSMIP Station No. 24236

Table C.6.1. Results of system identification in E-W (longitudinal) direction by WPCMIMO.

Mode No.	Frequency (Hz)	Damping	Part. Factor	Initial Disp.	Initial Velo.	Modal Cont.	Comments
1	0.5907	0.0827	-4.82E-02	1.69E-03	6.29E-03	2.82E-04	1st Mode*
2	1.2645	0.0085	-3.90E-02	-2.92E-03	1.38E-02	9.53E-03	
3	1.2758	0.0964	-1.34E-00	5.98E-03	-2.31E-02	8.41E-01	2nd Mode
4	4.7198	0.0900	-3.03E-02	4.92E-05	-2.84E-03	3.12E-03	
5	6.1129	0.0659	2.55E-02	-2.86E-05	-1.52E-03	4.48E-03	
6	7.8347	0.1198	3.57E-02	-3.46E-05	-5.27E-04	3.13E-03	

* 1st mode not visible in transfer function

Relative Error = 0.271 and Absolute Error = 0.703

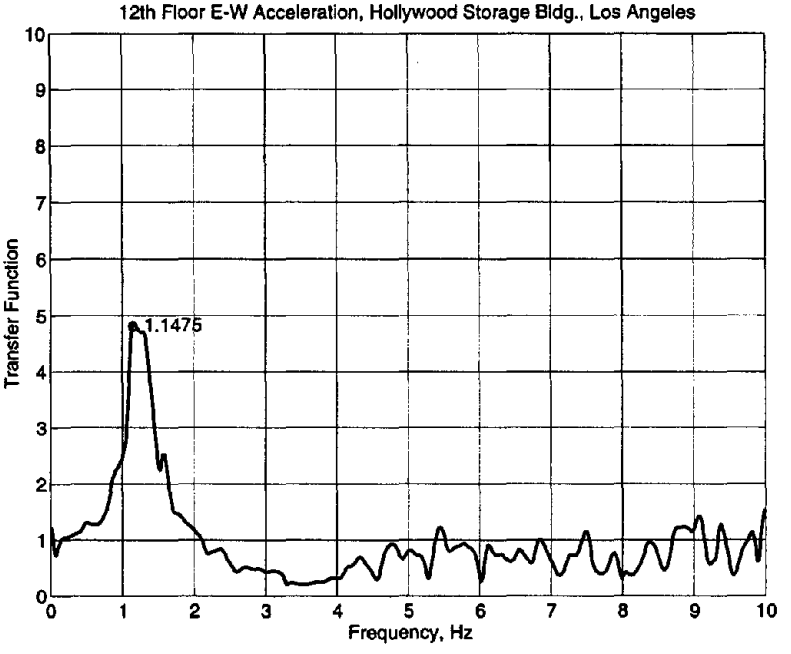

Figure C.6.2. Initial frequency estimates from transfer function in E-W direction.

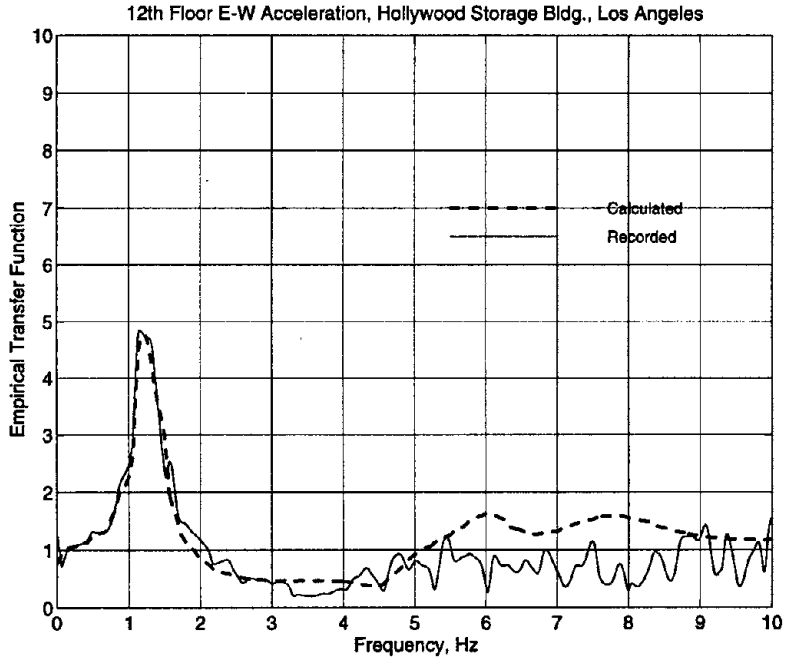

Figure C.6.3. Comparison of empirical transfer functions: recorded motions and calculated motions from WPCMIMO in E-W direction.

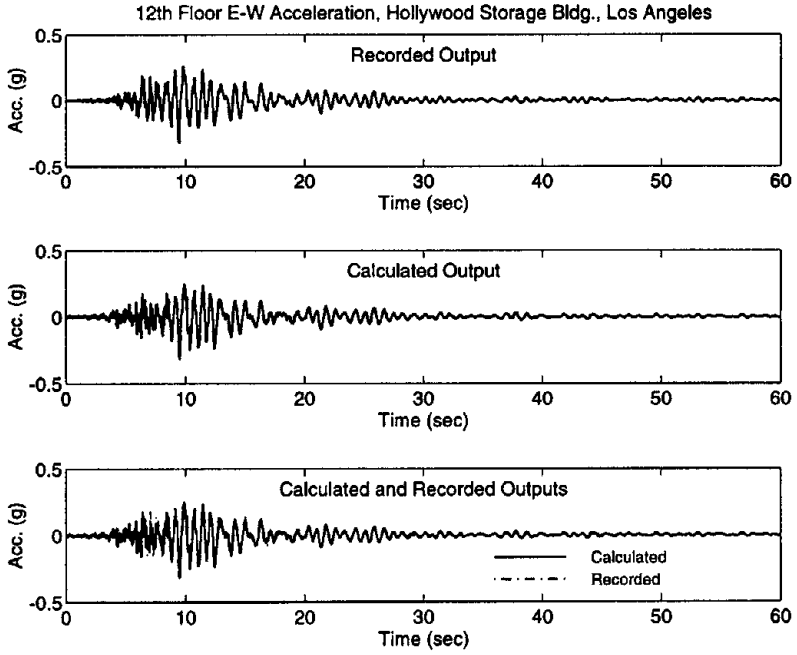

Figure C.6.4. Comparison of time-histories: recorded motions and calculated motions from WPCMIMO in E-W direction.

Table C.6.2. Results of system identification in N-S (transverse) direction by WPCMIMO.

Mode No.	Frequency (Hz)	Damping	Part. Factor	Initial Disp.	Initial Velo.	Modal Cont.	Comments
1	0.4397	0.0472	-7.61E-00	-9.23E-02	-5.59E-01	1.49E+00	1st Trans. Mode
2	0.4500	0.0436	2.53E-00	6.06E-02	5.89E-01	3.39E-01	1st Tor. Mode
3	1.5361	0.0801	5.39E-01	-1.08E-03	1.36E-02	2.72E-01	2nd Tran. Mode
4	1.8336	0.0437	1.24E-01	5.26E-04	4.02E-03	4.39E-02	2nd Tor. Mode
5	5.8838	0.0236	3.17E-01	-3.72E-04	-2.12E-02	2.28E+00	
6	7.7576	0.0757	6.66E-02	4.11E-05	1.74E-04	1.77E-02	
7	5.9003	0.0299	-3.81E-01	4.32E-04	2.48E-02	2.67E+00	
8	4.2006	0.0918	1.14E-01	-4.18E-05	2.68E-03	7.04E-02	

Relative Error = 0.478 and Absolute Error = 3.981

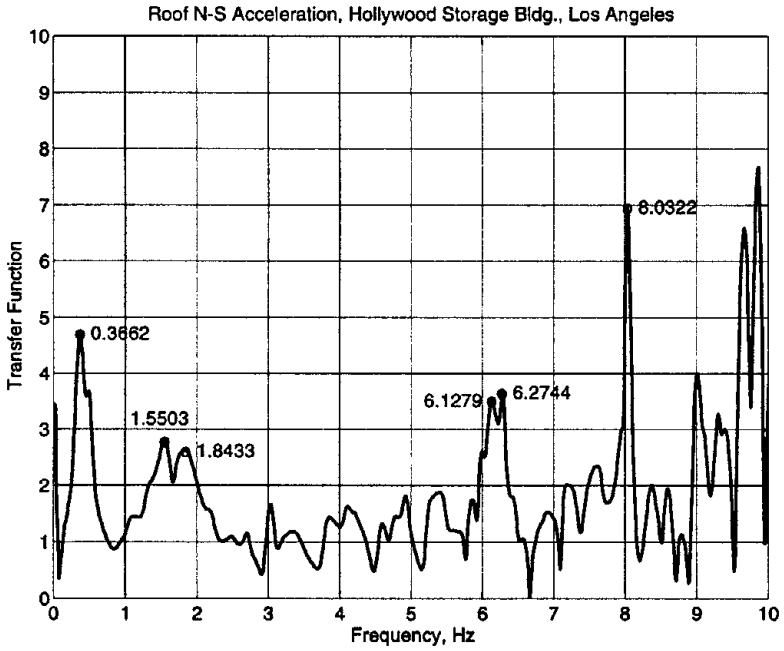

Figure C.6.5. Initial frequency estimates from transfer function in N-S direction.

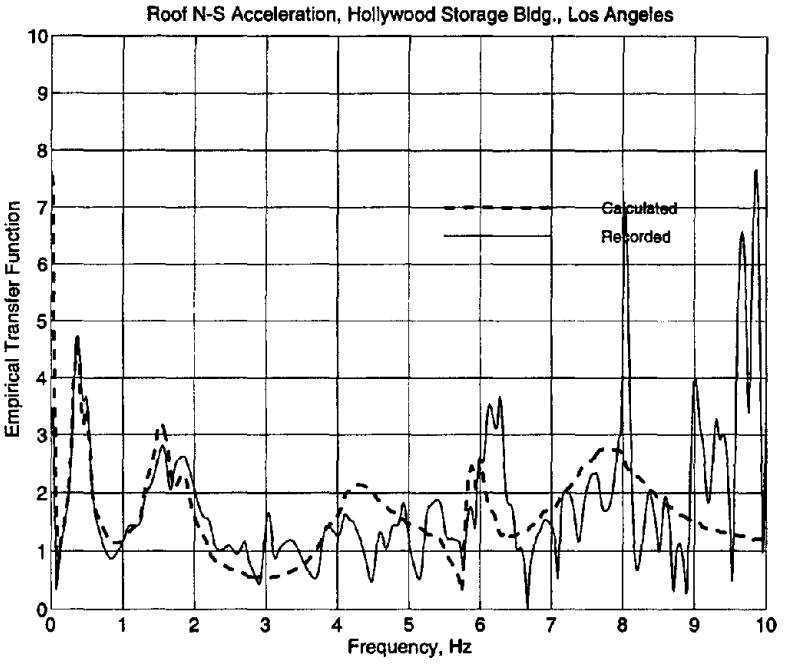

Figure C.6.6. Comparison of empirical transfer functions: recorded motions and calculated motions from WPCMIMO in N-S direction.

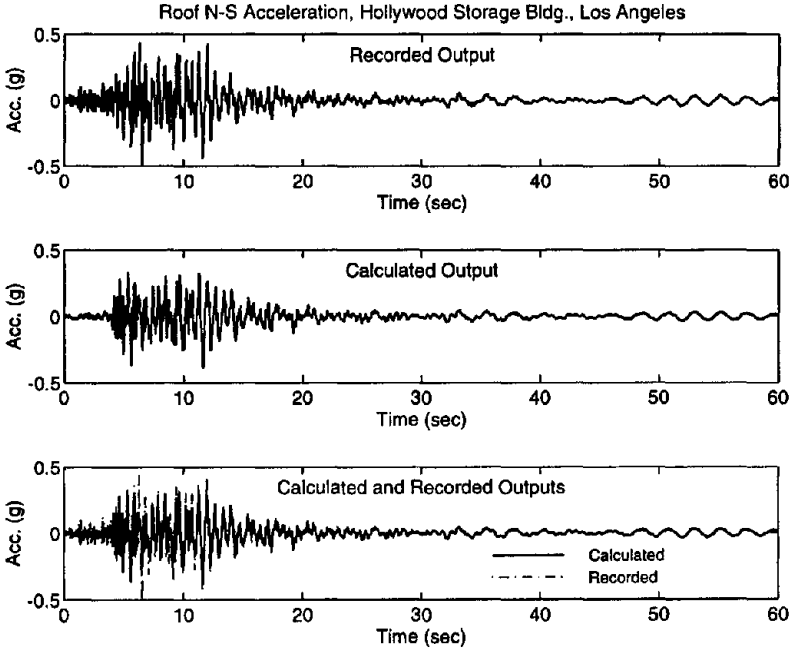

Figure C.6.7. Comparison of time-histories: recorded motions and calculated motions from WPCMIMO in N-S direction.

7. North Hollywood - 20-Story Hotel, CSMIP Station No. 24464

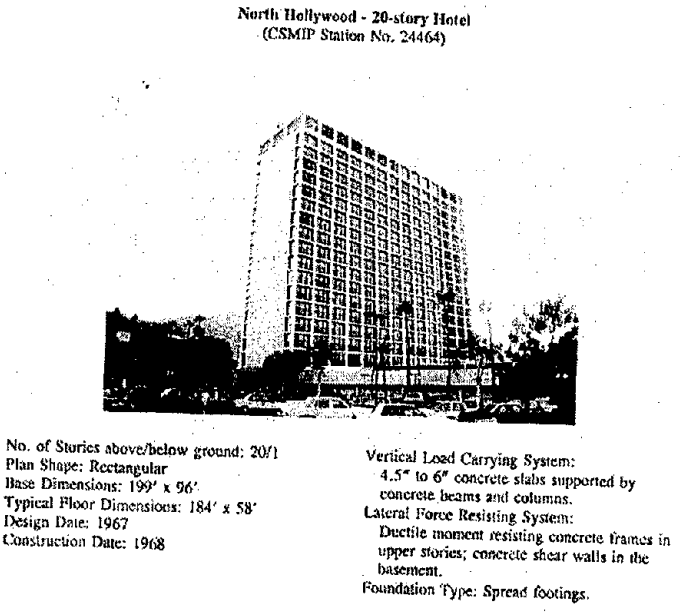

Figure C.7.1a. Details of 20-story hotel building, CSMIP Station No. 24464

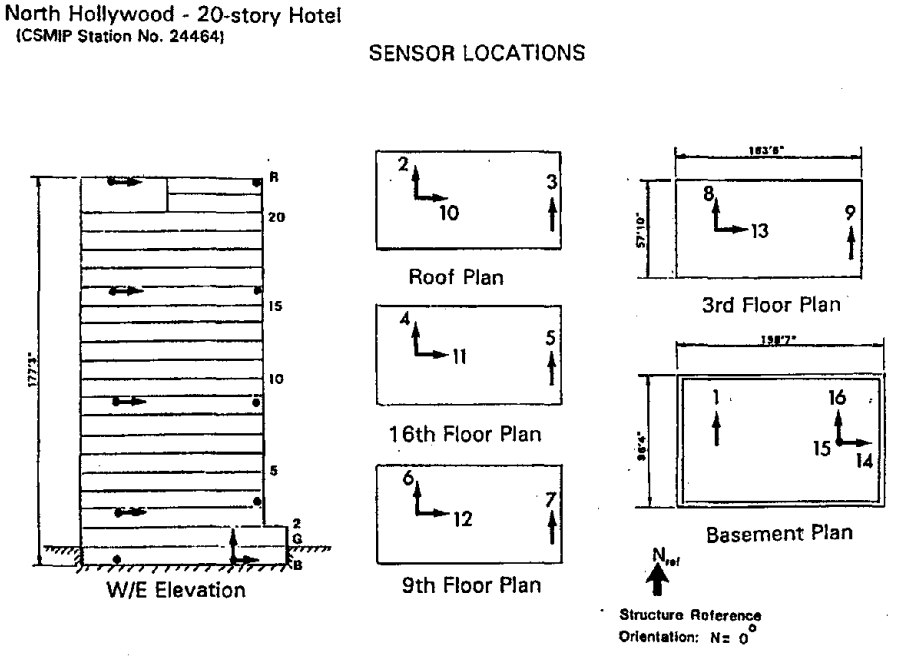

Figure C.7.1b. Sensor locations in 20-story hotel building, CSMIP Station No. 24464

Table C.7.1. Results of system identification in E-W (longitudinal) direction by WPCMIMO.

Mode No.	Frequency (Hz)	Damping	Part. Factor	Initial Disp.	Initial Velo.	Modal Cont.	Comments
1	0.3851	0.0587	-5.79E-00	3.35E-03	-9.30E-03	6.86E-01	1st Mode
2	1.1353	0.1578	8.28E-01	-7.65E-03	-2.71E-02	1.49E-01	
3	1.2817	0.0315	2.00E-01	1.80E-03	3.05E-02	6.31E-02	
4	2.9555	0.4005	-11.28E-0	1.09E-02	1.66E-01	7.45E+01	
5	2.9632	0.3350	9.49E-00	-9.24E-03	-1.34E-01	7.03E+01	
6	5.1417	0.0114	-2.11E-02	-1.19E-04	1.25E-03	2.58E-02	
7	5.4144	0.2175	7.15E-01	-8.31E-04	-4.32E-02	9.02E-01	
8	5.8070	0.0823	-1.79E-01	5.22E-04	1.68E-02	1.13E-01	
9	5.3661	0.0036	-1.15E-03	-4.82E-05	5.83E-03	7.59E-03	

Relative Error = 0.433 and Absolute Error = 1.055

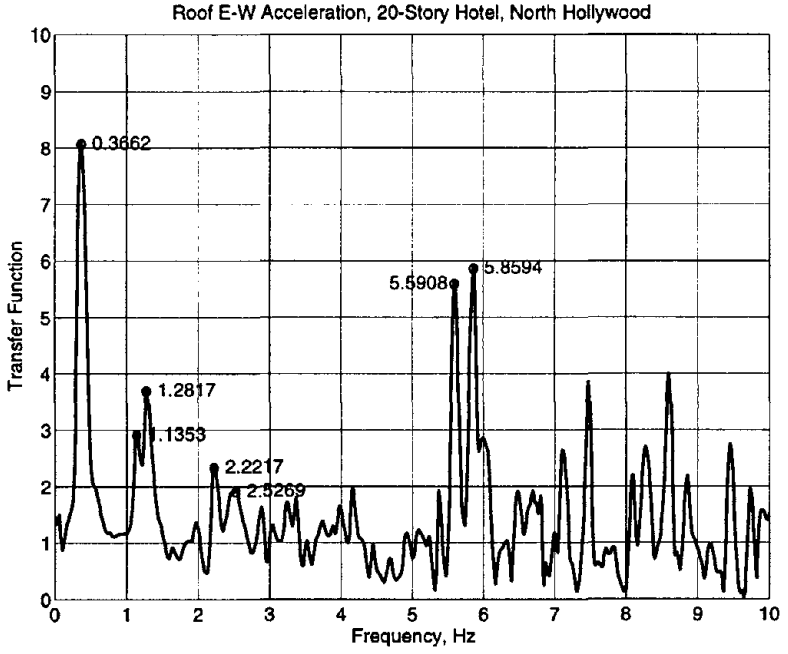

Figure C.7.2. Initial frequency estimates from transfer function in E-W direction.

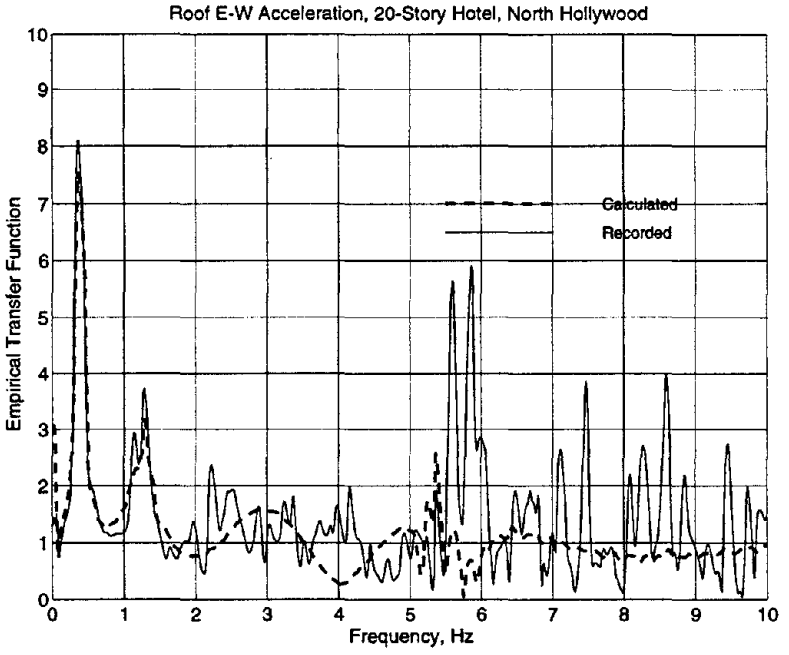

Figure C.7.3. Comparison of empirical transfer functions: recorded motions and calculated motions from WPCMIMO in E-W direction.

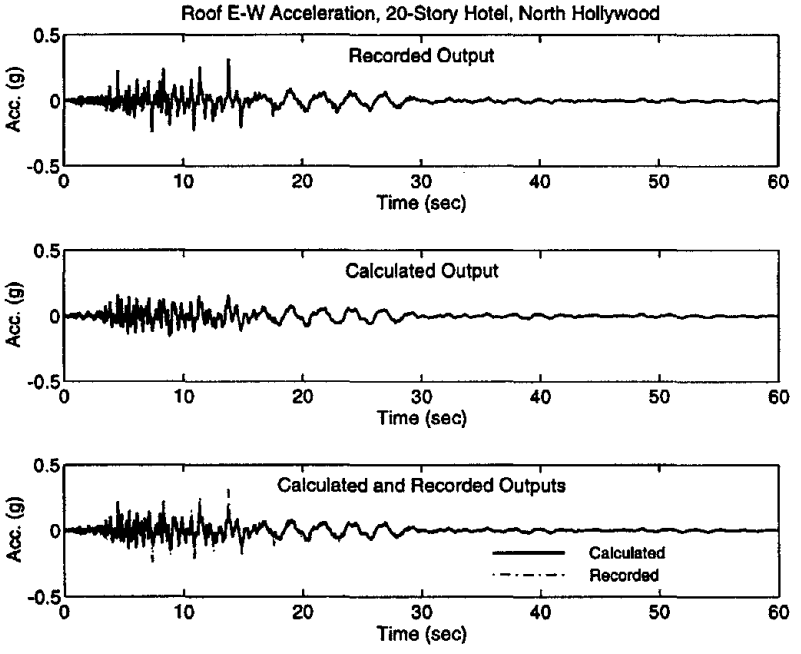

Figure C.7.4. Comparison of time-histories: recorded motions and calculated motions from WPCMIMO in E-W direction.

Table C.7.2. Results of system identification in N-S (transverse) direction by WPCMIMO.

Mode No.	Frequency (Hz)	Damping	Part. Factor	Initial Disp.	Initial Velo.	Model Cont.	Comments
1	0.3821	0.0650	-5.58E-00	-9.03E-03	5.69E-02	1.01E+00	1st Mode
2	1.2939	0.1325	5.02E-01	-1.10E-03	9.80E-03	3.30E-01	
3	1.1051	0.0298	9.54E-02	-1.78E-04	-1.18E-02	1.81E-02	
4	3.8197	0.0015	7.49E-03	-1.24E-04	-1.24E-03	2.25E-03	
5	3.9666	0.0083	8.38E-03	6.73E-06	3.09E-03	1.71E-03	
6	4.2187	0.0024	-1.25E-03	-3.81E-05	1.88E-03	7.20E-04	

Relative Error = 0.360 and Absolute Error = 0.891

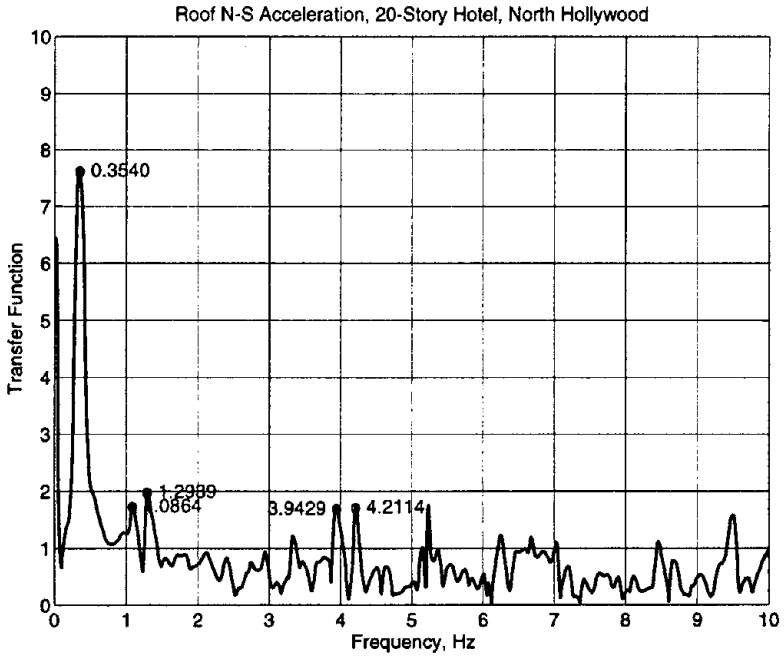

Figure C.7.5. Initial frequency estimates from transfer function in N-S direction.

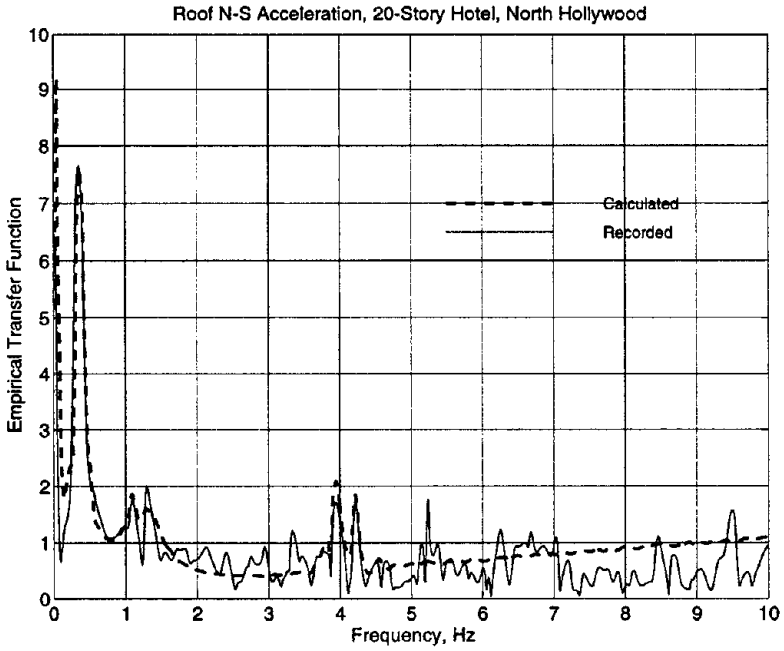

Figure C.7.6. Comparison of empirical transfer functions: recorded motions and calculated motions from WPCMIMO in N-S direction.

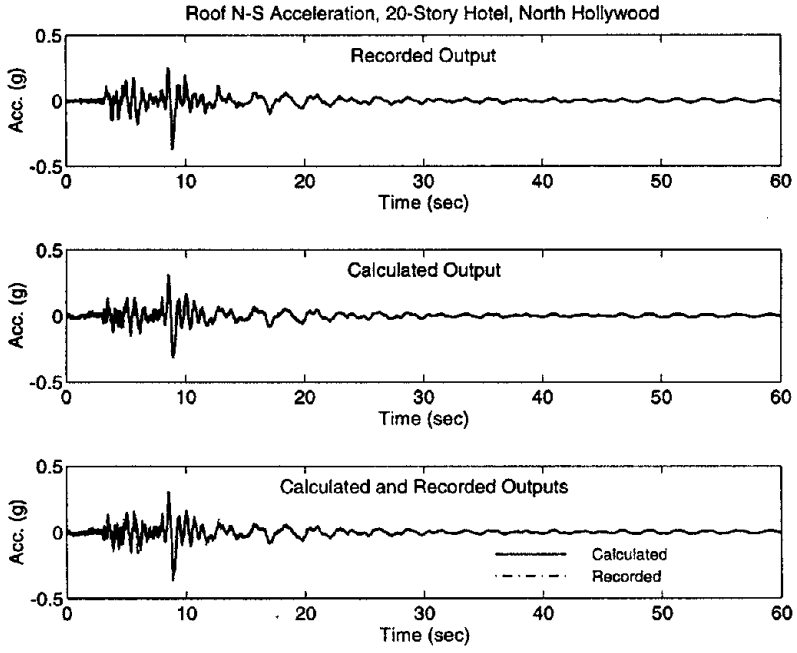

Figure C.7.7. Comparison of time-histories: recorded motions and calculated motions from WPCMIMO in N-S direction.

8. Milikan Library - NOAA Station No. N264-265

Table C.8.1. Results of system identification in E-W (longitudinal) direction by WPCMIMO.

Mode No.	Frequency (Hz)	Damping	Part. Factor	Initial Disp.	Initial Velo.	Modal Cont.	Comments
1	1.0466	0.0672	-2.03E-00	-2.42E-03	-8.54E-03	6.81E-01	1st Mode
2	1.4648	0.1070	-3.47E-01	-9.15E-04	5.59E-03	1.71E-02	
3	4.9699	0.0503	1.34E-01	-4.73E-05	-7.15E-04	2.75E-02	
4	5.5484	0.0025	1.65E-03	-4.84E-05	3.64E-03	2.08E-03	
5	11.2341	0.3176	-2.86E-01	4.61E-06	3.85E-03	4.92E-03	
6	11.9808	0.0237	1.61E-02	-3.27E-06	-1.21E-04	1.90E-04	

Relative Error = 0.443 and Absolute Error = 2.800

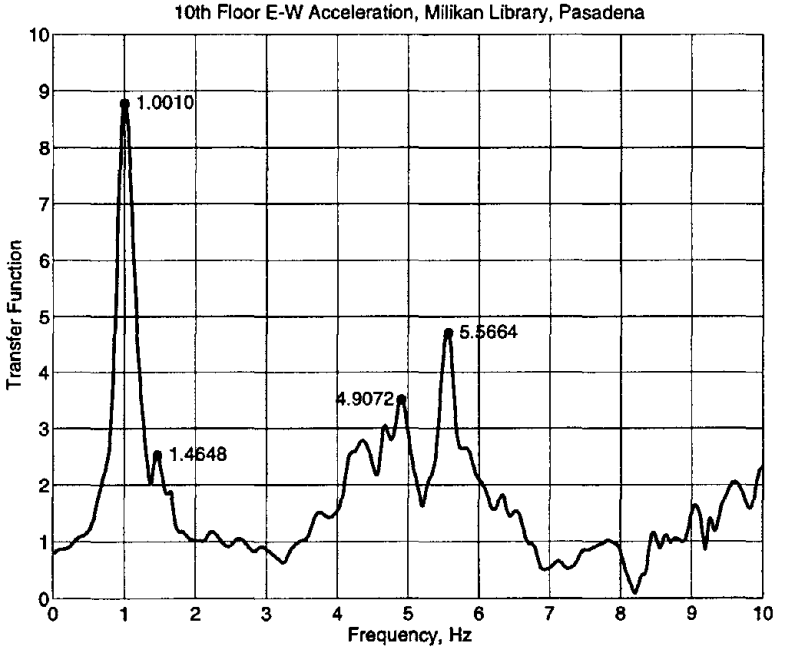

Figure C.8.1. Initial frequency estimates from transfer function in E-W direction.

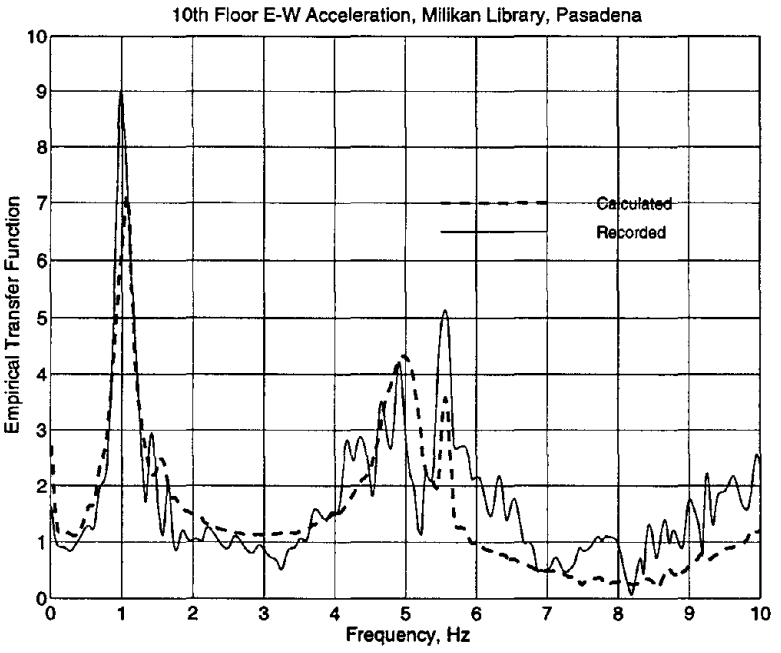

Figure C.8.2. Comparison of empirical transfer functions: recorded motions and calculated motions from WPCMIMO in E-W direction.

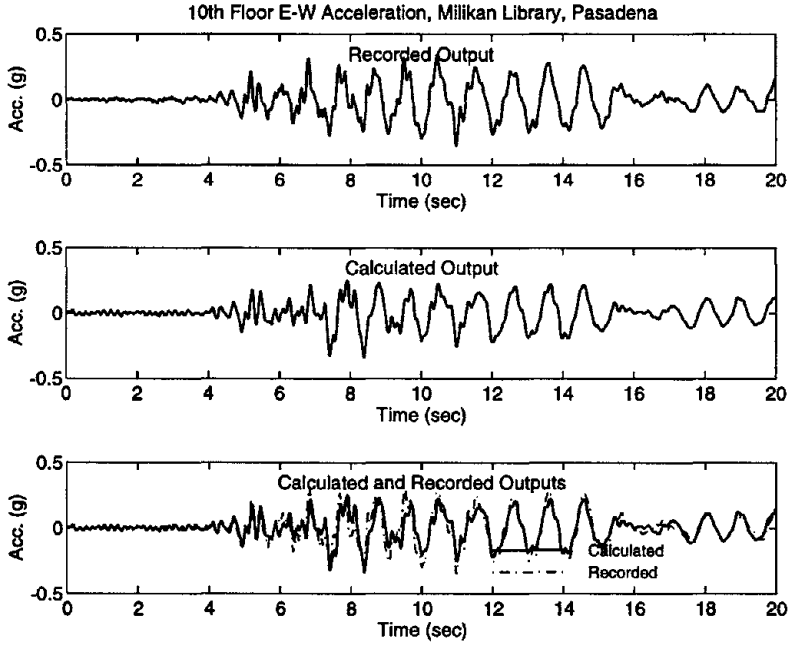

Figure C.8.3. Comparison of time-histories: recorded motions and calculated motions from WPCMIMO in E-W direction.

Table C.8.2. Results of system identification in N-S (transverse) direction by WPCMIMO.

Mode No.	Frequency (Hz)	Damping	Part. Factor	Initial Disp.	Initial Velo.	Modal Cont.	Comments
1	1.5897	0.0605	-1.24E-00	-1.58E-03	4.89E-02	6.32E-01	1st Mode
2	1.7578	0.0267	-2.08E-01	3.50E-03	-2.18E-02	3.58E-02	
3	6.4101	0.1372	6.96E-02	1.02E-04	3.51E-03	9.78E-03	
4	8.1378	0.0250	3.64E-02	-2.58E-05	-1.11E-03	6.00E-03	
5	7.8556	0.0021	1.94E-02	2.43E-05	8.60E-05	6.51E-03	
6	7.2776	0.0186	2.15E-02	1.22E-05	1.01E-04	1.44E-03	
7	7.2881	0.6551	-2.04E-01	2.46E-04	-1.65E-02	5.68E-03	
8	8.4907	0.0000	-2.72E-03	1.72E-05	-5.05E-04	7.72E-04	

Relative Error = 0.279 and Absolute Error = 0.718

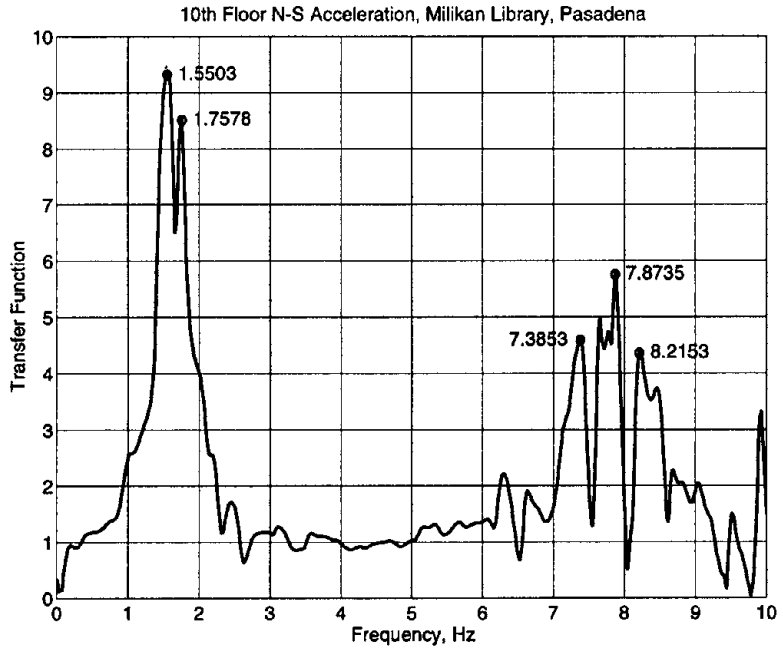

Figure C.8.4. Initial frequency estimates from transfer function in N-S direction.

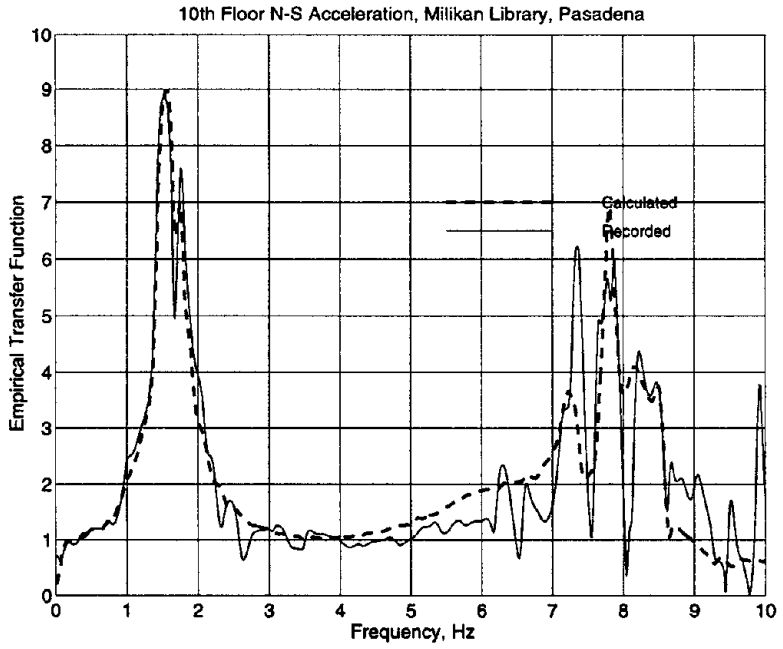

Figure C.8.5. Comparison of empirical transfer functions: recorded motions and calculated motions from WPCMIMO in N-S direction.

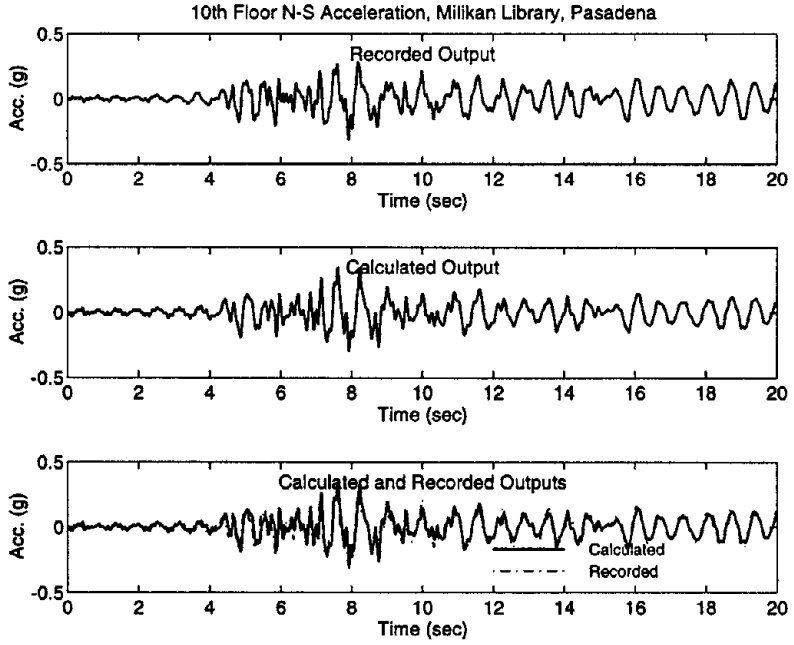

Figure C.8.6. Comparison of time-histories: recorded motions and calculated motions from WPCMIMO in N-S direction.

9. Los Angeles - 5-Story Warehouse, CSMIP Station No. 24463

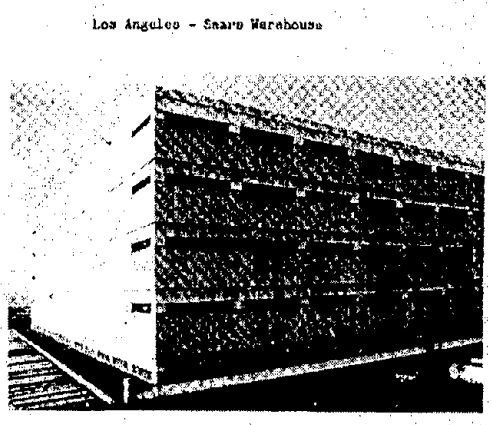

Address: 2555 East Olympic Blvd.
Los Angeles, CA
No. of Stories above/below ground: 5/1
Plan Shape: Rectangular
Base Dimensions: 360' x 280'
Typical Floor Dimensions: Same
Design Date: 1970

Vertical Load Carrying System:
Concrete slabs, beams and columns.
Lateral Force Resisting System:
Ductile reinforced concrete perimeter frame; basement shear walls; designed according to the 1970 Los Angeles Building Code.
Foundation Type:
Spread footings.

Note: This building is adjacent to a similar building; the buildings are separated by a seismic joint.

Figure C.9.1a. Details of 5-story warehouse, CSMIP Station No. 24463

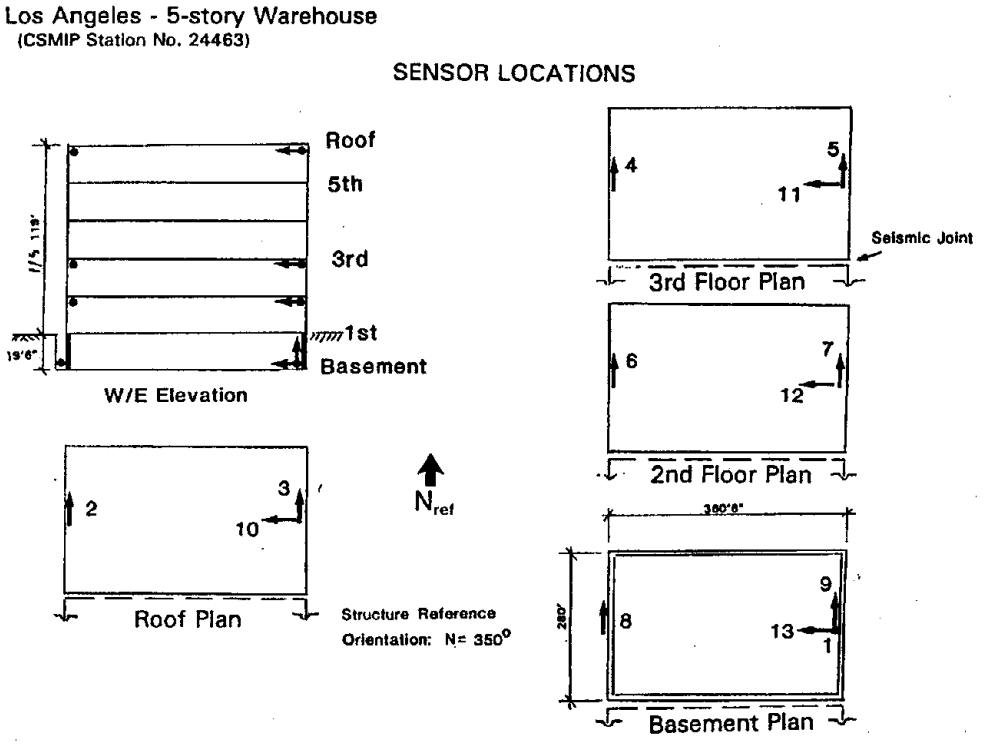

Figure C.9.1a. Sensor locations in 5-story warehouse, CSMIP Station No. 24463

Table C.9.1. Results of system identification in E-W (longitudinal) direction by WPCMIMO.

Mode No.	Frequency (Hz)	Damping	Part. Factor	Initial Disp.	Initial Velo.	Modal Cont.	Comments
1	0.6868	0.0552	-3.16E-00	-1.25E-03	-3.26E-03	8.13E-01	1st Mode
2	2.1240	0.0656	4.22E-01	-1.34E-05	7.84E-04	2.87E-01	2nd Mode
3	3.6467	0.0569	-1.11E-01	-1.66E-06	-3.18E-04	7.71E-02	
4	8.0107	0.0055	6.75E-02	-4.44E-04	-3.73E-02	5.76E-01	
5	8.0102	0.0061	-7.24E-02	4.38E-04	3.92E-02	5.83E-01	
6	7.9110	0.0028	3.03E-04	1.76E-05	-1.56E-03	1.14E-03	

Relative Error = 0.314 and Absolute Error = 0.635

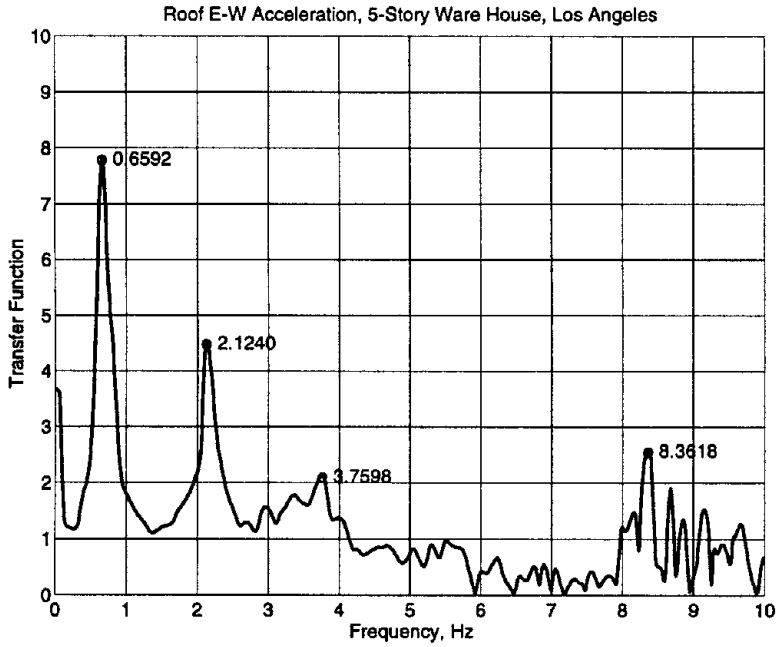

Figure C.9.2. Initial frequency estimates from transfer function in E-W direction.

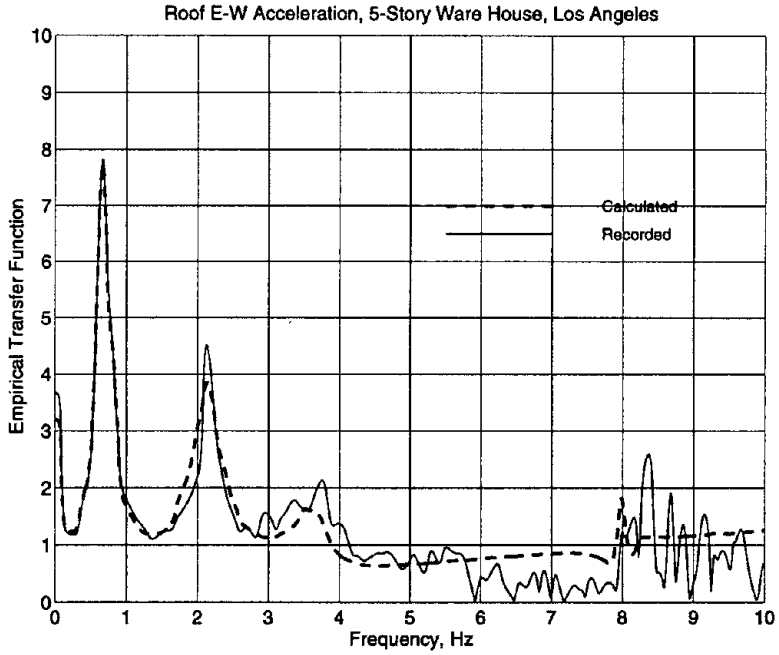

Figure C.9.3. Comparison of empirical transfer functions: recorded motions and calculated motions from WPCMIMO in E-W direction.

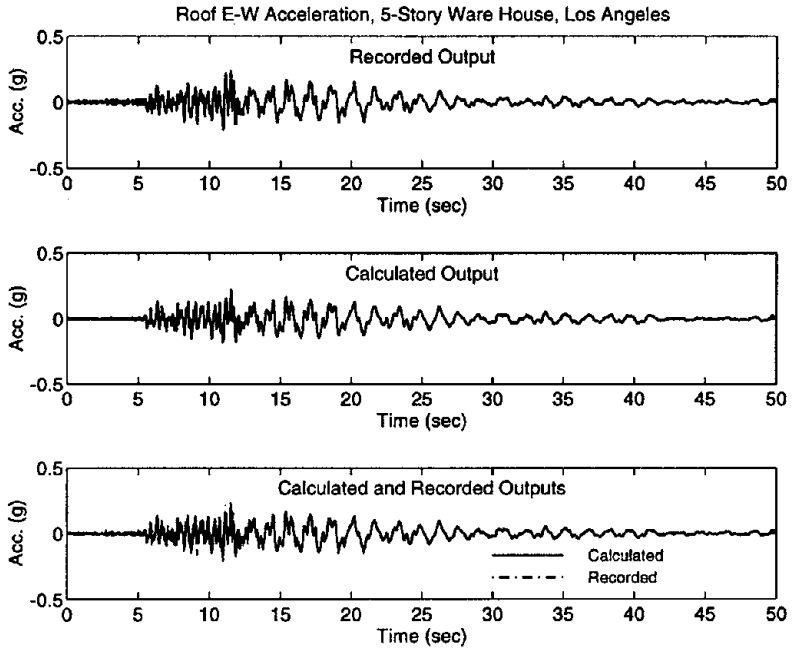

Figure C.9.4. Comparison of time-histories: recorded motions and calculated motions from WPCMIMO in E-W direction.

Table C.9.2. Results of system identification in N-S (transverse) direction by WPCMIMO.

Mode No.	Frequency (Hz)	Damping	Part. Factor	Initial Disp.	Initial Velo.	Modal Cont.	Comments
1	0.6230	0.0363	-3.25E-00	4.71E-03	5.75E-03	9.31E-01	1st Mode
2	1.8555	0.0721	-3.25E-00	4.01E-03	-3.11E-02	1.51E+01	2nd Mode
3	1.8597	0.0731	3.62E-00	-4.01E-03	2.88E-02	1.85E+01	
4	3.4478	0.0697	-9.83E-02	2.03E-05	-2.86E-05	4.77E-02	
5	4.7759	0.0609	2.40E-02	-1.58E-05	-8.12E-04	2.91E-03	

Relative Error = 0.164 and Absolute Error = 0.230

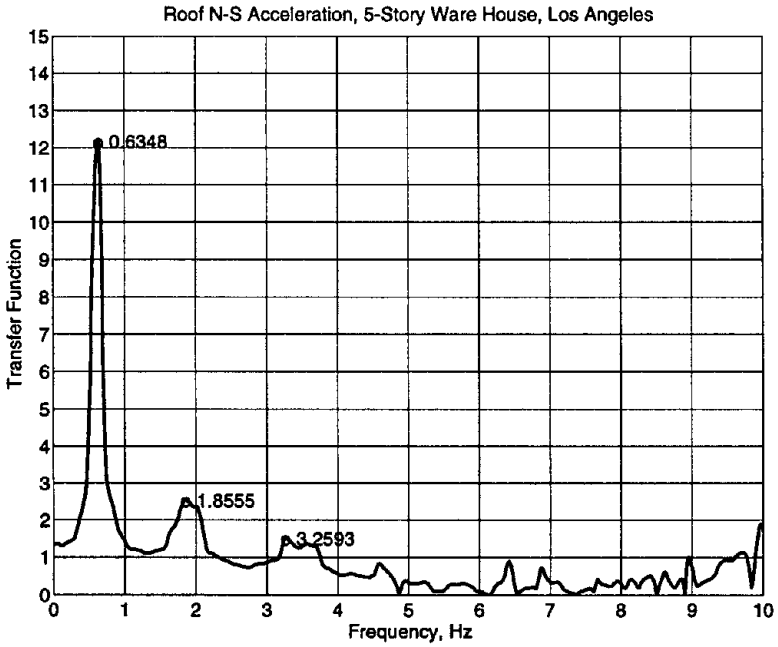

Figure C.9.5. Initial frequency estimates from transfer function in N-S direction.

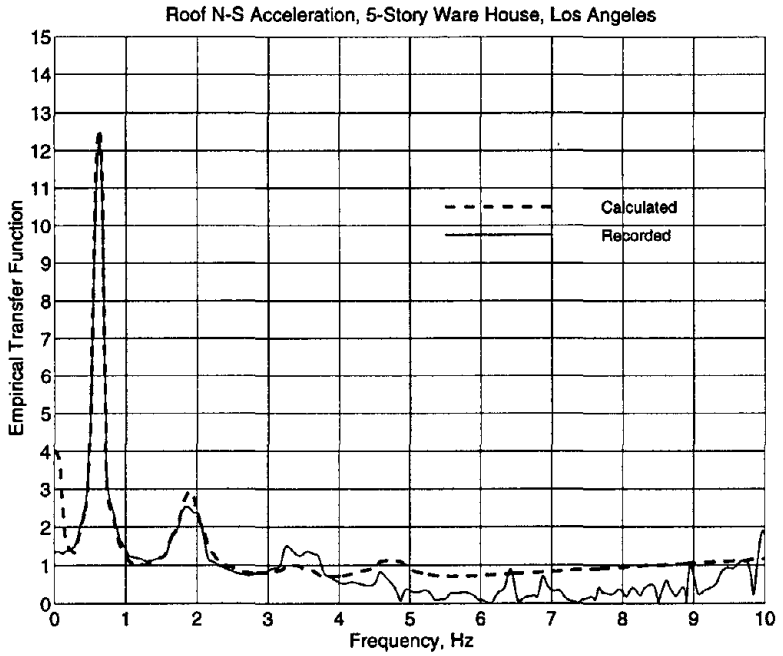

Figure C.9.6. Comparison of empirical transfer functions: recorded motions and calculated motions from WPCMIMO in N-S direction.

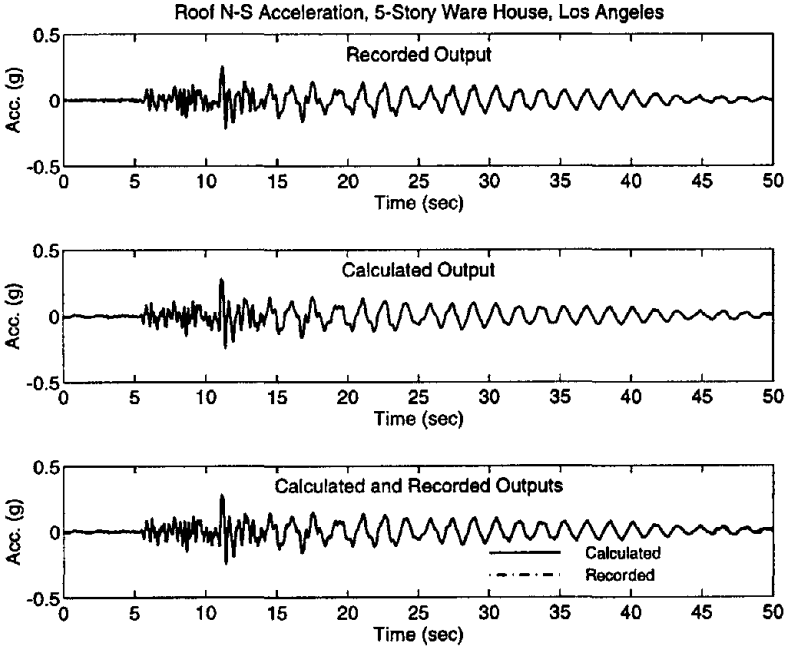

Figure C.9.7. Comparison of time-histories: recorded motions and calculated motions from WPCMIMO in N-S direction.

10. Los Angeles - 3-Story Commercial Building, CSMIP Station No. 24332

Los Angeles - 3-story Commercial Building
(CSMIP Station No. 24332)

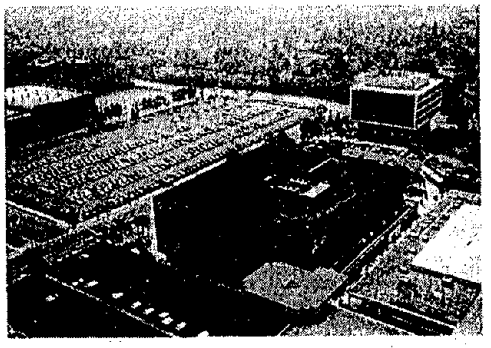

No. of Stories above/below ground: 3/2
Plan Shape: Rectangular
Base Dimensions: 520' x 227'
Typical Floor Dimensions: 241' x 219'
Design Date: 1974
Construction Date: 1975-76

Vertical Load Carrying System:
3.25" light-weight concrete slab over metal deck in upper three stories; 18" thick waffle slab in the basement.
Lateral Force Resisting System:
Steel braced frames in upper three stories; concrete shear walls in the basement.
Foundation Type:
Spread footings and drilled bell caissons.

Figure C.10.1a. Details of 3-story commercial building, CSMIP Station No. 24332

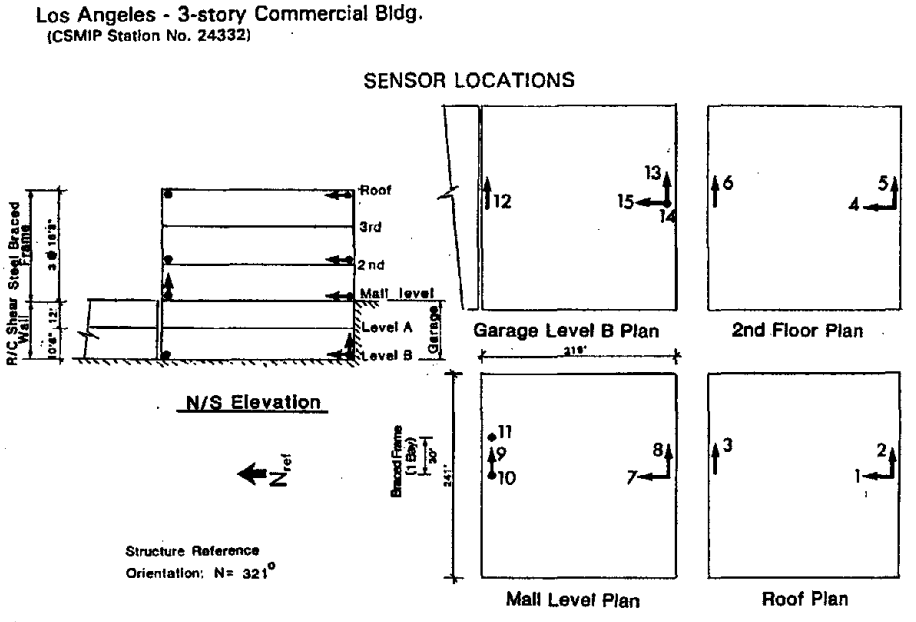

Figure C.10.1b. Sensor locations in 3-story commercial building, CSMIP Station No. 24332

Table C.10.1. Results of system identification in E-W (longitudinal) direction by WPCMIMO.

Mode No.	Frequency (Hz)	Damping	Part. Factor	Initial Disp.	Initial Velo.	Modal Cont.	Comments
1	1.7203	0.2343	-1.39E-00	-3.00E-03	4.76E-03	4.15E-01	
2	1.9897	0.0484	-5.94E-01	8.50E-04	9.96E-03	3.26E-01	1st Mode
3	2.6335	0.5218	1.53E-00	1.91E-03	-1.30E-02	2.96E-01	
4	4.4917	0.0362	5.82E-02	-8.27E-05	2.22E-03	1.87E-02	
5	5.4994	0.1164	-1.82E-01	-2.52E-05	-5.42E-04	4.95E-02	
6	6.5720	0.0600	1.94E-02	-7.30E-06	1.39E-03	8.91E-04	

Relative Error = 0.250 and Absolute Error = 1.995

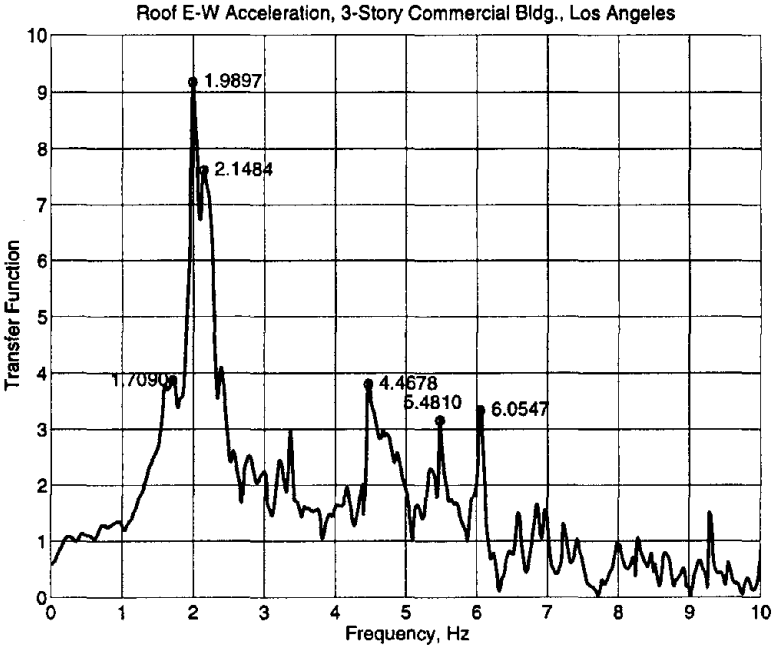

Figure C.10.2. Initial frequency estimates from transfer function in E-W direction.

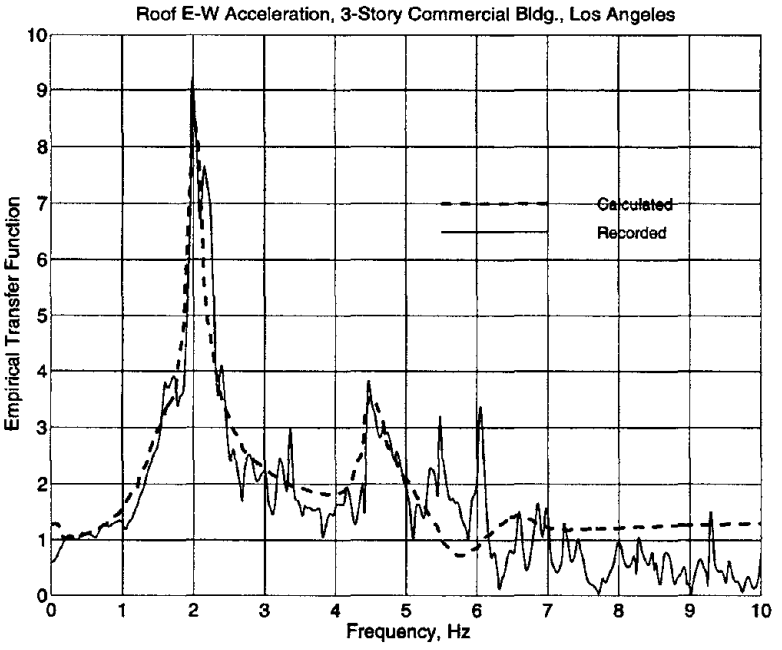

Figure C.10.3. Comparison of empirical transfer functions: recorded motions and calculated motions from WPCMIMO in E-W direction.

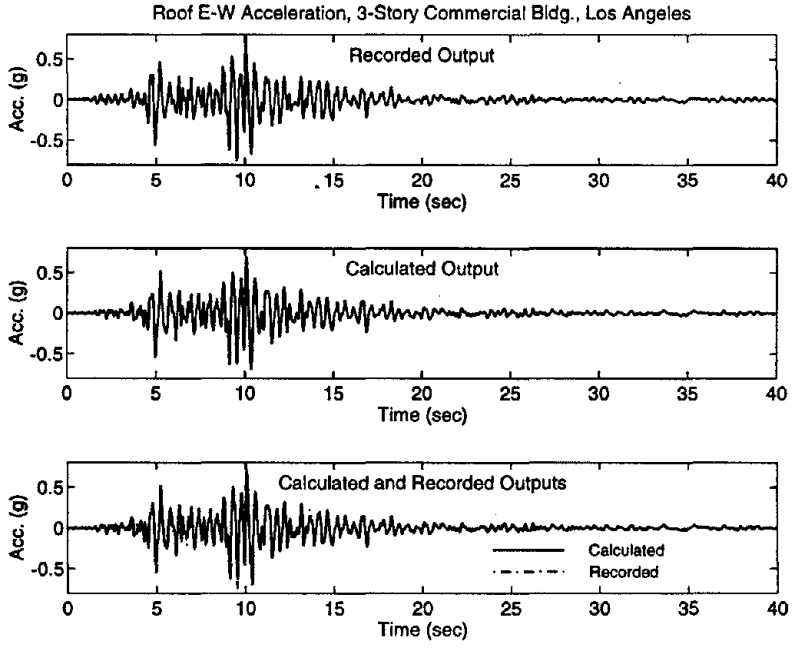

Figure C.10.4. Comparison of time-histories: recorded motions and calculated motions from WPCMIMO in E-W direction.

Table C.10.2. Results of system identification in N-S (transverse) direction by WPCMIMO.

Mode No.	Frequency (Hz)	Damping	Part. Factor	Initial Disp.	Initial Velo.	Modal Cont.	Comments
1	1.8938	0.4290	-328.2E-1	-1.98E-01	8.43E-01	1.59E+02	
2	1.8066	0.0071	-5.95E-02	3.04E-03	-1.64E-02	3.13E-02	1st Mode*
3	3.6306	0.0903	1.44E-01	4.51E-04	-1.64E-02	6.54E-02	
4	2.0896	0.3859	2.39E+01	1.24E-01	-6.05E-01	1.16E+02	
5	1.4502	0.3263	5.05E-00	6.08E-02	-1.73E-01	2.92E+00	
6	4.0497	0.0475	6.91E-02	-3.50E-04	-5.49E-03	4.10E-02	

* Damping is not reliable

Relative Error = 0.366 and Absolute Error = 4.888

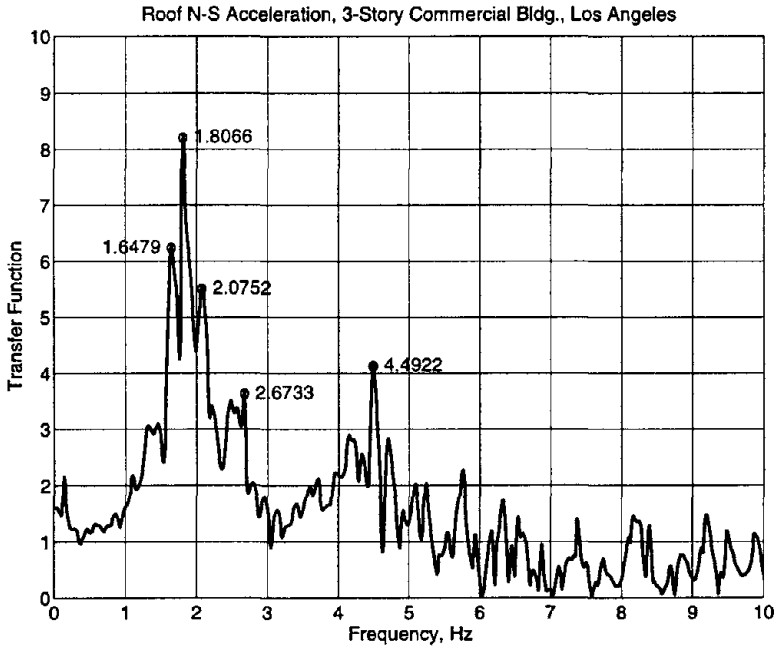

Figure C.10.5. Initial frequency estimates from transfer function in N-S direction.

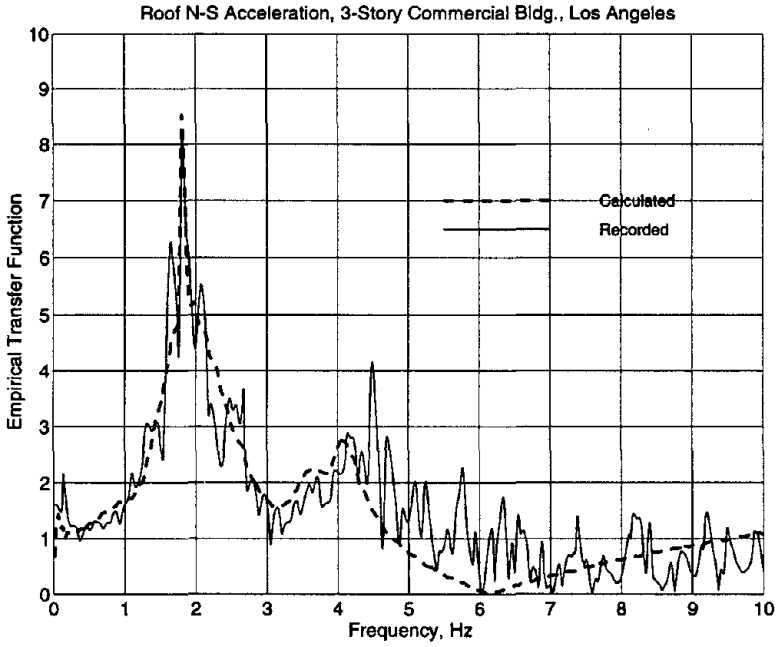

Figure C.10.6. Comparison of empirical transfer functions: recorded motions and calculated motions from WPCMIMO in N-S direction.

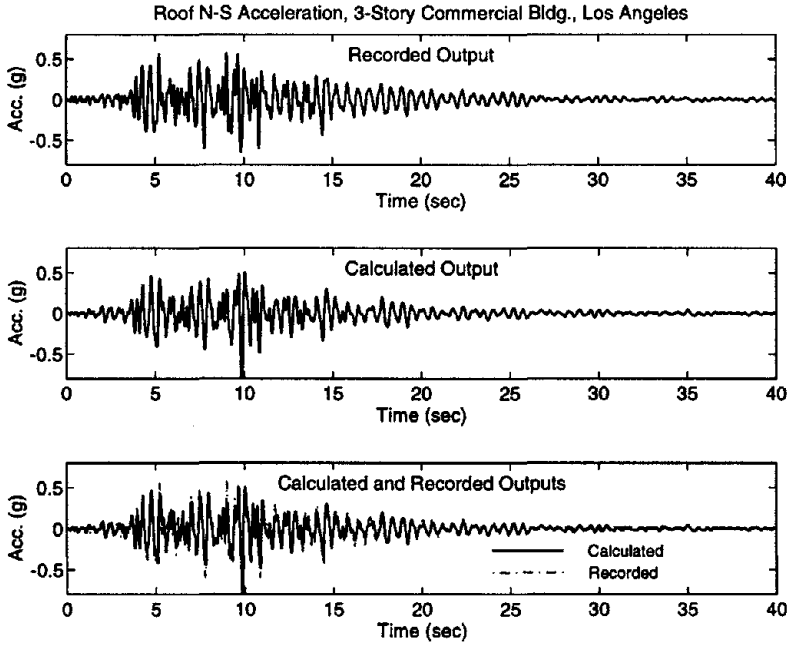

Figure C.10.7. Comparison of time-histories: recorded motions and calculated motions from WPCMIMO in N-S direction.

11. Los Angeles - 17-Story Residential Building, CSMIP Station No. 24601

Figure C.11.1a. Details of 17-story residential building, CSMIP Station No. 24601

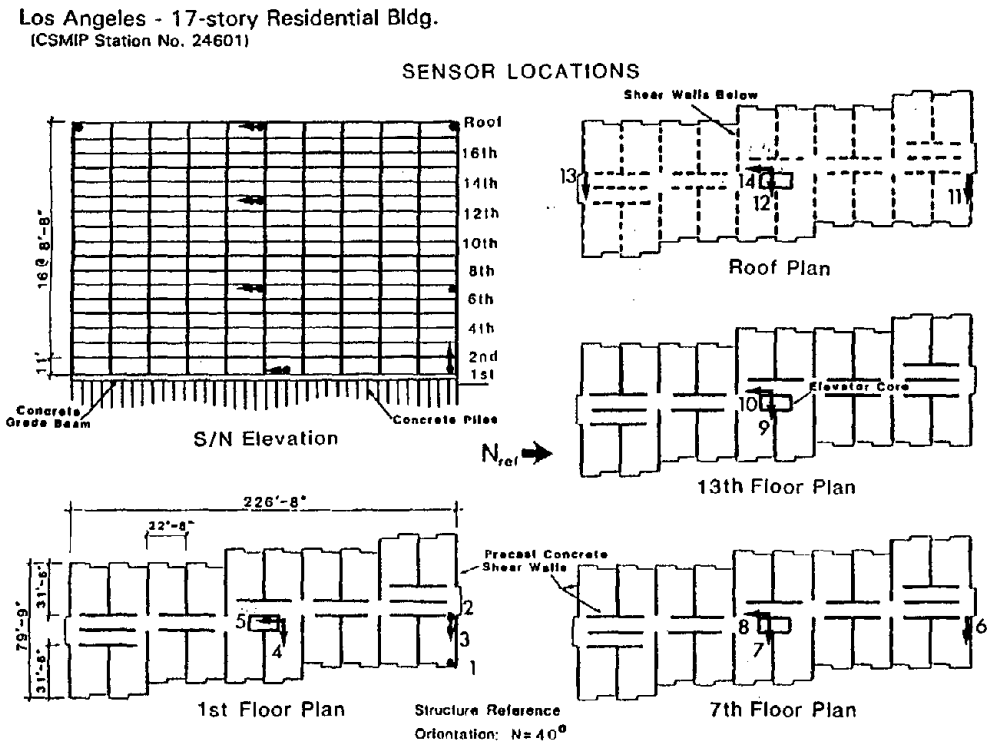

Figure C.11.1b. Sensor locations in 17-story residential building, CSMIP Station No. 24601

Table C.11.1. Results of system identification in N-S (longitudinal) direction by WPCMIMO.

Mode No.	Frequency (Hz)	Damping	Part. Factor	Initial Disp.	Initial Velo.	Modal Cont.	Comments
1	0.8493	0.0401	-3.18E-00	-1.47E-03	6.31E-03	8.09E-01	1st Mode
2	4.1504	0.1069	1.12E+01	-1.41E-03	-3.66E-02	9.39E+01	2nd Mode*
3	4.1576	0.1080	-1.10E+01	1.38E-03	3.78E-02	8.94E+01	
4	6.1290	0.0506	-7.70E-03	2.58E-06	1.40E-04	9.50E-05	
5	12.3674	0.0136	9.62E-04	2.47E-07	3.07E-09	2.00E-06	
6	8.2835	0.1204	-1.18E-01	4.55E-06	1.86E-04	3.57E-03	

Not reliable
Relative Error = 0.248 and Absolute Error = 3.265

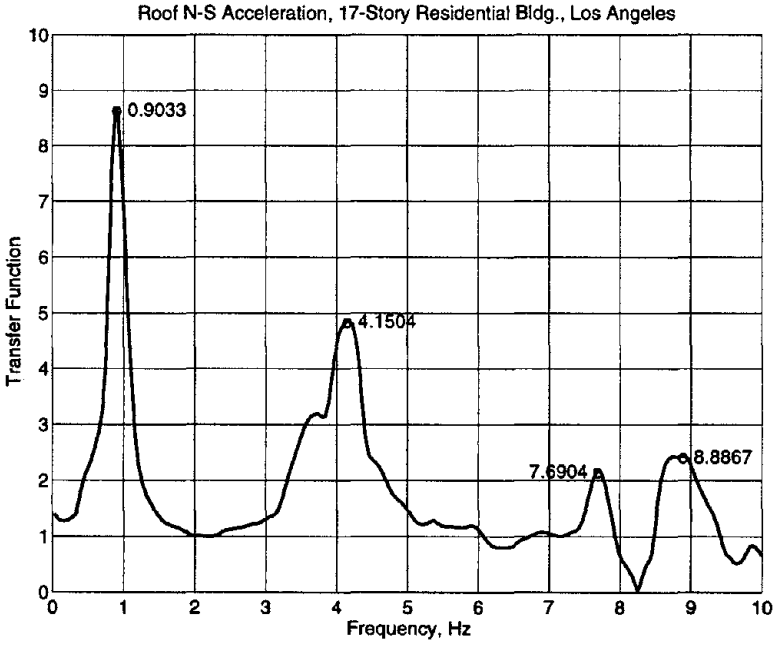

Figure C.11.2. Initial frequency estimates from transfer function in N-S direction.

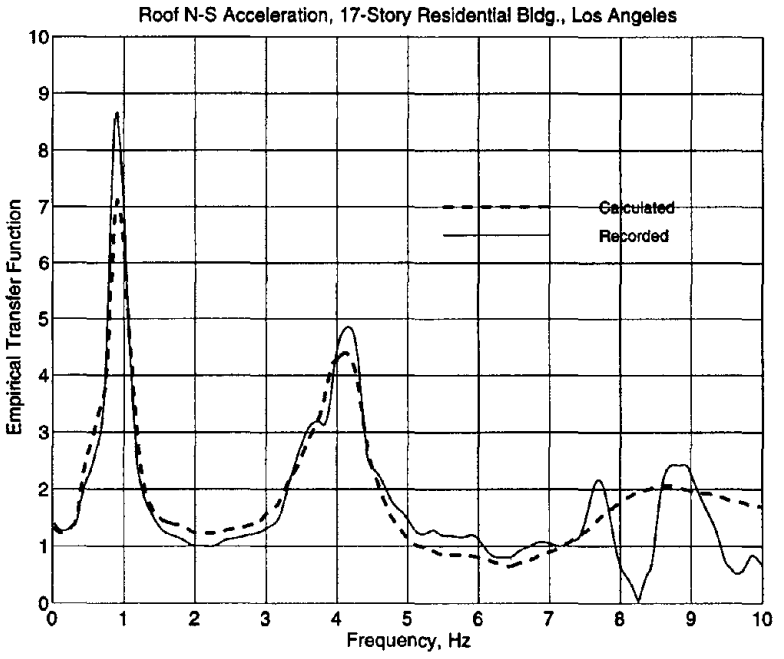

Figure C.11.3. Comparison of empirical transfer functions: recorded motions and calculated motions from WPCMIMO in N-S direction.

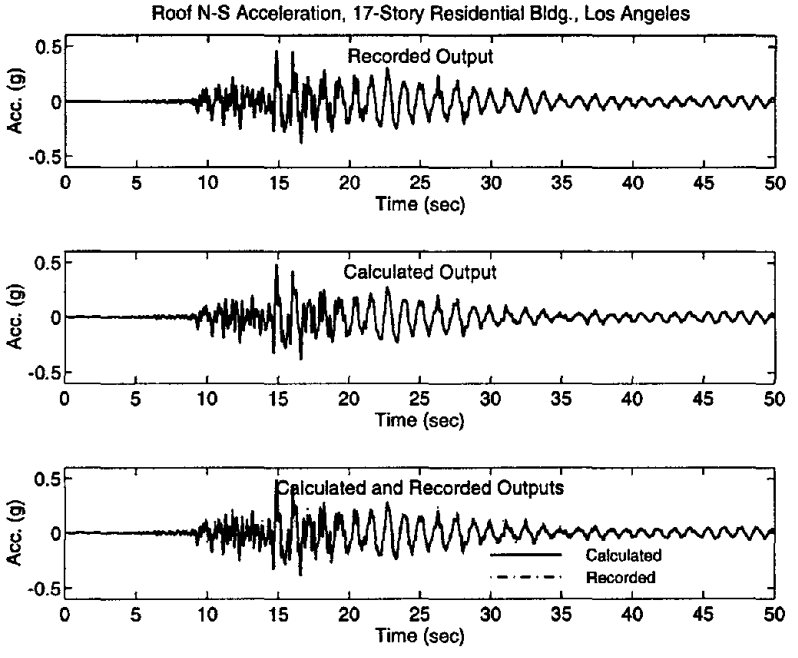

Figure C.11.4. Comparison of time-histories: recorded motions and calculated motions from WPCMIMO in N-S direction.

Table C.11.2. Results of system identification in E-W (transverse) direction by WPCMIMO.

Mode No.	Frequency (Hz)	Damping	Part. Factor	Initial Disp.	Initial Velo.	Modal Cont.	Comments
1	0.9506	0.0331	-2.43E-00	-1.79E-03	-3.31E-03	8.30E-01	1st Mode
2	4.5000	0.0115	3.34E-02	-4.18E-06	7.07E-04	2.74E-03	
3	4.7540	0.0090	3.60E-02	7.18E-06	-4.78E-04	4.35E-03	
4	5.3400	0.0902	9.89E-02	-1.43E-05	6.67E-04	5.76E-03	
5	10.3040	0.1082	-6.32E-02	4.36E-06	3.53E-04	1.29E-03	
6	7.3071	0.0468	-1.03E-02	-1.39E-07	3.23E-04	2.02E-04	

Relative Error = 0.352 and Absolute Error = 6.348

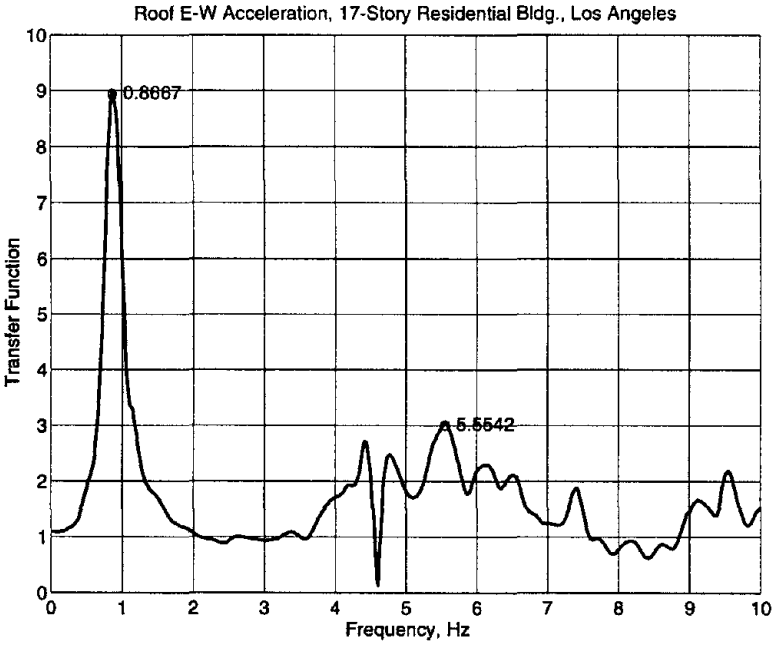

Figure C.11.5. Initial frequency estimates from transfer function in E-W direction.

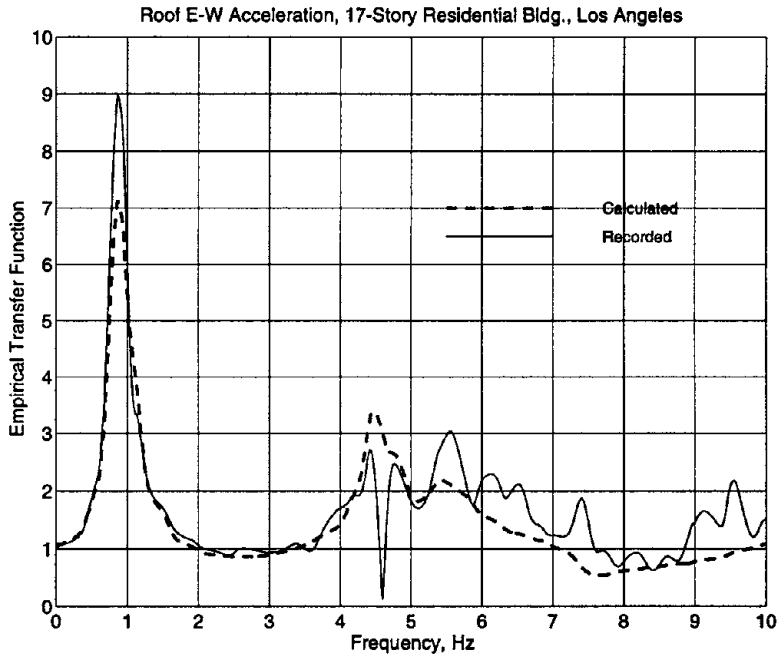

Figure C.11.6. Comparison of empirical transfer functions: recorded motions and calculated motions from WPCMIMO in E-W direction.

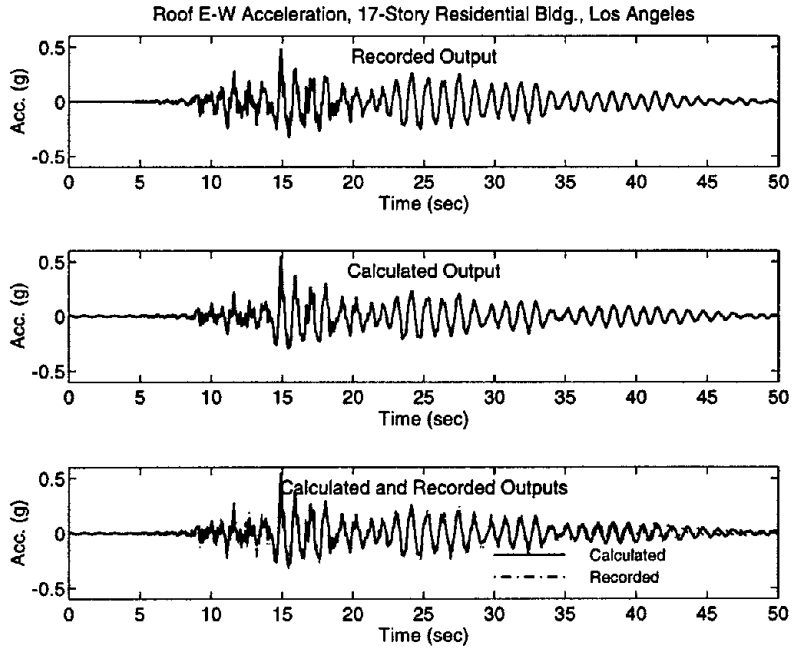

Figure C.11.7. Comparison of time-histories: recorded motions and calculated motions from WPCMIMO in E-W direction.

12. Los Angeles - 15-Story Govt. Office Building, CSMIP Station No. 24569

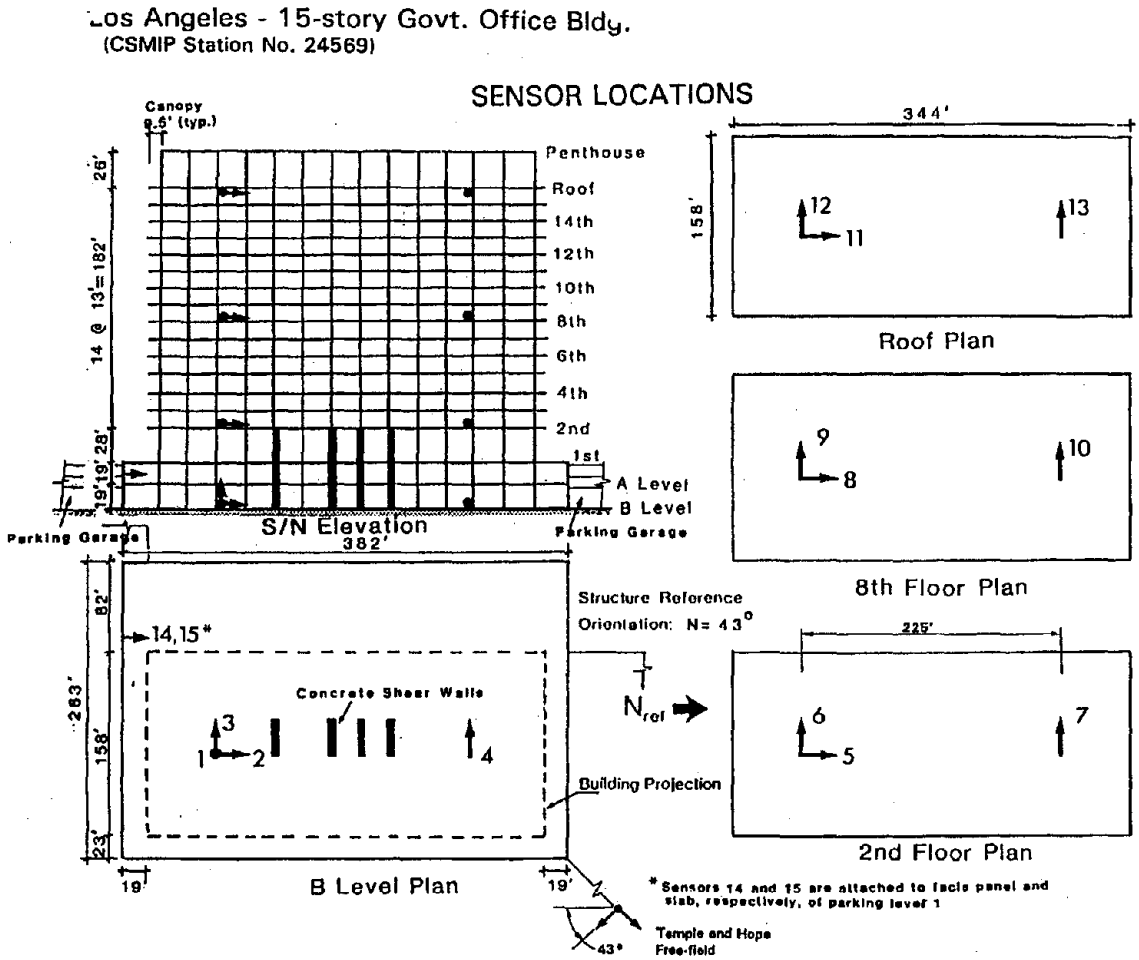

Figure C.12.1. Sensor locations in 15-story office building, CSMIP Station No. 24569

Table C.12.1. Results of system identification in N-S (longitudinal) direction by WPCMIMO.

Mode No.	Frequency (Hz)	Damping	Part. Factor	Initial Disp.	Initial Velo.	Modal Cont.	Comments
1	0.3220	0.0241	-6.99E-00	-3.78E-04	2.24E-03	1.06E+00	1st Mode
2	0.8667	0.0390	1.05E-00	4.76E-05	7.97E-04	3.28E-01	2nd Mode
3	1.4200	0.0887	-3.89E-01	2.11E-05	-3.86E-05	1.28E-01	
4	2.1877	0.0358	1.06E-01	4.05E-06	-4.07E-05	4.89E-02	

Relative Error = 0.326 and Absolute Error = 0.683

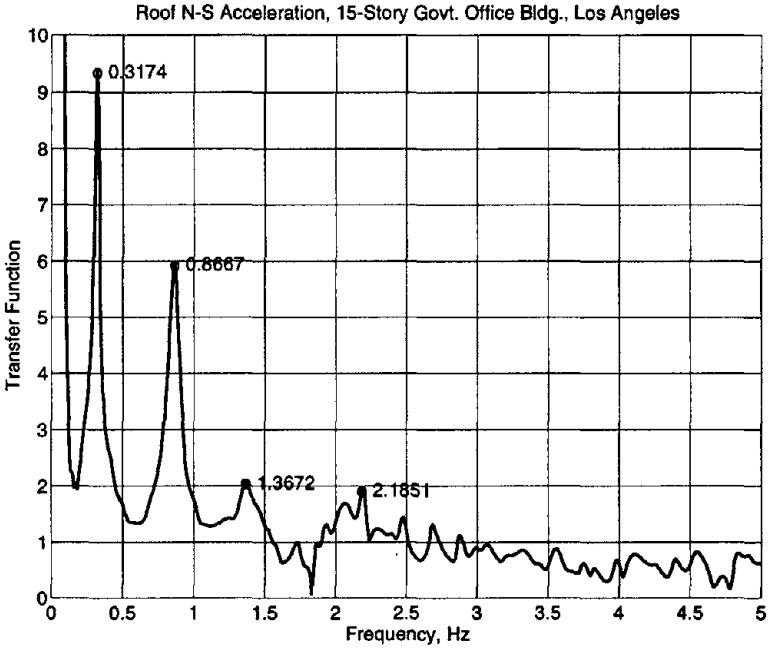

Figure C.12.2. Initial frequency estimates from transfer function in N-S direction.

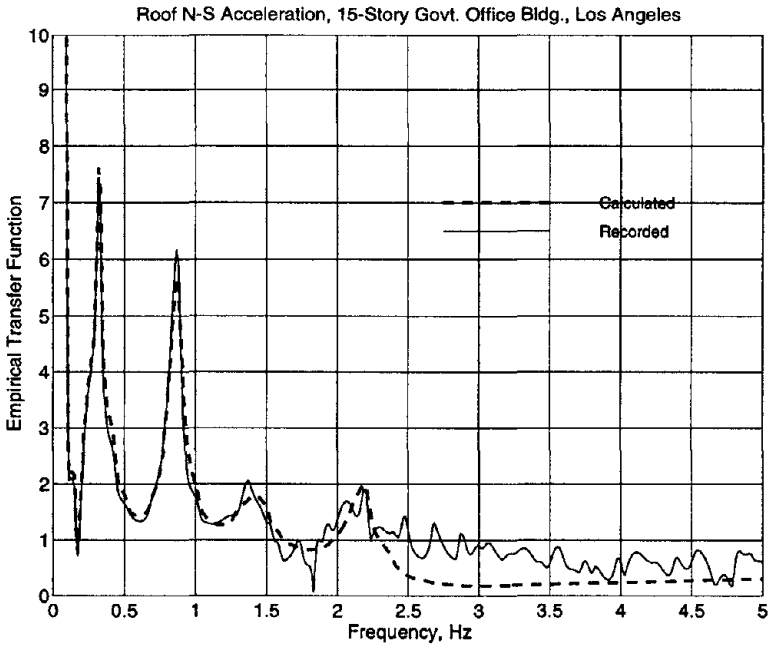

Figure C.12.3. Comparison of empirical transfer functions: recorded motions and calculated motions from WPCMIMO in N-S direction.

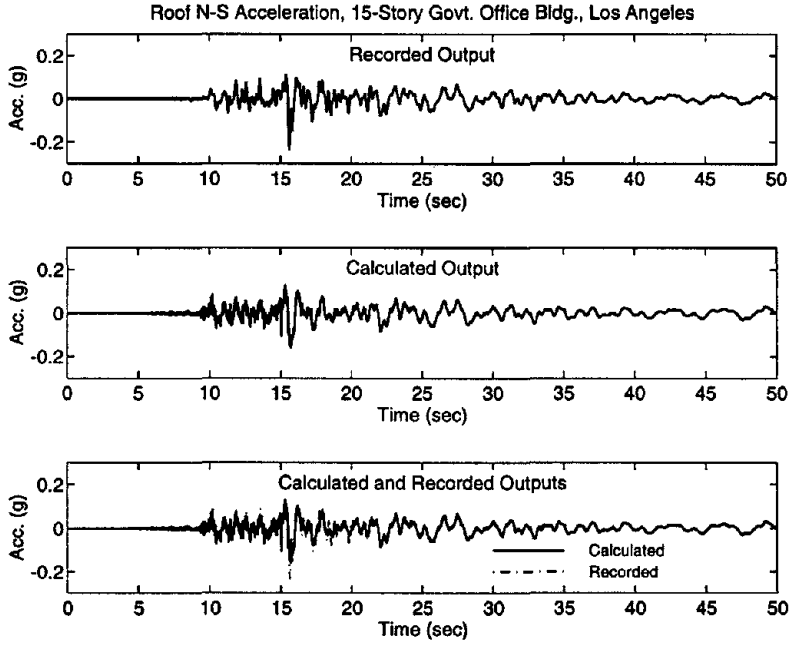

Figure C.12.4. Comparison of time-histories: recorded motions and calculated motions from WPCMIMO in N-S direction.

Table C.12.2. Results of system identification in E-W (transverse) direction by WPCMIMO.

Mode No.	Frequency (Hz)	Damping	Part. Factor	Initial Disp.	Initial Velo.	Modal Cont.	Comments
1	0.3133	0.0154	-6.47E-00	-7.86E-04	-1.40E-03	5.59E-01	1st Mode
2	0.8555	0.0321	1.01E-00	-6.49E-04	9.07E-04	3.84E-01	2nd Mode
3	1.9356	0.3273	-1.43E-00	-7.41E-04	6.63E-03	7.01E-01	
4	2.1726	0.1557	7.93E-01	5.30E-04	5.61E-04	6.00E-01	
5	2.3915	0.0172	1.11E-00	-3.02E-04	-3.29E-02	6.12E+00	
6	2.3915	0.0153	-1.00E-00	2.70E-04	3.07E-02	5.19E+00	
7	2.9069	0.0598	-1.58E-01	-1.95E-05	-9.07E-04	7.50E-02	
8	3.6051	0.0517	1.41E-01	-6.22E-06	-2.31E-04	1.14E-01	

Relative Error = 0.310 and Absolute Error = 0.556

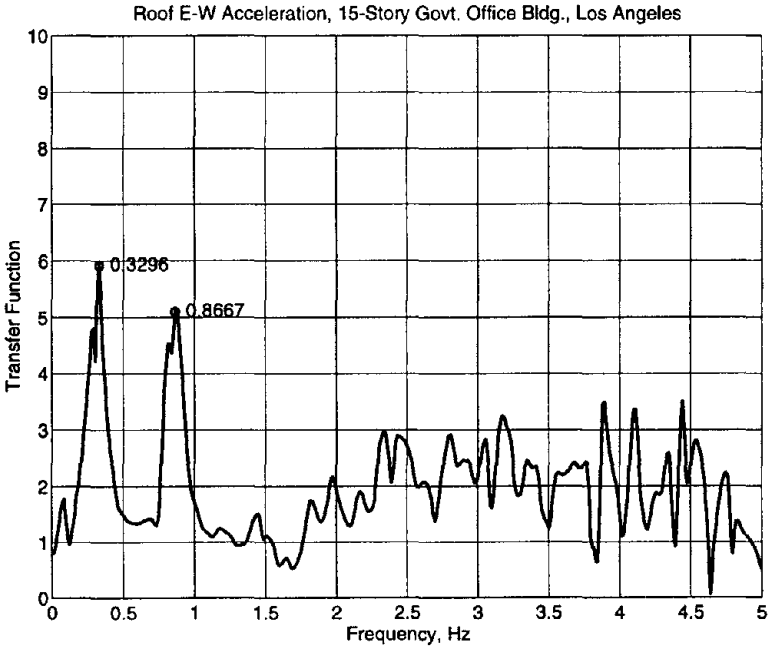

Figure C.12.5. Initial frequency estimates from transfer function in E-W direction.

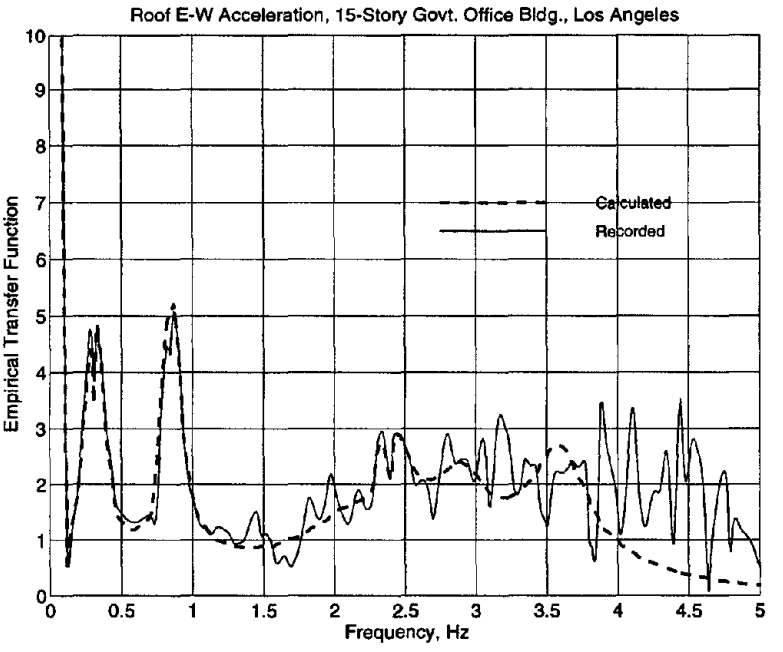

Figure C.12.6. Comparison of empirical transfer functions: recorded motions and calculated motions from WPCMIMO in E-W direction.

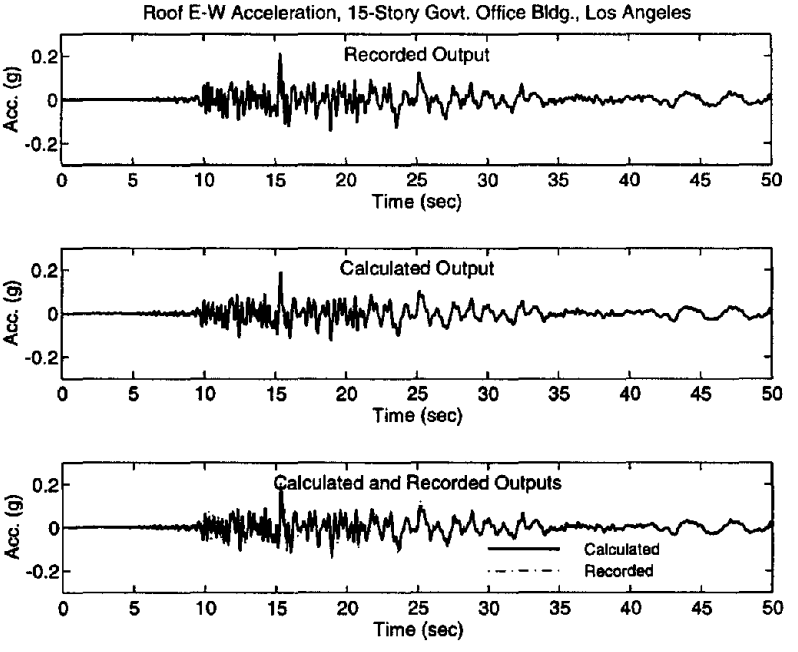

Figure C.12.7. Comparison of time-histories: recorded motions and calculated motions from WPCMIMO in E-W direction.

13. Los Angeles - 52-Story Office Building, CSMIP Station No. 24602

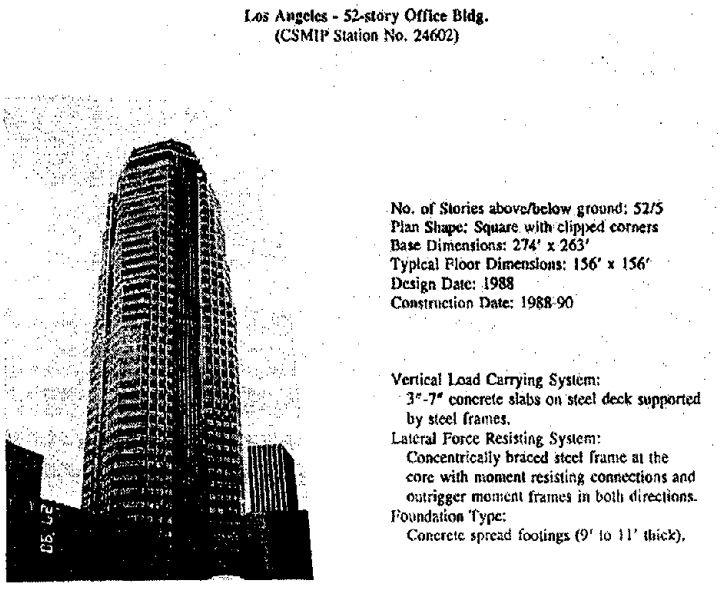

Figure C.13.1a. Details of 52-story office building, CSMIP Station No. 24602

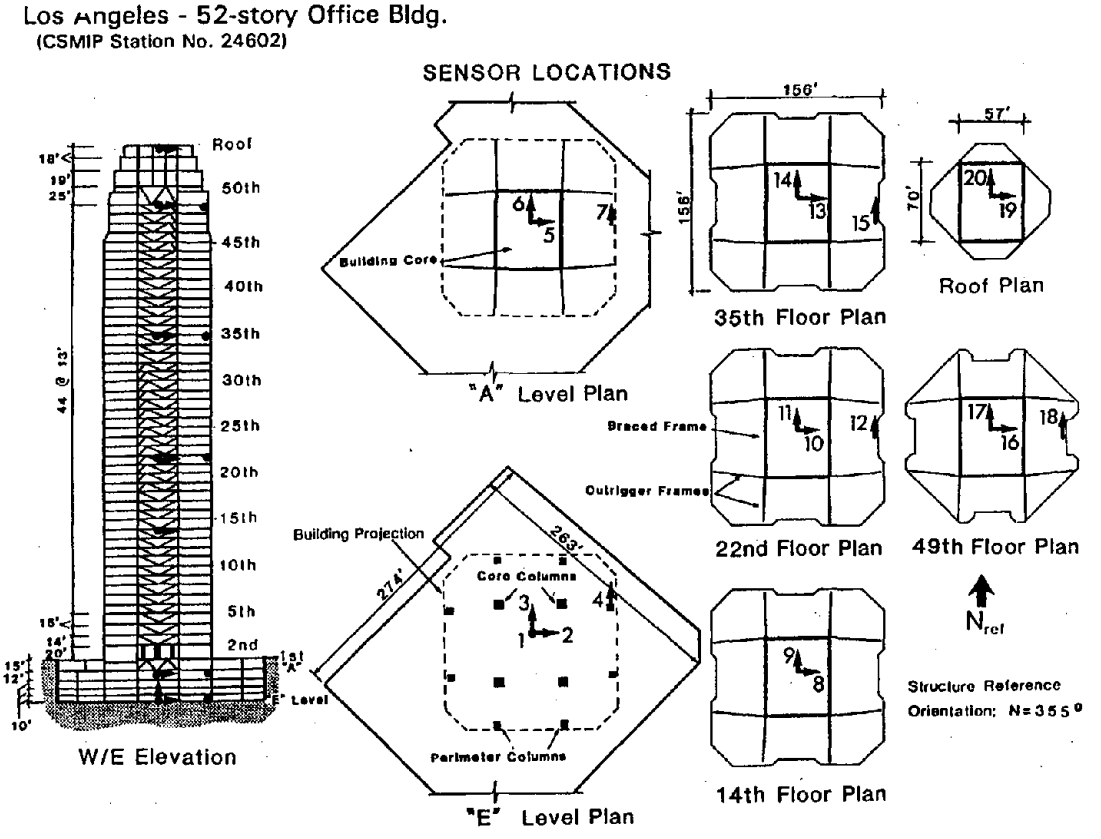

Figure C.13.1b. Sensor locations in 52-story office building, CSMIP Station No. 24602

Table C.13.1. Results of system identification in E-W (longitudinal) direction by WPCMIMO.

Mode No.	Frequency (Hz)	Damping	Part. Factor	Initial Disp.	Initial Velo.	Modal Cont.	Comments
1	0.1612	0.0065	-1.41E+01	-4.20E-03	-4.36E-04	1.92E-01	1st Mode
2	0.5371	0.0146	2.34E-00	-2.01E-03	-9.67E-03	3.84E-01	2nd Mode
3	1.0332	0.0177	-9.09E-01	-3.24E-04	3.89E-03	3.07E-01	
4	1.5220	0.0218	5.08E-01	1.10E-04	2.83E-04	1.41E-01	
5	1.9951	0.0303	-3.70E-01	5.04E-06	2.68E-04	8.11E-02	
6	2.4731	0.0198	1.52E-01	1.94E-05	-2.38E-04	3.37E-02	
7	3.2628	0.0194	7.60E-02	1.38E-05	4.45E-04	1.20E-02	
8	3.6766	0.0208	-4.04E-02	1.10E-05	1.75E-04	9.38E-03	
9	2.9215	0.0251	-1.58E-00	-4.53E-04	-1.54E-02	1.67E+00	
10	2.9367	0.0245	1.48E-00	3.46E-04	1.61E-02	1.52E+00	

Relative Error = 0.245 and Absolute Error = 1.071

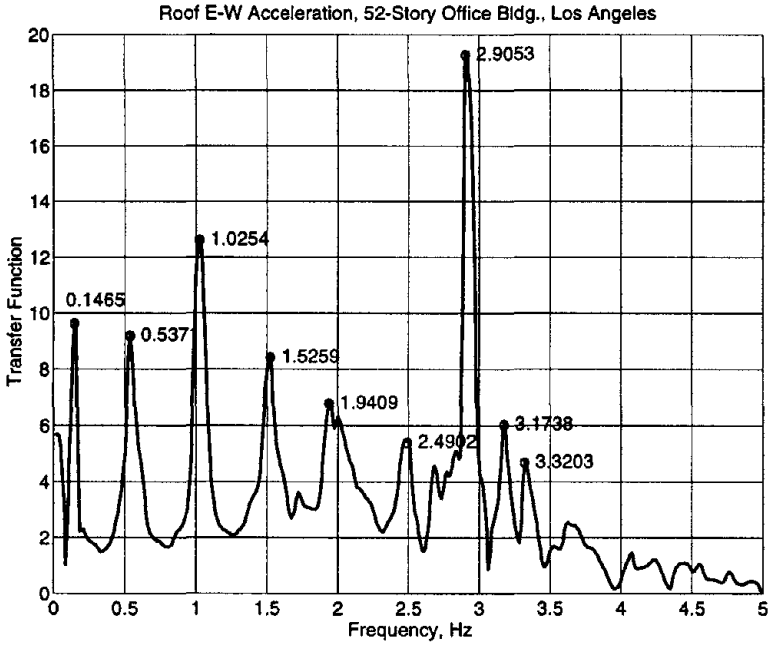

Figure C.13.2. Initial frequency estimates from transfer function in E-W direction.

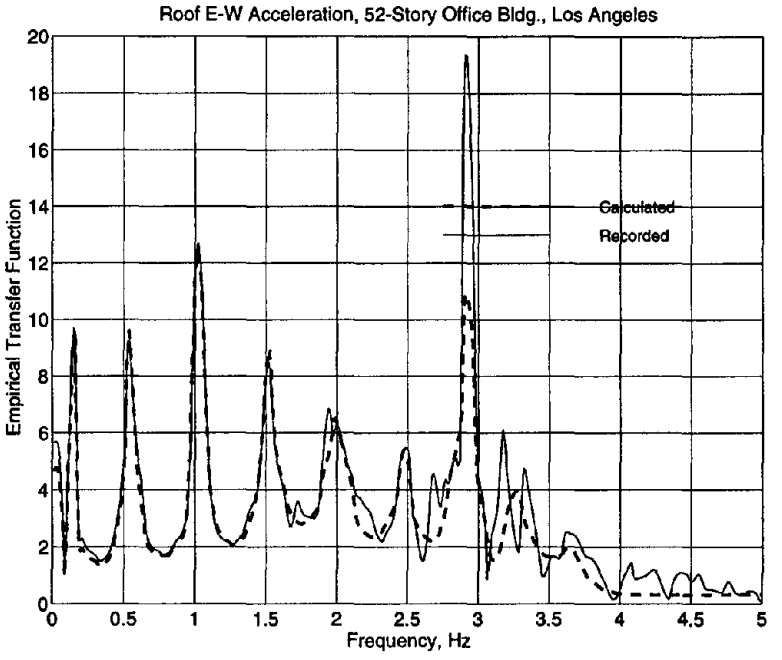

Figure C.13.3. Comparison of empirical transfer functions: recorded motions and calculated motions from WPCMIMO in E-W direction.

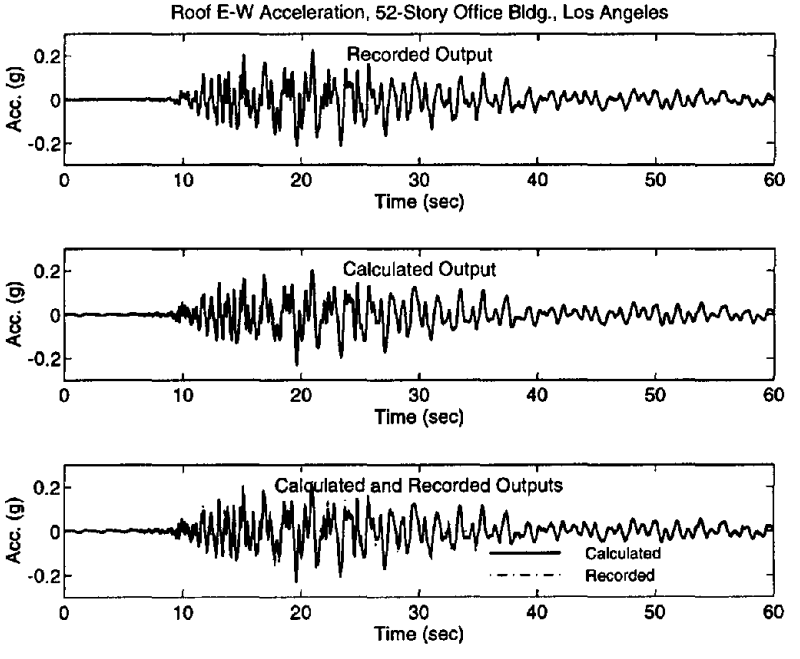

Figure C.13.4. Comparison of time-histories: recorded motions and calculated motions from WPCMIMO in E-W direction.

Table C.13.2. Results of system identification in N-S (transverse) direction by WPCMIMO.

Mode No.	Frequency (Hz)	Damping	Part. Factor	Initial Disp.	Initial Velo.	Modal Cont.	Comments
1	0.1673	0.0303	-2.13E+01	-2.25E-03	-1.07E-03	3.17E-01	1st Mode
2	0.5371	0.0509	4.16E-00	-3.91E-03	-6.53E-03	2.70E-01	2nd Mode
3	1.0178	0.0131	-7.33E-01	-1.96E-04	8.26E-05	1.97E-01	
4	1.4625	0.0228	4.77E-01	-7.38E-05	-4.71E-05	2.47E-01	
5	1.8992	0.0320	-3.61E-01	-1.52E-04	6.39E-04	8.10E-02	
6	3.1560	0.0300	9.21E-02	9.60E-05	-1.92E-03	1.80E-02	
7	2.3602	0.0113	1.18E-01	1.54E-04	6.99E-04	2.13E-02	
8	2.6214	0.0259	-1.54E-01	-2.56E-05	2.85E-03	2.22E-02	
9	2.2931	0.0463	1.91E-01	-4.20E-04	2.86E-03	2.42E-02	
10	2.9765	0.0059	2.16E-02	9.52E-05	9.84E-04	1.27E-03	
11	2.7816	0.0052	-8.66E-02	1.00E-04	1.75E-03	7.16E-03	

Relative Error = 0.448 and Absolute Error = 4.326

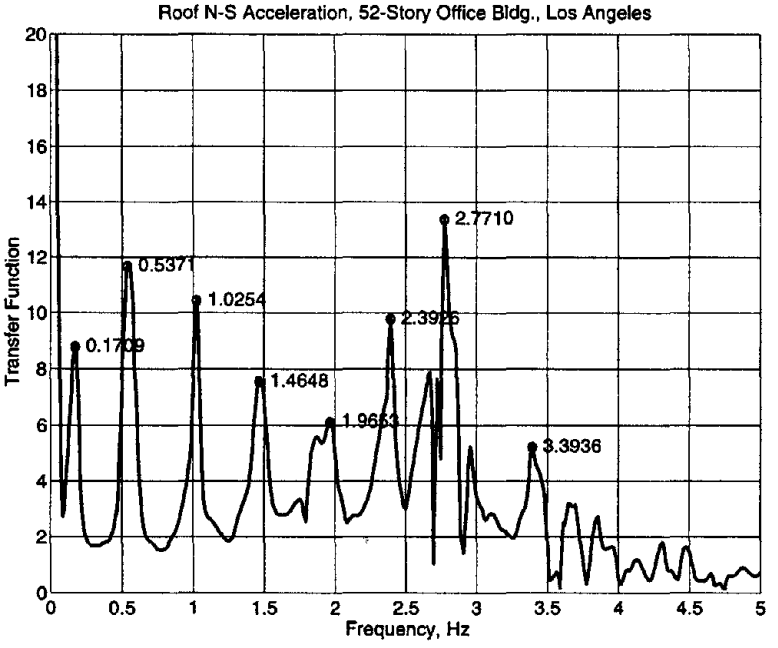

Figure C.13.5. Initial frequency estimates from transfer function in N-S direction.

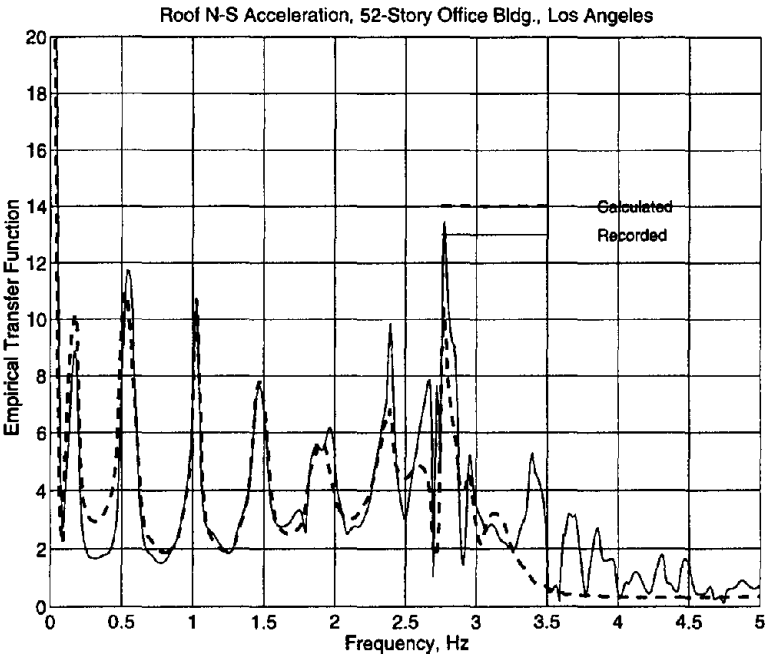

Figure C.13.6. Comparison of empirical transfer functions: recorded motions and calculated motions from WPCMIMO in N-S direction.

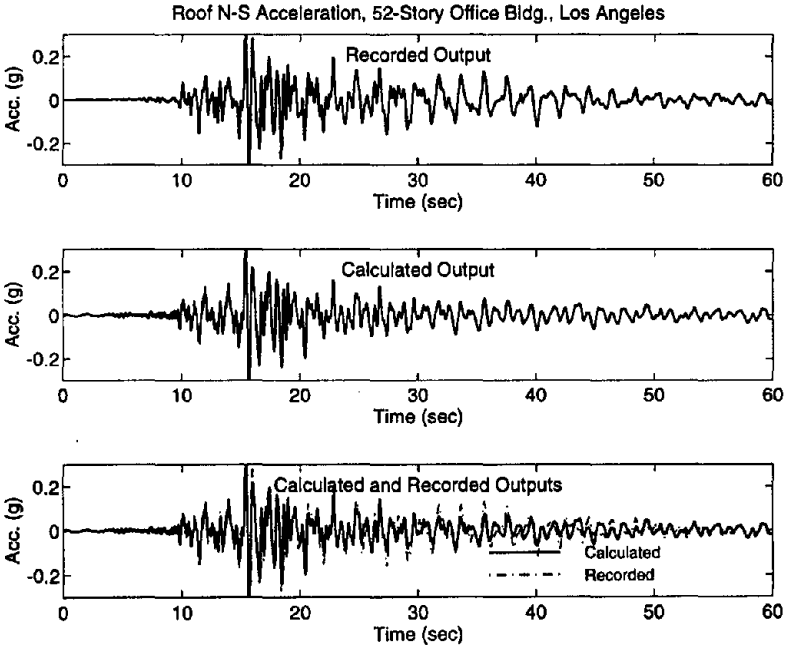

Figure C.13.7. Comparison of time-histories: recorded motions and calculated motions from WPCMIMO in N-S direction.

14. Los Angeles - 9-Story Office Building, CSMIP Station No. 24579

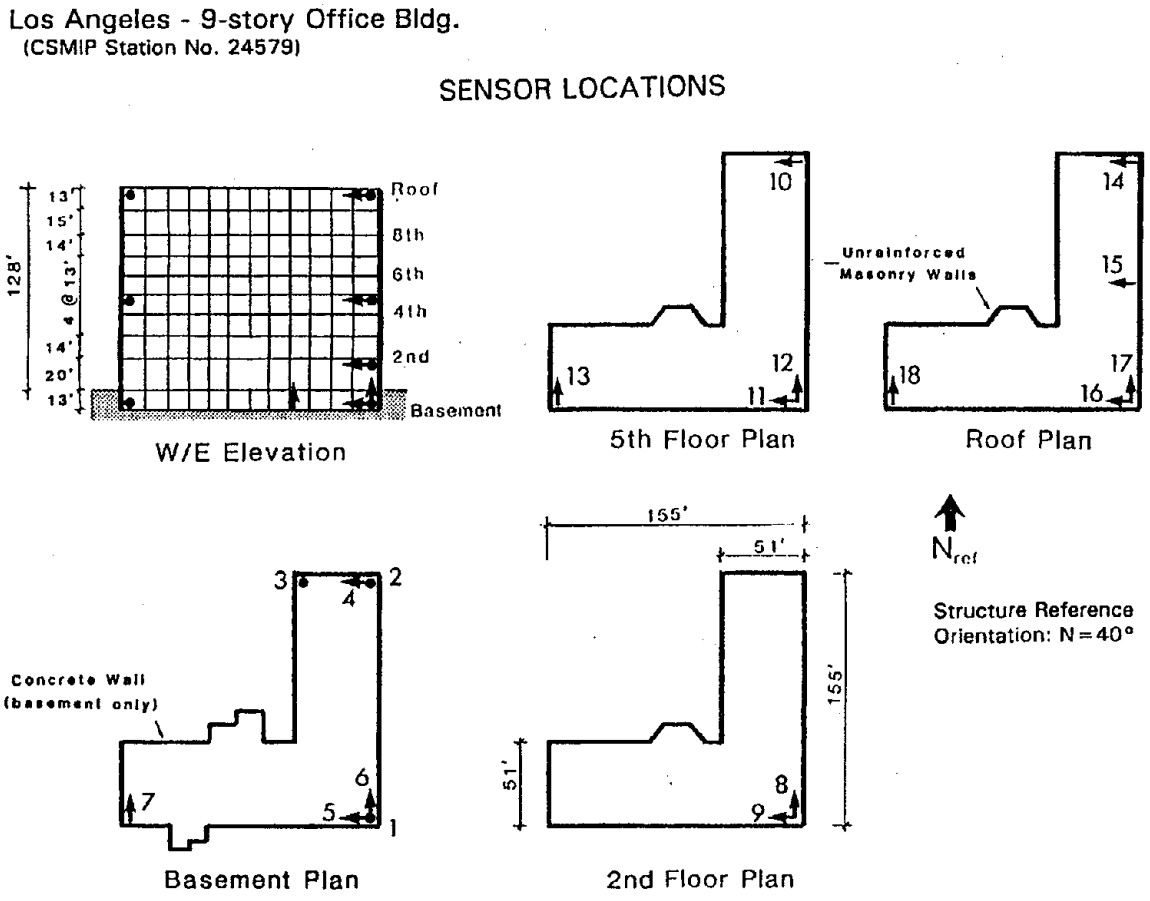

Figure C.14.1. Sensor locations in 9-story office building, CSMIP Station No. 24579

Table C.14.1. Results of system identification in E-W (longitudinal) direction by WPCMIMO.

Mode No.	Frequency (Hz)	Damping	Part. Factor	Initial Disp.	Initial Velo.	Modal Cont.	Comments
1	0.0143	0.0042	6.12E+01	1.23E-02	7.92E-03	5.51E-02	
2	0.6226	0.0136	-1.94E+01	-8.82E-01	-2.31E-00	1.37E+02	
3	0.7172	0.0830	-2.96E-00	-3.44E-03	1.99E-02	6.83E-01	1st Mode
4	0.8163	0.0135	-3.30E-01	-6.42E-04	-2.90E-04	3.24E-02	
5	0.6224	0.0134	1.87E+01	8.82E-01	2.28E-00	1.34E+02	
6	0.9218	0.0005	5.40E-03	-2.21E-04	5.60E-03	1.77E-03	
7	2.4321	0.0833	1.71E-01	7.72E-05	4.92E-03	8.40E-02	
8	2.8442	0.0018	1.92E-02	7.01E-05	-2.14E-03	8.65E-03	
9	2.7451	0.0044	1.41E-02	1.11E-05	-5.29E-04	4.79E-03	
10	3.8004	0.0097	-1.38E-02	-5.96E-06	-1.26E-04	5.02E-03	
11	4.2073	0.0715	-5.66E-02	4.28E-07	4.26E-04	1.55E-02	

Relative Error = 0.340 and Absolute Error = 1.352

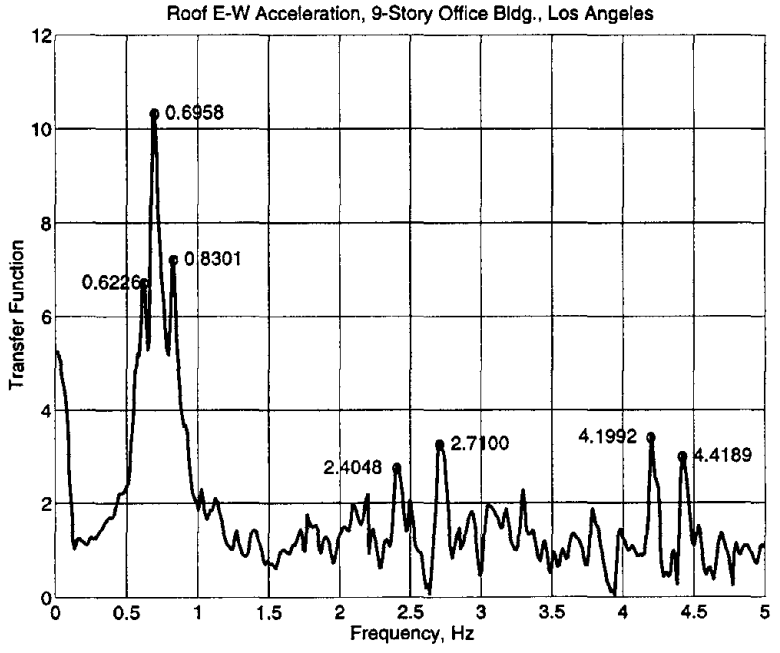

Figure C.14.2. Initial frequency estimates from transfer function in E-W direction.

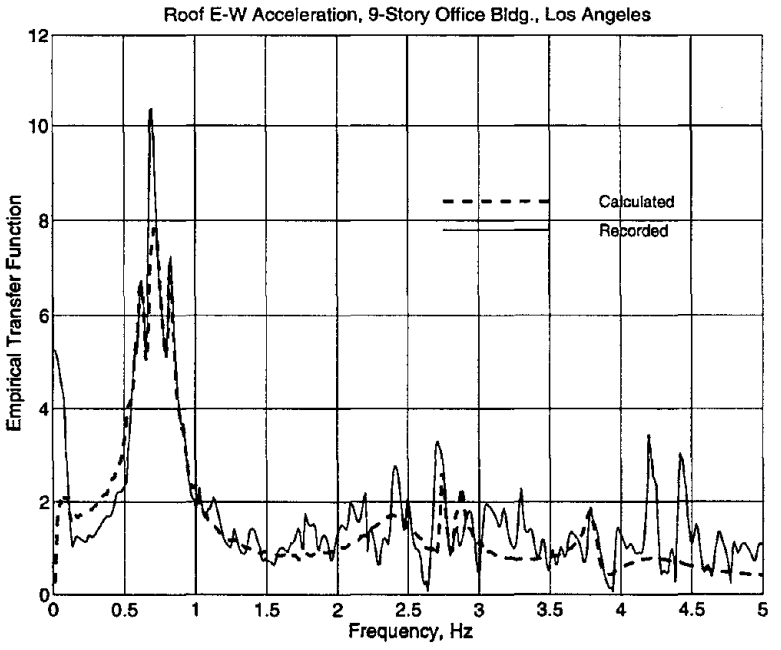

Figure C.14.3. Comparison of empirical transfer functions: recorded motions and calculated motions from WPCMIMO in E-W direction.

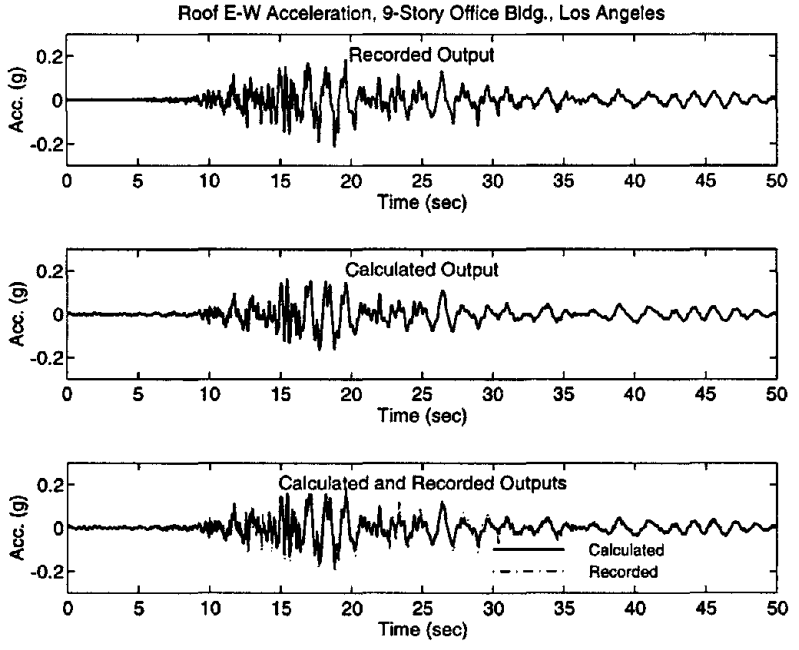

Figure C.14.4. Comparison of time-histories: recorded motions and calculated motions from WPCMIMO in E-W direction.

Table C.14.2. Results of system identification in N-S (transverse) direction by WPCMIMO.

Mode No.	Frequency (Hz)	Damping	Part. Factor	Initial Disp.	Initial Velo.	Modal Cont.	Comments
1	0.6408	0.0060	-1.44E-01	-7.83E-04	-1.28E-02	1.97E-02	
2	0.7813	0.0690	-1.70E-00	3.97E-03	-1.08E-01	2.87E-01	1st Mode
3	0.7588	0.0000	-6.78E-02	3.74E-03	4.90E-02	1.02E-01	
4	1.1144	0.6307	-7.89E-00	-3.46E-02	6.57E-02	2.53E+00	
5	1.3357	0.4244	4.14E-00	8.52E-03	6.82E-03	1.76E+00	
6	2.7573	0.1304	4.18E-01	4.58E-04	1.93E-03	1.80E-01	
7	2.4292	0.0501	9.99E-02	1.65E-08	1.61E-06	2.73E-02	
8	3.0762	0.0500	9.99E-02	1.34E-08	-1.28E-06	3.20E-02	

Relative Error = 0.502 and Absolute Error = 3.267

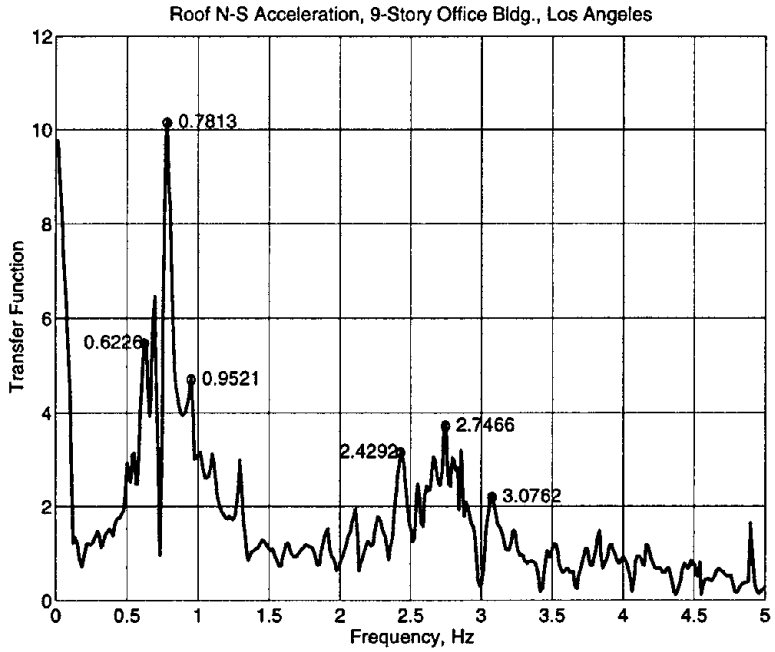

Figure C.14.5. Initial frequency estimates from transfer function in N-S direction.

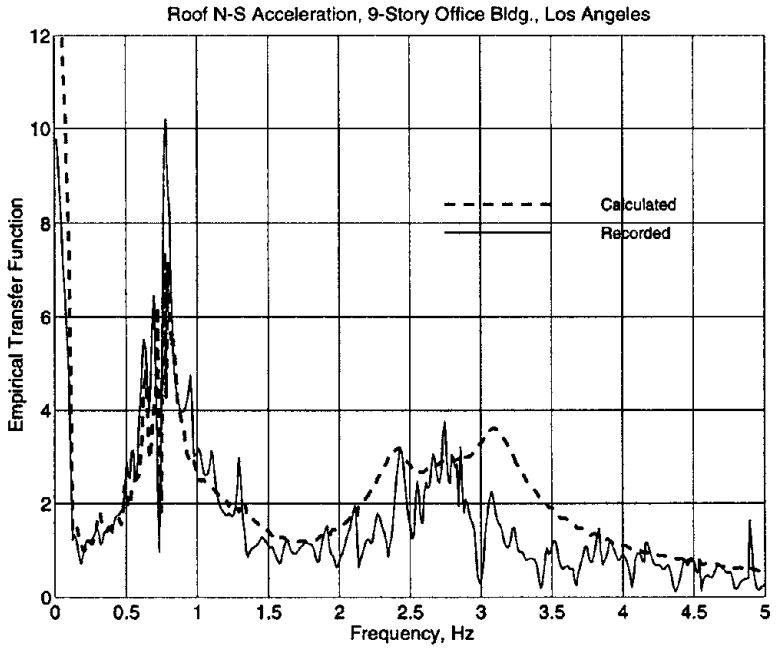

Figure C.14.6. Comparison of empirical transfer functions: recorded motions and calculated motions from WPCMIMO in N-S direction.

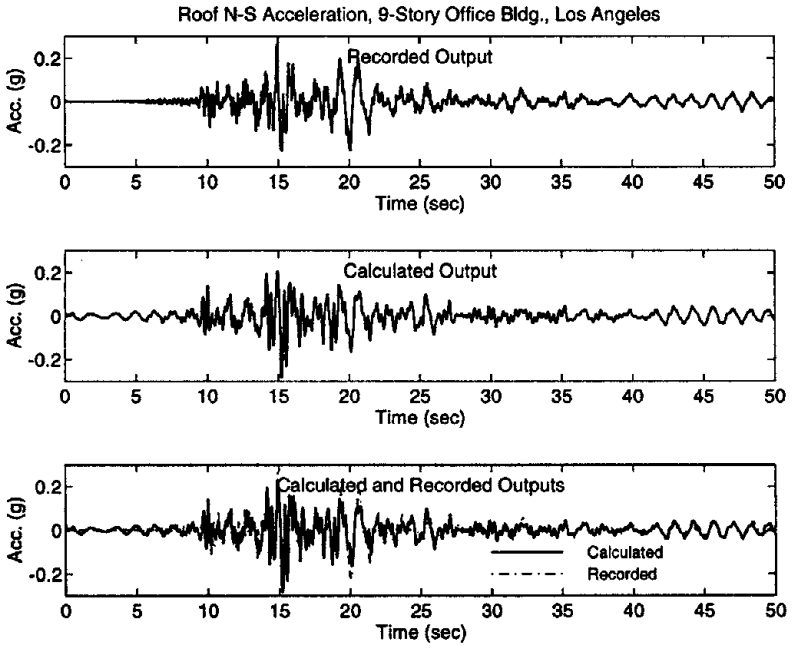

Figure C.14.7. Comparison of time-histories: recorded motions and calculated motions from WPCMIMO in N-S direction.

15. Los Angeles - 8-Story CSULA Administration Building, CSMIP Station No. 24468

Address: Calif. State University at LA
Los Angeles, CA
No. of Stories above/below ground: 8/1
Plan Shape: Rectangular
Base Dimensions: Irregular base shape
Typical Floor Dimensions: 154' x 63'
Design Date: 1967
Construction Date: 1969

Vertical Load Carrying System:
Concrete slabs supported by concrete beams and columns.
Lateral Force Resisting System:
Concrete shear walls except between levels 1 and 2 where composite concrete/steel columns resist lateral forces.
Foundation Type:
Spread footings and concrete caissons.

Figure C.15.1a. Details of 8-story CSULA administration building, CSMIP Station No. 24468

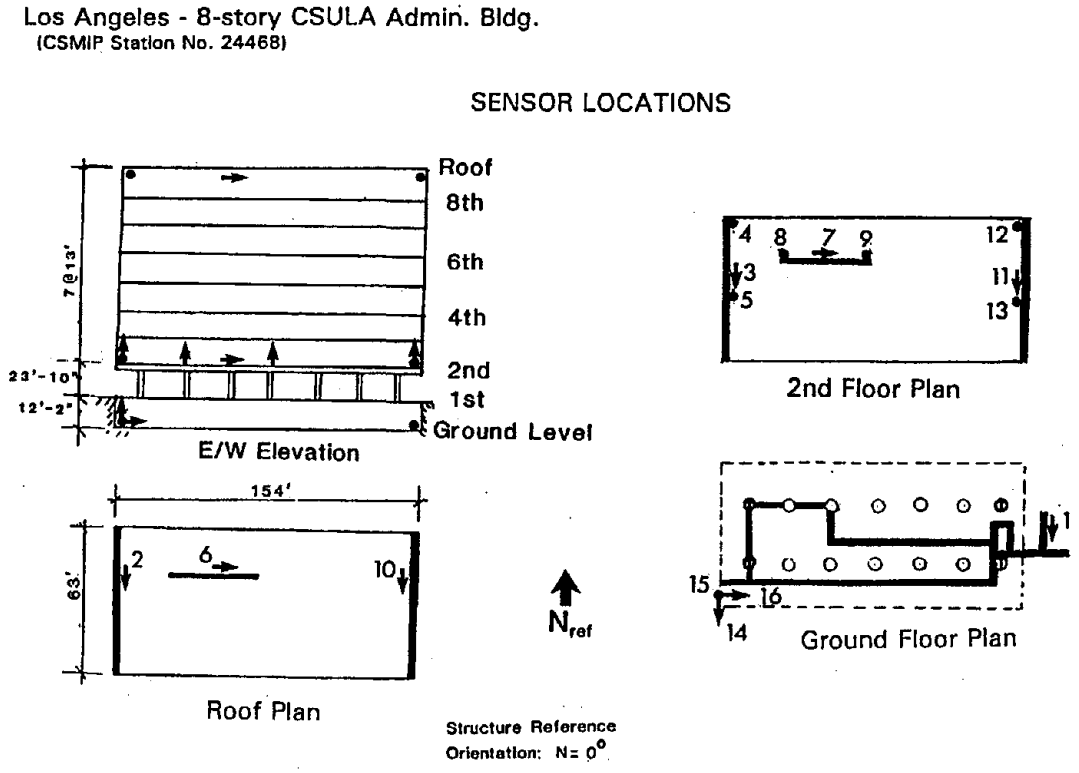

Figure C.15.1b. Sensor locations in 8-story administration building, CSMIP Station No. 24468

Table C.15.1. Results of system identification in E-W (longitudinal) direction by WPCMIMO.

Mode No.	Frequency (Hz)	Damping	Part. Factor	Initial Disp.	Initial Velo.	Modal Cont.	Comments
1	0.6479	0.0360	-3.08E-00	-4.72E-03	1.56E-02	8.78E-01	1st Long. Mode
2	0.7263	0.0304	-2.57E-01	5.14E-03	-4.06E-03	8.95E-03	1st Tor. Mode
3	1.8301	0.0724	3.87E-01	2.19E-04	3.65E-03	8.07E-02	
4	1.9892	0.0030	2.50E-02	2.47E-04	-2.01E-03	3.59E-03	
5	4.5171	0.0449	-2.23E-02	-1.05E-05	-2.67E-04	3.49E-03	
6	3.6944	0.0462	-1.33E-02	-7.75E-06	-5.72E-04	7.17E-04	

Relative Error = 0.240 and Absolute Error = 0.421

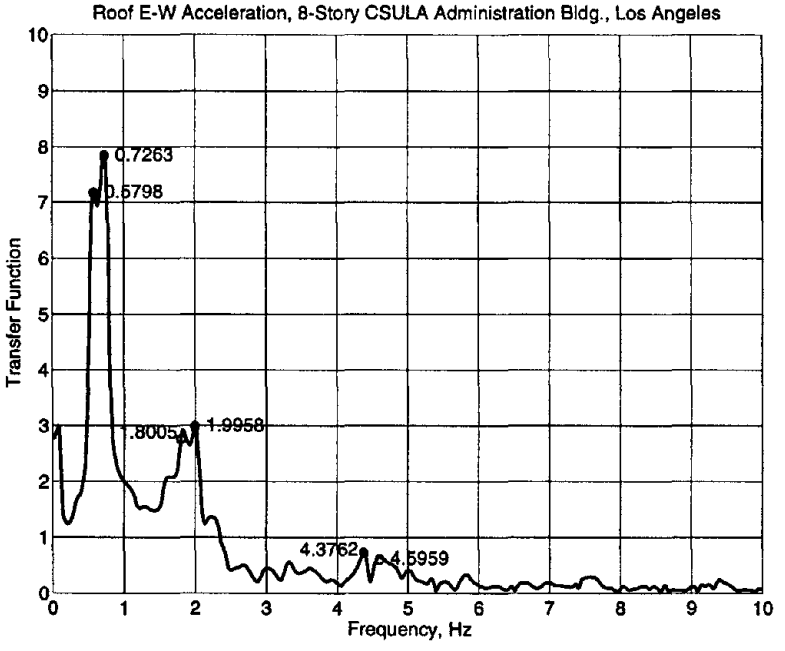

Figure C.15.2. Initial frequency estimates from transfer function in E-W direction.

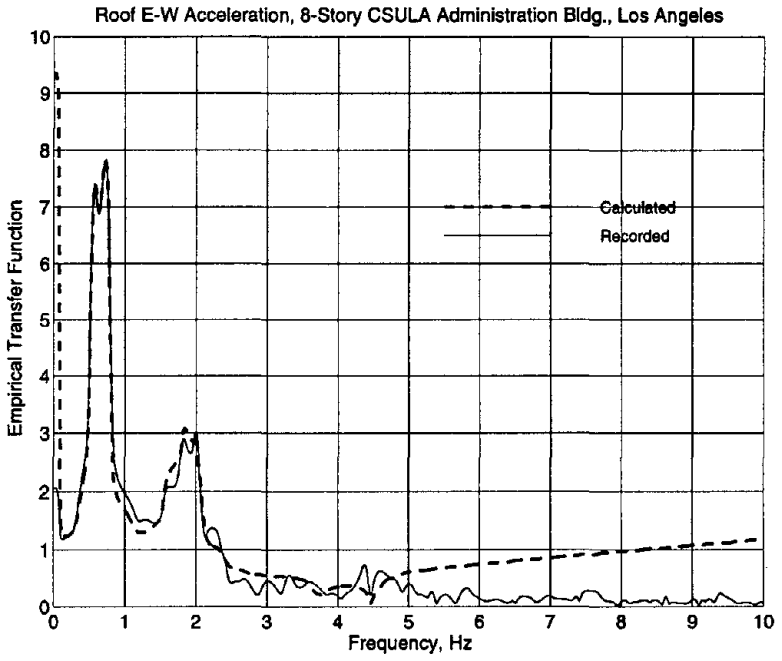

Figure C.15.3. Comparison of empirical transfer functions: recorded motions and calculated motions from WPCMIMO in E-W direction.

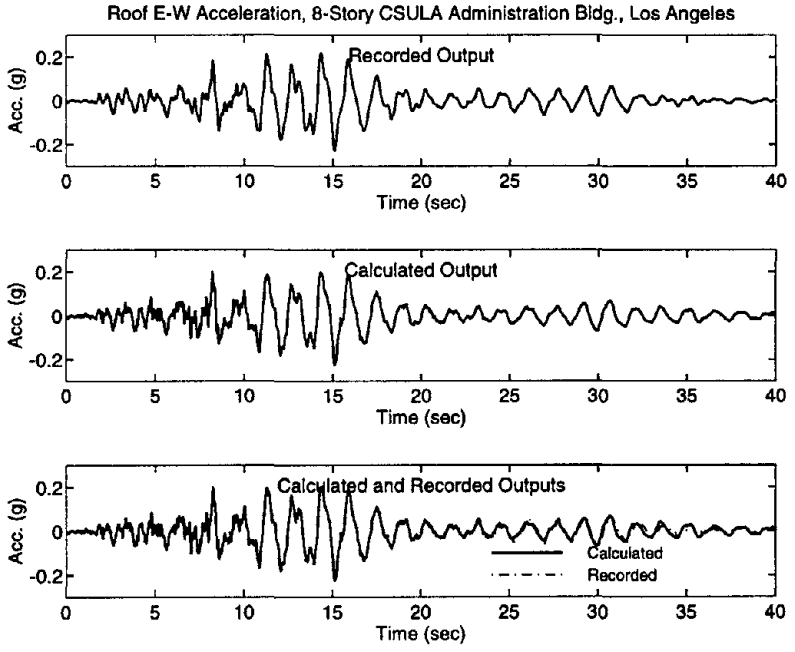

Figure C.15.4. Comparison of time-histories: recorded motions and calculated motions from WPCMIMO in E-W direction.

Table C.15.2. Results of system identification in N-S (transverse) direction by WPCMIMO.

Mode No.	Frequency (Hz)	Damping	Part. Factor	Initial Disp.	Initial Velo.	Modal Cont.	Comments
1	0.6188	0.0370	-4.27E-00	2.91E-03	2.07E-02	9.18E-01	1st Mode
2	1.9653	0.0582	4.56E-01	2.26E-04	2.80E-03	2.51E-01	2nd Mode
3	5.3866	0.4742	-1.72E-01	3.77E-04	-1.74E-02	1.51E-02	
4	5.5919	0.2183	7.03E-02	-6.67E-05	8.51E-03	1.08E-02	

Relative Error = 0.253 and Absolute Error = 0.412

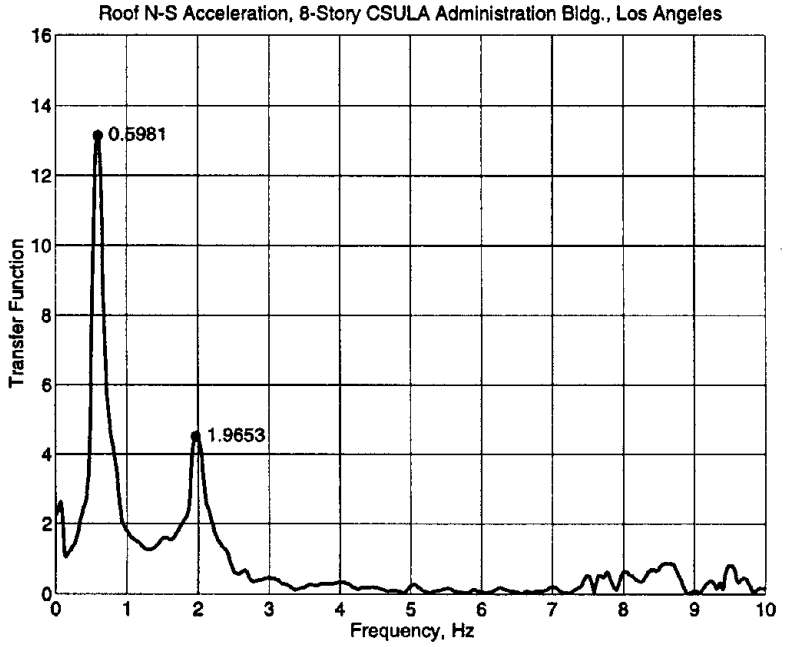

Figure C.15.5. Initial frequency estimates from transfer function in N-S direction.

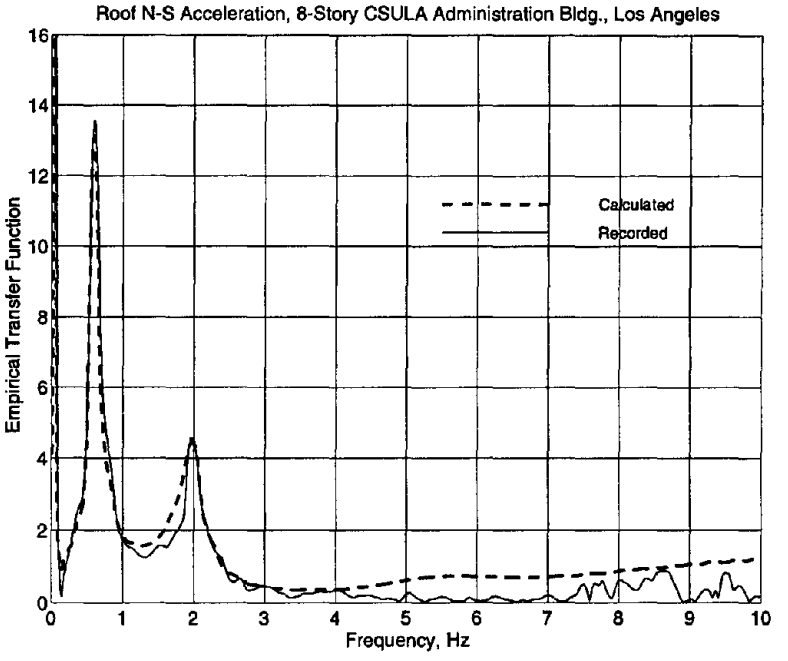

Figure C.15.6. Comparison of empirical transfer functions: recorded motions and calculated motions from WPCMIMO in N-S direction.

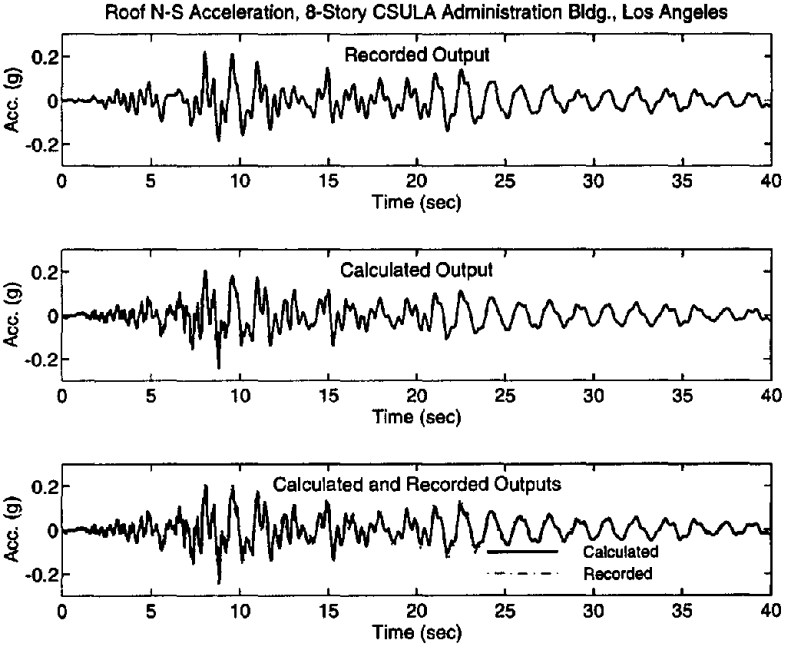

Figure C.15.7. Comparison of time-histories: recorded motions and calculated motions from WPCMIMO in N-S direction.

16. Pasadena - 6-Story Office Building, CSMIP Station No. 24541

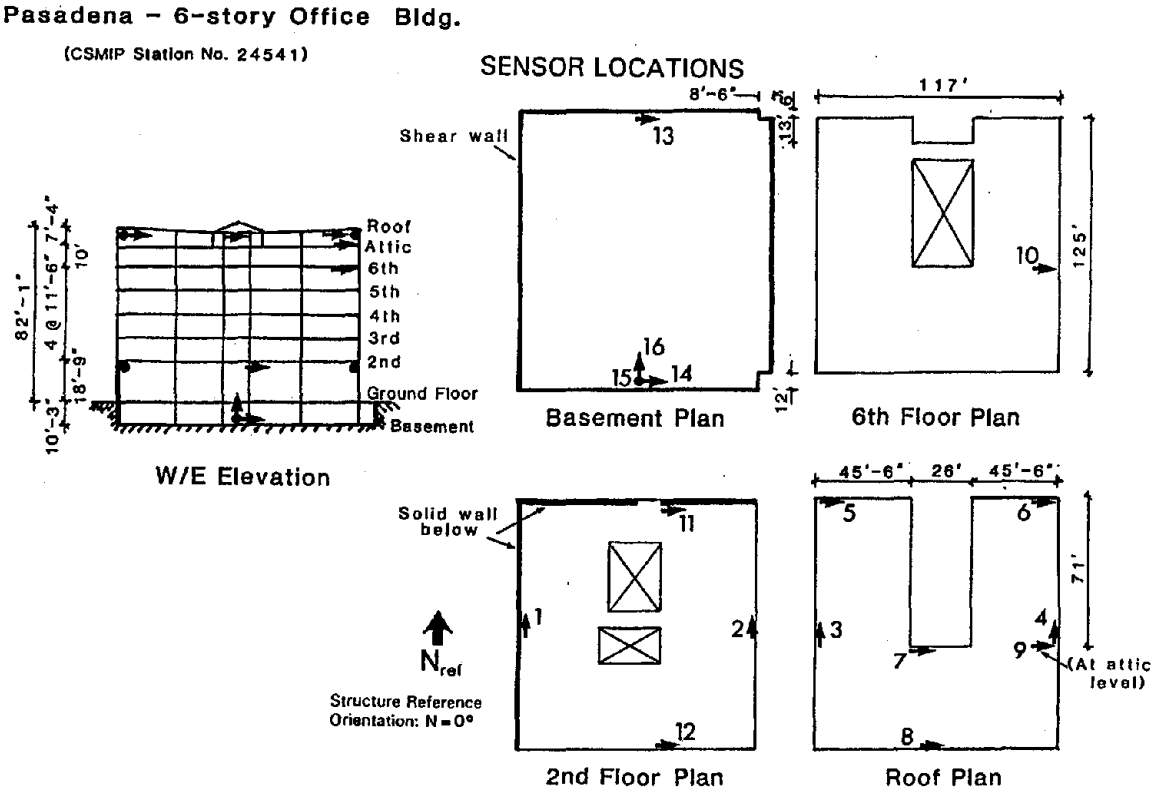

Figure C.16.1. Sensor locations in 6-story office building, CSMIP Station No. 24541

Table C.16.1. Results of system identification in E-W (longitudinal) direction by WPCMIMO.

Mode No.	Frequency (Hz)	Damping	Part. Factor	Initial Disp.	Initial Velo.	Modal Cont.	Comments
1	0.4564	0.0542	-4.47E-00	3.13E-03	-3.78E-03	6.59E-01	1st Mode
2	1.8677	0.0736	3.77E-01	8.35E-05	1.67E-04	4.13E-01	2nd Mode
3	3.5074	0.1201	-1.63E-01	1.61E-04	-2.09E-03	9.63E-02	
4	4.6060	0.0658	4.87E-02	-2.48E-05	-3.34E-03	2.22E-02	
5	5.1310	0.0000	-3.38E-03	-5.25E-05	1.44E-03	6.37E-03	
6	6.5609	0.0627	7.58E-03	1.14E-06	1.51E-05	3.41E-04	

Relative Error = 0.379 and Absolute Error = 0.268

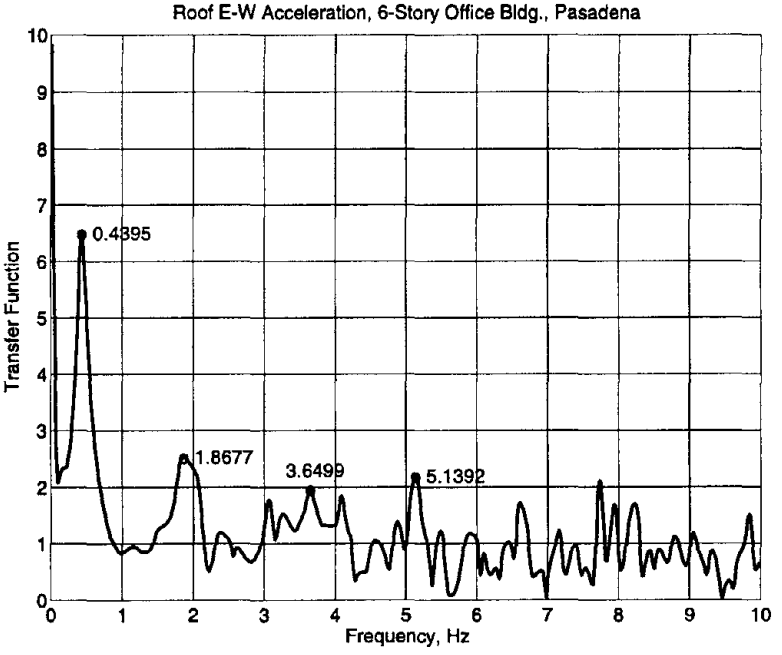

Figure C.16.2. Initial frequency estimates from transfer function in E-W direction.

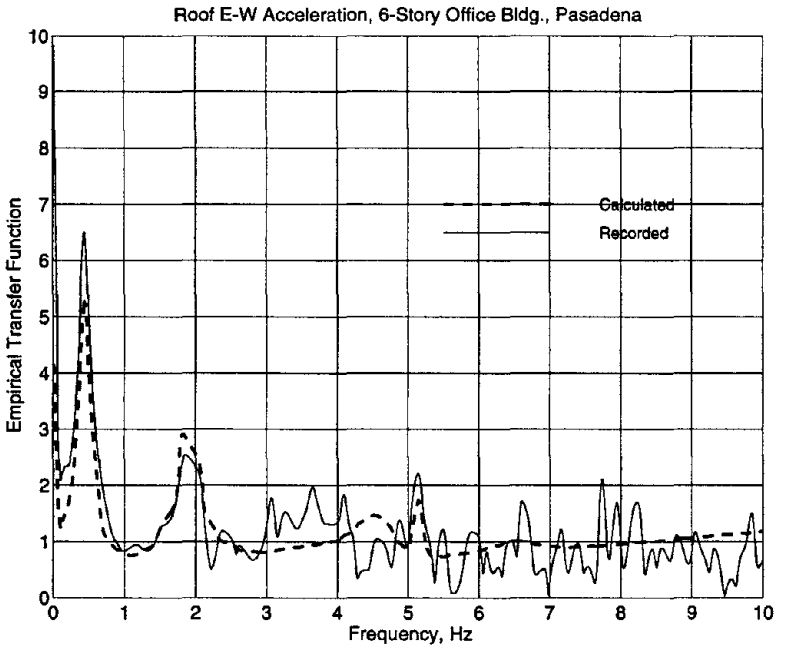

Figure C.16.3. Comparison of empirical transfer functions: recorded motions and calculated motions from WPCMIMO in E-W direction.

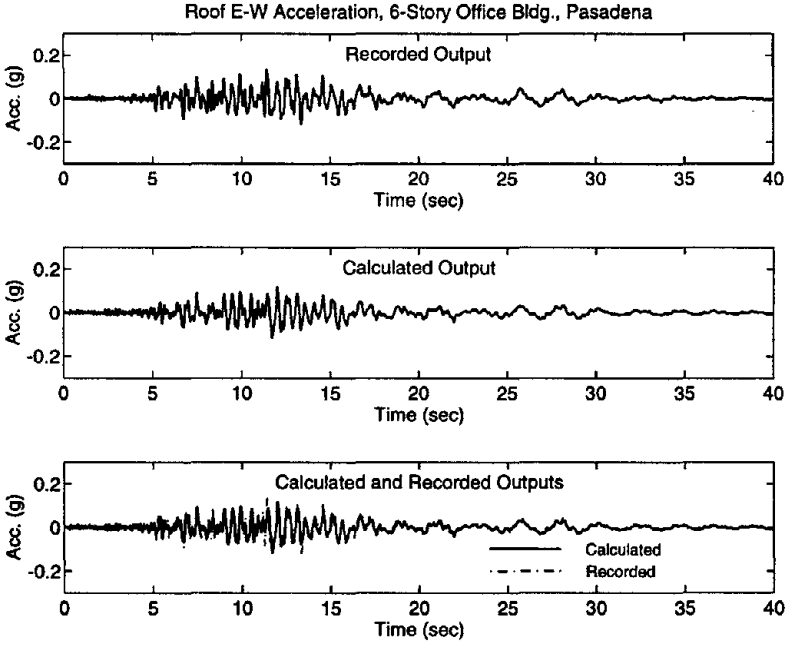

Figure C.16.4. Comparison of time-histories: recorded motions and calculated motions from WPCMIMO in E-W direction.

Table C.16.2. Results of system identification in N-S (transverse) direction by WPCMIMO.

Mode No.	Frequency (Hz)	Damping	Part. Factor	Initial Disp.	Initial Velo.	Modal Cont.	Comments
1	0.4760	0.2218	0.337229	0.001893	0.001131	3.62E-02	1st Tran. Mode*
2	0.5595	0.0908	-2.36E-00	-2.36E-04	3.57E-03	4.76E-01	1st Tor. Mode*
3	0.7813	0.0744	-9.89E-01	1.51E-03	1.69E-03	2.22E-01	
4	2.0093	0.1908	3.76E-01	2.09E-04	-3.00E-03	3.37E-01	2nd Tran. Mode*
5	4.9434	0.0264	-4.12E-03	-5.85E-05	9.34E-04	1.89E-03	
6	4.4202	0.0159	-3.96E-03	-8.64E-06	-7.25E-04	1.13E-03	
7	3.8488	0.0996	-5.86E-02	3.35E-05	-1.98E-03	3.62E-02	

* Damping is unreliable
Relative Error = 0.231 and Absolute Error = 0.100

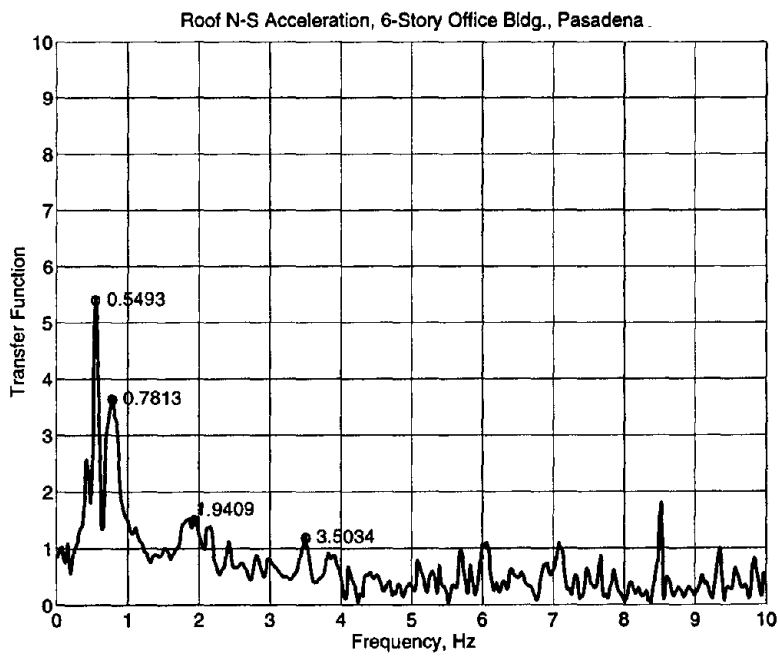

Figure C.16.5. Initial frequency estimates from transfer function in N-S direction.

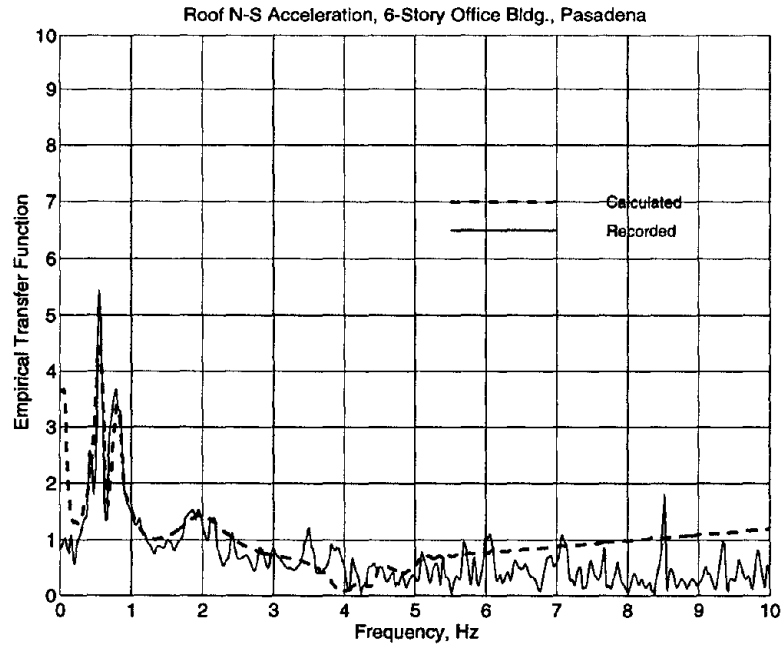

Figure C.16.6. Comparison of empirical transfer functions: recorded motions and calculated motions from WPCMIMO in N-S direction.

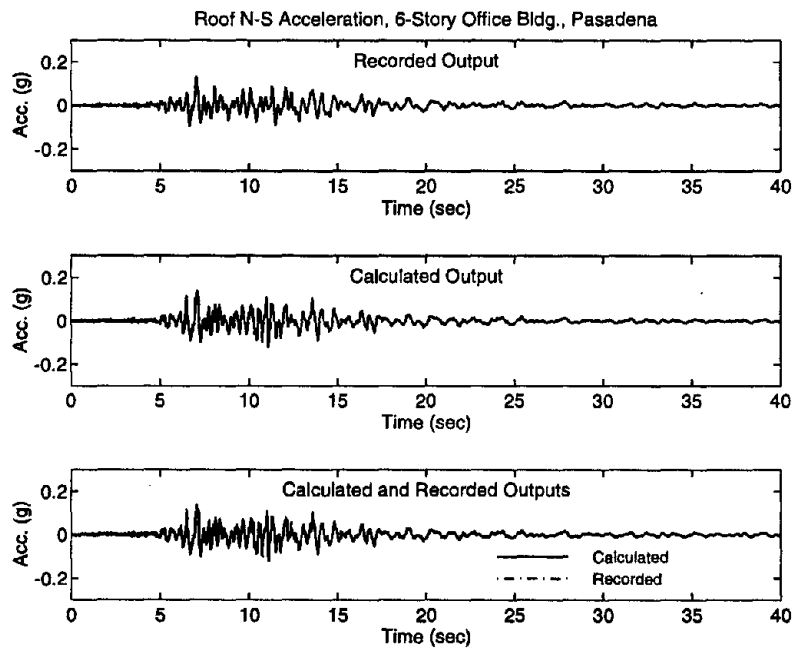

Figure C.16.7. Comparison of time-histories: recorded motions and calculated motions from WPCMIMO in N-S direction.

17. Whittier - 8-Story Hotel, CSMIP Station No. 14606

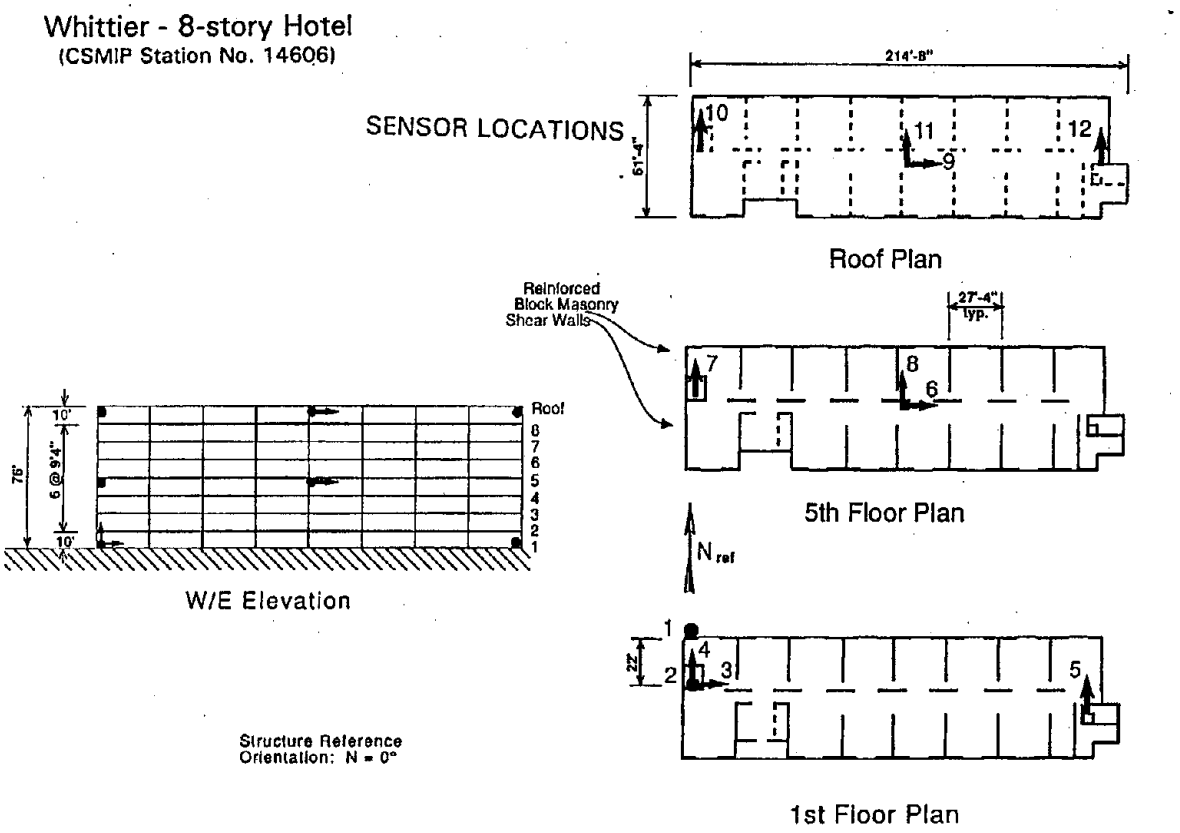

Figure C.17.1. Sensor locations in 8-story hotel, CSMIP Station No. 14606

Table C.17.1. Results of system identification in E-W (longitudinal) direction by WPCMIMO.

Mode No.	Frequency (Hz)	Damping	Part. Factor	Initial Disp.	Initial Velo.	Modal Cont.	Comments
1	1.4441	0.0519	-1.71E-00	-3.20E-05	2.82E-04	8.03E-01	1st Mode
2	5.5298	0.1125	1.60E-01	-4.79E-08	3.30E-05	1.01E-01	2nd Mode
3	12.2209	0.0912	-2.82E-02	5.32E-08	9.89E-06	1.66E-03	
4	20.9184	0.0570	-1.15E-02	2.68E-08	2.47E-06	4.10E-05	

Relative Error = 0.283 and Absolute Error = 1.077

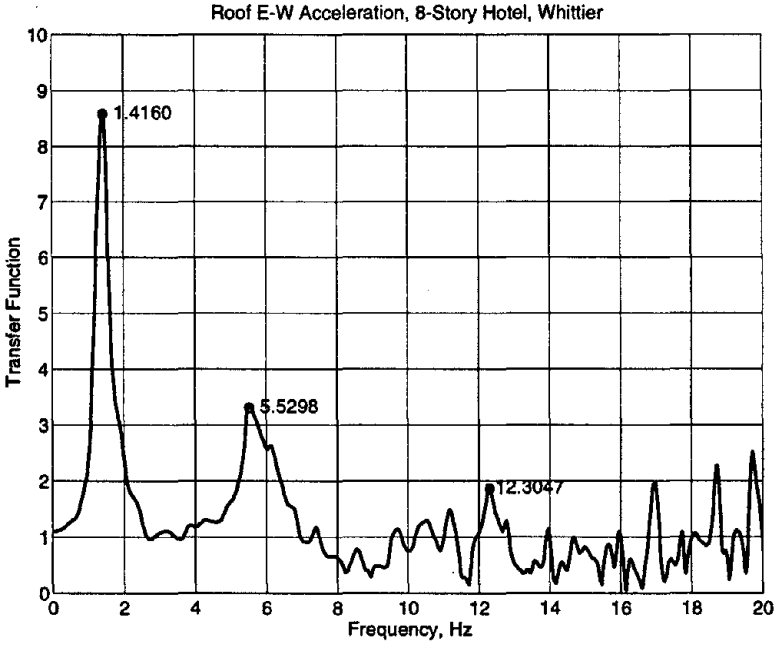

Figure C.17.2. Initial frequency estimates from transfer function in E-W direction.

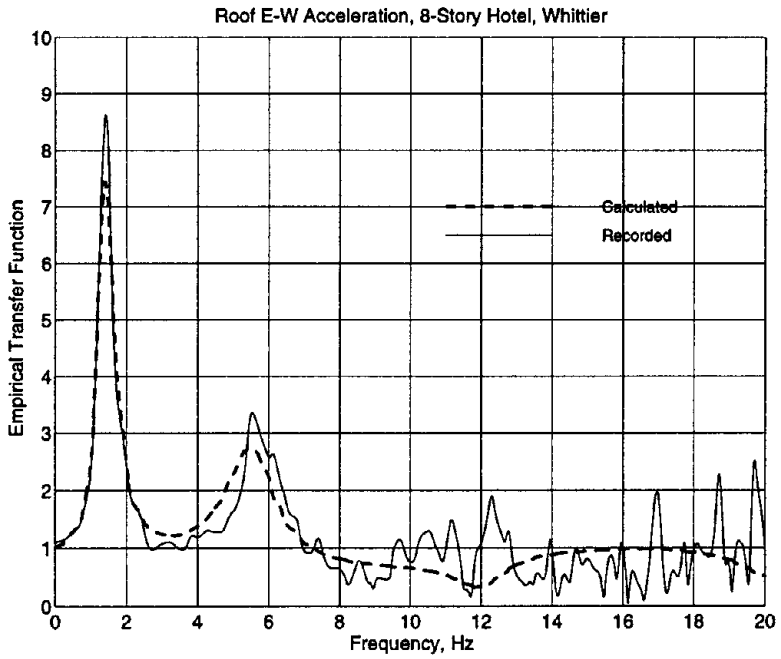

Figure C.17.3. Comparison of empirical transfer functions: recorded motions and calculated motions from WPCMIMO in E-W direction.

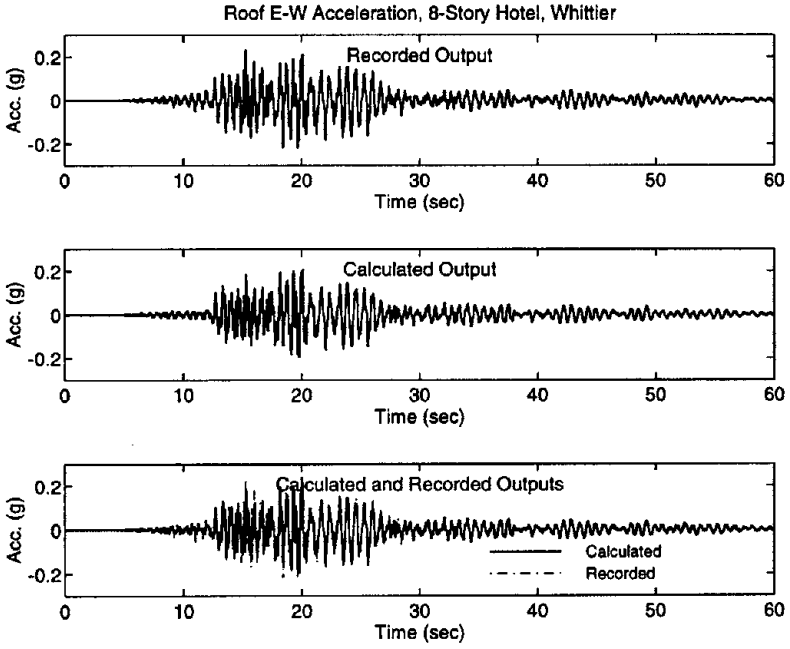

Figure C.17.4. Comparison of time-histories: recorded motions and calculated motions from WPCMIMO in E-W direction.

Table C.17.2. Results of system identification in N-S (transverse) direction by WPCMIMO.

Mode No.	Frequency (Hz)	Damping	Part. Factor	Initial Disp.	Initial Velo.	Modal Cont.	Comments
1	1.5956	0.1163	-1.11E-00	3.11E-06	4.20E-04	5.91E-01	1st Tran. Mode*
2	1.7822	0.0846	-2.41E-01	1.79E-05	-4.13E-04	4.96E-02	1st Tor. Mode *
3	3.2949	0.5232	2.56E-00	-5.63E-05	8.72E-04	2.22E+00	
4	3.2605	0.3913	-1.96E-00	4.19E-05	-8.58E-04	2.23E+00	
5	4.8955	0.0918	-4.75E-02	6.26E-07	-4.26E-05	1.25E-02	
6	5.5757	0.0438	-1.70E-02	-1.27E-06	-1.58E-05	2.52E-03	
7	9.5854	0.0329	1.09E-02	-6.25E-08	-1.94E-06	9.35E-04	

* Damping is not reliable
Relative Error = 0.355 and Absolute Error = 1.595

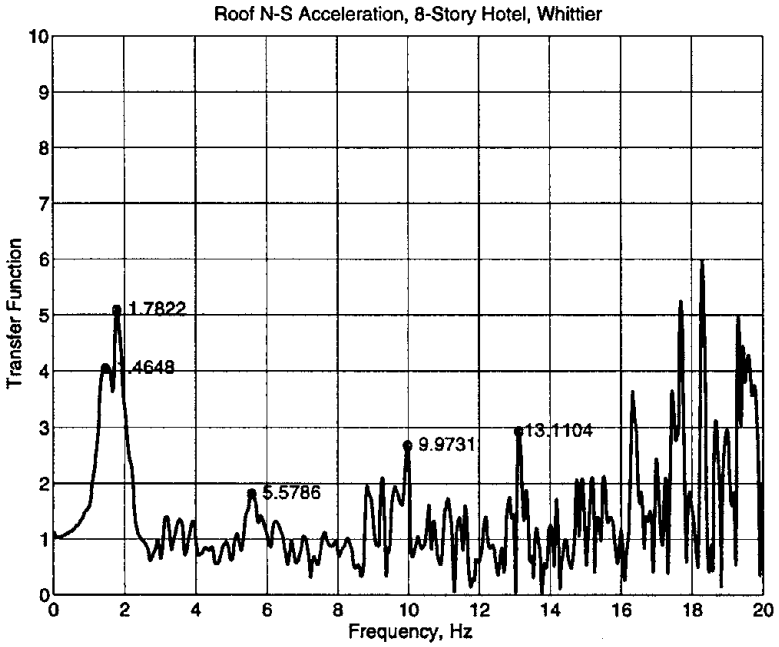

Figure C.17.5. Initial frequency estimates from transfer function in N-S direction.

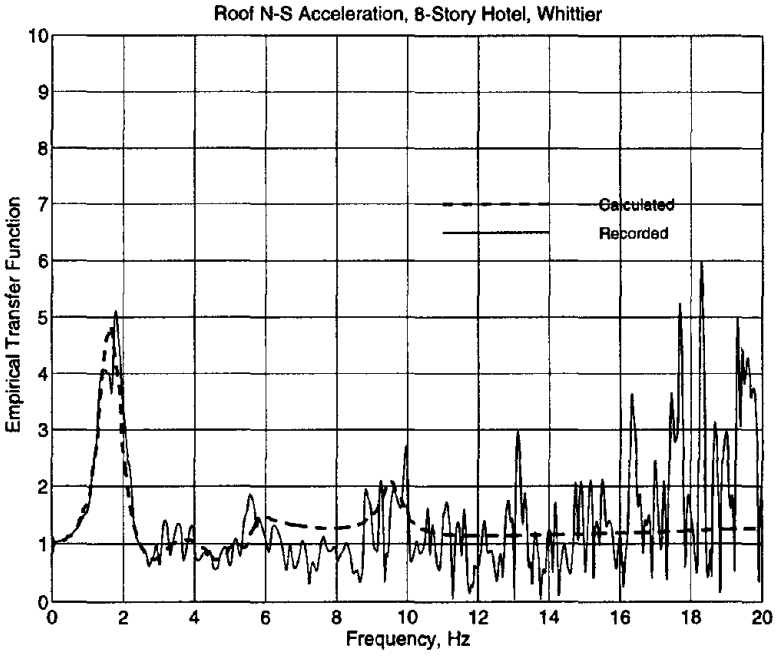

Figure C.17.6. Comparison of empirical transfer functions: recorded motions and calculated motions from WPCMIMO in N-S direction.

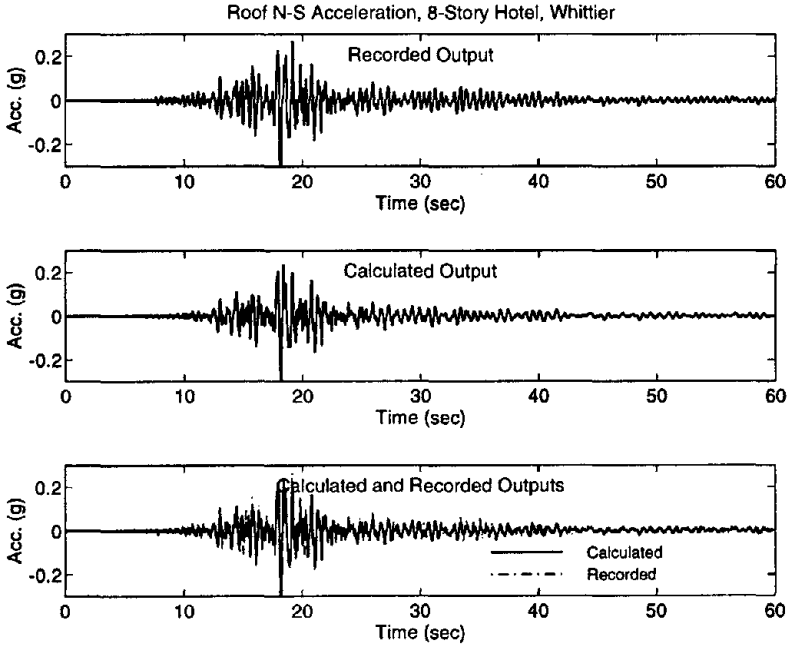

Figure C.17.7. Comparison of time-histories: recorded motions and calculated motions from WPCMIMO in N-S direction.

18. Los Angeles - 6-Story Office Building, CSMIP Station No. 24652

No. of Stories above/below ground: 5/1
Plan Shape: Square
Base Dimensions: 94' x 94'
Typical Floor Dimensions: 94' x 94'
Design Date: 1988
Construction Date: 1989

Vertical Load Carrying System:
Concrete slabs over metal deck supported by steel frames.
Lateral Force Resisting System:
Chevron type steel braced frames for lateral resistance; steel moment frames for torsional resistance.
Foundation Type:
Mat foundations for four towers; spread footings elsewhere.

Figure C.18.1a. Details of 6-story office building, CSMIP Station No. 24652

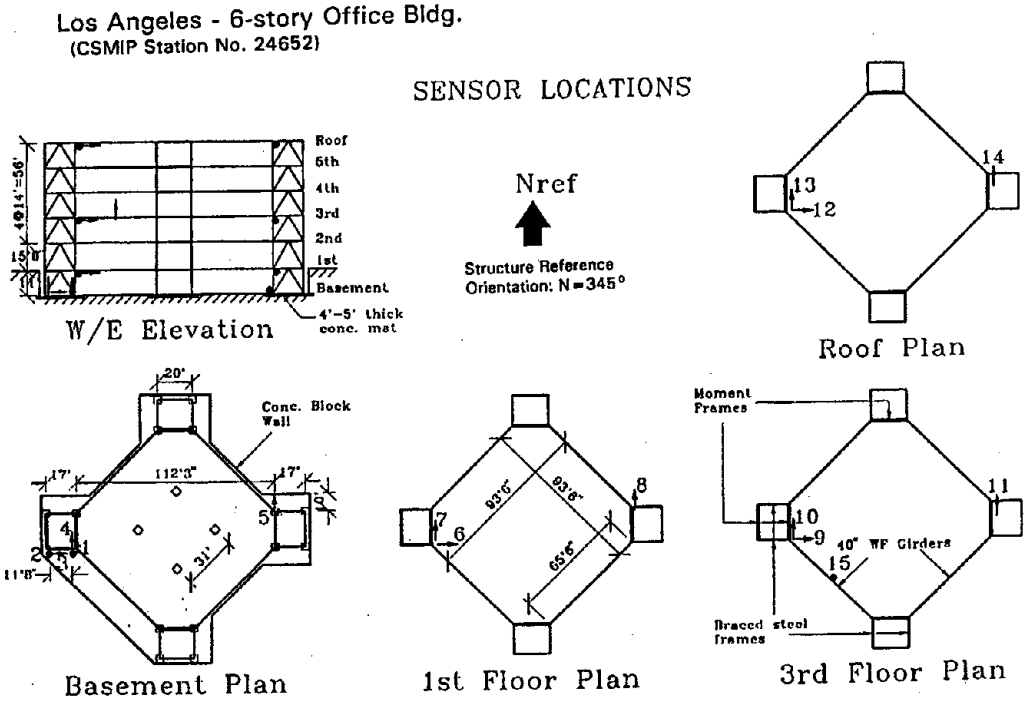

Figure C.18.1b. Sensor locations in 6-story office building, CSMIP Station No. 24652

Table C.18.1. Results of system identification in E-W (longitudinal) direction by WPCMIMO.

Mode No.	Frequency (Hz)	Damping	Part. Factor	Initial Disp.	Initial Velo.	Modal Cont.	Comments
1	1.1116	0.0394	-1.42E-00	-1.01E-03	3.61E-03	8.18E-01	1st Long. Mode
2	3.8208	0.0768	1.67E-01	-9.39E-07	1.87E-04	2.22E-02	2nd Long. Mode
3	1.2847	0.0367	-3.43E-01	4.85E-04	-1.03E-03	4.24E-02	1st Tor. Mode
4	6.1724	0.1110	-4.45E-02	3.25E-06	1.44E-04	1.79E-03	

Relative Error = 0.272 and Absolute Error = 2.695

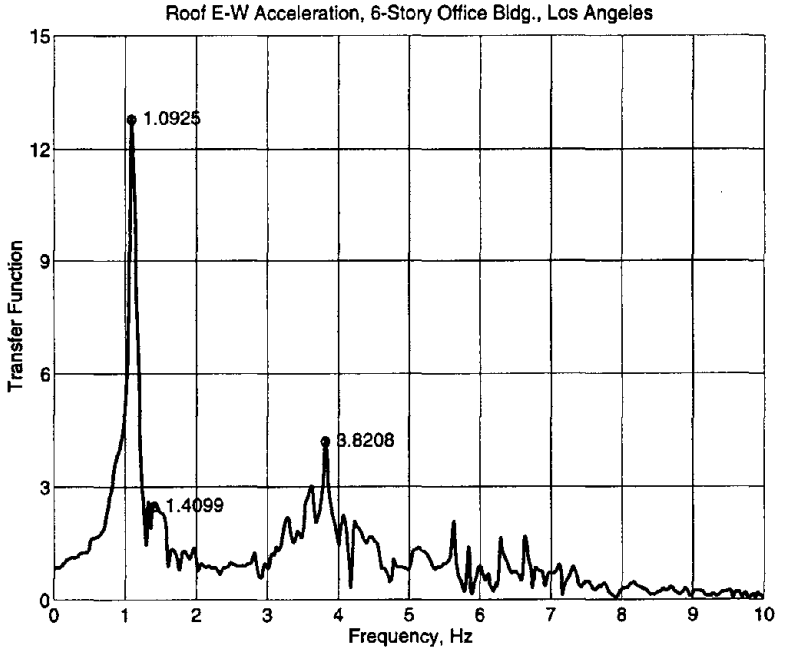

Figure C.18.2. Initial frequency estimates from transfer function in E-W direction.

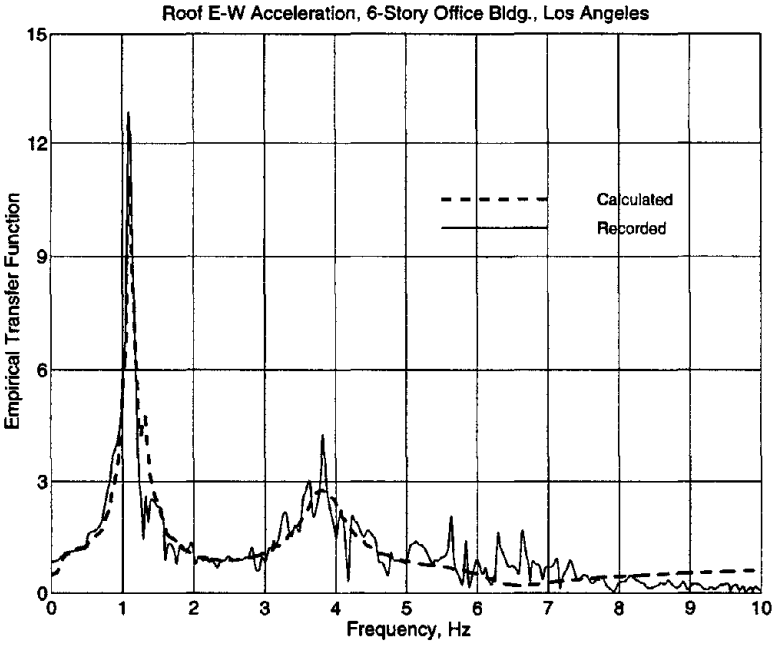

Figure C.18.3. Comparison of empirical transfer functions: recorded motions and calculated motions from WPCMIMO in E-W direction.

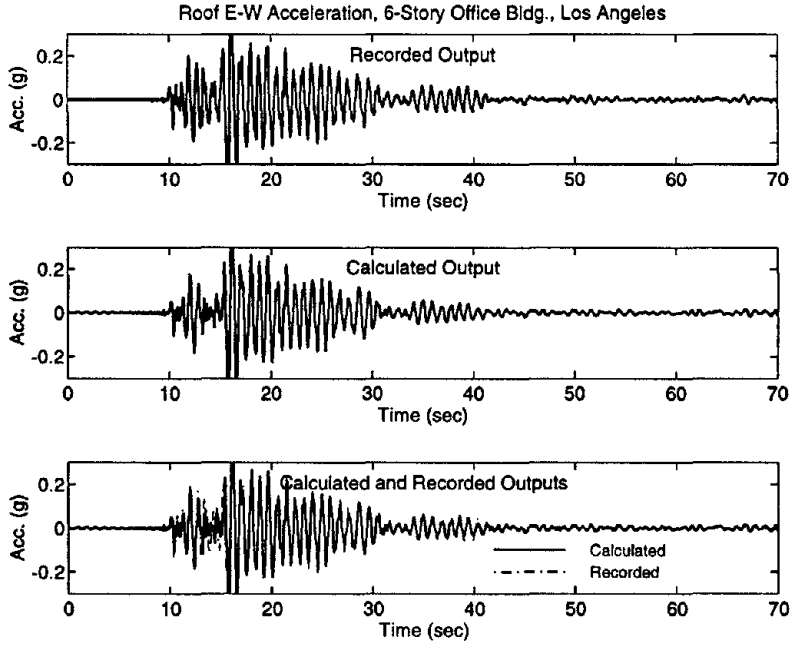

Figure C.18.4. Comparison of time-histories: recorded motions and calculated motions from WPCMIMO in E-W direction.

Table C.18.2. Results of system identification in N-S (transverse) direction by WPCMIMO.

Mode No.	Frequency (Hz)	Damping	Part. Factor	Initial Disp.	Initial Velo.	Modal Cont.	Comments
1	1.1584	0.0358	-1.80E-00	-1.44E-04	5.19E-03	8.65E-01	1st Mode
2	3.8818	0.0740	1.95E-01	8.08E-06	1.23E-04	5.60E-02	2nd Mode
3	6.6710	0.0976	-4.49E-02	3.17E-06	-4.19E-05	2.66E-03	
4	9.0754	0.0814	9.35E-03	-3.48E-07	-5.24E-05	1.94E-04	

Relative Error = 0.250 and Absolute Error = 1.518

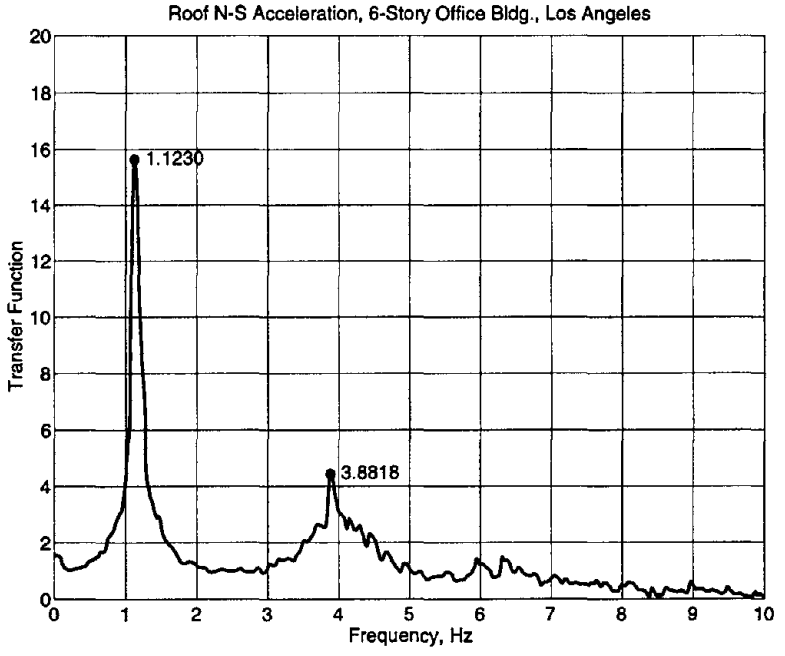

Figure C.18.5. Initial frequency estimates from transfer function in N-S direction.

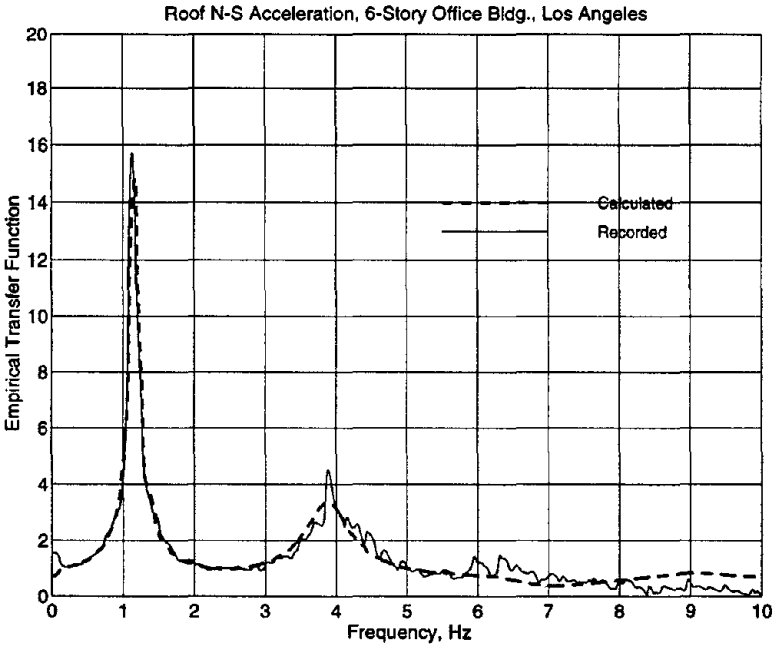

Figure C.18.6. Comparison of empirical transfer functions: recorded motions and calculated motions from WPCMIMO in N-S direction.

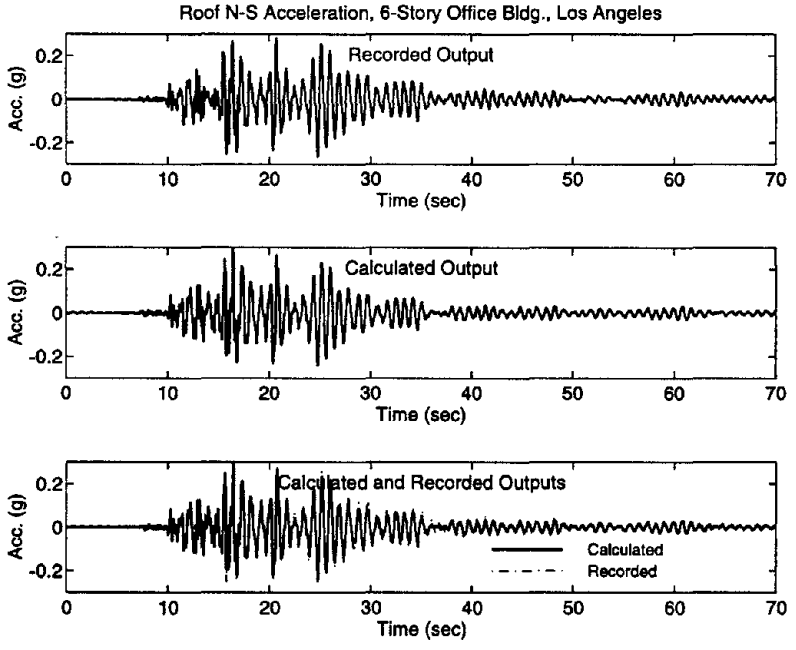

Figure C.18.7. Comparison of time-histories: recorded motions and calculated motions from WPCMIMO in N-S direction.

19. Alhambra: 900 South Fremont Street - 13-Story Steel Building, USGS Station No. 482

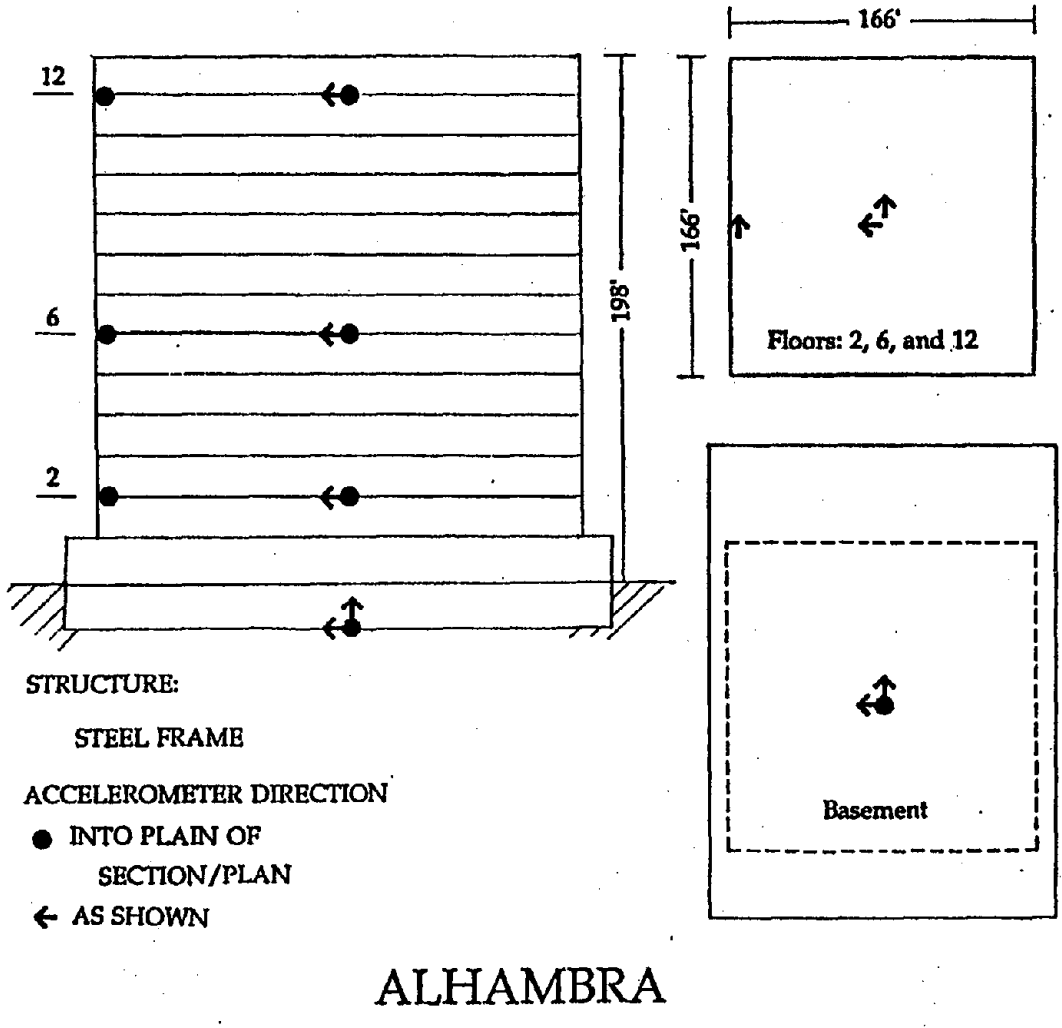

Figure C.19.1 Sensor locations in 13-story building, USGS Station No. 482

Table C.19.1. Results of system identification in E-W (longitudinal) direction by WPCMIMO.

Mode No.	Frequency (Hz)	Damping	Part. Factor	Initial Disp.	Initial Velo.	Modal Cont.	Comments
1	3.2271	0.1869	-2.00E-01	-1.95E-04	4.44E-03	1.05E-01	
2	0.4650	0.0119	-4.44E-00	-9.64E-03	-8.32E-03	1.02E+00	1st Mode
3	1.3052	0.0493	4.13E-01	7.99E-05	2.61E-03	1.79E-01	2nd Mode
4	3.8401	0.0721	1.17E-01	8.23E-05	4.56E-04	1.27E-01	

Relative Error = 0.236 and Absolute Error = 0.687

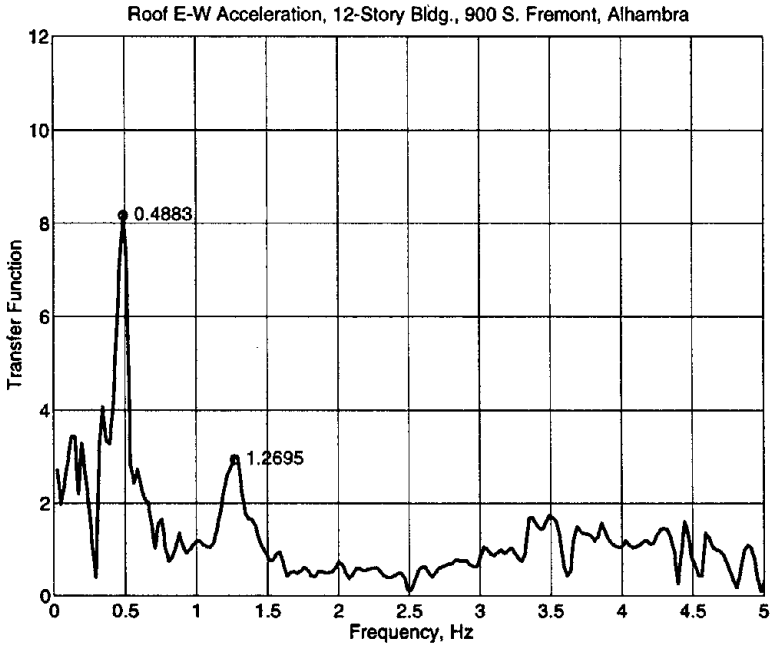

Figure C.19.2. Initial frequency estimates from transfer function in E-W direction.

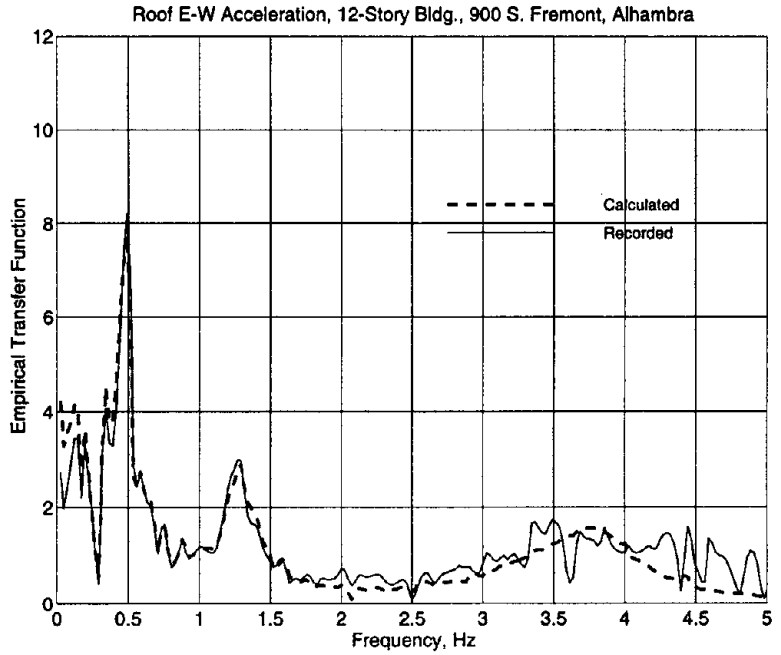

Figure C.19.3. Comparison of empirical transfer functions: recorded motions and calculated motions from WPCMIMO in E-W direction.

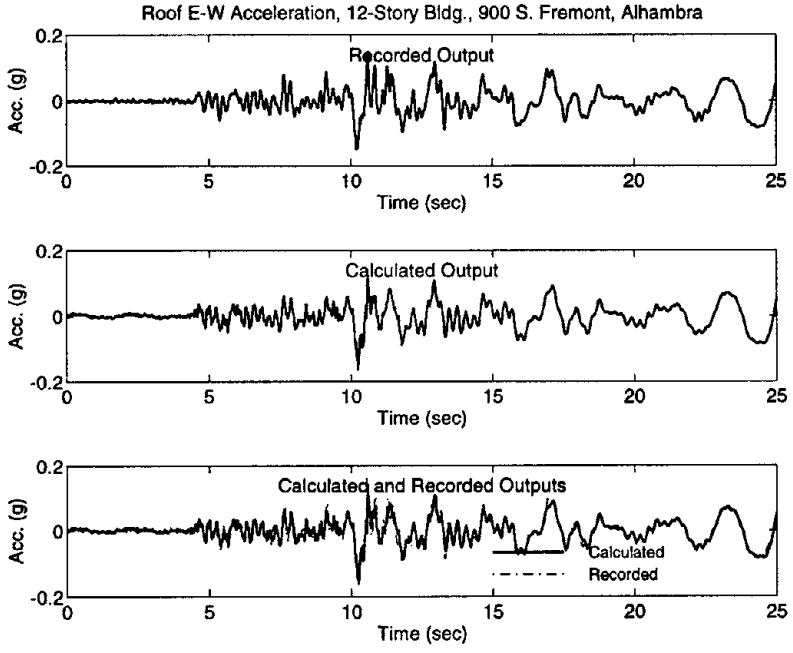

Figure C.19.4. Comparison of time-histories: recorded motions and calculated motions from WPCMIMO in E-W direction.

Table C.19.2. Results of system identification in N-S (transverse) direction by WPCMIMO.

Mode No.	Frequency (Hz)	Damping	Part. Factor	Initial Disp.	Initial Velo.	Modal Cont.	Comments
1	0.4204	0.0000	2.89E-00	7.57E-03	-2.01E-02	3.12E-01	
2	0.4505	0.0194	-7.09E-00	-1.03E-02	-7.15E-03	2.30E+00	1st Mode
3	1.2728	0.0643	4.04E-01	-2.80E-04	3.08E-03	1.96E-01	2nd Mode
4	2.9829	0.0788	-1.22E-01	3.05E-05	1.38E-03	7.49E-02	
5	3.7287	0.0383	3.67E-02	-3.29E-05	9.86E-04	2.74E-02	
6	4.0595	0.0092	5.18E-03	6.12E-05	3.87E-04	1.58E-03	

Relative Error = 0.323 and Absolute Error = 1.035

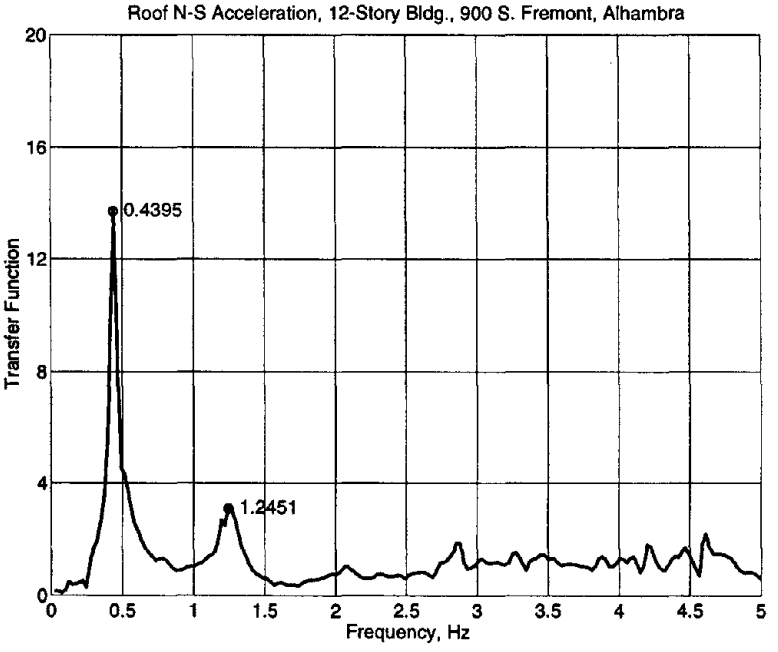

Figure C.19.5. Initial frequency estimates from transfer function in N-S direction.

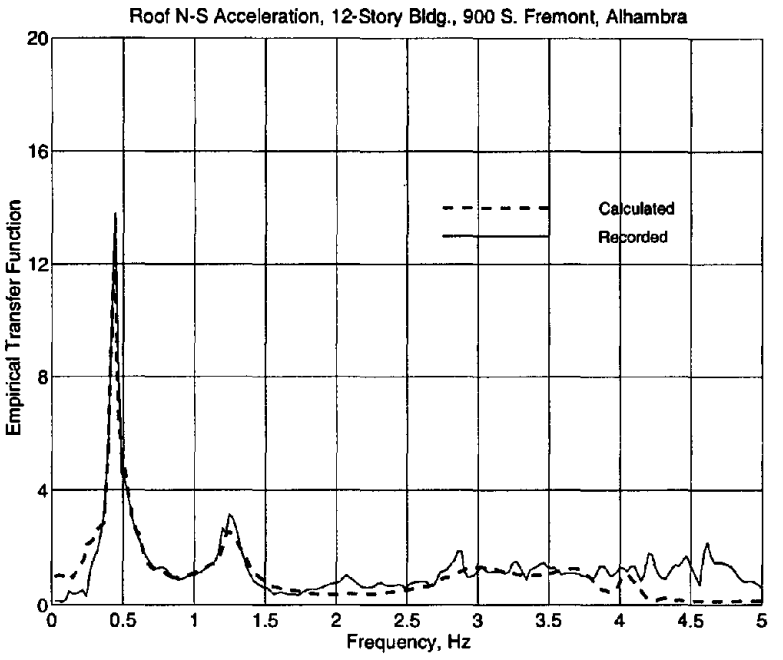

Figure C.19.6. Comparison of empirical transfer functions: recorded motions and calculated motions from WPCMIMO in N-S direction.

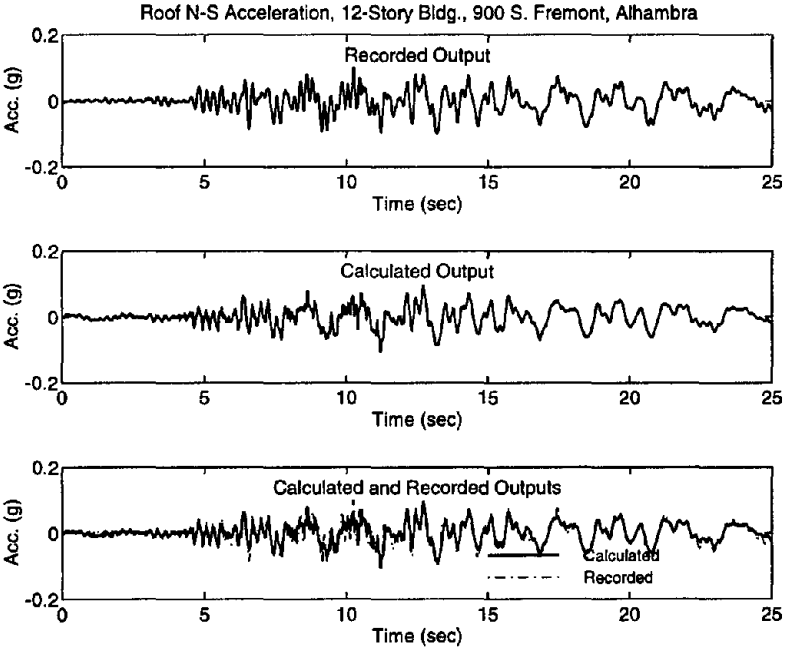

Figure C.19.7. Comparison of time-histories: recorded motions and calculated motions from WPCMIMO in N-S direction.

20. Los Angeles: 1100 Wilshire Blvd. - 32-Story Building, USGS Station No. 5233

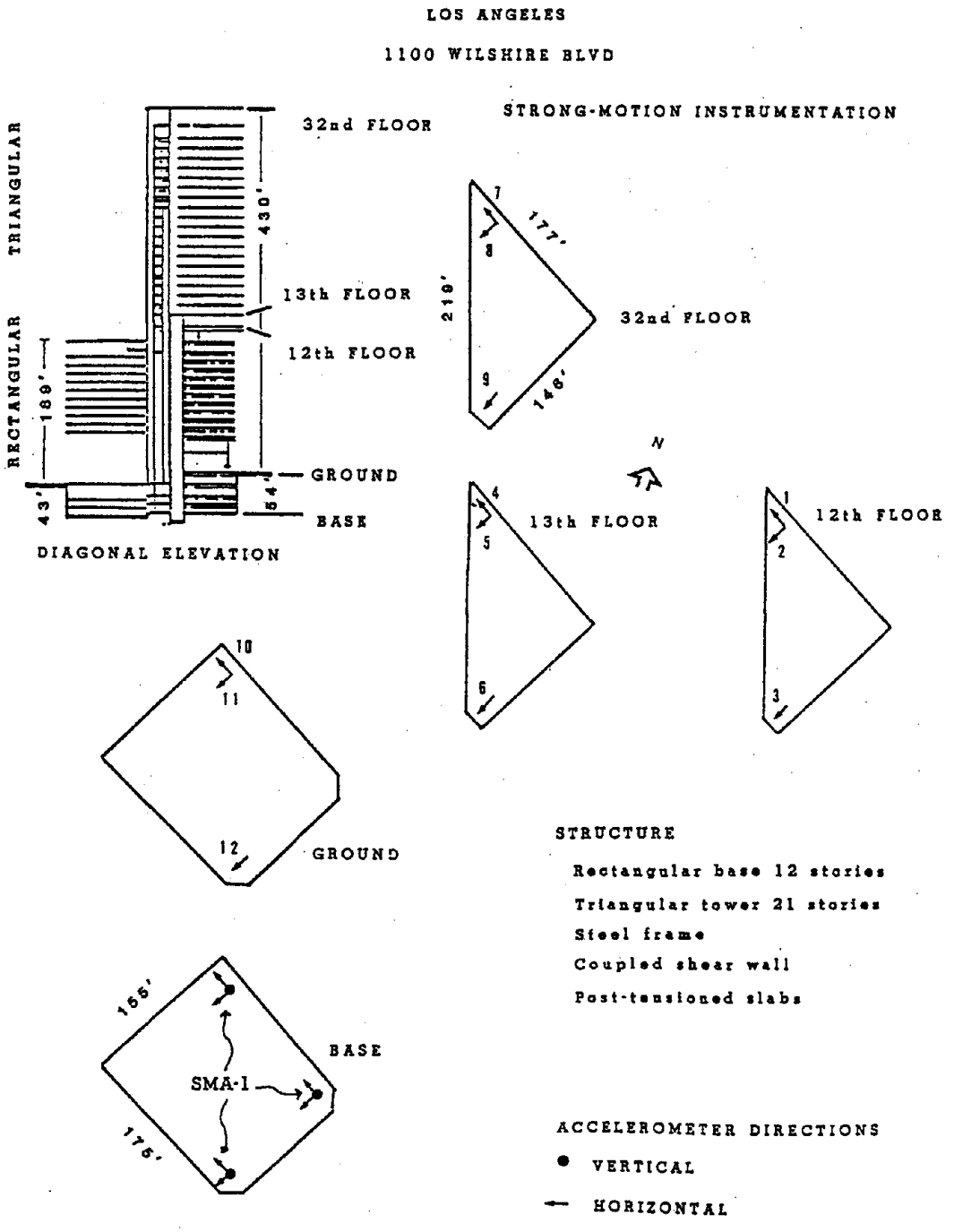

43

Figure C.20.1. Sensor locations in 32-story building, USGS Station No. 5233

Table C.20.1. Results of system identification in E-W (longitudinal) direction by WPCMIMO.

Mode No.	Frequency (Hz)	Damping	Part. Factor	Initial Disp.	Initial Velo.	Modal Cont.	Comments
1	0.5907	0.0329	1.59E+01	-5.70E-01	4.58E-00	9.92E+01	2nd Tor. Mode
2	0.2808	0.0413	-1.43E+01	1.07E-01	-8.97E-02	1.31E+00	1st Tor. Mode
3	-0.0062	0.0055	1.22E+01	-1.65E+01	3.38E-01	1.84E-03	
4	0.2296	0.0090	-1.01E+01	6.15E-02	7.36E-02	4.69E-01	
5	0.2919	0.0165	1.43E+01	-6.31E-02	1.08E-02	1.44E+00	1st Long. Mode
6	0.5881	0.0355	-1.90E+01	6.34E-01	-4.95E-00	1.09E+02	2nd Long. Mode
7	0.5548	0.0030	3.17E-00	-4.42E-02	2.69E-01	1.00E+00	
8	1.0561	0.0167	-2.36E-01	1.20E-03	-2.72E-03	4.38E-02	
9	1.0867	0.2598	6.71E-01	-1.12E-02	7.21E-03	5.39E-02	
10	1.4649	0.0066	-5.09E-03	9.33E-04	3.07E-02	3.99E-02	
11	1.5024	0.0076	7.23E-02	1.02E-03	-2.97E-02	2.82E-02	

Relative Error = 0.377 and Absolute Error = 2.521

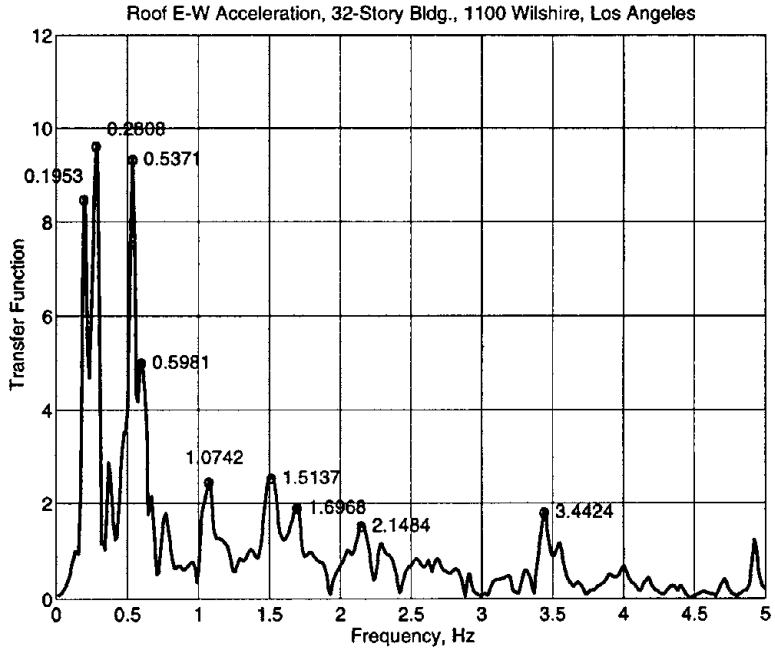

Figure C.20.2. Initial frequency estimates from transfer function in E-W direction.

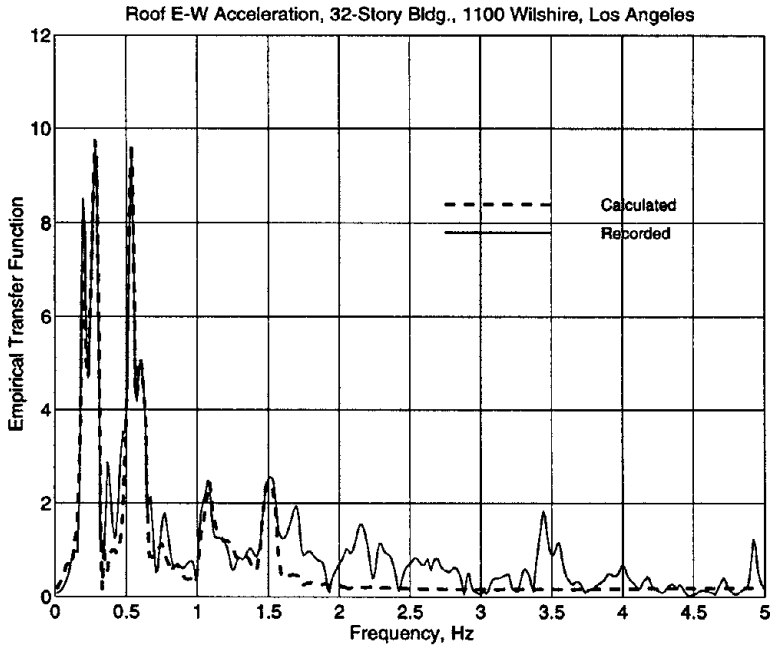

Figure C.20.3. Comparison of empirical transfer functions: recorded motions and calculated motions from WPCMIMO in E-W direction.

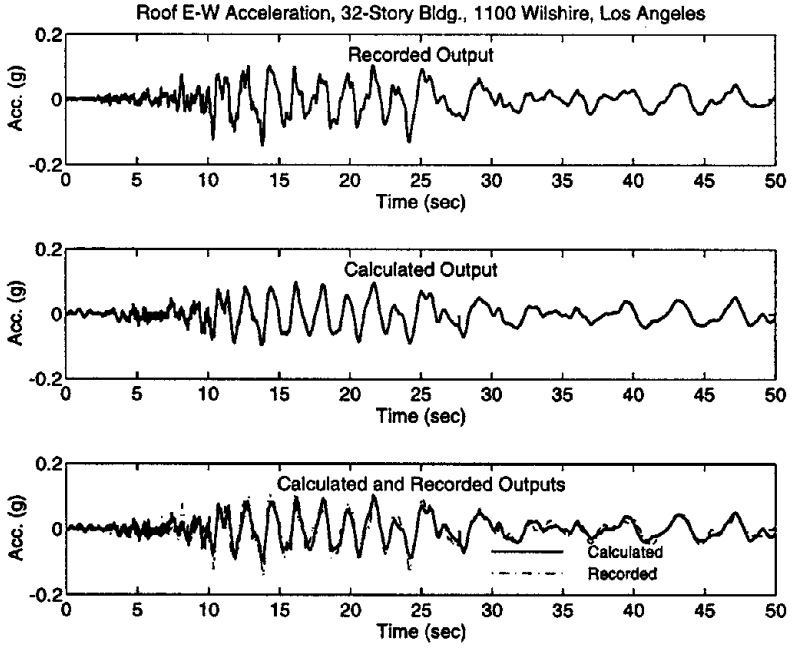

Figure C.20.4. Comparison of time-histories: recorded motions and calculated motions from WPCMIMO in E-W direction.

Table C.20.2. Results of system identification in N-S (transverse) direction by WPCMIMO.

Mode No.	Frequency (Hz)	Damping	Part. Factor	Initial Disp.	Initial Velo.	Modal Cont.	Comments
1	0.6689	0.0294	-1.87E-00	-1.01E-02	-3.99E-02	1.29E-01	
2	0.2295	0.0177	-1.11E+01	4.36E-02	-5.32E-02	2.83E-01	1st Mode
3	0.5538	0.0299	2.70E-00	2.25E-03	-7.37E-02	4.54E-01	2nd Mode
4	1.0586	0.0012	-2.26E-01	-4.65E-03	-6.55E-03	2.23E-02	
5	1.2360	0.0184	4.39E-01	-2.17E-03	2.84E-02	6.80E-02	
6	2.2550	0.0532	1.94E-01	-6.09E-04	2.38E-02	5.80E-02	
7	1.6792	0.0076	9.09E-02	1.24E-03	1.30E-02	1.18E-02	
8	1.8565	0.0355	-2.39E-01	4.89E-04	-1.31E-02	5.24E-02	
9	2.2729	0.0000	1.68E-02	2.26E-04	-1.12E-02	4.02E-03	

Relative Error = 0.419 and Absolute Error = 10.187

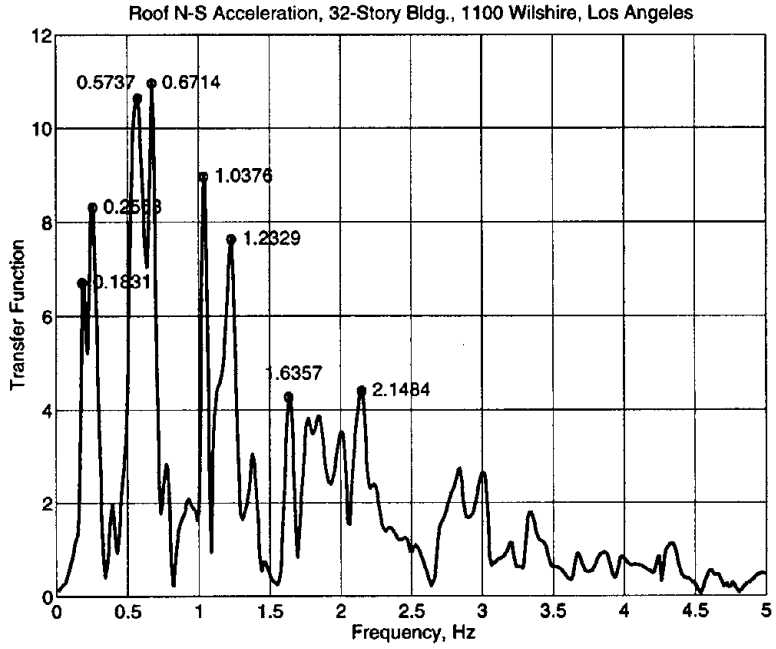

Figure C.20.5. Initial frequency estimates from transfer function in N-S direction.

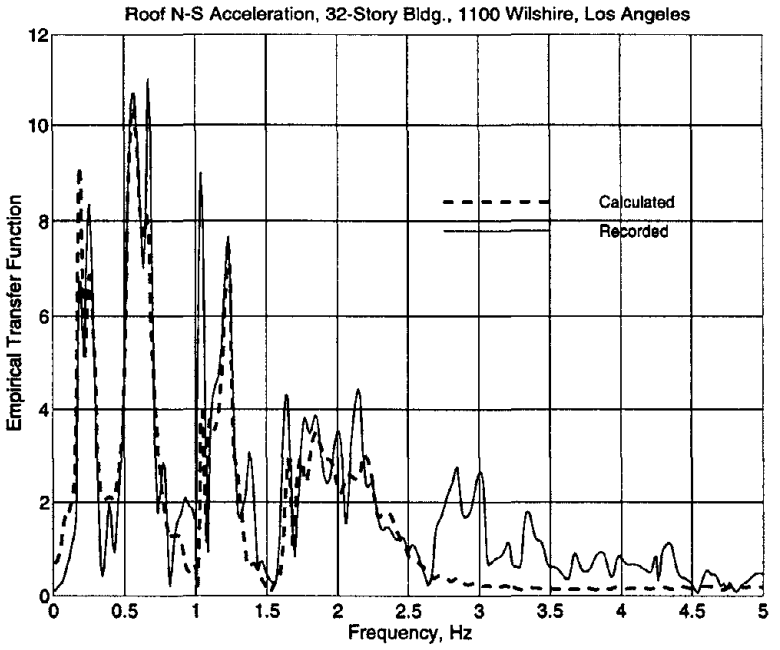

Figure C.20.6. Comparison of empirical transfer functions: recorded motions and calculated motions from WPCMIMO in N-S direction.

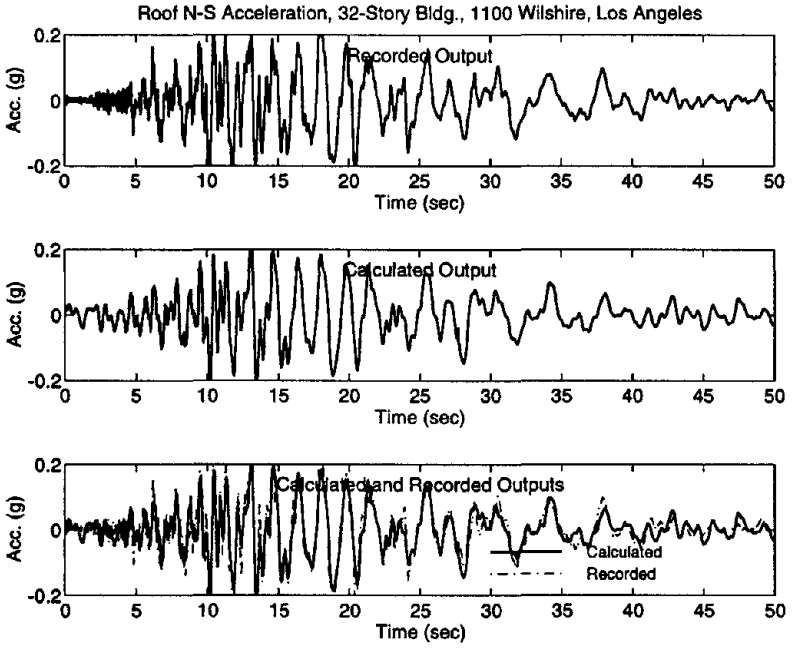

Figure C.20.7. Comparison of time-histories: recorded motions and calculated motions from WPCMIMO in N-S direction.

21. Los Angeles - 6-Story Wadsworth VA Hospital Building, USGS Station No. 5082

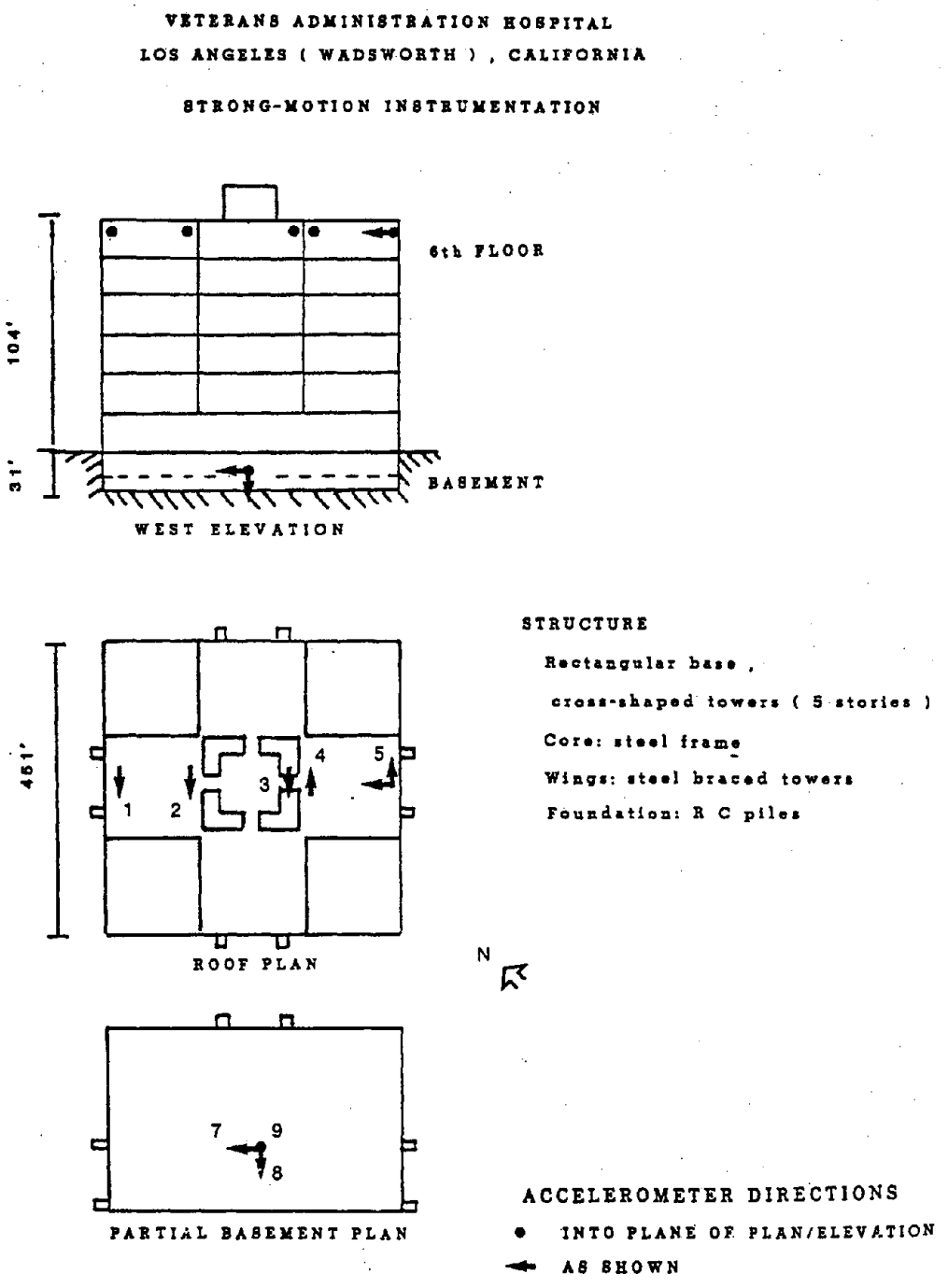

Figure C.21.1. Sensor locations in 6-story hospital building, USGS Station No. 5082

Table C.21.1. Results of system identification in E-W (longitudinal) direction by WPCMIMO.

Mode No.	Frequency (Hz)	Damping	Part. Factor	Initial Disp.	Initial Velo.	Modal Cont.	Comments
1	1.0648	0.0516	-2.58E-00	4.38E-03	2.34E-02	7.04E-01	1st Mode
2	3.1250	0.3305	1.58E-00	3.29E-03	-4.25E-02	6.30E-01	
3	3.1434	0.0400	7.21E-02	-1.56E-04	-1.55E-04	1.16E-02	
4	3.6626	0.1114	-3.90E-01	-6.76E-04	-5.05E-03	1.58E-01	
5	4.3789	0.1321	-3.86E-01	-4.69E-04	8.74E-03	2.00E-01	

Relative Error = 0.343 and Absolute Error = 8.968

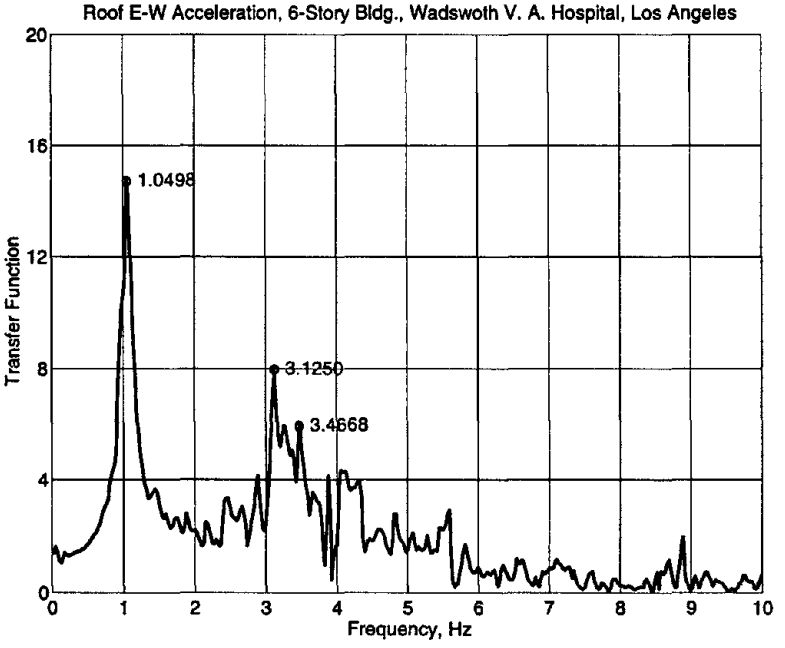

Figure C.21.2. Initial frequency estimates from transfer function in E-W direction.

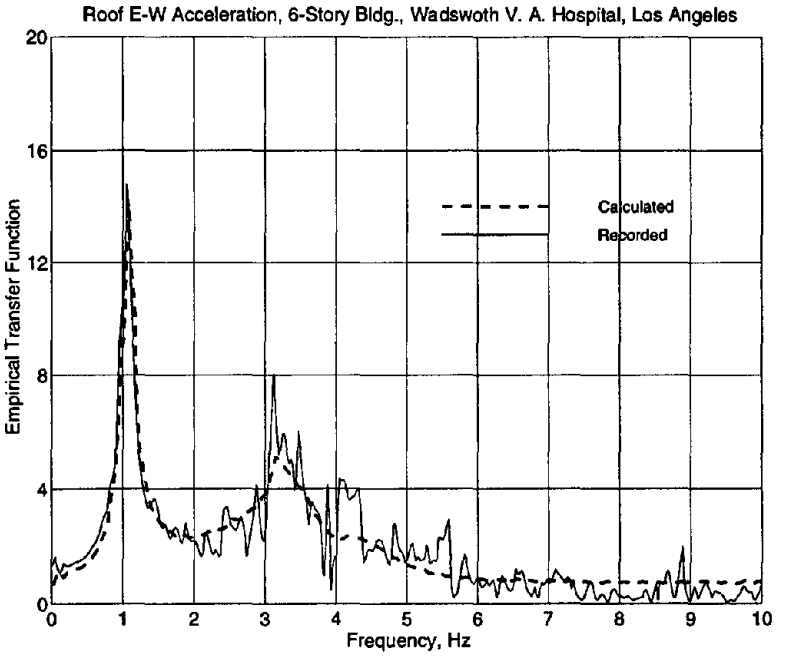

Figure C.21.3. Comparison of empirical transfer functions: recorded motions and calculated motions from WPCMIMO in E-W direction.

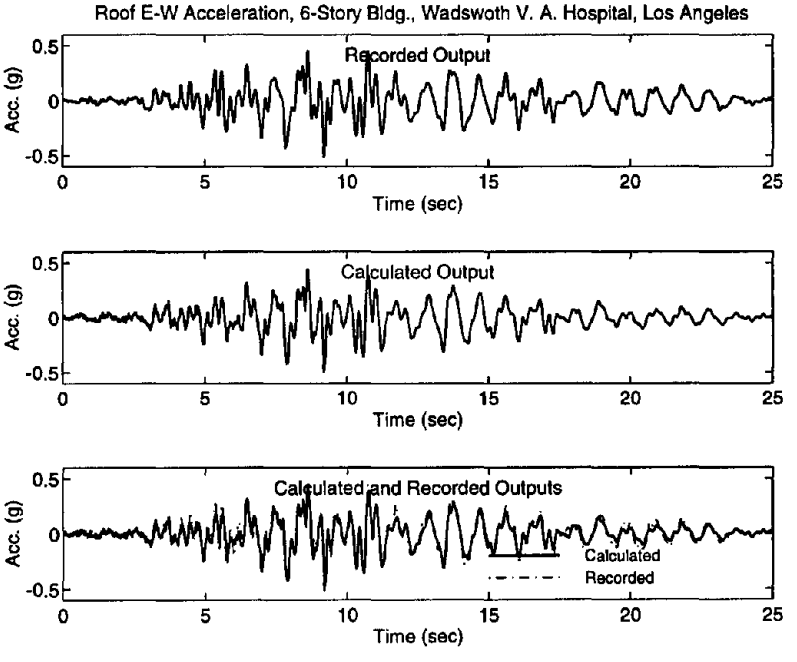

Figure C.21.4. Comparison of time-histories: recorded motions and calculated motions from WPCMIMO in E-W direction.

Table C.21.2. Results of system identification in N-S (transverse) direction by WPCMIMO.

Mode No.	Frequency (Hz)	Damping	Part. Factor	Initial Disp.	Initial Velo.	Modal Cont.	Comments
1	1.0376	0.0427	-2.31E-00	-1.43E-03	5.53E-03	9.68E-01	1st Mode
2	3.2715	0.0835	1.80E-01	-1.11E-04	9.02E-03	4.32E-02	

Relative Error = 0.261 and Absolute Error = 5.600

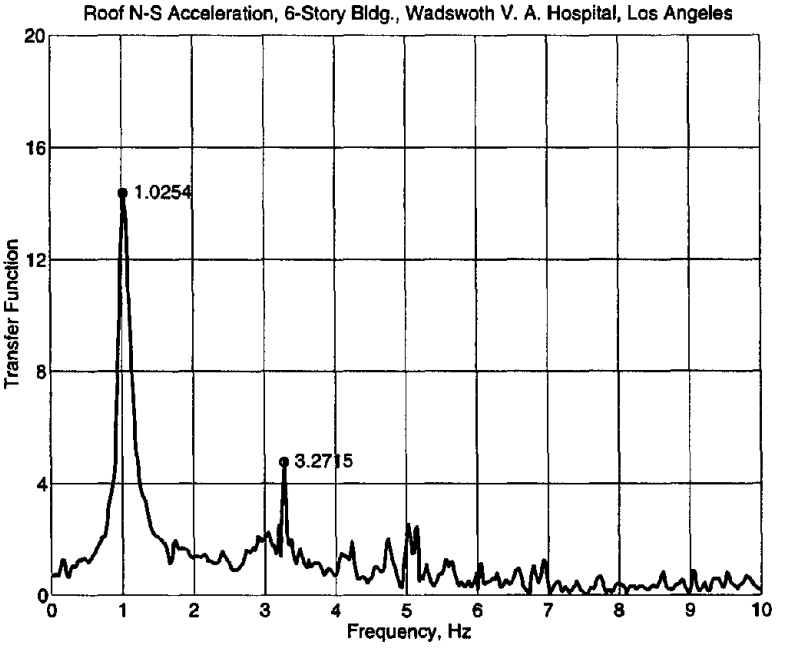

Figure C.21.5. Initial frequency estimates from transfer function in N-S direction.

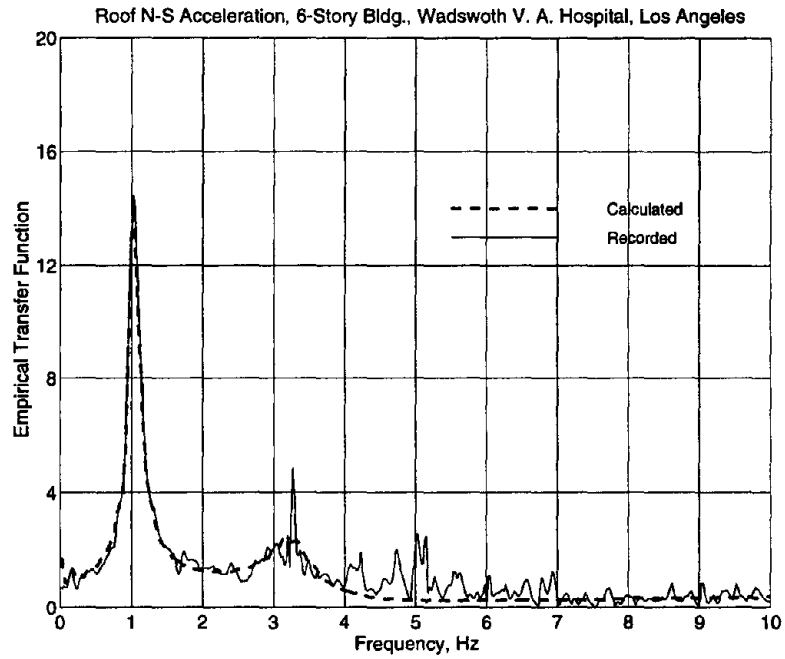

Figure C.21.6. Comparison of empirical transfer functions: recorded motions and calculated motions from WPCMIMO in N-S direction.

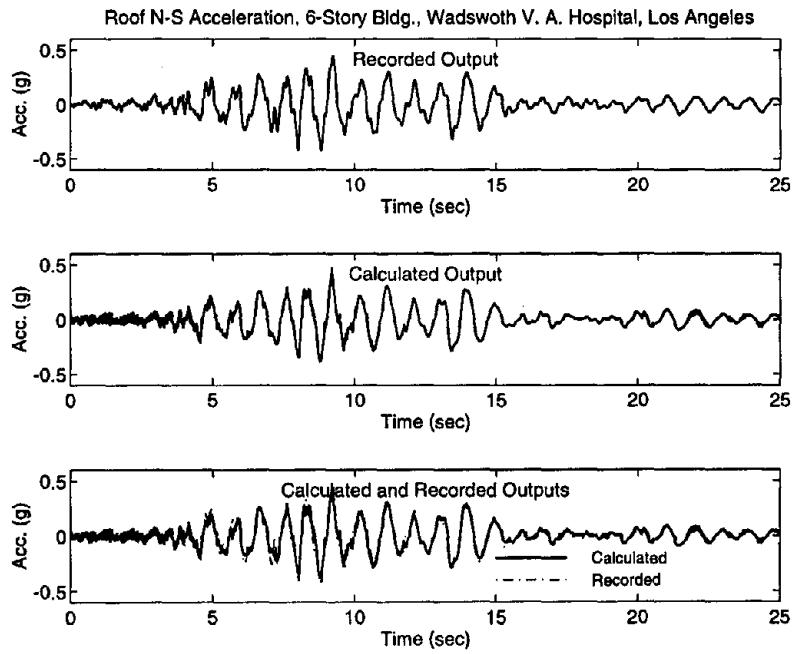

Figure C.21.7. Comparison of time-histories: recorded motions and calculated motions from WPCMIMO in N-S direction.

22. Los Angeles - 13-Story Office Building, CSMIP Station No. 24567

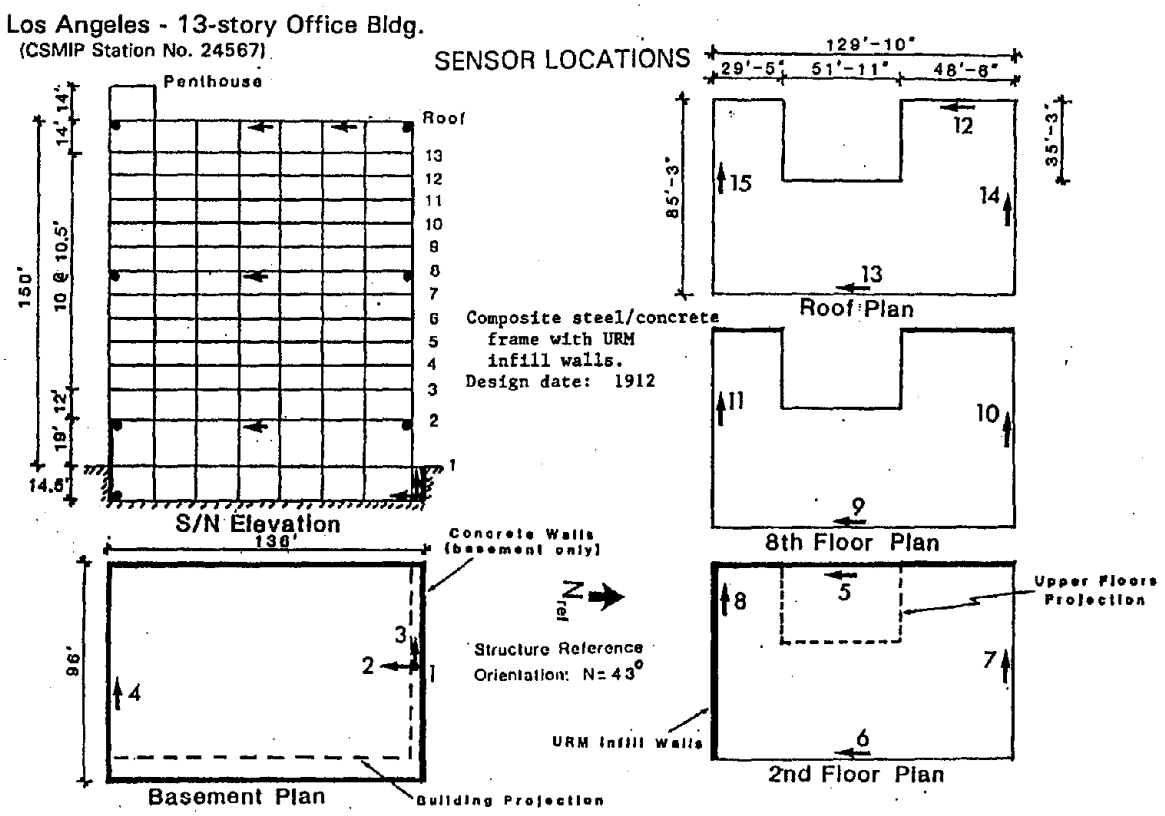

Figure C.22.1. Sensor locations in 13-story office building, CSMIP Station No. 24567

Table C.22.1 Results of system identification in E-W (transverse) direction by WPCMIMO.

Mode No.	Frequency (Hz)	Damping	Part. Factor	Initial Disp.	Initial Velo.	Modal Cont.	Comments
1	0.3803	0.0802	-8.22E-01	8.05E-04	2.55E-04	7.85E-01	1st Mode
2	1.0986	0.1489	1.95E-01	5.89E-05	-3.26E-04	5.88E-01	2nd Mode*
3	2.0581	0.1332	-5.07E-02	1.78E-05	-2.18E-04	2.03E-01	
4	3.5180	0.1559	4.62E-01	1.98E-04	-2.17E-03	3.05E+01	
5	3.5545	0.1579	-4.50E-01	-2.00E-04	1.79E-03	2.90E+01	
6	5.7913	0.0472	2.70E-03	-6.38E-07	5.25E-06	4.19E-03	

* Damping is not reliable

Relative Error = 0.466 and Absolute Error = 3.341

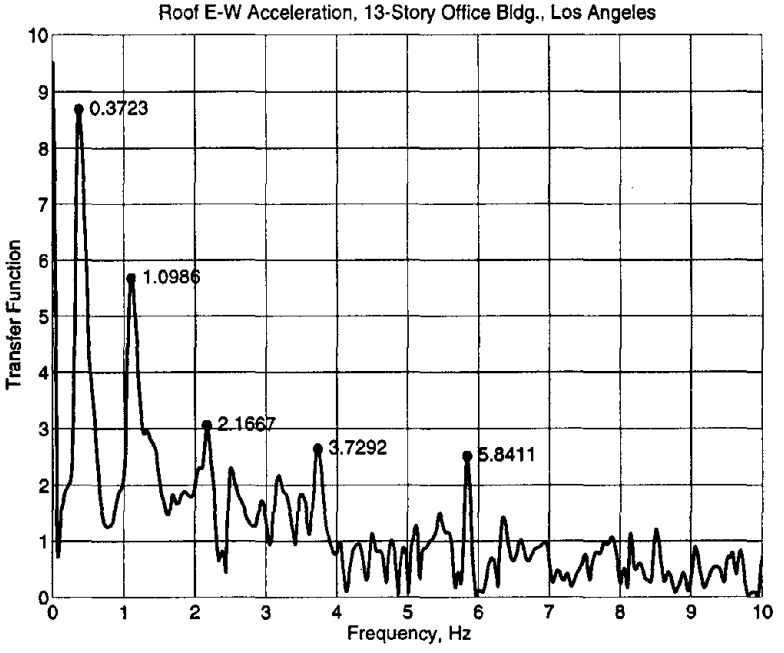

Figure C.22.2 Initial frequency estimates from transfer function in E-W direction.

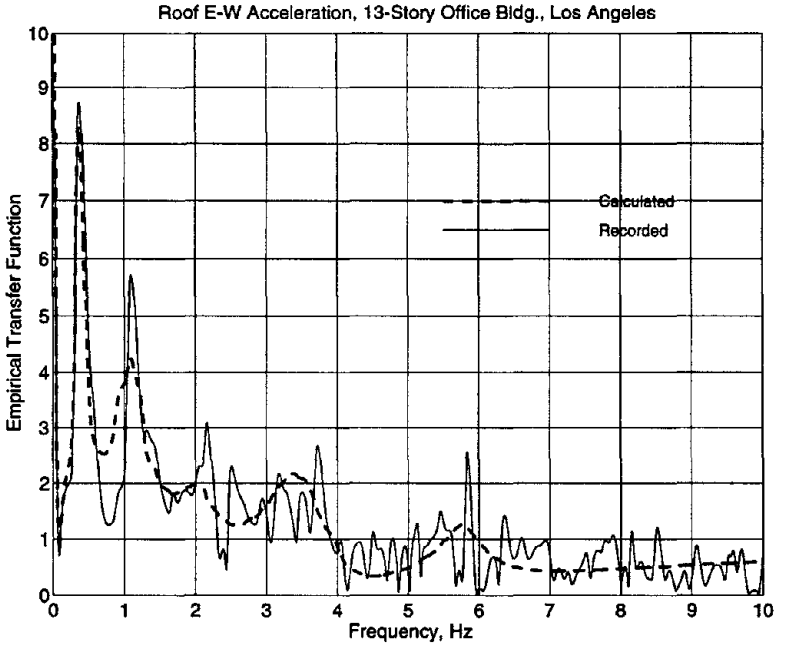

Figure C.22.3. Comparison of empirical transfer functions: recorded motions and calculated motions from WPCMIMO in E-W direction.

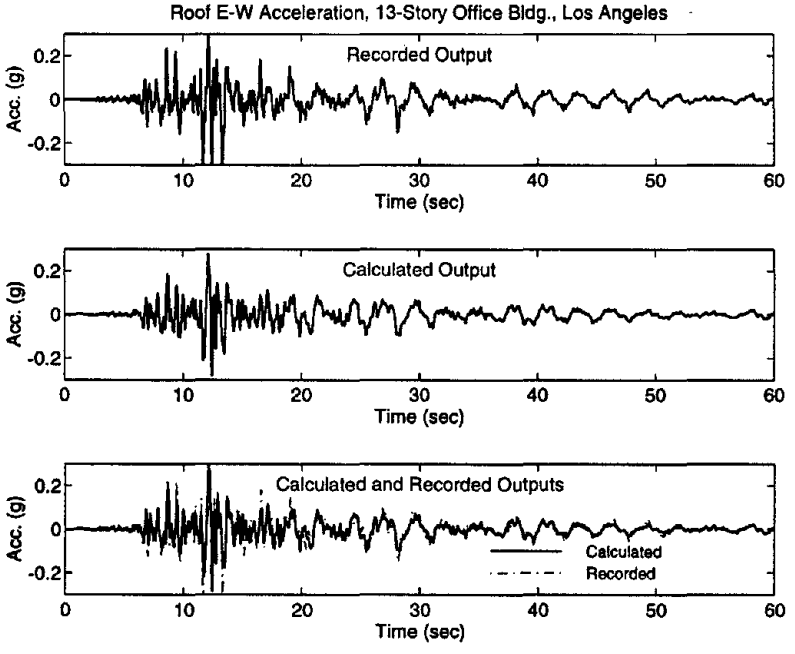

Figure C.22.4. Comparison of time-histories: recorded motions and calculated motions from WPCMIMO in E-W direction.

Table C.22.2 Results of system identification in N-S (longitudinal) direction by WPCMIMO.

Mode No.	Frequency (Hz)	Damping	Part. Factor	Initial Disp.	Initial Velo.	Modal Cont.	Comments
1	0.4356	0.0927	-4.77E-01	-4.80E-05	4.93E-04	5.92E-01	1st Mode
2	1.1353	0.2527	1.17E-01	3.74E-05	5.01E-05	2.65E-01	
3	2.2378	0.1570	-4.82E-02	9.98E-06	-6.84E-05	3.87E-01	
4	3.2740	0.1390	1.44E-02	2.22E-06	-1.40E-04	6.69E-02	
5	4.4041	0.0463	-3.95E-03	-1.37E-06	-6.89E-05	1.56E-02	
6	5.0297	0.0000	-1.43E-04	-2.26E-06	4.22E-05	7.78E-04	

Relative Error = 0.535 and Absolute Error = 2.324

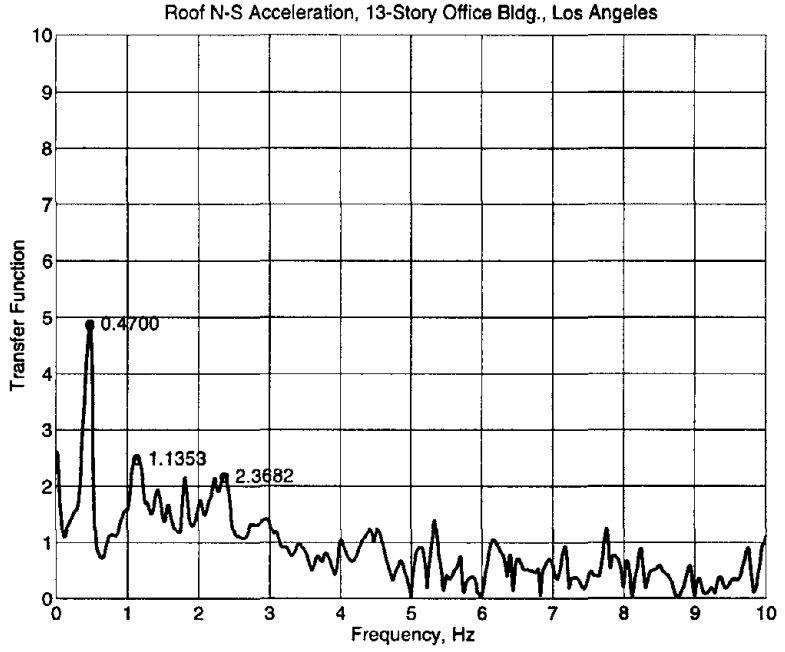

Figure C.22.5 Initial frequency estimates from transfer function in N-S direction.

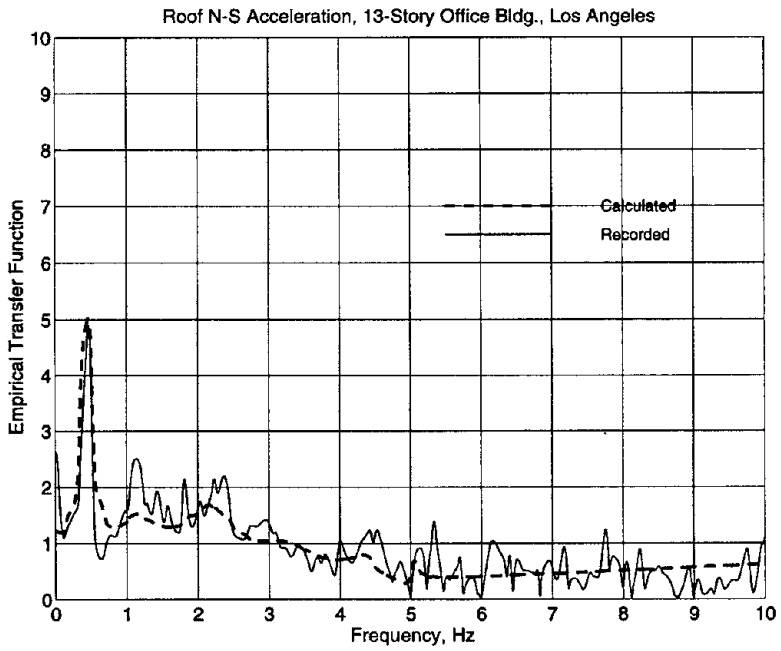

Figure C.22.6. Comparison of empirical transfer functions: recorded motions and calculated motions from WPCMIMO in N-S direction.

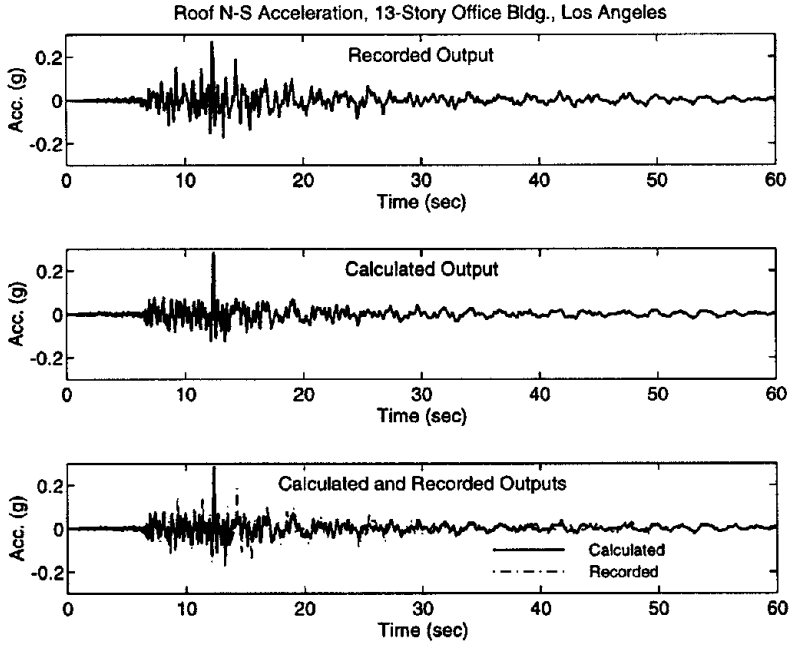

Figure C.22.7. Comparison of time-histories: recorded motions and calculated motions from WPCMIMO in N-S direction.

APPENDIX D: BASIS FOR CODE FORMULA

The period formula specified in current US codes is based on the following assumptions:

1. Equivalent lateral forces are distributed linearly over height of the building.
2. Base shear is proportional to $1/T^{\alpha}$.
3. Weight of the building is distributed uniformly over its height.
4. Deflection of the building due to the equivalent lateral force distribution is linear over its height implying that the inter-story drift, Δ, is constant over height of the building.

For these assumptions, period of a building, idealized as a cantilever with uniform mass, may be estimated using the Rayleigh's method as follows:

$$T = 2\pi\sqrt{(\int m\delta^2(x)) \div (g\int f(x)\delta(x)dx)} \tag{D-1}$$

in which $\delta(x)$ is the deflected shape of the building due to the equivalent lateral force $f(x)$. Utilizing assumption (1) to (3) regarding distribution of lateral forces leads to:

$$f(x) = 2mg\frac{C}{T^{\alpha}}\frac{x}{H} \tag{D-2}$$

in which C is the constant related to the seismic coefficient, and H is total height of the building, and assumption (4) for deflected shape of the building gives:

$$\delta(x) = \Delta x \tag{D-3}$$

Utilizing Eqs. (D-2) and (D-3) in (D-1) leads to:

$$T = \left[(2\pi)^2\frac{\Delta}{2gC}\right]^{\frac{1}{2-\alpha}} H^{\frac{1}{2-\alpha}} \tag{D-4}$$

For $\alpha = 0$, which corresponds to base shear independent of the period, Eq. (D-4) gives:

$$T = 2\pi\sqrt{\frac{\Delta}{2gC}}\sqrt{H} \tag{D-5}$$

For $\alpha = 1$, implying base shear proportional to $1/T$, Eq. (D-4) leads to:

$$T = (2\pi)^2\frac{\Delta}{2gC}H \tag{D-6}$$

For $\alpha = 2/3$, indicating base shear proportional to $1/T^{2/3}$, Eq. (D-4) results in:

$$T = \left[(2\pi)^2\frac{\Delta}{2gC}\right]^{3/4} H^{3/4} \tag{D-7}$$

Eq. (D-7) is consistent with the formula $T = C_t H^{3/4}$ in US seismic codes that specify base shear proportional to $1/T^{2/3}$ in the velocity-controlled region of the design spectrum.

APPENDIX E: THEORETICAL FORMULA FOR MRF BUILDINGS

Derived in this appendix are the theoretical formulas for fundamental period of frame buildings using the Rayleigh's method. The formulas are derived for the shear buildings, that is buildings with rigid girders (or beams).

Using Rayleigh's method, the fundamental period of a shear building is:

$$T = 2\pi \sqrt{\frac{\sum_{j=1}^{N} m_j \psi_j^2}{\sum_{j=1}^{N} k_j \left(\psi_j - \psi_{j-1}\right)^2}} \tag{E-1}$$

in which m_j is the mass and ψ_j is the deflection at jth floor of the building; and , k_j is the stiffness of the jth story. For equal mass at all floors, i.e., $m_j = m$ for $j = 1 - N$, and linear deflected shape of the building, i.e., $\psi_j = j/N$, Eq. (E-1) leads to:

$$T = 2\pi \sqrt{\frac{\frac{m}{N^2}\sum_{j=1}^{N} j^2}{\sum_{j=1}^{N} k_j \left(\frac{j}{N} - \frac{j-1}{N}\right)^2}} = 2\pi \sqrt{\frac{m\sum_{j=1}^{N} j^2}{\sum_{j=1}^{N} k_j}} \tag{E-2}$$

Buildings with Uniform Stiffness Over Height

For uniform building stiffness over height, i.e., $k_j = k$ for $j = 1 - N$, Eq. (E-2) simplifies to:

$$T = 2\pi \sqrt{\frac{\frac{m}{N^2}\sum_{j=1}^{N} j^2}{k\sum_{j=1}^{N} 1}} = 2\pi \sqrt{\frac{m}{k}\frac{\sum_{j=1}^{N} j^2}{N}} \tag{E-3}$$

Eq. (E-3) can be further simplified by utilizing the following result:

$$\sum_{j=1}^{N} j^2 = \frac{N(N+1)(2N+1)}{6} \tag{E-4}$$

to obtain

$$T = 2\pi\sqrt{\frac{m}{k}\frac{(N+1)(2N+1)}{6}} = 2\pi\sqrt{\frac{m}{k}\frac{2N^2+3N+1}{6}} \tag{E-5}$$

For N > 6, i.e., building with more than 6 stories, the N^2 term in Eq. (E-5) would dominate and the following relationship may be used to estimate the fundamental period:

$$T = C_1 N \tag{E-6}$$

in which the coefficient C_1 depends on the unit mass and stiffness properties among other constants in Eq. (E-5). For buildings with uniform story height, Eq. (E-6) may also be written in terms of the total building height, H, as:

$$T = \overline{C}_1 H \tag{E-7}$$

Buildings with Linearly Decreasing Stiffness Over Height

For linearly decreasing stiffness with height,

$$k_j = k_N(N - j + 1) \tag{E-8}$$

in which k_N is the stiffness at the top story level. This leads to

$$\sum_{j=1}^{N} k_j = k_N \sum_{j=1}^{N}(N+1-j) = k_N(N+1)\sum_{j=1}^{N}1 - k_N\sum_{j=1}^{N} j = k_N(N+1)N - k_N\frac{(N+1)N}{2} = \frac{1}{2}k_N \tag{E-9}$$

Utilizing Eqs. (E-9) and (E-4) in Eq. (E-2) leads to:

$$T = 2\pi\sqrt{\frac{m}{k_N}\frac{(2N+1)}{3}} \tag{E-10}$$

For N > 3, Eq. (E-10) may be approximated as:

$$T = C_2\sqrt{N} \tag{E-11}$$

or

$$T = \overline{C}_2 \sqrt{H} \tag{E-12}$$

Buildings with Linear Deflection Due toTriangular Load

For linear deflection under the triangular loading, the stiffness required at the jth story is given as:

$$k_j = \frac{k_N}{N} \sum_{i=j}^{N} i \tag{E-13}$$

which leads to:

$$\sum_{j=1}^{N} k_j = \frac{k_N}{N} \sum_{j=1}^{N} \sum_{i=j}^{N} i = \frac{k_N}{N} \frac{N(N+1)(2N+1)}{6} \tag{E-14}$$

Utilizing Eqs. (E-4) and (E-14) in Eq. (E-2) leads to:

$$T = 2\pi \sqrt{\frac{m}{k_N} N} \tag{E-15}$$

which can obviously be written as:

$$T = C_3 \sqrt{\mathrm{N}} \tag{E-16}$$

or

$$T = \overline{C}_3 \sqrt{H} \tag{E-17}$$

APPENDIX F: REGRESSION ANALYSIS METHOD

The fundamental period of a building can be expressed as:

$$T = \alpha \overline{H}^{\beta} \tag{F-1}$$

For MRF buildings $\overline{H} = H$ and α and β are the numerical constants to be determined from regression analysis. For SW buildings $\overline{H} = H \div \sqrt{\overline{A_e}}$, β is fixed at one, and α is the numerical constant to be determined from regression analysis. Eq. (F-1) may be recast as:

$$y = a + \beta x \tag{F-2}$$

where $y = log(T)$, $a = log(\alpha)$, and $x = \log(\overline{H})$. Equation (F-2) represents a straight line with intercept a and slope β. Therefore, the power relationship of Eq. (F-1) becomes a linear relationship in the log-log space as shown in Figure F.1.

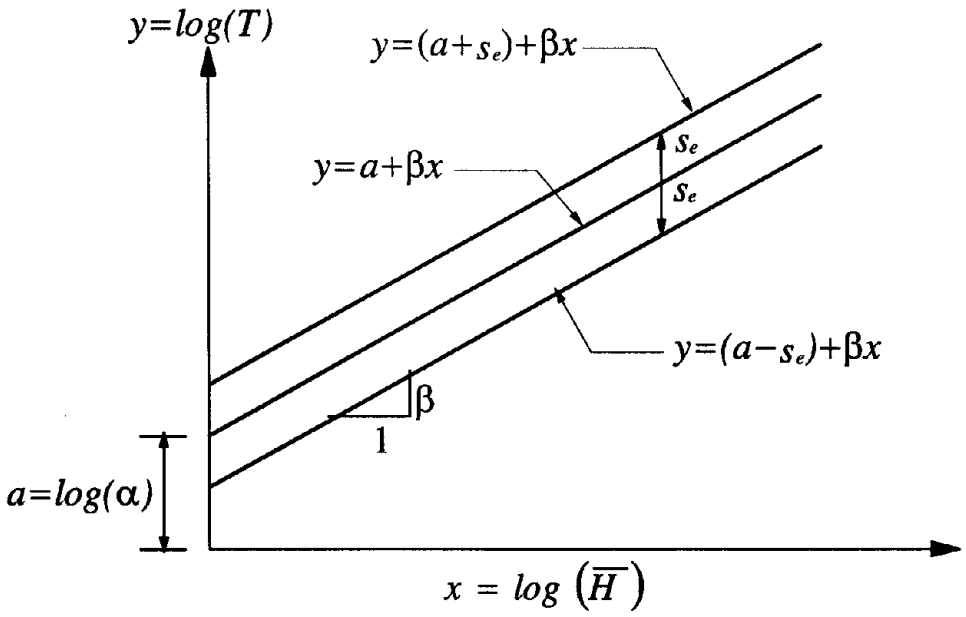

Figure F.1. Conceptual explanation of regression analysis.

In the regression analysis, the intercept a and slope β of the line in Figure F.1 were determined by minimizing the squared error between the measured and computed periods, and then the numerical constant α was back calculated from the relationship $a = log(\alpha)$.

The goodness of the fit is represented by the standard error of estimate defined as:

$$s_e = \sqrt{\frac{\sum_{i=1}^{n}\left[y_i - (a+\beta x_i)\right]^2}{(n-2)}} \qquad \text{(F-3)}$$

in which $y_i = \log(T_i)$ is the observed value (with $T_i =$ measured period) and $(a+\beta x_i) = \log(\alpha) + \beta\log(\overline{H})$ is the computed value of the ith data, and n is the number of data points. The s_e represents scatter in the data and approaches, for large n, the standard deviation of the measured period data from the best-fit equation.

This procedure leads to the value of α_R for Eq. (F-1) to represent the best-fit, in the least squared sense, to the measured period data. However, for code applications the formula should provide a lower value of the period and this was obtained by lowering the best-fit line (Eq. F-2) by s_e without changing its slope (Figure F.1). Thus α_L, the lower value of α, is computed from:

$$\log(\alpha_L) = \log(\alpha_R) - s_e \qquad \text{(F-4)}$$

Since s_e approaches the standard deviation for large number of samples and if y is assumed to be log-normal, α_L is the mean-minus-one-standard-deviation or 15.9 percentile value, implying that 15.9 percent of the measured periods would fall below the curve corresponding to α_L (subsequently referred to as the best-fit – 1σ curve). If desired, α_L corresponding to other non-exceedance probabilities may be selected.

As mentioned previously, codes also specify an upper limit on the period calculated by a "rational" analysis. This limit is established in this investigation by raising the best-fit line (Eq. F-2) by s_e without changing its slope (Figure F.1). Thus α_U, the upper value of α corresponding to the upper limit, is computed from:

$$\log(\alpha_U) = \log(\alpha_R) + s_e \qquad \text{(F-5)}$$

Eq. (F-1) with α_U represents the best-fit + 1σ curve which will be exceeded by 15.9 percent of the measured periods.

Regression analysis in the log-log space (Eq. F-2) is preferred over the direct regression on Eq. (F-1) because it permits convenient development of the best-fit − 1σ and best-fit + 1σ curves. Also note that β is fixed at one for SW buildings and only α is determined from the regression analysis.

APPENDIX G: THEORETICAL FORMULAS FOR SW BUILDINGS

Rayleigh's Method

For a cantilever with uniformly distributed mass and stiffness properties, the fundamental period may be calculated from:

$$T = 2\pi\sqrt{\frac{\int m(x)\delta^2(x)dx}{\int f(x)\delta(x)dx}} \tag{G-1}$$

in which $m(x)$ = mass per unit length, $f(x)$ = applied force, and $\delta(x)$ = deflection due to the applied force at height = x from base of the cantilever. For a cantilever with uniform mass $m(x) = m$ and a triangular distribution of applied force $f(x) = f_o x/H$, Eq. (G-1) becomes:

$$T = 2\pi\sqrt{\frac{m\int\delta^2(x)dx}{\frac{f_o}{H}\int x\delta(x)dx}} \tag{G-2}$$

The triangular distribution of forces over the height of the cantilever is similar to that specified in building codes. For such a height-wise distribution of forces, variations of shear force and bending moment with height of the cantilever are given as:

$$V(x) = \frac{1}{2}\frac{f_o}{H}\left(H^2 - x^2\right) \tag{G-3}$$

$$M(x) = \frac{1}{6}\frac{f_o}{H}\left(2H^3 - 3H^2x + x^3\right) \tag{G-4}$$

The deflection at location x can be calculated by the principle of virtual work as:

$$\delta(x) = \int_0^x \frac{v(\zeta)}{\kappa GA}V(\zeta)d\zeta + \int_0^x \frac{\overline{m}(\zeta)}{EI}M(\zeta)d\zeta = \delta_S(x) + \delta_F(x) \tag{G-5}$$

in which $v(\zeta)$ and $\overline{m}(\zeta)$ are the shear force and bending moment, respectively, at location ζ due to a virtual unit force at location x; E and G are the Young's modulus and shear modulus, respectively; and κ is the shape factor for the cantilever. The first term in Eq. (G-5) is the

contribution due to shear deformation whereas the second term is the contribution due to flexural deformation. For the cantilever with triangular loading, the deflections due to shear and flexure are:

$$\delta_S(x) = \int_0^x \frac{1}{\kappa GA}\frac{1}{2}\frac{f_o}{H}\left(H^2-\zeta^2\right)d\zeta = \frac{1}{6}\frac{f_o}{H}\frac{1}{\kappa GA}\left(3H^2x-x^3\right) \tag{G-6}$$

$$\delta_F(x) = \int_0^x \frac{(x-\zeta)}{EI}\frac{1}{6}\frac{f_o}{H}\left(H^3-H^2\zeta+\zeta^3\right)d\zeta = \frac{1}{120}\frac{f_o}{H}\frac{1}{EI}\left(20H^3x^2-10H^2x^3+x^5\right) \tag{G-7}$$

Deflection due to Shear Alone

Considering deflections due to shear alone (Eq. G-6), the numerator and denominator in Eq. (G-2) are:

$$\int_0^H m\delta_S^2(x)dx = \int_0^H m\left[\frac{1}{6}\frac{f_o}{H}\frac{1}{\kappa GA}\left(3H^3x-x^3\right)\right]^2 dx = \frac{17}{315}\left(\frac{f_o}{\kappa GA}\right)^2 mH^5 \tag{G-8}$$

$$\int_0^H f(x)\delta_S(x)dx = \int_0^H \frac{f_o}{H}x\left[\frac{1}{6}\frac{f_o}{H}\frac{1}{\kappa GA}\left(3H^2x-x^3\right)\right]dx = \frac{2}{15}\frac{f_o^2}{\kappa GA}H^3 \tag{G-9}$$

Utilizing Eqs. G-8 and G-9 in Eq. G-2 leads to:

$$T = 2\pi\sqrt{\frac{\frac{17}{315}\left(\frac{f_o}{\kappa GA}\right)^2 mH^5}{\frac{2}{15}\frac{f_o^2}{\kappa GA}H^3}} = 2\pi\sqrt{\frac{17}{42}\frac{m}{\kappa G}}\frac{H}{\sqrt{A}} = 3.997\sqrt{\frac{m}{\kappa G}}\frac{H}{\sqrt{A}} \tag{G-10}$$

This formula compares well with the following exact solution for a shear cantilever:

$$T = 4\sqrt{\frac{m}{\kappa G}}\frac{H}{\sqrt{A}} \tag{G-11}$$

Deflection due to Flexure Alone

Considering deflections due to flexure alone (Eq. G-7), the numerator and denominator in Eq. (G-2) are:

$$\int_0^H m\,\delta_F^2(x)dx = \int_0^H m\left[\frac{1}{120}\frac{f_o}{H}\frac{1}{EI}\left(20H^3x^2-10H^2x^3+x^5\right)\right]^2 dx = \frac{21128}{9979200}\left(\frac{f_o}{EI}\right)^2 m H^9 \tag{G-12}$$

$$\int_0^H f(x)\,\delta_F(x)dx = \int_0^H \frac{f_o}{H}x\left[\frac{1}{120}\frac{f_o}{H}\frac{1}{EI}\left(20H^3x^2-10H^2x^3+x^5\right)\right]dx = \frac{11}{420}\frac{f_o^2}{EI}H^5 \tag{G-13}$$

Utilizing Eqs. G-12 and G-13 in Eq. G-2 leads to:

$$T = 2\pi\sqrt{\frac{\frac{21128}{9979200}\left(\frac{f_o}{EI}\right)^2 m H^9}{\frac{11}{420}\frac{f_o^2}{EI}H^5}} = 2\pi\sqrt{\frac{2641}{32670}\frac{m}{E}\frac{H^2}{\sqrt{I}}} = 1.786\sqrt{\frac{m}{E}}\frac{H^2}{\sqrt{I}} \tag{G-14}$$

which also compares well with the following exact solution for a flexural cantilever:

$$T = \frac{2\pi}{3.516}\sqrt{\frac{m}{E}}\frac{H^2}{\sqrt{I}} = 1.787\sqrt{\frac{m}{E}}\frac{H^2}{\sqrt{I}} \tag{G-15}$$

Recognizing that $I = A\,D^2/12$, in which A is the area and D is the dimension of shear wall along the direction under consideration, Eq. G-14 and G-15 may be re-written as:

$$T = 1.786\sqrt{\frac{m}{E}}\frac{H^2}{\sqrt{\frac{A\,D^2}{12}}} = 6.188\sqrt{\frac{m}{E}}\frac{H}{D}\frac{1}{\sqrt{A}}H = \overline{C}_5\frac{H}{D}\frac{1}{\sqrt{A}}H \tag{G-16}$$

$$T = 1.787\sqrt{\frac{m}{E}}\frac{H^2}{\sqrt{\frac{A\,D^2}{12}}} = 6.190\sqrt{\frac{m}{E}}\frac{H}{D}\frac{1}{\sqrt{A}}H \tag{G-17}$$

Deflections Due to Shear and Flexure

Considering deflections due to shear as well as flexure, the numerator and denominator in Eq. (G-2) are:

$$\begin{aligned}\int_0^H m\delta^2(x)dx &= \int_0^H m\left(\delta_S(x)+\delta_F(x)\right)^2 dx \\ &= \int_0^H m\delta_S^2(x)dx + \int_0^H m\delta_F^2(x)dx + 2\int_0^H m\delta_S(x)\delta_F(x)dx \\ &= \frac{17}{315}\left(\frac{f_o}{\kappa GA}\right)^2 mH^5 + \frac{21128}{9979200}\left(\frac{f_o}{EI}\right)^2 mH^9 + \frac{467}{22680}\frac{f_o}{\kappa GA}\frac{f_o}{EI}mH^7\end{aligned} \tag{G-18}$$

$$\begin{aligned}\int_0^{h_n} f(x)\delta(x)dx &= \int_0^H f(x)\left(\delta_S(x)+\delta_F(x)\right)dx = \int_0^H f(x)\delta_S(x)dx + \int_0^H f(x)\delta_F(x)dx \\ &= \frac{2}{15}\frac{f_o^2}{\kappa GA}H^3 + \frac{11}{420}\frac{f_o^2}{EI}H^5\end{aligned} \tag{G-19}$$

Utilizing Eqs. (G-18) and (G-19) in Eq. (G-2) gives:

$$\begin{aligned}T &= 2\pi\sqrt{\frac{\frac{17}{315}\left(\frac{f_o}{\kappa GA}\right)^2 mH^5 + \frac{2641}{1247400}\left(\frac{f_o}{EI}\right)^2 mH^9 + \frac{467}{22680}\frac{f_o}{\kappa GA}\frac{f_o}{EI}mH^7}{\frac{2}{15}\frac{f_o^2}{\kappa GA}H^3 + \frac{11}{420}\frac{f_o^2}{EI}H^5}} \\ &= 2\pi\sqrt{\frac{m}{E}}\frac{H}{\sqrt{A}}\sqrt{\frac{\left[\frac{17}{315}\left(\frac{E}{\kappa G}\right)^2 + \frac{2641}{1247400}\left(\frac{12}{D^2}\right)^2 H^4 + \frac{467}{22680}\frac{E}{\kappa G}\frac{12}{D^2}H^2\right]}{\left[\frac{2}{15}\frac{E}{\kappa G} + \frac{11}{420}\frac{12}{D^2}H^2\right]}} \\ &= 2\pi\sqrt{\frac{m}{E}}\frac{H}{\sqrt{A}}\sqrt{\frac{\left[\frac{17}{315}\left(\frac{E}{\kappa G}\right)^2 + \frac{5282}{17325}\left(\frac{H^2}{D^2}\right)^2 + \frac{467}{1890}\frac{E}{\kappa G}\frac{H^2}{D^2}\right]}{\left[\frac{2}{15}\frac{E}{\kappa G} + \frac{11}{35}\frac{H^2}{D^2}\right]}}\end{aligned} \tag{G-20}$$

Dunkerley's Method

Single Shear Wall

Based on Dunkerley's method, the fundamental period of a cantilever considering flexural and shear deformations, can be computed from:

$$\frac{1}{\omega^2}=\frac{1}{\omega_F^2}+\frac{1}{\omega_S^2}, \text{ or}$$

$$\frac{1}{f^2}=\frac{1}{f_F^2}+\frac{1}{f_S^2}, \text{ or} \qquad \text{(G-21)}$$

$$T^2=T_F^2+T_S^2$$

in which $T_F=1/f_F=2\pi/\omega_F$ and $T_S=1/f_S=2\pi/\omega_S$ are the periods of the fundamental periods of pure-flexural and pure-shear cantilevers, respectively. For uniform cantilevers, these periods are given by:

$$T_F=\frac{2\pi}{3.516}\sqrt{\frac{m}{EI}}H^2 \qquad \text{(G-22)}$$

and

$$T_S=4\sqrt{\frac{m}{\kappa G}}\frac{H}{\sqrt{A}} \qquad \text{(G-23)}$$

In Eqs. (G-22) and (G-23), m is the mass per unit height, E is the modulus of elasticity, G is the shear modulus, I is the section moment of inertia, A is the section area, and κ is the shape factor to account for nonuniform distribution of shear stresses (= 5/6 for rectangular sections). Utilizing Eqs. (G-22) and (G-23) in (G-21) gives:

$$T=\left[\frac{4\pi^2}{3.516^2}\frac{m}{EI}H^4+16\frac{m}{\kappa GA}H^2\right]^{1/2}=4\sqrt{\frac{m}{\kappa G}}\left[0.2\frac{\kappa G}{E}\frac{H^2}{I}+\frac{1}{A}\right]^{1/2}H \qquad \text{(G-27)}$$

Since $I=AD^2\div 12$, Eq. (G-27) can be further simplified to:

$$T=4\sqrt{\frac{m}{\kappa G}}\left[\frac{1}{A}\left\{1+2.4\frac{\kappa G}{E}\left(\frac{H}{D}\right)^2\right\}\right]^{1/2}H \qquad \text{(G-28)}$$

Recognizing that $G=E\div 2(1+\mu)$, where the Poison's ratio $\mu = 0.2$ for concrete, leads to:

$$T = 4\sqrt{\frac{m}{\kappa G}}\frac{1}{\sqrt{A_e}}H \tag{G-29}$$

with

$$A_e = \frac{A}{\left[1+0.83\left(\frac{H}{D}\right)^2\right]} \tag{G-30}$$

where D is the plan dimension of the cantilever in the direction under consideration.

Several Shear Walls

Now consider a class of symmetric-plan buildings -- symmetric in the lateral direction considered -- with lateral-force resisting system comprised of a number of uncoupled (i.e., without coupling beams) shear walls connected through rigid floor diaphragms. Assuming that the stiffness properties of each wall are uniform over its height, Eq. (G-27) may be written as:

$$\begin{aligned} T &= \left[\sum_{i=1}^{NW}\left\{\frac{4\pi^2}{3.516^2}\frac{m}{EI_i}H_i^4+16\frac{m}{\kappa G A_i}H_i^2\right\}\right]^{1/2} \\ &= 4\sqrt{\frac{m}{\kappa G}}\left[\sum_{i=1}^{NW}\left(\frac{H_i}{H}\right)^2\frac{1}{A_i}\left\{1+2.4\frac{\kappa G}{E}\left(\frac{H_i}{D_i}\right)^2\right\}\right]^{1/2}H \end{aligned} \tag{G-31}$$

in which A_i, H_i, and D_i are the area, height, and dimension in the direction under consideration of the ith shear wall, and NW is the number of shear walls. Eq. (G-31) may be written in the same form as Eq. (G-29) if A_e is defined as:

$$A_e = \sum_{i=1}^{NW}\left(\frac{H}{H_i}\right)^2\frac{A_i}{\left[1+0.83\left(\frac{H_i}{D_i}\right)^2\right]} \tag{G-32}$$

Equation (G-29) can be expressed in a form convenient for buildings:

$$T = 40\sqrt{\frac{\rho}{\kappa G}}\frac{1}{\sqrt{\overline{A}_e}}H \tag{G-33}$$

where ρ is the average mass density, defined as the total building mass (= mH) divided by the total building volume (= $A_B H$ -- A_B is the building plan area), i.e., $\rho = m/A_B$; and $\overline{A}_e$ is the equivalent shear area expressed as a percentage of A_B, i.e.,

$$\overline{A}_e = 100\frac{A_e}{A_B} \tag{G-34}$$

APPENDIX H: COMPUTED PERIODS OF SW BUILDINGS

1. Burbank - 10 Story Residential Building, CSMIP Station No. 24385

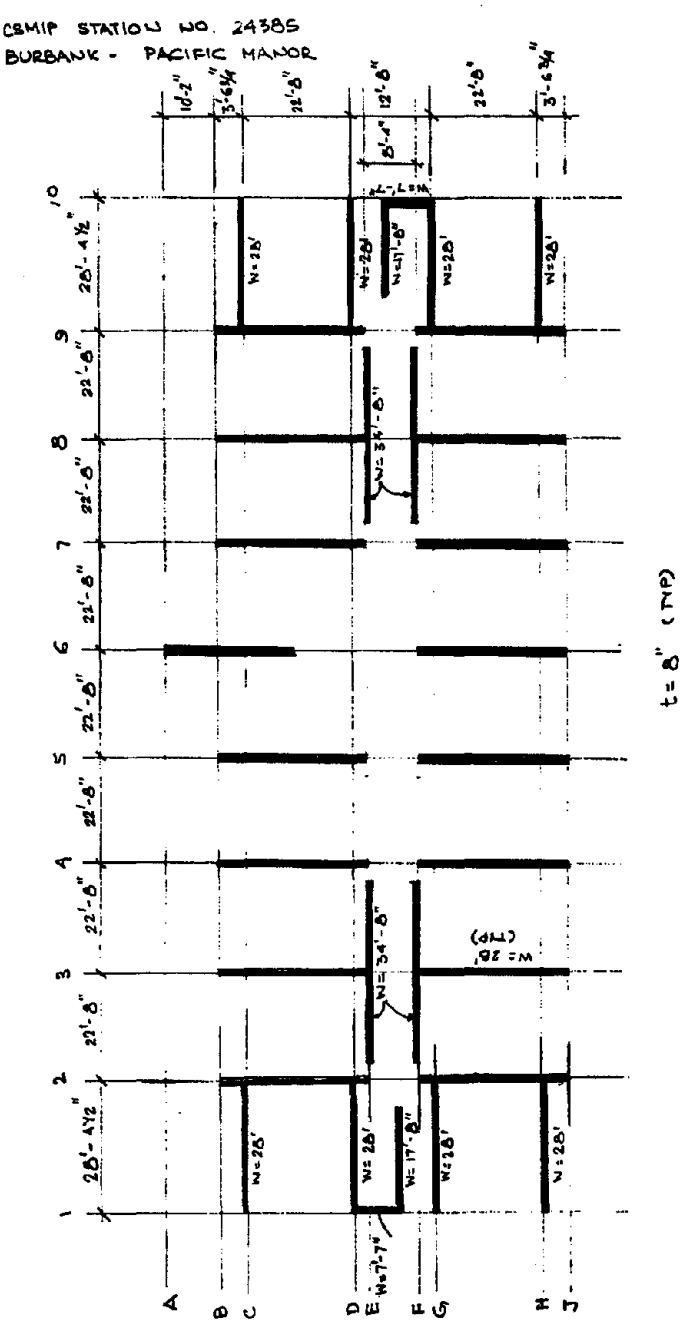

Figure H.1.1. Sketch of shear walls in CSMIP Station No. 24385

Location	Burbank
Occupancy	Residential
Station ID	24385
Name	Pacific Manor
Address	609 Glenoaks Blvd
Height	88 ft
Building Plan Area	16125 sq. ft

Period Calculations				
Direction	Code Formula		New Formula	
	A_c (sq. ft)	T (sec)	$\overline{A}_e$ (%)	T (sec)
Longitudinal	83.48	0.3145	0.1978	0.3760
Transverse	92.07	0.2994	0.2019	0.3721

Calculation of Equivalent Shear Wall Areas: Transverse Direction

Wall ID	Width (ft)	Thickness (ft)	Area (sq. ft)	D_i/H	Area for Code Formula		Area for New Formula	
					$0.2+(D_i/H)^2$	A_{ci} (sq. ft)	$1/(1+0.83(H/D_i)^2)$	A_{ei} (sq. ft)
1-DEF	7.58	0.67	5.06	0.09	0.21	1.05	0.009	0.045
2-BE	28.00	0.67	18.67	0.32	0.30	5.62	0.109	2.029
2-FJ	28.00	0.67	18.67	0.32	0.30	5.62	0.109	2.029
3-BE	28.00	0.67	18.67	0.32	0.30	5.62	0.109	2.029
3-FJ	28.00	0.67	18.67	0.32	0.30	5.62	0.109	2.029
4-BE	28.00	0.67	18.67	0.32	0.30	5.62	0.109	2.029
4-FJ	28.00	0.67	18.67	0.32	0.30	5.62	0.109	2.029
5-BE	28.00	0.67	18.67	0.32	0.30	5.62	0.109	2.029
5-FJ	28.00	0.67	18.67	0.32	0.30	5.62	0.109	2.029
6-AC	28.00	0.67	18.67	0.32	0.30	5.62	0.109	2.029
6-FJ	28.00	0.67	18.67	0.32	0.30	5.62	0.109	2.029
7-BE	28.00	0.67	18.67	0.32	0.30	5.62	0.109	2.029
7-FJ	28.00	0.67	18.67	0.32	0.30	5.62	0.109	2.029
8-BE	28.00	0.67	18.67	0.32	0.30	5.62	0.109	2.029
8-FJ	28.00	0.67	18.67	0.32	0.30	5.62	0.109	2.029
9-BE	28.00	0.67	18.67	0.32	0.30	5.62	0.109	2.029
9-FJ	28.00	0.67	18.67	0.32	0.30	5.62	0.109	2.029
10-EG	7.58	0.67	5.06	0.09	0.21	1.05	0.009	0.045
					$\sum A_{ci}$	92.07	$\sum A_{ei}$	32.56

Calculation of Equivalent Shear Wall Areas: Longitudinal Direction

Wall ID	Width (ft)	Thickness (ft)	Area (sq. ft)	D_i/H	Area for Code Formula		Area for New Formula	
					$0.2+(D_i/H)^2$	A_{ci} (sq. ft)	$1/(1+0.83(H/D_i)^2)$	A_{ei} (sq. ft)
C-12	28.00	0.67	18.67	0.32	0.30	5.62	0.109	2.029
D-12	28.00	0.67	18.67	0.32	0.30	5.62	0.109	2.029
F-12	17.67	0.67	11.78	0.20	0.24	2.83	0.046	0.545
G-12	28.00	0.67	18.67	0.32	0.30	5.62	0.109	2.029
H-12	28.00	0.67	18.67	0.32	0.30	5.62	0.109	2.029
E-24	34.67	0.67	23.11	0.39	0.36	8.21	0.158	3.640
F-24	34.67	0.67	23.11	0.39	0.36	8.21	0.158	3.640
E-79	34.67	0.67	23.11	0.39	0.36	8.21	0.158	3.640
F-79	34.67	0.67	23.11	0.39	0.36	8.21	0.158	3.640
C-910	28.00	0.67	18.67	0.32	0.30	5.62	0.109	2.029
D-910	28.00	0.67	18.67	0.32	0.30	5.62	0.109	2.029
EF-910	17.67	0.67	11.78	0.20	0.24	2.83	0.046	0.545
G-910	28.00	0.67	18.67	0.32	0.30	5.62	0.109	2.029
H-910	28.00	0.67	18.67	0.32	0.30	5.62	0.109	2.029
					$\sum A_{ci}$	83.48	$\sum A_{ei}$	31.89

2. Los Angeles - 8 Story Administration Building, CSMIP Station No. 24468

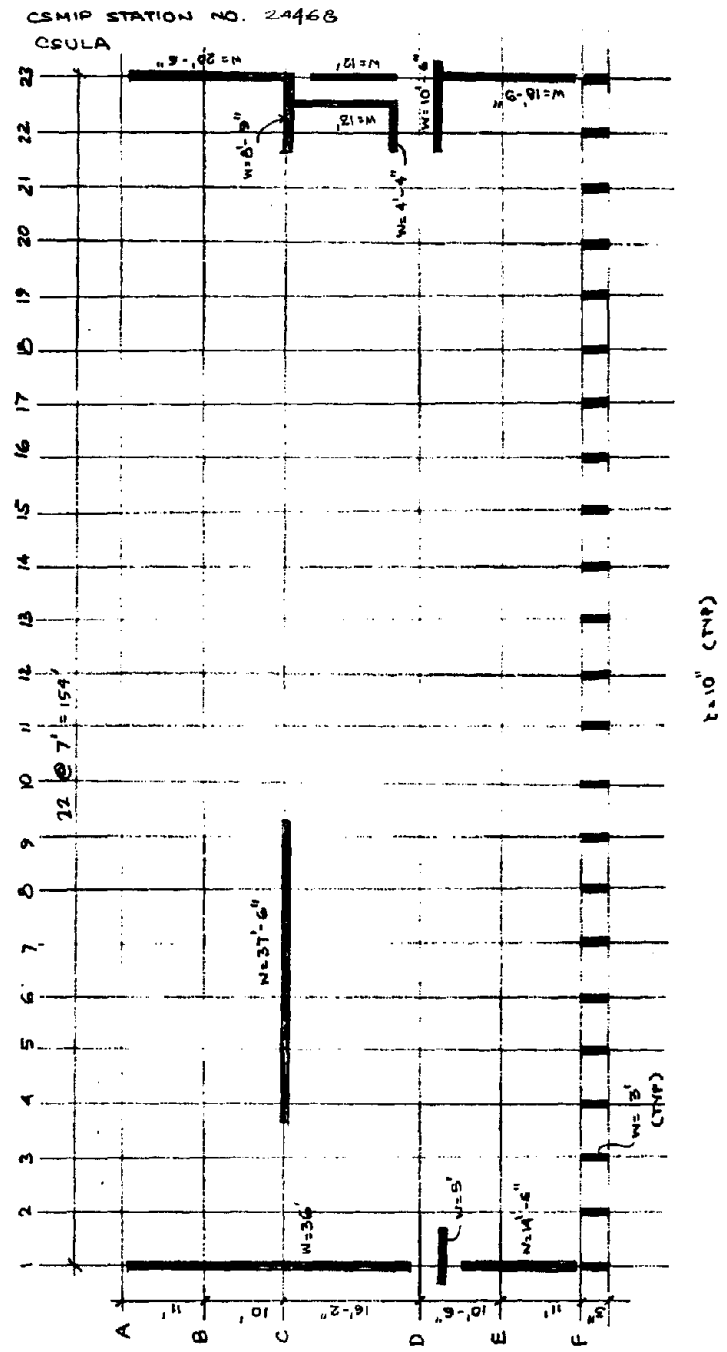

Figure H.2.1. Sketch of shear walls in CSMIP Station No. 24468

Location	Los Angeles
Occupancy	Administration
Station ID	24468
Name	CSULA
Height	127 ft
Building Plan Area	9702 sq. ft

Period Calculations				
Direction	Code Formula		New Formula	
	A_c (sq. ft)	T (sec)	$\overline{A}_e$ (%)	T (sec)
Longitudinal	13.84	1.0168	0.0319	1.3507
Transverse	34.21	0.6468	0.0416	1.1833

Calculation of Equivalent Shear Wall Areas: Transverse Direction

Wall ID	Width (ft)	Thickness (ft)	Area (sq. ft)	D_i/H	Area for Code Formula		Area for New Formula	
					$0.2+(D_i/H)^2$	A_{ci} (sq. ft)	$1/(1+0.83(H/D_i)^2)$	A_{ei} (sq. ft)
1-AD	36.00	0.83	30.00	0.28	0.28	8.41	0.088	2.648
1-DEF	14.50	0.83	12.08	0.11	0.21	2.57	0.015	0.187
1-F	3.00	0.83	2.50	0.02	0.20	0.50	0.001	0.002
2-F	3.00	0.83	2.50	0.02	0.20	0.50	0.001	0.002
3-F	3.00	0.83	2.50	0.02	0.20	0.50	0.001	0.002
4-F	3.00	0.83	2.50	0.02	0.20	0.50	0.001	0.002
5-F	3.00	0.83	2.50	0.02	0.20	0.50	0.001	0.002
6-F	3.00	0.83	2.50	0.02	0.20	0.50	0.001	0.002
7-F	3.00	0.83	2.50	0.02	0.20	0.50	0.001	0.002
8-F	3.00	0.83	2.50	0.02	0.20	0.50	0.001	0.002
9-F	3.00	0.83	2.50	0.02	0.20	0.50	0.001	0.002
10-F	3.00	0.83	2.50	0.02	0.20	0.50	0.001	0.002
11-F	3.00	0.83	2.50	0.02	0.20	0.50	0.001	0.002
12-F	3.00	0.83	2.50	0.02	0.20	0.50	0.001	0.002
13-F	3.00	0.83	2.50	0.02	0.20	0.50	0.001	0.002
14-F	3.00	0.83	2.50	0.02	0.20	0.50	0.001	0.002
15-F	3.00	0.83	2.50	0.02	0.20	0.50	0.001	0.002
16-F	3.00	0.83	2.50	0.02	0.20	0.50	0.001	0.002
17-F	3.00	0.83	2.50	0.02	0.20	0.50	0.001	0.002
18-F	3.00	0.83	2.50	0.02	0.20	0.50	0.001	0.002
19-F	3.00	0.83	2.50	0.02	0.20	0.50	0.001	0.002
20-F	3.00	0.83	2.50	0.02	0.20	0.50	0.001	0.002
21-F	3.00	0.83	2.50	0.02	0.20	0.50	0.001	0.002
22-F	3.00	0.83	2.50	0.02	0.20	0.50	0.001	0.002
23-F	3.00	0.83	2.50	0.02	0.20	0.50	0.001	0.002
23-AC	20.50	0.83	17.08	0.16	0.23	3.86	0.030	0.520
23-CD	12.00	0.83	10.00	0.09	0.21	2.09	0.011	0.106
23-DF	18.75	0.83	15.63	0.15	0.22	3.47	0.026	0.400
2223-CD	13.00	0.83	10.83	0.10	0.21	2.28	0.012	0.135
					ΣA_{ci}	34.21	ΣA_{ei}	4.03

Calculation of Equivalent Shear Wall Areas: Longitudinal Direction

Wall ID	Width (ft)	Thickness (ft)	Area (sq. ft)	D_i/H	Area for Code Formula		Area for New Formula	
					$0.2+(D_i/H)^2$	A_{ci} (sq. ft)	$1/(1+0.83(H/D_i)^2)$	A_{ei} (sq. ft)
DE-12	5.00	0.83	4.17	0.04	0.20	0.84	0.002	0.008
C-49	37.50	0.83	31.25	0.30	0.29	8.97	0.095	2.971
C-2223	8.75	0.83	7.29	0.07	0.20	1.49	0.006	0.041
D-2122	4.33	0.83	3.61	0.03	0.20	0.73	0.001	0.005
D21-23	10.50	0.83	8.75	0.08	0.21	1.81	0.008	0.071
					ΣA_{ci}	13.84	ΣA_{ei}	3.10

3. Los Angeles - 10 Story Residential Building, CSMIP Station No. 24601

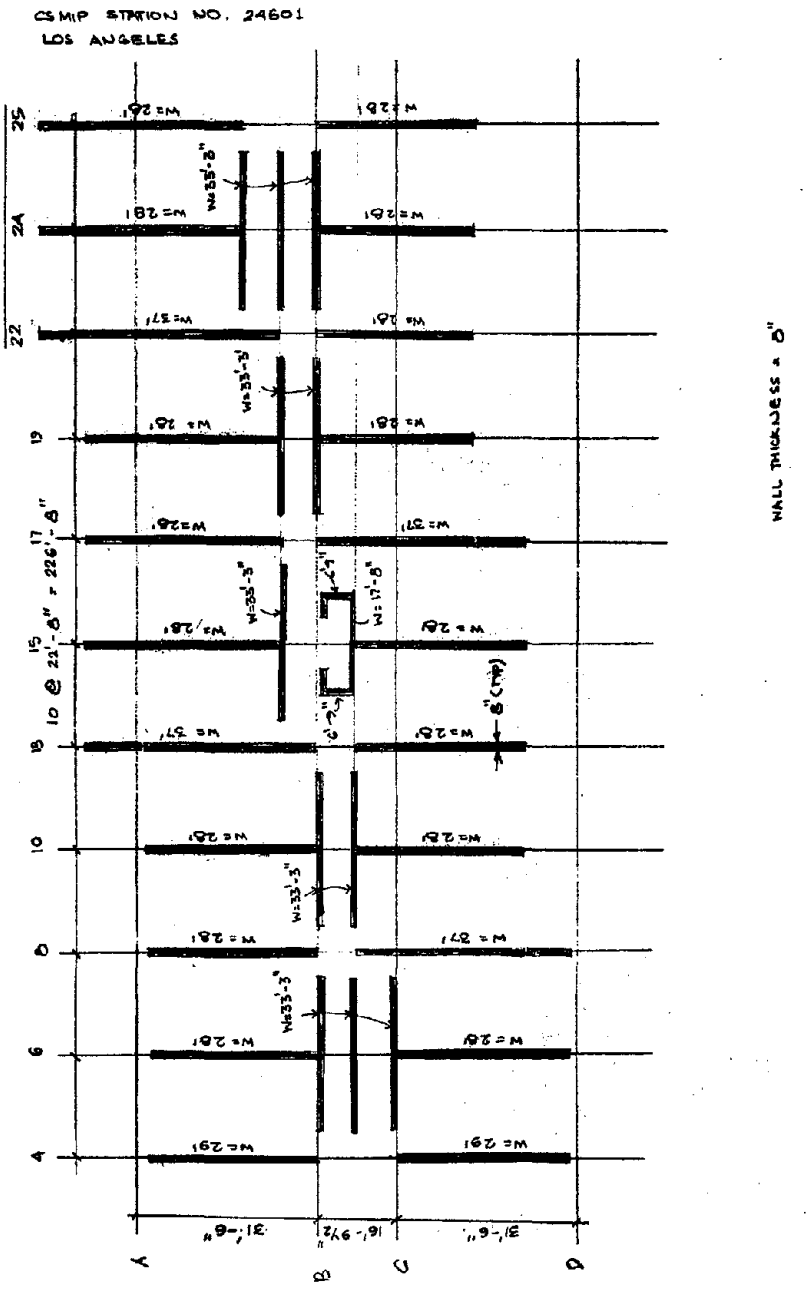

Figure H.3.1. Sketch of shear walls in CSMIP Station No. 24601

Location Los Angeles
Occupancy Residential
Station ID 24601
Height 149.7 ft
Building Plan Area 18160 sq. ft

Period Calculations				
Direction	Code Formula		New Formula	
	A_c (sq. ft)	T (sec)	$\overline{A}_e$ (%)	T (sec)
Longitudinal	63.37	0.5376	0.0765	1.0286
Transverse	106.95	0.4138	0.1131	0.8458

Calculation of Equivalent Shear Wall Areas: Transverse Direction								
Wall ID	Width (ft)	Thickness (ft)	Area (sq. ft)	D_i/H	Area for Code Formula		Area for New Formula	
					$0.2+(D_i/H)^2$	A_{ei} (sq. ft)	$1/(1+0.83(H/D_i)^2)$	A_{ei} (sq. ft)
4-1	29.00	0.67	19.33	0.194	0.24	4.59	0.043	0.836
4-2	29.00	0.67	19.33	0.194	0.24	4.59	0.043	0.836
6-1	28.00	0.67	18.67	0.187	0.23	4.39	0.040	0.755
6-2	28.00	0.67	18.67	0.187	0.23	4.39	0.040	0.755
8-1	28.00	0.67	18.67	0.187	0.23	4.39	0.040	0.755
8-2	37.00	0.67	24.67	0.247	0.26	6.44	0.069	1.691
10-1	28.00	0.67	18.67	0.187	0.23	4.39	0.040	0.755
10-2	28.00	0.67	18.67	0.187	0.23	4.39	0.040	0.755
13-1	37.00	0.67	24.67	0.247	0.26	6.44	0.069	1.691
13-2	28.00	0.67	18.67	0.187	0.23	4.39	0.040	0.755
15-1	28.00	0.67	18.67	0.187	0.23	4.39	0.040	0.755
15-2	28.00	0.67	18.67	0.187	0.23	4.39	0.040	0.755
17-1	28.00	0.67	18.67	0.187	0.23	4.39	0.040	0.755
17-2	37.00	0.67	24.67	0.247	0.26	6.44	0.069	1.691
19-1	28.00	0.67	18.67	0.187	0.23	4.39	0.040	0.755
19-2	28.00	0.67	18.67	0.187	0.23	4.39	0.040	0.755
22-1	37.00	0.67	24.67	0.247	0.26	6.44	0.069	1.691
22-2	28.00	0.67	18.67	0.187	0.23	4.39	0.040	0.755
24-1	28.00	0.67	18.67	0.187	0.23	4.39	0.040	0.755
24-2	28.00	0.67	18.67	0.187	0.23	4.39	0.040	0.755
25-1	28.00	0.67	18.67	0.187	0.23	4.39	0.040	0.755
25-2	28.00	0.67	18.67	0.187	0.23	4.39	0.040	0.755
Core-1	6.75	0.67	4.50	0.045	0.20	0.91	0.002	0.011
Core-2	6.75	0.67	4.50	0.045	0.20	0.91	0.002	0.011
					$\sum A_{ci}$	106.95	$\sum A_{ei}$	20.54

Calculation of Equivalent Shear Wall Areas: Longitudinal Direction								
Wall ID	Width (ft)	Thickness (ft)	Area (sq. ft)	D_i/H	Area for Code Formula		Area for New Formula	
					$0.2+(D_i/H)^2$	A_{ei} (sq. ft)	$1/(1+0.83(H/D_i)^2)$	A_{ei} (sq. ft)
B-48	33.25	0.67	22.28	0.22	0.25	5.55	0.056	1.250
BC-48	33.25	0.67	22.28	0.22	0.25	5.55	0.056	1.250
C-48	33.25	0.67	22.17	0.22	0.25	5.53	0.056	1.244
B-813	33.25	0.67	22.17	0.22	0.25	5.53	0.056	1.244
BC-813	33.25	0.67	22.17	0.22	0.25	5.53	0.056	1.244
AB-1317	33.25	0.67	22.17	0.22	0.25	5.53	0.056	1.244
B-1722	33.25	0.67	22.17	0.22	0.25	5.53	0.056	1.244
AB-1722	33.25	0.67	22.17	0.22	0.25	5.53	0.056	1.244
B-2225	33.25	0.67	22.17	0.22	0.25	5.53	0.056	1.244
AB-2225	33.25	0.67	22.17	0.22	0.25	5.53	0.056	1.244
AAB-2225	33.25	0.67	22.17	0.22	0.25	5.53	0.056	1.244
Core-1	17.67	0.67	11.78	0.12	0.21	2.52	0.017	0.194
					$\sum A_{ci}$	63.37	$\sum A_{ei}$	13.89

4. Palm Desert - 4 Story Medical Building, CSMIP Station No. 12284

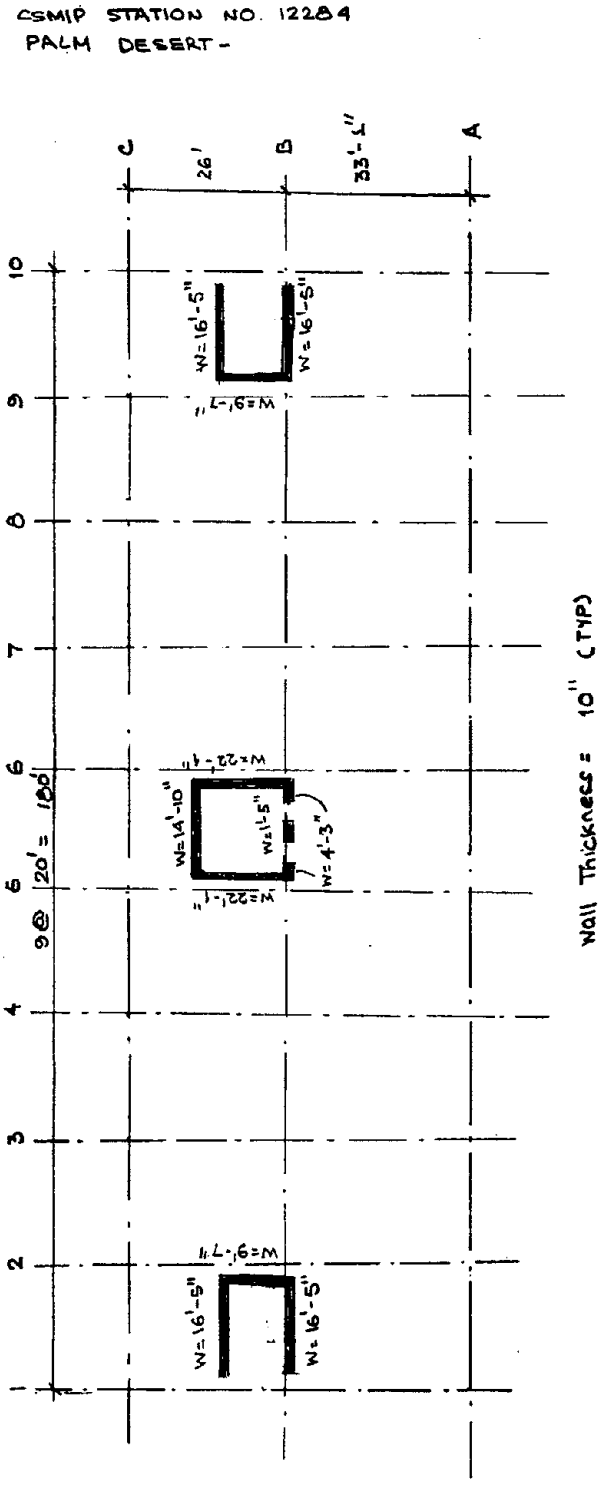

Figure H.4.1. Sketch of shear walls in CSMIP Station No. 12284

Location	Palm Desert
Occupancy	Medical Center
Station ID	12284
Name	Kiewit Bldg
Address	39000 Bob Hope Drive
Height	52.2 ft
Building Plan Area	10800 sq. ft

Period Calculations				
Direction	Code Formula		New Formula	
	A_c (sq. ft)	T (sec)	$\overline{A}_e$ (%)	T (sec)
Longitudinal	21.53	0.4186	0.0646	0.3901
Transverse	17.68	0.4618	0.0662	0.3854

Calculation of Equivalent Shear Wall Areas: Transverse Direction								
Wall ID	Width (ft)	Thickness (ft)	Area (sq. ft)	D_i/H	Area for Code Formula		Area for New Formula	
					$0.2+(D_i/H)^2$	A_{ci} (sq. ft)	$1/(1+0.83(H/D_i)^2)$	A_{ei} (sq. ft)
Core-L	9.58	0.83	7.99	0.18	0.23	1.87	0.039	0.312
Core-C1	22.08	0.83	18.40	0.42	0.38	6.97	0.177	3.264
Core-C2	22.08	0.83	18.40	0.42	0.38	6.97	0.177	3.264
Core-R	9.58	0.83	7.99	0.18	0.23	1.87	0.039	0.312
					$\sum A_{ci}$	17.68	$\sum A_{ei}$	7.15

Calculation of Equivalent Shear Wall Areas: Longitudinal Direction								
Wall ID	Width (ft)	Thickness (ft)	Area (sq. ft)	D_i/H	Area for Code Formula		Area for New Formula	
					$0.2+(D_i/H)^2$	A_{ci} (sq. ft)	$1/(1+0.83(H/D_i)^2)$	A_{ei} (sq. ft)
Core-R1	16.42	0.83	13.68	0.31	0.30	4.09	0.106	1.457
Core-R2	16.42	0.83	13.68	0.31	0.30	4.09	0.106	1.457
Core-C1	14.83	0.83	12.36	0.28	0.28	3.47	0.089	1.096
Core-C2	1.42	0.83	1.18	0.03	0.20	0.24	0.001	0.001
Core-C3	4.25	0.83	3.54	0.08	0.21	0.73	0.008	0.028
Core-C4	4.25	0.83	3.54	0.08	0.21	0.73	0.008	0.028
Core-L1	16.42	0.83	13.68	0.31	0.30	4.09	0.106	1.457
Core-L2	16.42	0.83	13.68	0.31	0.30	4.09	0.106	1.457
					$\sum A_{ci}$	21.53	$\sum A_{ei}$	6.98

5. Piedmont - 3 Story School Building, CSMIP Station No. 58334

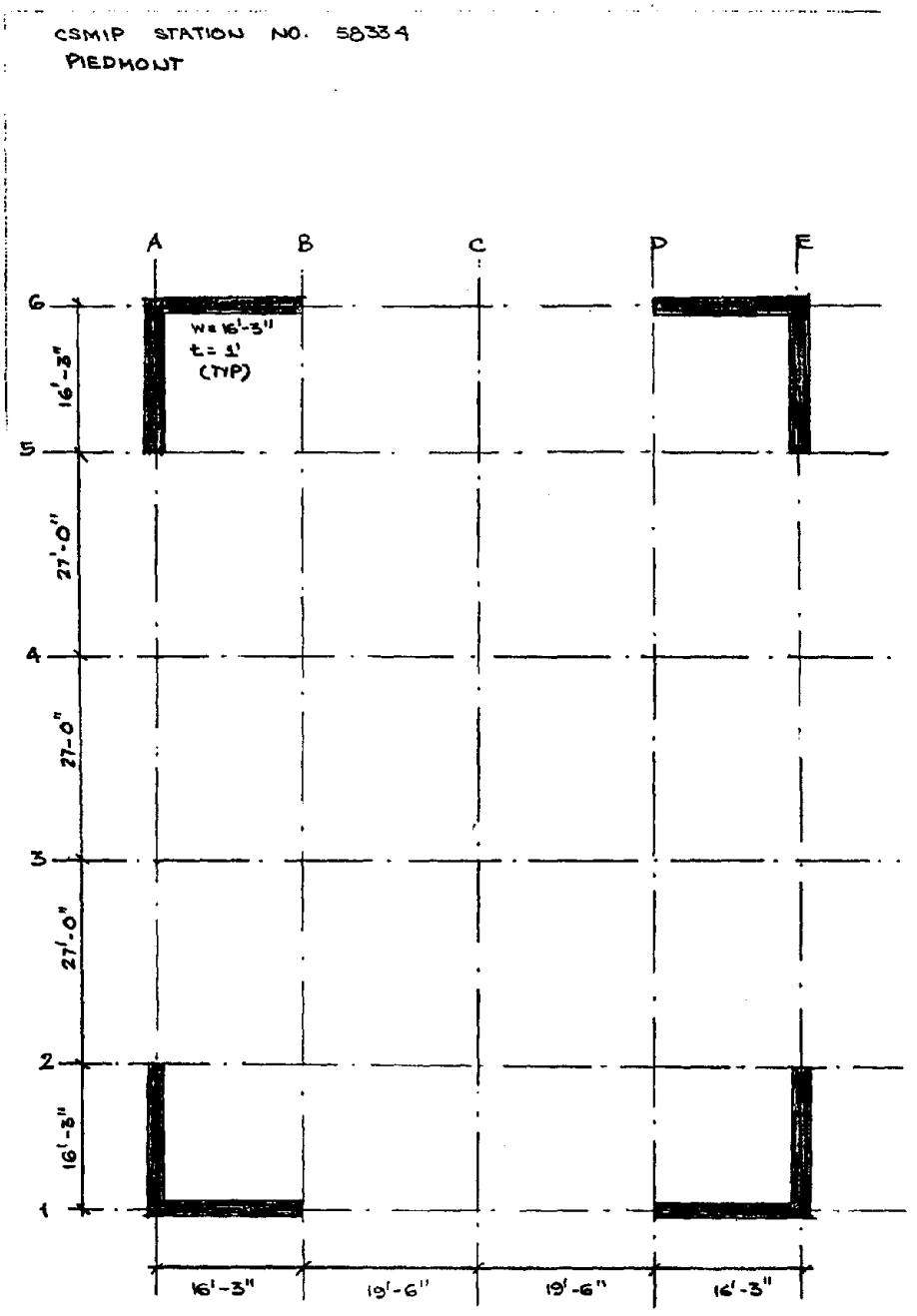

Figure H.5.1. Sketch of shear walls in CSMIP Station No. 58334

Location	Piedmont
Occupancy	School
Station ID	58334
Name	Piedmont Jr. High
Height	36 ft
Building Plan Area	8115.25 sq. ft

Period Calculations				
Direction	Code Formula		New Formula	
	A_c (sq. ft)	T (sec)	$\overline{A}_e$ (%)	T (sec)
Longitudinal	26.24	0.2869	0.1579	0.1722
Transverse	26.24	0.2869	0.1579	0.1722

Calculation of Equivalent Shear Wall Areas: Transverse Direction								
Wall ID	Width (ft)	Thickness (ft)	Area (sq. ft)	D_i/H	Area for Code Formula		Area for New Formula	
					$0.2+(D_i/H)^2$	A_{ci} (sq. ft)	$1/(1+0.83(H/D_i)^2)$	A_{ei} (sq. ft)
1-AB	16.25	1.00	16.25	0.45	0.40	6.56	0.197	3.203
1-DE	16.25	1.00	16.25	0.45	0.40	6.56	0.197	3.203
6-AB	16.25	1.00	16.25	0.45	0.40	6.56	0.197	3.203
6-DE	16.25	1.00	16.25	0.45	0.40	6.56	0.197	3.203
					ΣA_{ci}	26.24	ΣA_{ei}	12.81

Calculation of Equivalent Shear Wall Areas: Longitudinal Direction								
Wall ID	Width (ft)	Thickness (ft)	Area (sq. ft)	D_i/H	Area for Code Formula		Area for New Formula	
					$0.2+(D_i/H)^2$	A_{ci} (sq. ft)	$1/(1+0.83(H/D_i)^2)$	A_{ei} (sq. ft)
A-12	16.25	1.00	16.25	0.45	0.40	6.56	0.197	3.203
A-56	16.25	1.00	16.25	0.45	0.40	6.56	0.197	3.203
E-12	16.25	1.00	16.25	0.45	0.40	6.56	0.197	3.203
E-56	16.25	1.00	16.25	0.45	0.40	6.56	0.197	3.203
					ΣA_{ci}	26.24	ΣA_{ei}	12.81

6. Pleasant Hill - 3 Story Commercial Building, CSMIP Station No. 58348

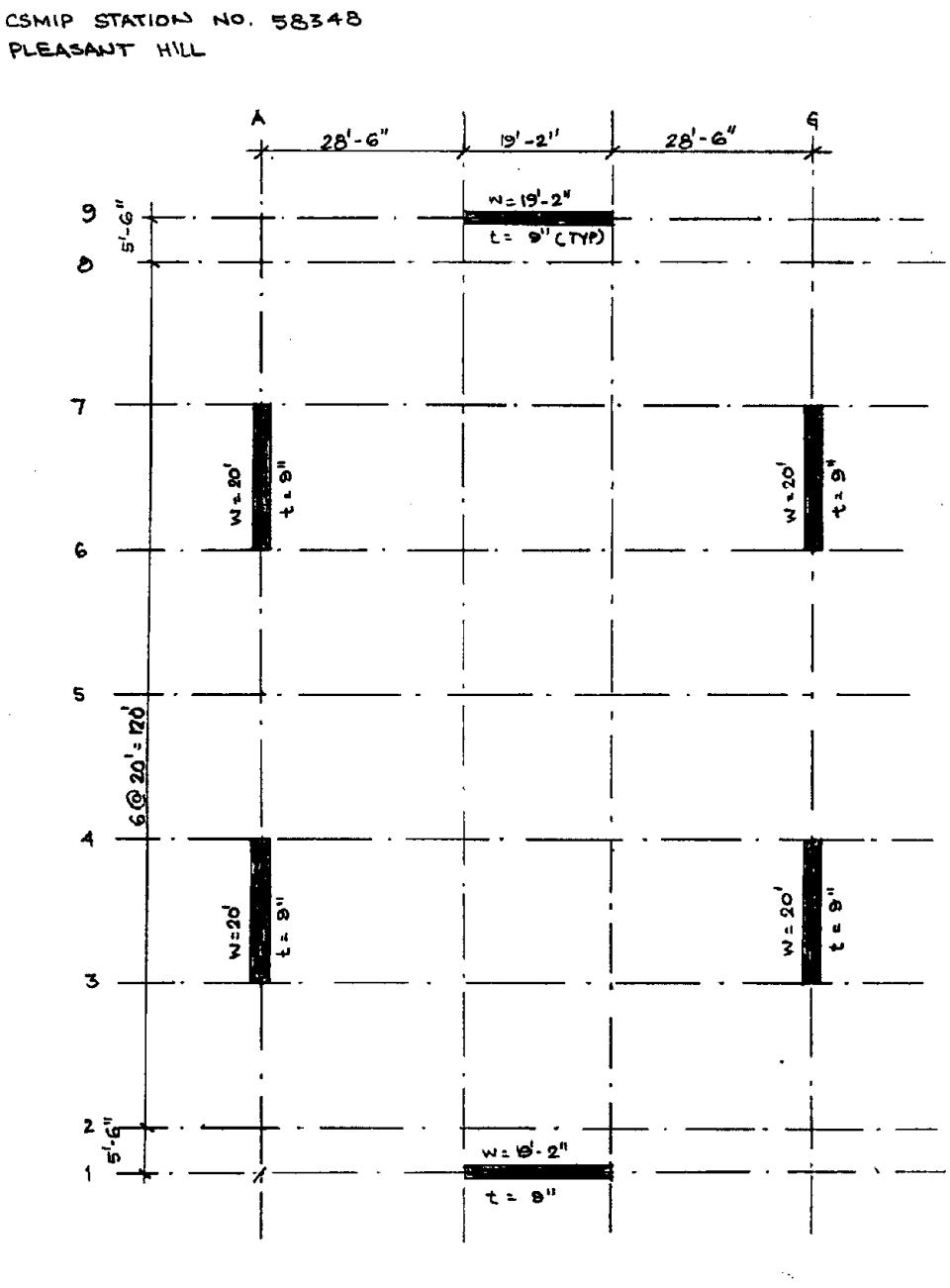

Figure H.6.1. Sketch of shear walls in CSMIP Station No. 58348

Location	Pleasant Hill
Occupancy	Commercial
Station ID	58348
Height	40.6 ft
Building Plan Area	10087 sq. ft

Period Calculations				
Direction	Code Formula		New Formula	
	A_c (sq. ft)	T (sec)	$\overline{A}_e$ (%)	T (sec)
Longitudinal	26.56	0.3121	0.1346	0.2103
Transverse	12.16	0.4613	0.0603	0.3141

Calculation of Equivalent Shear Wall Areas: Transverse Direction								
Wall ID	Width (ft)	Thickness (ft)	Area (sq. ft)	D_i/H	Area for Code Formula		Area for New Formula	
					$0.2+(D_i/H)^2$	A_{ci} (sq. ft)	$1/(1+0.83(H/D_i)^2)$	A_{ei} (sq. ft)
1-AG	19.17	0.75	14.38	0.47	0.42	6.08	0.212	3.043
9-AG	19.17	0.75	14.38	0.47	0.42	6.08	0.212	3.043
					$\sum A_{ci}$	12.16	$\sum A_{ei}$	6.09

Calculation of Equivalent Shear Wall Areas: Longitudinal Direction								
Wall ID	Width (ft)	Thickness (ft)	Area (sq. ft)	D_i/H	Area for Code Formula		Area for New Formula	
					$0.2+(D_i/H)^2$	A_{ci} (sq. ft)	$1/(1+0.83(H/D_i)^2)$	A_{ei} (sq. ft)
A-34	20.00	0.75	15.00	0.49	0.44	6.64	0.226	3.393
A-67	20.00	0.75	15.00	0.49	0.44	6.64	0.226	3.393
G-34	20.00	0.75	15.00	0.49	0.44	6.64	0.226	3.393
G-67	20.00	0.75	15.00	0.49	0.44	6.64	0.226	3.393
					$\sum A_{ci}$	26.56	$\sum A_{ei}$	13.57

7. San Bruno - 9 Story Office Building, CSMIP Station No. 58394

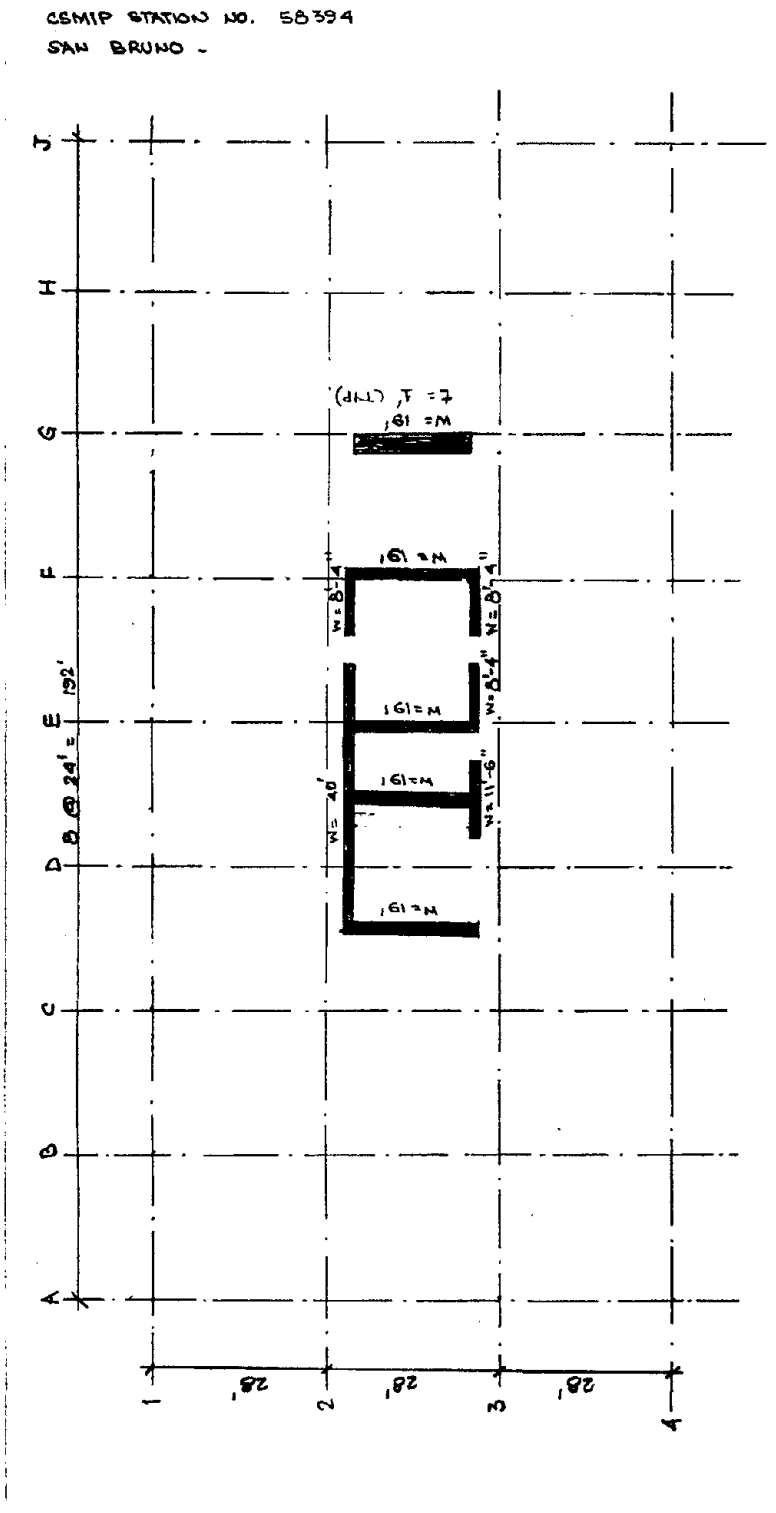

Figure H.7.1. Sketch of shear walls in CSMIP Station No. 58394

Location	San Bruno
Occupancy	Office
Station ID	58394
Height	104 ft
Building Plan Area	16128 sq. ft

Period Calculations				
Direction	Code Formula		New Formula	
	A_c (sq. ft)	T (sec)	$\overline{A}_c$ (%)	T (sec)
Longitudinal	21.52	0.7021	0.0397	0.9912
Transverse	22.17	0.6916	0.0228	1.3095

Calculation of Equivalent Shear Wall Areas: Transverse Direction								
Wall ID	Width (ft)	Thickness (ft)	Area (sq. ft)	D_i/H	Area for Code Formula		Area for New Formula	
					$0.2+(D_i/H)^2$	A_{ci} (sq. ft)	$1/(1+0.83(H/D_i)^2)$	A_{ei} (sq. ft)
Core-1	19.00	1.00	19.00	0.18	0.23	4.43	0.039	0.735
Core-2	19.00	1.00	19.00	0.18	0.23	4.43	0.039	0.735
Core-3	19.00	1.00	19.00	0.18	0.23	4.43	0.039	0.735
Core-4	19.00	1.00	19.00	0.18	0.23	4.43	0.039	0.735
Core-5	19.00	1.00	19.00	0.18	0.23	4.43	0.039	0.735
					$\sum A_{ci}$	22.17	$\sum A_{ei}$	3.67

Calculation of Equivalent Shear Wall Areas: Longitudinal Direction								
Wall ID	Width (ft)	Thickness (ft)	Area (sq. ft)	D_i/H	Area for Code Formula		Area for New Formula	
					$0.2+(D_i/H)^2$	A_{ci} (sq. ft)	$1/(1+0.83(H/D_i)^2)$	A_{ei} (sq. ft)
Core-1	40.00	1.00	40.00	0.38	0.35	13.92	0.151	6.051
Core-2	8.33	1.00	8.33	0.08	0.21	1.72	0.008	0.064
Core-3	11.50	1.00	11.50	0.11	0.21	2.44	0.015	0.167
Core-4	8.33	1.00	8.33	0.08	0.21	1.72	0.008	0.064
Core-5	8.33	1.00	8.33	0.08	0.21	1.72	0.008	0.064
					$\sum A_{ci}$	21.52	$\sum A_{ei}$	6.41

8. San Jose - 10 Story Commercial Building, CSMIP Station No. 57355

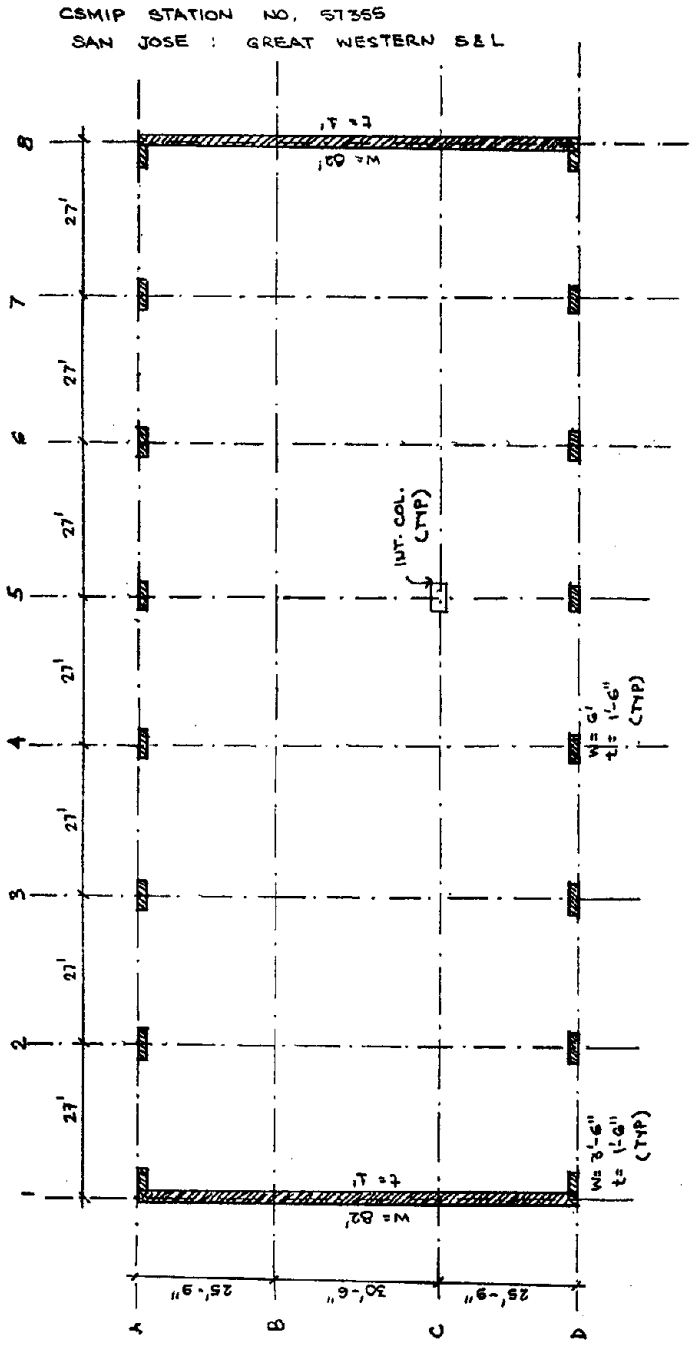

Figure H.8.1. Sketch of shear walls in CSMIP Station No. 57355

Location	San Jose
Occupancy	Commercial
Station ID	57355
Name	Great Western S&L
Height	124 ft
Building Plan Area	17100 sq. ft

Period Calculations				
Direction	Code Formula		New Formula	
	A_c (sq. ft)	T (sec)	$\overline{A}_c$ (%)	T (sec)
Longitudinal	NA	NA	NA	NA
Transverse	104.52	0.3635	0.3309	0.4095

Calculation of Equivalent Shear Wall Areas: Transverse Direction								
Wall ID	Width (ft)	Thickness (ft)	Area (sq. ft)	D_i/H	Area for Code Formula		Area for New Formula	
					$0.2+(D_i/H)^2$	A_{ci} (sq. ft)	$1/\left(1+0.83\left(H/D_i\right)^2\right)$	A_{ei} (sq. ft)
Wall-L	82.00	1.00	82.00	0.66	0.64	52.26	0.345	28.295
Wall-R	82.00	1.00	82.00	0.66	0.64	52.26	0.345	28.295
					$\sum A_{ci}$	104.52	$\sum A_{ei}$	56.59

9. San Jose - 10 Story Residential Building, CSMIP Station No. 57356

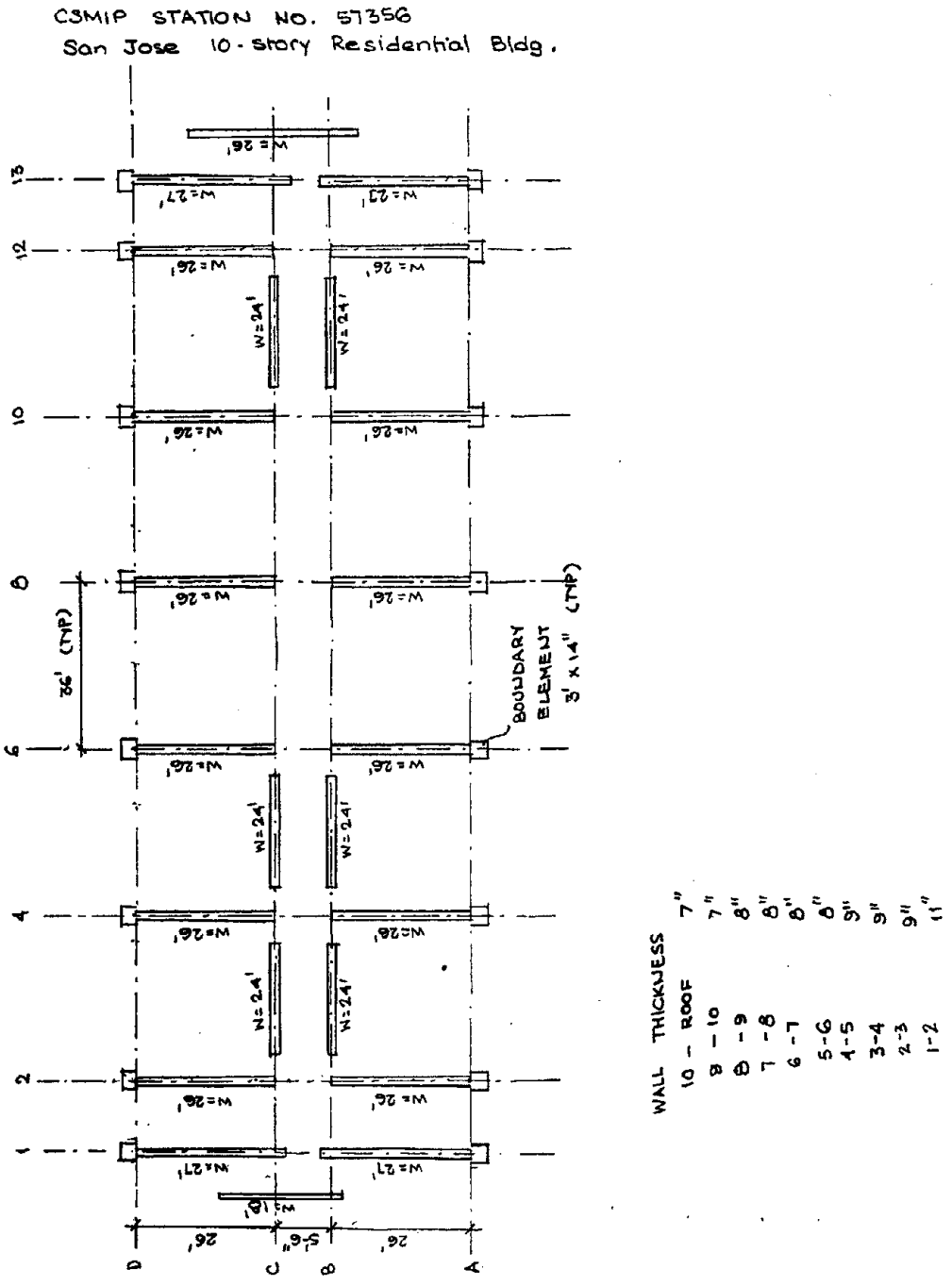

Figure H.9.1. Sketch of shear walls in CSMIP Station No. 57356

Location	San Jose
Occupancy	Residential
Station ID	57356
Name	Town Park Tower Apartment
Height	96 ft
Building Plan Area	13440 sq. ft

Period Calculations				
Direction	Code Formula		New Formula	
	A_c (sq. ft)	T (sec)	$\overline{A}_e$ (%)	T (sec)
Longitudinal	83.41	0.3358	0.2120	0.3962
Transverse	116.20	0.2845	0.2563	0.3603

Calculation of Equivalent Shear Wall Areas: Transverse Direction								
Wall ID	Width (ft)	Thickness (ft)	Area (sq. ft)	D_i/H	Area for Code Formula		Area for New Formula	
					$0.2+(D_i/H)^2$	A_{ci} (sq. ft)	$1/(1.2+(H/D_i)^2)$	A_{ei} (sq. ft)
1-BC	18.00	0.92	16.50	0.19	0.24	3.88	0.041	0.670
1-CD	27.00	0.92	24.75	0.28	0.28	6.91	0.087	2.154
1-AB	27.00	0.92	24.75	0.28	0.28	6.91	0.087	2.154
2-CD	26.00	0.92	23.83	0.27	0.27	6.51	0.081	1.935
2-AB	26.00	0.92	23.83	0.27	0.27	6.51	0.081	1.935
4-CD	26.00	0.92	23.83	0.27	0.27	6.51	0.081	1.935
4-AB	26.00	0.92	23.83	0.27	0.27	6.51	0.081	1.935
6-CD	26.00	0.92	23.83	0.27	0.27	6.51	0.081	1.935
6-AB	26.00	0.92	23.83	0.27	0.27	6.51	0.081	1.935
8-CD	26.00	0.92	23.83	0.27	0.27	6.51	0.081	1.935
8-AB	26.00	0.92	23.83	0.27	0.27	6.51	0.081	1.935
10-CD	26.00	0.92	23.83	0.27	0.27	6.51	0.081	1.935
10-AB	26.00	0.92	23.83	0.27	0.27	6.51	0.081	1.935
12-CD	26.00	0.92	23.83	0.27	0.27	6.51	0.081	1.935
12-AB	26.00	0.92	23.83	0.27	0.27	6.51	0.081	1.935
13-CD	27.00	0.92	24.75	0.28	0.28	6.91	0.087	2.154
13-AB	27.00	0.92	24.75	0.28	0.28	6.91	0.087	2.154
13-BC	26.00	0.92	23.83	0.27	0.27	6.51	0.081	1.935
					$\sum A_{ci}$	116.20	$\sum A_{ei}$	34.44

Calculation of Equivalent Shear Wall Areas: Longitudinal Direction								
Wall ID	Width (ft)	Thickness (ft)	Area (sq. ft)	D_i/H	Area for Code Formula		Area for New Formula	
					$0.2+(D_i/H)^2$	A_{ci} (sq. ft)	$1/(1.2+(H/D_i)^2)$	A_{ei} (sq. ft)
C-24	24.00	0.92	22.00	0.25	0.26	5.78	0.070	1.541
B-24	24.00	0.92	22.00	0.25	0.26	5.78	0.070	1.541
C-46	24.00	0.92	22.00	0.25	0.26	5.78	0.070	1.541
B-46	24.00	0.92	22.00	0.25	0.26	5.78	0.070	1.541
C-1012	24.00	0.92	22.00	0.25	0.26	5.78	0.070	1.541
B-1012	24.00	0.92	22.00	0.25	0.26	5.78	0.070	1.541
B-1722	33.25	0.92	30.48	0.35	0.32	9.75	0.126	3.849
AB-1722	33.25	0.92	30.48	0.35	0.32	9.75	0.126	3.849
B-2225	33.25	0.92	30.48	0.35	0.32	9.75	0.126	3.849
AB-2225	33.25	0.92	30.48	0.35	0.32	9.75	0.126	3.849
AAB-2225	33.25	0.92	30.48	0.35	0.32	9.75	0.126	3.849
					$\sum A_{ci}$	83.41	$\sum A_{ei}$	28.49

APPENDIX I: BIBLIOGRAPHY

System Identification

Beck, J. L. (1978). *Determining Models of Structures from Earthquake records*, Report No. EERL 78-01, Earthquake Engineering Research Laboratory, California Institute of Technology, Pasadena, CA, June.

Beck, R. T. and Beck, J. L. (1985). *Comparison Between Transfer Function and Modal Minimization Methods for System Identification*, Report No. EERL 85-06, Earthquake Engineering Research Laboratory, California Institute of Technology, Pasadena, CA, November.

Beck, J. L. and Jennings, P.C. (1980). "Structural Identification Using Linear Models and Earthquake records," *Earthquake Engineering and Structural Dynamics*, 8, 145-160.

Genatios, C., Lafuente, M. and Lopez, O. (1994). "On the Identification of Structural Dynamic Properties: Parametric Evaluation of the Experimental Techniques," *Proceedings of Fifth U. S. National Conference of Earthquake Engineering*, Vol. II, 743-752, July.

Hart, G. C. and Yao, J. T. P. (1977). "System Identification in Structural Dynamics," *Journal of Engineering Mechanics*, 103(EM6), 1089-1104.

Hong, K.-S. and Yun, C.-B. (1993). "Improved Method for Frequency Domain Identification of Structures," *Engineering Structures*, 15(3), 179-188.

Imai, H., Yun, C. B., Maruyama, O., Shinozuka, M. (1989). "Fundamentals of System Identification in Structural Dynamics," *Probabilistic Engineering Mechanics*, 4(4), 162-173.

Li, Y. and Mau, S. T. (1991). "A Case Study of MIMO System Identification Applied to Building Seismic Records," *Earthquake Engineering and Structural Dynamics*, 20, 1045-1064.

Ljung, L. (1987). *System Identification: Theory for the User*, Prentice Hall, Englewood Cliffs, NJ.

McVerry, G. H. (1979). *Frequency Domain Identification of Structural Models from Earthquake Records*, Report No. EERL 79-02, Earthquake Engineering research Laboratory, California Institute of Technology, Pasadena, CA, October.

Safak, E. (1989). "Adaptive Modeling, Identification, and Control of Dynamic Structural Systems. I. Theory," *Journal of Engineering Mechanics*, ASCE, 115(11), 2386-2405.

Safak, E. (1989). "Adaptive Modeling, Identification, and Control of Dynamic Structural Systems. II. Applications," *Journal of Engineering Mechanics*, ASCE, 115(11), 2406-2426.

Safak, E. (1988). *Analysis of Recordings in Structural Engineering: Adaptive Filtering, Prediction, and Control*, Open-file Report 88-647, U.S. Geological Survey, Menlo Park, CA.

Safak, E. (1991). "Identification of Linear Structures Using Discrete-Time Filters," *Journal of Structural Engineering*, ASCE, 117 (10), 3064-3085.

Safak, E. and Celebi, M. (1991). "Seismic Response of Transamerica Building. II: System Identification," *Journal of Structural Engineering*, ASCE, 117(8), 2405-2425.

Safak. E. and Celebi, M. (1992). "Recorded Seismic Response of Pacific Park Plaza. II. System Identification," *Journal of Structural Engineering*, ASCE, 118(6), 1566-1589.

Werner, S. D., Beck J. L. and Levine, M. B. (1987). "Seismic Response Evaluation of Meloland Road Overpass Using 1979 Imperial Valley Earthquake Records," *Earthquake Engineering and Structural Dynamics*, 15, 249-274.

Werner, S. D., Nisar, A., and Beck, J. L. (1992). *Assessment of UBC Seismic Design Provisions Using Recorded Building Motions from Morgan Hill, Mount Lewis, and Loma Prieta Earthquakes*, Dames and Moor, Oakland, California, April.

Periods and Damping

Beck, J. L. (1978). *Determining Models of Structures from Earthquake records*, Report No. EERL 78-01, Earthquake Engineering Research Laboratory, California Institute of Technology, Pasadena, CA, June.

Beck, J. L. and Jennings, P.C. (1980). "Structural Identification Using Linear Models and Earthquake records," *Earthquake Engineering and Structural Dynamics*, 8, 145-160.

Bendimerad, F. M., Shah, H. C., and Hoskins, T. (1991). *Extension of Study on Fundamental Period of Reinforced Concrete Moment-Resisting Frame Structures*, Report No. 96, John A. Blume Earthquake Engineering Center, Stanford University, CA, June.

Bertero, V. V., Bendimerad, F. M., and Shah, H. C. (1988). *Fundamental Period of Reinforced Concrete Moment-Resisting Frame Structures*, Report No. 87, John A. Blume Earthquake Engineering Center, Stanford University, CA, October.

Boroschek, R. L., Mahin, S. A. and Zeris, C. A. (1990). "Seismic Response and Analytical Modeling of Three Instrumented Buildings," *Proceedings of Fourth U. S. National Conference of Earthquake Engineering*, Vol. II, 219-228, May.

Celebi, M. (1992). "Highlights of Loma Prieta Responses of Four Tall Buildings," *Proceedings of Tenth World Conference on Earthquake Engineering*, 4039-4044.

Celebi, M. (1993). "Seismic Response of Eccentrically Braced Tall Building," *Journal of Structural Engineering*, ASCE, 119(4), 1188-1205.

Celebi, M. (1993). "Loma Prieta Response of an Eccentrically Braced Tall Building," *Proceedings of the Structures Congress '93*, Vol. 2, 1545-1550, April.

Celebi, M. (1993). "Seismic Response of Two Adjacent Buildings. I. Data and Analyses," *Journal of the Structural Engineering*, ASCE, 119(8), 2461-2476.

Celebi, M. (1993). "Seismic Response of Two Adjacent Buildings. II. Interaction," *Journal of the Structural Engineering*, ASCE, 119(8), 2477-2492.

Celebi, M. (1994). "Seismic Response of A Thirteen-Story Building," *Proceedings of Fifth U. S. National Conference of Earthquake Engineering*, Vol. I, 87-96, July.

Celebi, M. and Safak, E. (1991). "Seismic Response of Transamerica Building. I: Data and Preliminary Analyses," *Journal of Structural Engineering*, ASCE, 117(8), 2389-2404.

Celebi, M. and Safak, E. (1992). "Seismic Response of Pacific Park Plaza. I. Data and Preliminary Analyses," *Journal of Structural Engineering*, ASCE, 118(6), 1547-1565.

Cole, E. E., Tokas, C. V. and Meehan, J. F. (1992). "Analysis of Recorded Building Data to Verify or Improve 1991 Uniform Building Code (UBC) Period of Vibration Formulas," *Proceedings of SMIP92*, Strong Motion Instrumentation Program, Division of Mines and Geology, California Department of Conservation, Sacramento, 6-1 - 6-12, May.

Coats, D. W. (1989). *Damping in Building Structures During Earthquakes*, Report No. NUREG/CR-3006, U.S. Nuclear Regulatory Commission, Washington, DC, January.

De la Llera, J. C. and Chopra, A. K. (1992). "Evaluation of Code-Accidental Torsion Provisions Using Earthquake Records from Three Nominally Symmetric-Plan Buildings," *Proceedings*

of SMIP92, Strong Motion Instrumentation Program, Division of Mines and Geology, California Department of Conservation, Sacramento, May.

Earthquake Investigations in California 1934-1935. (1936). Special Publication No. 201, U. S. Government Printing Office, Washington.

Fenves, G. L. (1990). "Evaluation of Lateral Force Procedures for Buildings," *Proceedings of SMIP90*, Strong Motion Instrumentation Program, Division of Mines and Geology, California Department of Conservation, Sacramento, 6-1 - 6-10, July.

Foutch, D. A., Housner, G. W., Jennings, P. C. (1975). *Dynamic Responses of Six Multistory Buildings During the San Fernando Earthquake*, Report No. EERL 75-02, Earthquake Engineering Research Laboratory, California Institute of Technology, Pasadena, CA, October.

Freeman, S. A. and Honda, K. K. (1973). *Response of Two Identical Seven-Story Structures to the San Fernando Earthquake of February 9, 1971*, John A. Blume & Associates, San Francisco, CA, October.

Gates, W. E., Hart, G. C., Gupta, S. and Srinivasan, M. (1994). "Evaluation of Overturning Forces of Shear Wall Buildings," *Proceedings of SMIP94*, Strong Motion Instrumentation Program, Division of Mines and Geology, California Department of Conservation, Sacramento, 105-120, May.

Hart, G. C. and Vasudevan, R. (1975). "Earthquake Design of Buildings: Damping," *Journal of the Structural Division*, ASCE, 101(ST1), 11-30.

Hart, G. C., DiJulio, R. M. and Lew, M. (1975). "Torsional Response of High-Rise Buildings," *Journal of the Structural Division*, ASCE, 101(ST2), 397-416.

Hashimoto, P. S., Steele, L. K., Johnson, J. J., and Mensing, R. W. (1993). *Review of Structure Damping Value for Elastic Seismic Analysis of Nuclear Power Plant*, Report No. NUREG/CR-6011, U.S. Nuclear Regulatory Commission, Washington, DC.

Hashimoto, P. S., Tiong, L. W., Steele, L. K., Johnson, J. J., and Beck, J. L. (1993). *Stiffness and Damping Properties of a Low Aspect Ratio Shear Wall Building Based on Recorded Earthquake Responses*, Report No. NUREG/CR-6012, U.S. Nuclear Regulatory Commission, Washington, DC.

Haviland, R. (1976). *A Study of the Uncertainties in the Fundamental Translational Periods and Damping Values for Real Buildings*, Publication No. R76-12, Department of Civil Engineering, Massachusetts Institute of Technology, Mass., February.

Housner, G. W. and Brady, A. G. (1963). "Natural Periods of Vibration of Buildings," *Journal of Engineering Mechanics Division*, ASCE, 89(EM4), 31-65.

Jeary, A. P. (1986). "Damping in Tall Buildings - A Mechanism and A Predictor," *Earthquake Engineering and Structural Dynamics*, 14(5), 733-750.

Li, Y. and Mau, S. T. (1991). "A Case Study of MIMO System Identification Applied to Building Seismic Records," *Earthquake Engineering and Structural Dynamics*, 20, 1045-1064.

Lin, B. C. and Papageorgiou, A. S. (1989). "Demonstration of Torsional Coupling Caused by Closely Spaced Periods - 1984 Morgan Hill Earthquake Response of the Santa Clara County Building," *Earthquake Spectra*, 5(3), 539-556.

Marshall, R. D., Phan, L. T. and Celebi, M. (1994). "Full-Scale Measurement of Building Response to Ambient Vibration and the Loma Prieta Earthquake," *Proceedings of Fifth U. S. National Conference of Earthquake Engineering*, Vol. II, 661-670, July.

McVerry, G. H. (1979). *Frequency Domain Identification of Structural Models from Earthquake Records*, Report No. EERL 79-02, Earthquake Engineering research Laboratory, California Institute of Technology, Pasadena, CA, October.

Papageorgiou, A. S. and Lin, B. C. (1989). "Influence of Lateral-Load-Resisting System on the Earthquake Response of Structures-A System Identification Study," *Earthquake Engineering and Structural Dynamics*, 18(6), 799-814.

Safak, E. and Celebi, M. (1991). "Seismic Response of Transamerica Building. II: System Identification," *Journal of Structural Engineering*, ASCE, 117(8), 2405-2425.

Safak. E. and Celebi, M. (1992). "Recorded Seismic Response of Pacific Park Plaza. II. System Identification," *Journal of Structural Engineering*, ASCE, 118(6), 1566-1589.

Sedarat, H., Gupta, S. and Werner, S. (1994). *Torsional Response Characteristics of Regular Buildings Under Different Seismic Excitation Levels*, Data Utilization Report CSMIP/94-01, Strong Motion Instrumentation Program, Division of Mines and Geology, California Department of Conservation, Sacramento, January.

Werner, S. D., Nisar, A. and Beck, J. L. (1992). *Assessment of UBC Seismic Design provisions Using Recorded Building Motion from the Morgan Hill, Mount Lewis, and Loma Prieta Earthquakes*, Dames and Moor, Oakland, CA, April.

Wood, J. H. (1972). *Analysis of the Earthquake Response of a Nine-Story Steel Frame Building During the San Fernando Earthquake*, Report No. EERL 72-04, Earthquake Engineering Research Laboratory, California Institute of Technology, Pasadena, CA, October.

Recorded Motions

Etheredge, E. C. and Porcella, R. L. (1987). *Strong-Motion Data fom the October 1, 1987 Whittier Narrows Earthquake,* Open-File Report 87-616, U.S. Geological Survey, Menlo Park, CA.

Hudson, D. E., Editor. (1971). *Strong-Motion Instrumental Data on the San Fernando Earthquake of Feb. 9, 1971,* Earthquake Engineering Research Laboratory, California Institute of Technology and Seismological Field Survey, NOAA, February.

Porcella, R. L., Etheredge, E. C., Maley, R. P., and Acosta, A. V. (1994). *Accelrograms Recorded at USGS National Strong-Motion Network Stations During the Ms=6.6 Northridge, California Earthquake of January 17, 1994*, Open-File Report 94-141, U.S. Geological Survey, Menlo Park, CA.

Shakal, A. F. and Huang, M. J. (1986). "Torsional Response of Three Instrumented Buildings During the 1984 Morgan Hill Earthquake," *Proceedings of Third U. S. National Conference of Earthquake Engineering,* 1639-1650.

Huang, M. et al. (1986). *CSMIP Strong-Motion Records from the Palm Springs, California Earthquake of 8 July, 1986,* Report No. OSMS 86-05, California Department of Conservation, Division of Mines and Geology, Office of Strong Motion Studies, Sacramento, CA.

Shakal, A. et al. (1987). *CSMIP Strong-Motion Records from the Whittier, California Earthquake of 1 October, 1987*, Report No. OSMS 87-05, California Department of Conservation, Division of Mines and Geology, Office of Strong Motion Studies, Sacramento, CA.

Huang, M. et al. (1989). *CSMIP Strong-Motion Records from the Santa Cruz Mountains (Loma Prieta), California Earthquake of 17 October 1989,* Report No. OSMS 89-06, California Department of Conservation, Division of Mines and Geology, Office of Strong Motion Studies, Sacramento, CA.

Shakal, A. et al. (1990). *Quick Report on CSMIP Strong-Motion Records from the February 28, 1990 Earthquake near Upland, California,* Report No. OSMS 90-02, California Department of Conservation, Division of Mines and Geology, Office of Strong Motion Studies, Sacramento, CA.

Shakal, A. et al. (1991). *CSMIP Strong-Motion Records from the Sierra Madre, California Earthquake of 28 June 1991,* Report No. OSMS 91-03, California Department of Conservation, Division of Mines and Geology, Office of Strong Motion Studies, Sacramento, CA.

Shakal, A. et al. (1994). *CSMIP Strong-Motion Records from the Northridge, California Earthquake of January 17, 1994*, Report No. OSMS 94-07, California Department of Conservation, Division of Mines and Geology, Office of Strong Motion Studies, Sacramento, CA.

Shakal, A. F., Huang, M. J. and Darragh, R. B. (1994). "Some Implications of Strong-Motion Records from the 1994 Northridge Earthquake," *Proceedings of SMIP94*, Strong Motion Instrumentation Program, Division of Mines and Geology, California Department of Conservation, Sacramento, May.

General

Chopra, A. K. (1995). *Dynamics of Structures: Theory and Applications to Earthquake Engineering*, Prentice Hall, Englewood Cliffs, NJ.

Housner, G. W. and Jennings, P.C. (1982). *Earthquake Design Criteria*, Engineering Monograph, Earthquake Engineering Research Institute. CA.

MATLAB User's Guide. (1992). The MathWorks, Inc., Natick, Mass.

NEHRP Recommended Provisions for the Development of seismic Regulations for New Buildings. (1994). Building Seismic Safety Council, Washington, D. C.

Newmark, N. M. (1967). *Design Criteria for Nuclear Reactors Subjected to Earthquake Hazards*, Urbana, Illinois, May.

Newmark, N. M., and Hall, W. J. (1978). *Development of Criteria for Seismic Review of Selected Nuclear Power Plants*, Nuclear Regulatory Commission Report NUREG/CR-0098, Washington, DC.

Newmark, N. M. and Hall, W. J. (1982). *Earthquake Spectra and Design*, Engineering Monograph, Earthquake Engineering Research Institute. CA.

Priestley, M. J. N. and Hart, G. C. (1989). *Design Recommendations for the Period of Vibration of Masonry Wall Buildings*, Report No. SSRP-89/05, Structural Systems Research Report, University of California at San Diego and Los Angeles, CA, November.

Recommended Lateral Force Requirements and Commentary. (1990). Seismological Committee, Structural Engineers Association of California, San Francisco, CA.

Tentative Provisions for the Development of Seismic Regulations for Buildings. (1978). ATC3-06, Applied Technological Council, Palo Alto, CA.

User's Guide: System Identification Toolbox for Use with MATLAB. (1993). The Math Works, Inc., Natick, Mass.

Uniform Building Code. (1997). International Conference of Building Officials, Whittier, CA.

EERC REPORTS

EERC reports are available from the National Information Service for Earthquake Engineering (NISEE) and from the National Technical Information Service (NTIS). To order EERC Reports, please contact the Earthquake Engineering Research Center, 1301 S. 46th Street, Richmond, California 94804-4698, ph 510-231-9468.

UCB/EERC-97/14 Vibration Properties of Buildings Determined from Recorded Earthquake Motions, by Goel, R. K. and Chopra, A., December 1997. $26

UCB/EERC-97/13: Fatigue Life Evaluation of Changeable Message Sign Structures -- Volume 2: Retrofitted Specimens, by Chavez, J.W., Gilani, A.S., and Whittaker, A.S., December, 1997. $20

UCB/EERC-97/12: New Design and Analysis Procedures for Intermediate Hinges in Multiple-Frame Bridges, by DesRoches, R. and Fenves, G. L., December, 1997. $26

UCB/EERC-97/11: Viscous Heating of Fluid Dampers During Seismic and Wind Excitations--Analytical Solutions and Design Formulae, by Makris, N., Roussos, Y., Whittaker, A.S., and Kelly, J.M., November, 1997. $15

UCB/EERC-97/10: Fatigue Life Evaluation of Changeable Message Sign Structures -- Volume 1: As-Built Specimens, by Gilani, A.M., Chavez, J.W., and Whittaker, A.S., November, 1997. $20

UCB/EERC-97/09: Second U.S.-Japan Workshop on Seismic Retrofit of Bridges, edited by Kawashima, K. and Mahin, S.A., September, 1997. $57

UCB/EERC-97/08: Implications of the Landers and Big Bear Earthquakes on Earthquake Resistant Design of Structures, by Anderson, J.C. and Bertero, V.V., July 1997. $20

UCB/EERC-97/07: Analysis of the Nonlinear Response of Structures Supported on Pile Foundations, by Badoni, D. and Makris, N., July 1997. $20

UCB/EERC-97/06: Executive Summary on: Phase 3: Evaluation and Retrofitting of Multilevel and Multiple-Column Structures -- An Analytical, Experimental, and Conceptual Study of Retrofitting Needs and Methods, by Mahin, S.A., Fenves, G.L., Filippou, F.C., Moehle, J.P., Thewalt, C.R., May, 1997. $20

UCB/EERC-97/05: The EERC-CUREe Symposium to Honor Vitelmo V. Bertero, February 1997. $26

UCB/EERC-97/04: Design and Evaluation of Reinforced Concrete Bridges for Seismic Resistance, by Aschheim, M., Moehle, J.P. and Mahin, S.A., March 1997. $26

UCB/EERC-97/03: U.S.-Japan Workshop on Cooperative Research for Mitigation of Urban Earthquake Disasters: Learning from Kobe and Northridge -- Recommendations and Resolutions, by Mahin, S., Okada, T., Shinozuka, M. and Toki, K., February 1997. $15

UCB/EERC-97/02: Multiple Support Response Spectrum Analysis of Bridges Including the Site-Response Effect & MSRS Code, by Der Kiureghian, A., Keshishian, P. and Hakobian, A., February 1997. $20

UCB/EERC-97/01: Analysis of Soil-Structure Interaction Effects on Building Response from Earthquake Strong Motion Recordings at 58 Sites, by Stewart, J.P. and Stewart, A.F., February 1997. $57

UCB/EERC-96/05: Application of Dog Bones for Improvement of Seismic Behavior of Steel Connections, by Popov, E.P., Blondet, M. and Stepanov, L., June 1996. $13

UCB/EERC-96/04: Experimental and Analytical Studies of Base Isolation Applications for Low-Cost Housing, by Taniwangsa, W. and Kelly, J.M., July 1996. $20

UCB/EERC-96/03: Experimental and Analytical Evaluation of a Retrofit Double-Deck Viaduct Structure: Part I of II, by Zayati, F., Mahin, S. A. and Moehle, J. P., June 1996. $33

UCB/EERC-96/02: Field Testing of Bridge Design and Retrofit Concepts. Part 2 of 2: Experimental and Analytical Studies of the Mt. Diablo Blvd. Bridge, by Gilani, A.S., Chavez, J.W. and Fenves, G.L., June 1996. $20

UCB/EERC-96/01: Earthquake Engineering Research at Berkeley -- 1996: Papers Presented at the 11th World Conference on Earthquake Engineering, by EERC, May 1996. $26

UCB/EERC-95/14: Field Testing of Bridge Design and Retrofit Concepts. Part 1 of 2: Field Testing and Dynamic Analysis of a Four-Span Seismically Isolated Viaduct in Walnut Creek, California, by Gilani, A.S., Mahin, S.A., Fenves, G.L., Aiken, I.D. and Chavez, J.W., December 1995. $26

UCB/EERC-95/13: Experimental and Analytical Studies of Steel Connections and Energy Dissipators, by Yang, T.-S. and Popov, E.P., December 1995. $26

UCB/EERC-95/12: Natural Rubber Isolation Systems for Earthquake Protection of Low-Cost Buildings, by Taniwangsa, W., Clark, P. and Kelly, J.M., June 1996. $20

UCB/EERC-95/11: Studies in Steel Moment Resisting Beam-to-Column Connections for Seismic-Resistant Design, by Blackman, B. and Popov, E.P., October 1995, PB96-143243. $20

UCB/EERC-95/10: Seismological and Engineering Aspects of the 1995 Hyogoken-Nanbu (Kobe) Earthquake, by EERC, November 1995. $26

UCB/EERC-95/09: Seismic Behavior and Retrofit of Older Reinforced Concrete Bridge T-Joints, by Lowes, L.N. and Moehle, J.P., September 1995, PB96-159850. $20

UCB/EERC-95/08: Behavior of Pre-Northridge Moment Resisting Steel Connections, by Yang, T.-S. and Popov, E.P., August 1995, PB96-143177. $15

UCB/EERC-95/07: Earthquake Analysis and Response of Concrete Arch Dams, by Tan, H. and Chopra, A.K., August 1995, PB96-143185. $20

UCB/EERC-95/06: Seismic Rehabilitation of Framed Buildings Infilled with Unreinforced Masonry Walls Using Post-Tensioned Steel Braces, by Teran-Gilmore, A., Bertero, V.V. and Youssef, N., June 1995, PB96-143136. $26

UCB/EERC-95/05: Final Report on the International Workshop on the Use of Rubber-Based Bearings for the Earthquake Protection of Buildings, by Kelly, J.M., May 1995. $20

UCB/EERC-95/04: Earthquake Hazard Reduction in Historical Buildings Using Seismic Isolation, by Garevski, M., June 1995. $15

UCB/EERC-95/03: Upgrading Bridge Outrigger Knee Joint Systems, by Stojadinovic, B. and Thewalt, C.R., June 1995, PB95-269338. $20

UCB/EERC-95/02: The Attenuation of Strong Ground Motion Displacements, by Gregor, N.J., June 1995, PB95-269346. $26

UCB/EERC-95/01: Geotechnical Reconnaissance of the Effects of the January 17, 1995, Hyogoken-Nanbu Earthquake, Japan, August 1995, PB96-143300. $26

UCB/EERC-94/12: Response of the Northwest Connector in the Landers and Big Bear Earthquakes, by Fenves, G.L. and Desroches, R., December 1994. $20

UCB/EERC-94/11: Earthquake Analysis and Response of Two-Level Viaducts, by Singh, S.P. and Fenves, G.L., October 1994, PB96-133756 (A09). $20

UCB/EERC-94/10: Manual for Menshin Design of Highway Bridges: Ministry of Construction, Japan, by Sugita, H. and Mahin, S., August 1994, PB95-192100(A08). $20

UCB/EERC-94/09: Performance of Steel Building Structures During the Northridge Earthquake, by Bertero, V.V., Anderson, J.C. and Krawinkler, H., August 1994, PB95-112025(A10). $26

UCB/EERC-94/08: Preliminary Report on the Principal Geotechnical Aspects of the January 17, 1994 Northridge Earthquake, by Stewart, J.P., Bray, J.D., Seed, R.B. and Sitar, N., June 1994, PB94203635(A12). $26

UCB/EERC-94/07: Accidental and Natural Torsion in Earthquake Response and Design of Buildings, by De la Llera, J.C. and Chopra, A.K., June 1994, PB94-203627(A14). $33

UCB/EERC-94/05: Seismic Response of Steep Natural Slopes, by Sitar, N. and Ashford, S.A., May 1994, PB94-203643(A10). $26

UCB/EERC-94/04: Insitu Test Results from Four Loma Prieta Earthquake Liquefaction Sites: SPT, CPT, DMT and Shear Wave Velocity, by Mitchell, J.K., Lodge, A.L., Coutinho, R.Q., Kayen, R.E., Seed, R.B., Nishio, S. and Stokoe II, K.H., April 1994,

PB94-190089(A09). $20

UCB/EERC-94/03: The Influence of Plate Flexibility on the Buckling Load of Elastomeric Isolators, by Kelly, J.M., March 1994, PB95-192134(A04). $15

UCB/EERC-94/02: Energy Dissipation with Slotted Bolted Connections, by Grigorian, C.E. and Popov, E.P., February 1994, PB94-164605. $26

UCB/EERC-94/01: Preliminary Report on the Seismological and Engineering Aspects of the January 17, 1994 Northridge Earthquake, by EERC, January 1994, (PB94 157 666/AS)A05. $15

UCB/EERC-93/13: On the Analysis of Structures with Energy Dissipating Restraints, by Inaudi, J.A., Nims, D.K. and Kelly, J.M., December 1993, PB94-203619(A07). $20

UCB/EERC-93/12: Synthesized Strong Ground Motions for the Seismic Condition Assessment of the Eastern Portion of the San Francisco Bay Bridge, by Bolt, B.A. and Gregor, N.J., December 1993, PB94-165842(A10). $26

UCB/EERC-93/11: Nonlinear Homogeneous Dynamical Systems, by Inaudi, J.A. and Kelly, J.M., October 1995. $20

UCB/EERC-93/09: A Methodology for Design of Viscoelastic Dampers in Earthquake-Resistant Structures, by Abbas, H. and Kelly, J.M., November 1993, PB94-190071(A10). $26

UCB/EERC-93/08: Model for Anchored Reinforcing Bars under Seismic Excitations, by Monti, G., Spacone, E. and Filippou, F.C., December 1993, PB95-192183(A05). $15

UCB/EERC-93/07: Earthquake Analysis and Response of Concrete Gravity Dams Including Base Sliding, by Chavez, J.W. and Fenves, G.L., December 1993, (PB94 157 658/AS)A10. $26

UCB/EERC-93/06: On the Analysis of Structures with Viscoelastic Dampers, by Inaudi, J.A., Zambrano, A. and Kelly, J.M., August 1993, PB94-165867(A06). $20

UCB/EERC-93/05: Multiple-Support Response Spectrum Analysis of the Golden Gate Bridge, by Nakamura, Y., Der Kiureghian, A. and Liu, D., May 1993, (PB93 221 752)A05. $15

UCB/EERC-93/04: Seismic Performance of a 30-Story Building Located on Soft Soil and Designed According to UBC 1991, by Teran-Gilmore, A. and Bertero, V.V., 1993, (PB93 221 703)A17. $33

UCB/EERC-93/03: An Experimental Study of Flat-Plate Structures under Vertical and Lateral Loads, by Hwang, S.-H. and Moehle, J.P., February 1993, (PB94 157 690/AS)A13. $26

UCB/EERC-93/02: Evaluation of an Active Variable-Damping-Structure, by Polak, E., Meeker, G., Yamada, K. and Kurata, N., 1993, (PB93 221 711)A05. $15

UCB/EERC-92/18: Dynamic Analysis of Nonlinear Structures using State-Space Formulation and Partitioned Integration Schemes, by Inaudi, J.A. and De la Llera, J.C., December 1992, (PB94 117 702/AS/A05. $15

UCB/EERC-92/17: Performance of Tall Buildings During the 1985 Mexico Earthquakes, by Teran-Gilmore, A. and Bertero, V.V., December 1992, (PB93 221 737)A11. $26

UCB/EERC-92/16: Tall Reinforced Concrete Buildings: Conceptual Earthquake-Resistant Design Methodology, by Bertero, R.D. and Bertero, V.V., December 1992, (PB93 221 695)A12. $26

UCB/EERC-92/15: A Friction Mass Damper for Vibration Control, by Inaudi, J.A. and Kelly, J.M., October 1992, (PB93 221 745)A04. $15

UCB/EERC-92/14: Earthquake Risk and Insurance, by Brillinger, D.R., October 1992, (PB93 223 352)A03.

UCB/EERC-92/13: Earthquake Engineering Research at Berkeley - 1992, by EERC, October 1992, PB93-223709(A10). $13

UCB/EERC-92/12: Application of a Mass Damping System to Bridge Structures, by Hasegawa, K. and Kelly, J.M., August 1992, (PB93 221 786)A06. $26

UCB/EERC-92/11: Mechanical Characteristics of Neoprene Isolation Bearings, by Kelly, J.M. and Quiroz, E., August 1992, (PB93 221 729)A07. $20

UCB/EERC-92/10: Slotted Bolted Connection Energy Dissipators, by Grigorian, C.E., Yang, T.-S. and Popov, E.P., July 1992, (PB92 120 285)A03. $20

UCB/EERC-92/09: Evaluation of Code Accidental-Torsion Provisions Using Earthquake Records from Three

Nominally Symmetric-Plan Buildings, by De la Llera, J.C. and Chopra, A.K., September 1992, (PB94 117 611)A08. $13

UCB/EERC-92/08: Nonlinear Static and Dynamic Analysis of Reinforced Concrete Subassemblages, by Filippou, F.C., D'Ambrisi, A. and Issa, A., August, 1992. $20

UCB/EERC-92/07: A Beam Element for Seismic Damage Analysis, by Spacone, E., Ciampi, V. and Filippou, F.C., August 1992, (PB95-192126)A06. $20

UCB/EERC-92/06: Seismic Behavior and Design of Semi-Rigid Steel Frames, by Nader, M.N. and Astaneh-Asl, A., May 1992, PB93-221760(A17). $33

UCB/EERC-92/05: Parameter Study of Joint Opening Effects on Earthquake Response of Arch Dams, by Fenves, G.L., Mojtahedi, S. and Reimer, R.B., April 1992, (PB93 120 301)A04. $15

UCB/EERC-92/04: Shear Strength and Deformability of RC Bridge Columns Subjected to Inelastic Cyclic Displacements, by Aschheim, M. and Moehle, J.P., March 1992, (PB93 120 327)A06. $20

UCB/EERC-92/03: Models for Nonlinear Earthquake Analysis of Brick Masonry Buildings, by Mengi, Y., McNiven, H.D. and Tanrikulu, A.K., March 1992, (PB93 120 293)A08. $20

UCB/EERC-92/02: Response of the Dumbarton Bridge in the Loma Prieta Earthquake, by Fenves, G.L., Filippou, F.C. and Sze, D.T., January 1992, (PB93 120 319)A09. $20

UCB/EERC-92/01: Studies of a 49-Story Instrumented Steel Structure Shaken During the Loma Prieta Earthquake, by Chen, C.-C., Bonowitz, D. and Astaneh-Asl, A., February 1992, (PB93 221 778)A08. $20

UCB/EERC-91/18: Investigation of the Seismic Response of a Lightly-Damped Torsionally-Coupled Building, by Boroschek, R. and Mahin, S.A., December 1991, (PB93 120 335)A13. $26

UCB/EERC-91/17: A Fiber Beam-Column Element for Seismic Response Analysis of Reinforced Concrete Structures, by Taucer, F., Spacone, E. and Filippou, F.C., December 1991, (PB94 117 629AS)A07. $20

UCB/EERC-91/16: Evaluation of the Seismic Performance of a Thirty-Story RC Building, by Anderson, J.C., Miranda, E., Bertero, V.V. and The Kajima Project Research Team, July 1991, (PB93 114 841)A12. $26

UCB/EERC-91/15: Design Guidelines for Ductility and Drift Limits: Review of State-of-the-Practice and State-of-the-Art in Ductility and Drift-Based Earthquake-Resistant Design of Buildings, by Bertero, V.V., Anderson, J.C., Krawinkler, H., Miranda, E. and The CUREe and The Kajima Research Teams, July 1991, (PB93 120 269)A08. $20

UCB/EERC-91/14: Cyclic Response of RC Beam-Column Knee Joints: Test and Retrofit, by Mazzoni, S., Moehle, J.P. and Thewalt, C.R., October 1991, (PB93 120 277)A03. $13

UCB/EERC-91/13: Shaking Table - Structure Interaction, by Rinawi, A.M. and Clough, R.W., October 1991, (PB93 114 917)A13. $26

UCB/EERC-91/12: Performance of Improved Ground During the Loma Prieta Earthquake, by Mitchell, J.K. and Wentz, Jr., F.J., October 1991, (PB93 114 791)A06. $20

UCB/EERC-91/11: Seismic Performance of an Instrumented Six-Story Steel Building, by Anderson, J.C. and Bertero, V.V., November 1991, (PB93 114 809)A07. $20

UCB/EERC-91/10: Evaluation of Seismic Performance of a Ten-Story RC Building During the Whittier Narrows Earthquake, by Miranda, E. and Bertero, V.V., October 1991, (PB93 114 783)A06. $20

UCB/EERC-91/09: A Preliminary Study on Energy Dissipating Cladding-to-Frame Connections, by Cohen, J.M. and Powell, G.H., September 1991, (PB93 114 510)A05. $15

UCB/EERC-91/08: A Response Spectrum Method for Multiple-Support Seismic Excitations, by Der Kiureghian, A. and Neuenhofer, A., August 1991, (PB93 114 536)A04. $15

UCB/EERC-91/07: Estimation of Seismic Source Processes Using Strong Motion Array Data, by Chiou, S.-J., July 1991, (PB93 114 551/AS)A08. $20

UCB/EERC-91/06: Computation of Spatially Varying Ground Motion and Foundation-Rock Impedance Matrices for Seismic Analysis of Arch Dams, by Zhang, L. and Chopra, A.K., May

1991, (PB93 114 825)A07. $20

UCB/EERC-91/05: Base Sliding Response of Concrete Gravity Dams to Earthquakes, by Chopra, A.K. and Zhang, L., May 1991, (PB93 114 544/AS)A05. $15

UCB/EERC-91/04: Dynamic and Failure Characteristics of Bridgestone Isolation Bearings, by Kelly, J.M., April 1991, (PB93 114 528)A05. $15

UCB/EERC-91/03: A Long-Period Isolation System Using Low-Modulus High-Damping Isolators for Nuclear Facilities at Soft-Soil Sites, by Kelly, J.M., March 1991, (PB93 114 577/AS)A10. $26

UCB/EERC-91/02: Displacement Design Approach for Reinforced Concrete Structures Subjected to Earthquakes, by Qi, X. and Moehle, J.P., January 1991, (PB93 114 569/AS)A09. $20

UCB/EERC-90/21: Observations and Implications of Tests on the Cypress Street Viaduct Test Structure, by Bollo, M., Mahin, S.A., Moehle, J.P., Stephen, R.M. and Qi, X., December 1990, (PB93 114 775)A13. $26

UCB/EERC-90/20: Seismic Response Evaluation of an Instrumented Six Story Steel Building, by Shen, J.-H. and Astaneh-Asl, A., December 1990, (PB91 229 294/AS)A04. $15

UCB/EERC-90/19: Cyclic Behavior of Steel Top-and-Bottom Plate Moment Connections, by Harriott, J.D. and Astaneh-Asl, A., August 1990, (PB91 229 260/AS)A05. $15

UCB/EERC-90/18: Material Characterization of Elastomers used in Earthquake Base Isolation, by Papoulia, K.D. and Kelly, J.M., 1990, PB94-190063(A08). $15

UCB/EERC-90/17: Behavior of Peak Values and Spectral Ordinates of Near-Source Strong Ground-Motion over a Dense Array, by Niazi, M., June 1990, (PB93 114 833)A07. $20

UCB/EERC-90/14: Inelastic Seismic Response of One-Story, Asymmetric-Plan Systems, by Goel, R.K. and Chopra, A.K., October 1990, (PB93 114 767)A11. $26

UCB/EERC-90/13: The Effects of Tectonic Movements on Stresses and Deformations in Earth Embankments, by Bray, J. D., Seed, R. B. and Seed, H. B., September 1989, PB92-192996(A18). $39

UCB/EERC-90/12: Effects of Torsion on the Linear and Nonlinear Seismic Response of Structures, by Sedarat, H. and Bertero, V.V., September 1989, (PB92 193 002/AS)A15. $33

UCB/EERC-90/11: Seismic Hazard Analysis: Improved Models, Uncertainties and Sensitivities, by Araya, R. and Der Kiureghian, A., March 1988, PB92-193010(A08). $20

UCB/EERC-90/10: Experimental Testing of the Resilient-Friction Base Isolation System, by Clark, P.W. and Kelly, J.M., July 1990, (PB92 143 072)A08. $20

UCB/EERC-90/09: Influence of the Earthquake Ground Motion Process and Structural Properties on Response Characteristics of Simple Structures, by Conte, J.P., Pister, K.S. and Mahin, S.A., July 1990, (PB92 143 064)A15. $33

UCB/EERC-90/08: Soil Conditions and Earthquake Hazard Mitigation in the Marina District of San Francisco, by Mitchell, J.K., Masood, T., Kayen, R.E. and Seed, R.B., May 1990, (PB 193 267/AS)A04. $15

UCB/EERC-90/07: A Unified Earthquake-Resistant Design Method for Steel Frames Using ARMA Models, by Takewaki, I., Conte, J.P., Mahin, S.A. and Pister, K.S., June 1990, PB92-192947(A06). $15

UCB/EERC-90/05: Preliminary Report on the Principal Geotechnical Aspects of the October 17, 1989 Loma Prieta Earthquake, by Seed, R.B., Dickenson, S.E., Riemer, M.F., Bray, J.D., Sitar, N., Mitchell, J.K., Idriss, I.M., Kayen, R.E., Kropp, A., Harder, L.F., Jr. and Power, M.S., April 1990, (PB 192 970)A08. $20

UCB/EERC-90/03: Earthquake Simulator Testing and Analytical Studies of Two Energy-Absorbing Systems for Multistory Structures, by Aiken, I.D. and Kelly, J.M., October 1990, (PB92 192 988)A13. $26

UCB/EERC-90/02: Javid's Paradox: The Influence of Preform on the Modes of Vibrating Beams, by Kelly, J.M., Sackman, J.L. and Javid, A., May 1990, (PB91 217 943/AS)A03. $13

UCB/EERC-89/16: Collapse of the Cypress Street Viaduct as a Result of the Loma Prieta Earthquake, by

Nims, D.K., Miranda, E., Aiken, I.D., Whittaker, A.S. and Bertero, V.V., November 1989, (PB91 217 935/AS)A05. $15

UCB/EERC-89/15: Experimental Studies of a Single Story Steel Structure Tested with Fixed, Semi-Rigid and Flexible Connections, by Nader, M.N. and Astaneh-Asl, A., August 1989, (PB91 229 211/AS)A10. $26

UCB/EERC-89/14: Preliminary Report on the Seismological and Engineering Aspects of the October 17, 1989 Santa Cruz (Loma Prieta) Earthquake, by EERC, October 1989, (PB92 139 682/AS)A04. $15

UCB/EERC-89/13: Mechanics of Low Shape Factor Elastomeric Seismic Isolation Bearings, by Aiken, I.D., Kelly, J.M. and Tajirian, F.F., November 1989, (PB92 139 732/AS)A09. $20

UCB/EERC-89/12: ADAP-88: A Computer Program for Nonlinear Earthquake Analysis of Concrete Arch Dams, by Fenves, G.L., Mojtahedi, S. and Reimer, R.B., September 1989, (PB92 139 674/AS)A07. $20

UCB/EERC-89/11: Static Tilt Behavior of Unanchored Cylindrical Tanks, by Lau, D.T. and Clough, R.W., September 1989, (PB92 143 049)A10. $26

UCB/EERC-89/10: Measurement and Elimination of Membrane Compliance Effects in Undrained Triaxial Testing, by Nicholson, P.G., Seed, R.B. and Anwar, H., September 1989, (PB92 139 641/AS)A13. $26

UCB/EERC-89/09: Feasibility and Performance Studies on Improving the Earthquake Resistance of New and Existing Buildings Using the Friction Pendulum System, by Zayas, V., Low, S., Mahin, S.A. and Bozzo, L., July 1989, (PB92 143 064)A14. $33

UCB/EERC-89/08: Seismic Performance of Steel Moment Frames Plastically Designed by Least Squares Stress Fields, by Ohi, K. and Mahin, S.A., August 1989, (PB91 212 597)A05. $15

UCB/EERC-89/07: EADAP - Enhanced Arch Dam Analysis Program: Users's Manual, by Ghanaat, Y. and Clough, R.W., August 1989, (PB91 212 522)A06. $20

UCB/EERC-89/06: Effects of Spatial Variation of Ground Motions on Large Multiply-Supported Structures, by Hao, H., July 1989, (PB91 229 161/AS)A08. $20

UCB/EERC-89/05: The 1985 Chile Earthquake: An Evaluation of Structural Requirements for Bearing Wall Buildings, by Wallace, J.W. and Moehle, J.P., July 1989, (PB91 218 008/AS)A13. $26

UCB/EERC-89/04: Earthquake Analysis and Response of Intake-Outlet Towers, by Goyal, A. and Chopra, A.K., July 1989, (PB91 229 286/AS)A19. $39

UCB/EERC-89/03: Implications of Site Effects in the Mexico City Earthquake of Sept. 19, 1985 for Earthquake-Resistant Design Criteria in the San Francisco Bay Area of California, by Seed, H.B. and Sun, J.I., March 1989, (PB91 229 369/AS)A07. $20

UCB/EERC-89/02: Earthquake Simulator Testing of Steel Plate Added Damping and Stiffness Elements, by Whittaker, A., Bertero, V.V., Alonso, J. and Thompson, C., January 1989, (PB91 229 252/AS)A10. $26

UCB/EERC-89/01: Behavior of Long Links in Eccentrically Braced Frames, by Engelhardt, M.D. and Popov, E.P., January 1989, (PB92 143 056)A18. $39

UCB/EERC-88/20: Base Isolation in Japan, 1988, by Kelly, J.M., December 1988, (PB91 212 449)A05. $15

UCB/EERC-88/19: Steel Beam-Column Joints in Seismic Moment Resisting Frames, by Tsai, K.-C. and Popov, E.P., November 1988, (PB91 217 984/AS)A20. $39

UCB/EERC-88/18: Use of Energy as a Design Criterion in Earthquake-Resistant Design, by Uang, C.-M. and Bertero, V.V., November 1988, (PB91 210 906/AS)A04. $15

UCB/EERC-88/17: Earthquake Engineering Research at Berkeley - 1988, by EERC, November 1988, (PB91 210 864)A10. $26

UCB/EERC-88/16: Reinforced Concrete Flat Plates Under Lateral Load: An Experimental Study Including Biaxial Effects, by Pan, A. and Moehle, J.P., October 1988, (PB91 210 856)A13. $26

UCB/EERC-88/15: Dynamic Moduli and Damping Ratios for Cohesive Soils, by Sun, J.I., Golesorkhi, R. and Seed, H.B., August 1988, (PB91 210 922)A04. $15

UCB/EERC-88/14: An Experimental Study of the Behavior of Dual Steel Systems, by Whittaker, A.S.,

Uang, C.-M. and Bertero, V.V., September 1988, (PB91 212 712)A16. $33

UCB/EERC-88/13: Implications of Recorded Earthquake Ground Motions on Seismic Design of Building Structures, by Uang, C.-M. and Bertero, V.V., November 1988, (PB91 212 548)A06. $20

UCB/EERC-88/12: Nonlinear Analysis of Reinforced Concrete Frames Under Cyclic Load Reversals, by Filippou, F.C. and Issa, A., September 1988, (PB91 212 589)A07. $20

UCB/EERC-88/11: Liquefaction Potential of Sand Deposits Under Low Levels of Excitation, by Carter, D.P. and Seed, H.B., August 1988, (PB91 210 880)A15. $33

UCB/EERC-88/10: The Landslide at the Port of Nice on October 16, 1979, by Seed, H.B., Seed, R.B., Schlosser, F., Blondeau, F. and Juran, I., June 1988, (PB91 210 914)A05. $15

UCB/EERC-88/09: Alternatives to Standard Mode Superposition for Analysis of Non-Classically Damped Systems, by Kusainov, A.A. and Clough, R.W., June 1988, (PB91 217 992/AS)A04. $15

UCB/EERC-88/08: Analysis of Near-Source Waves: Separation of Wave Types Using Strong Motion Array Recordings, by Darragh, R.B., June 1988, (PB91 212 621)A08. $20

UCB/EERC-88/07: Theoretical and Experimental Studies of Cylindrical Water Tanks in Base-Isolated Structures, by Chalhoub, M.S. and Kelly, J.M., April 1988, (PB91 217 976/AS)A05. $15

UCB/EERC-88/06: DRAIN-2DX User Guide, by Allahabadi, R. and Powell, G.H., March 1988, (PB91 212 530)A12. $26

UCB/EERC-88/05: Experimental Evaluation of Seismic Isolation of a Nine-Story Braced Steel Frame Subject to Uplift, by Griffith, M.C., Kelly, J.M. and Aiken, I.D., May 1988, (PB91 217 968/AS)A07. $20

UCB/EERC-88/04: Re-evaluation of the Slide in the Lower San Fernando Dam in the Earthquake of Feb. 9, 1971, by Seed, H.B., Seed, R.B., Harder, L.F. and Jong, H.-L., April 1988, (PB91 212 456/AS)A07. $20

UCB/EERC-88/03: Cyclic Behavior of Steel Double Angle Connections, by Astaneh-Asl, A. and Nader, M.N., January 1988, (PB91 210 872)A05. $15

UCB/EERC-88/02: Experimental Evaluation of Seismic Isolation of Medium-Rise Structures Subject to Uplift, by Griffith, M.C., Kelly, J.M., Coveney, V.A. and Koh, C.G., January 1988, (PB91 217 950/AS)A09. $20

UCB/EERC-88/01: Seismic Behavior of Concentrically Braced Steel Frames, by Khatib, I., Mahin, S.A. and Pister, K.S., January 1988, (PB91 210 898/AS)A11. $26